Elucidation of the role of the linker motifs of *Plasmodium falciparum* Hsp70-1 and Hsp70-z

by

Graham Chakafana

submitted in fulfilment of the requirements for the degree of

Doctor of Philosophy

in the subject of

Biochemistry

at

the University of Venda

Promoter: Prof. A. Shonhai

Co-promoter: Dr. T. Zininga

Submitted on

23 March 2020

Abstract

The main malaria agent, *Plasmodium falciparum*, exhibits a complex life cycle. The parasite initially develops in a poikilothermic mosquito vector before it is subsequently transmitted to a homeothermic human host. As such, the parasite depends on heat shock proteins (Hsps) for maintenance of proteostasis under the physiologically diverse conditions characterising its life cycle. Some of the parasite Hsp70 family members, amongst them, PfHsp70-1 and PfHsp70-z, are essential for parasite survival. PfHsp70-1 is a canonical Hsp70, which closely resembles *Escherichia coli* Hsp70, DnaK. On the other hand, PfHsp70-z is a non-canonical Hsp70 which belongs to the Hsp110 subfamily. Hsp70s exhibit a highly conserved structural architecture characterized by an N-terminal nucleotide-binding domain (NBD) and a C-terminal substrate-binding domain (SBD) adjoined by a linker motif. Although canonical Hsp70 linkers are highly conserved, Hsp110 linkers are less conserved. Moreover, sequence analysis data revealed that PfHsp70-z possesses a highly charged linker motif that is markedly different from that of the most studied Hsp110, *Saccharomyces cerevisiae* Sse1. To date, the function of the linkers of Hsp110s and PfHsp70-1 largely remains unknown. By creating linker swap versions of PfHsp70-1 and PfHsp70-z, this study sought to elucidate the roles of the linkers of the two chaperones in modulating their functions. A DnaK mutant harbouring a PfHsp70-z linker insertion was also characterized towards further elucidating the function of the PfHsp70-z linker. *In silico* and biophysical characterization revealed structural variations induced by linker mutations. It was established that the linker of PfHsp70-z confers improved stability to protein structure. On the other hand, the insertion of the PfHsp70-z linker into PfHsp70-1 and DnaK compromised the perturbation of the conformations of these two canonical Hsp70s in response to nucleotide binding. Additionally, the PfHsp70-1 linker induced a 3-fold increase in basal ATPase activity of PfHsp70-z. However, the PfHsp70-z linker reduced PfHsp70-1 basal ATPase activity by half. The PfHsp70-z linker also reduced the affinity of PfHsp70-1 for PfHsp40. This possibly accounted for the lack of PfHsp40-induced stimulation of ATPase activity in the PfHsp70-1 linker mutant. Moreover, there was a marked reduction in the refolding efficiency of PfHsp70-1 and PfHsp70-z linker mutants, respectively. Taken together, this study provided evidence that PfHsp70-1 and PfHsp70-z linkers dictate the structural conformation and functional specifications of the respective proteins. The unique linker PfHsp70-z appears to regulate the chaperone function of this medically important protein.

Key words: linker motif, *Plasmodium falciparum*, chaperone, motif, Hsp70, Hsp110

Declaration

I, Graham Chakafana hereby declare that the thesis for the Doctor of Philosophy in Biochemistry degree at the University of Venda, hereby submitted by me, has not previously been submitted for a degree at this or any other university, and that it is my own work in design and execution and that all reference material contained therein has been duly acknowledged.

Signature:  **Date: 24 Aug 2020**

Dedication

I dedicate this thesis to my parents, Mr Dennis and Mrs Farai Chakafana who to this stage have been my greatest educators.

Preface

This thesis is comprised of six chapters. The outlines for each chapter are provided below.

Chapter 1: This is a general introduction encompassing all the background to the suggested broad aim and specific objectives. It also highlights the broad problem statement and spells out the study hypothesis.

Chapter 2: This chapter reports the *in silico* analyses conducted in order to decipher the possible roles of the linker motifs of PfHsp70-1, PfHsp70-z and DnaK.

Chapter 3: This chapter highlights the recombinant production of PfHsp70-1, PfHsp70-z, DnaK and their linker substitution mutants. In this chapter, the biophysical characterization of the proteins is described.

Chapter 4: This chapter describes the effects of the introduced linker mutations on the functions of PfHsp70-1, PfHsp70-z and DnaK *in vitro.*

Chapter 5: This chapter encompasses the evaluation of the role of the linkers of PfHsp70-1, PfHsp70-z and DnaK with respect to their association with respective co-chaperones.

Chapter 6.:This chapter covers conclusive remarks and future perspectives.

Acknowledgments

I wish to thank God for giving me the strength to complete this study. I am also grateful to my promoter, Prof. A. Shonhai and co-promoter, Dr. T. Zininga for their mentorship, guidance and motivation throughout the duration of the project. Their support and patience helped me develop a deeper understanding and passion in Protein Biochemistry.

I also wish to express my appreciation to the following people for the technical support provided during this study:

- Dr. I. Achilonu and Prof. H. Dirr; Protein Structure-Function Research Unit, University of the Witwatersrand, South Africa.

I wish to extend further acknowledgments to the:

- Deutsche Forschungsgemeinschaft (DFG) and the National Research Fund (NRF) for funding the project and study bursary
- University of Venda Research Committee (South Africa) for student research funding

Finally, special thanks go to all the members of the Protein Biochemistry and Malaria (ProBioM) research team who were the family I had at the University of Venda. Special mention goes to Dr. Stanley Makumire who took time to provide technical support during the study. I would also want to thank the staff members of the Biochemistry department who also supported me in many ways throughout the duration of the study. Finally, I wish to extend my gratitude to my family and friends that always supported me throughout this journey

Table of Contents

List of Figures

List of Tables

List of Symbols

Abbreviations of units and symbol interpretation

%	percent
µl	microlitre
A320	absorbance at 320 nanometres
A360	absorbance at 360 nanometres
A595	absorbance at 595 nanometres
A600	absorbance at 600 nanometres
bp	base pair
kDa	kilodalton
µM	micromolar
pM	picomolar
°C	degree celsius
ml	millilitre
l	litres
w/v	weight per volume
v/v	volume per volume
µg	microgram
g	gram
α	alpha
β	beta

List of Outputs

Journal articles

Chakafana, G., Zininga, T., Shonhai, A. (2019). Comparative structure-function features of Hsp70s of *Plasmodium falciparum* and human origins. *Biophysical reviews* **6:**591-602. doi: 10.1007/s12551-019-00563-w

Chakafana, G., Zininga, T., Shonhai, A. (2019). The link that binds: the linker of Hsp70 as a helm of protein function. *Biomolecules* **9**: 543-563. doi: 10.3390/biom9100543.

Seraphim, T.V, Chakafana, G., Shonhai, A., Houry, W.A. (2019). *Plasmodium falciparum* R2TP complex: drivers of parasite Hsp90s. *Biophysical Reviews* **11:**1007-1015. doi: 10.1007/s12551-019-00605-3.

Chakafana, G., Zininga, T., Achilonu, I., Dirr, H., Shonhai, A. (2020). Characterization of the unique linker segment of *P. falciparum* Hsp110. (Manuscript in preparation)

Conference/Workshop Proceedings

Chakafana, G., Zininga, T., Shonhai, A. Biophysical analysis of the linker motifs of *P. falciparum* Hsp70-1 and Hsp70-z. Biophysics and Structural Biology at Synchrotrons Workshop. 16 -24 Jan 2019. University of Cape Town (South Africa).

Chakafana, G., Zininga, T., Shonhai, A. Elucidation of the role of the linker motif of *Plasmodium falciparum* Hsp70-1 in modulating its interaction with co-chaperones. Southern Africa Malaria Research Conference, University of Pretoria, 2019

Chakafana, G. National Research Fund (NRF) & British Council Fame Lab "Heat shock proteins of *P. falciparum* as potential antimalarial drug targets" University of Venda, 2019

CHAPTER 1

Literature review

1.1 Malaria

Global estimates indicate that approximately 3.2 billion people are at risk of malaria transmission based on the World Health Organisation (WHO) 2019 world malaria report. As such, half of the world's population is thought to be living in regions where malaria is endemic (WHO, 2019). In the year 2018, malaria accounted for approximately 228 million clinical cases and 405 000 deaths globally (WHO, 2019). The majority of the malaria cases reported (88%) were from Sub Saharan Africa (WHO, 2019). In addition, Africa accounts for approximately 94% of all malaria deaths worldwide (WHO, 2019). Various factors such as socio-economic instability and a sub-tropical environment that is conducive for the breeding of mosquito vectors account for the high malaria prevalence in sub-Saharan Africa (CDC, 2018).

Malaria is caused by the Apicomplexan intracellular parasites of the *Plasmodium* genus. The Apicomplexan family consists of obligate intracellular, unicellular organisms that are characterised by an apical complex located at the anterior end of the parasites (Lim and McFadden, 2010). Human malaria is caused by 5 species of the *Plasmodium* genus which include *P. falciparum*, *P. vivax, P. knowlesi, P. malariae* and *P. ovale (*Schmitz *et al*., 2010). *P. falciparum* is responsible for approximately 99.7% of malaria cases in Africa(WHO, 2018). Furthermore, *P. falciparum* is responsible for the most severe forms of malaria due to its complicated life cycle (Pasvol *et al*., 2005).

1.2 Life cycle of *P. falciparum*

The malaria parasite exhibits a complex life-cycle in which it develops in a poikilothermic mosquito vector (*Anopheles* mosquito) before it is subsequently transmitted to a homeothermic human host (Figure 1.1). In the human host, *P. falciparum* infection is initiated when sporozoites are injected into the bloodstream from the salivary glands of a feeding mosquito (Figure 1.1). The sporozoites migrate through the circulatory system to the liver where they invade hepatocytes (Sinnis *et al*., 1997). It is estimated that the injection of only between two to ten sporozoites can initiate *P. falciparum* infection (Khusmith *et al*., 1994). In addition, the invasion of

hepatocytes by sporozoites is a rapid and efficient process which is thought to occur approximately two minutes after intravenous injection (Amino *et al*., 2006; Hopp *et al*., 2015).

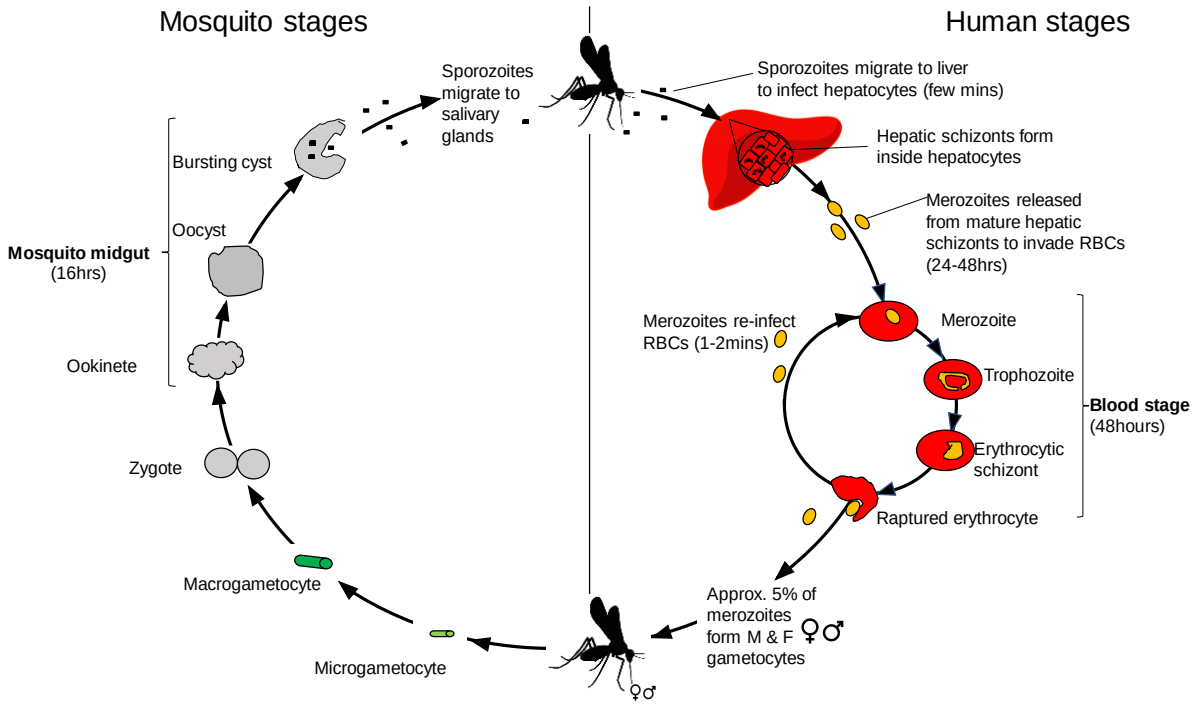

Figure 1.1. Life cycle of *Plasmodium falciparum*

P. falciparum parasites are injected into the warm-blooded human host in the form of sporozoites when the *Anopheles* mosquito vector takes a blood meal. The sporozoites subsequently migrate to the liver where they infect hepatocytes. Inside the hepatocytes, the sporozoites develop and multiply via schizogony to rupture and release merozoites, which then infect erythrocytes Once inside the erythrocytes, the merozoites multiply via schizogony asexually. The infected erythrocytes then burst, releasing more merozoites which re-infect new erythrocytes within 48 hours. Some of the merozoites differentiate into gametocytes, which are then taken up by the mosquito when it ingests a blood-meal. The sexual reproduction stage occurs through gametocytes that fuse together and differentiate in the mosquito midgut to form new sporozoites. The sporozoites can be further injected into the human host starting another cycle. (Adapted from Seraphim *et al*., 2019).

Inside the hepatocytes, sporozoites undergo exoerythrocytic schizogony which is thought to last approximately one week before it culminates into the production of merozoites (Wiser, 2016). When the hepatic schizonts burst, they release the merozoites into the bloodstream where they invade erythrocytes to initiate the erythrocytic stage (Cowman *et al*., 2006). It is thought that, approximately 10 000 to 30 000 merozoites are released from a single schizont into the circulatory system

(Alvarez *et al*., 2006; Zheng *et al*., 2014). Merozoites are highly susceptible to phagocytosis and should therefore avoid contact with macrophages (Baer *et al*., 2007). As such, merozoites only have a short life span of approximately 1-2 mins within which they must infect erythrocytes (Yahata *et al*., 2012).

Upon entry into the erythrocytes, merozoites undergo asexual replication via schizogony, which is known to last for approximately 48 hours (Sinnis *et al*., 1997). During the erythrocytic stage, merozoites undergo a trophic period in which they enlarge to form trophozoites (Bousema *et al*., 2014; Figure1.1). The early trophozoite is referred to as the 'ring form' because of its' morphology. Trophozoite enlargement is accompanied by active metabolism which includes the ingestion of host cytoplasm and proteolysis of haemoglobin to release amino acids and heme. The amino acids are then utilised for parasite protein synthesis (Abu Bakar *et al*., 2010; Wiser, 2016). Heme is toxic to the parasite and as such it is converted into a crystalline less toxic form, hemozoin (Rinehart *et al*., 2016). The end of the trophic period is marked by multiple rounds of nuclear division without cytokinesis which subsequently results in the formation of an early schizont (Tuteja *et al*., 2007). During erythrocytic schizogony, maturation is the last stage which culminates in the release of approximately 16–32 daughter merozoites into the bloodstream (Figure 1.1; Bousema *et al*., 2014; Absalon *et al*., 2016).

Most of the released merozoites then invade new erythrocytes and thus reinitiate another round of the asexual erythrocyte-stage replicative cycle. Some of the released merozoites (approximately 0.1 - 5%) differentiate into gametocytes to form microgametocytes (male) and macrogametocytes (female) which are the sexual forms of the parasite (Sinden 1983). Gametocytogenesis is thought to be triggered by stress from the host immune system, nutrition deprivation and high parasitemia (Talman *et al*., 2004). *P. falciparum* gametocytes differentiate and mature through a process that takes approximately 8-10 days in the erythrocytes (Hawking *et al*. 1971; Sinden *et al*. 1978).

P. falciparum gametocytes are typically large parasites which fill up the erythrocytes as they mature (Figure 1.1; Meibalan *et al*., 2017). When a mosquito takes another blood meal from an infected human, it ingests the gametocytes (Figure 1.1). Once the gametocytes are inside the mosquito midgut, fertilization is induced by the drop in temperature, increase in pH and increased xanthurenic acid concentration (Billker *et al*. 1998, 2000). When the flagellated microgametes fertilize the macrogamete a zygote is formed. The zygote then develops into motile ookinetes, which subsequently penetrate the mosquito midgut and develop into oocysts (Figure 1.1). *P. falciparum* oocysts mature over a period of approximately 11-16 days to form sporozoites (Meis *et al*. 1992). The sporozoites then migrate to the salivary glands of the mosquito awaiting release into the human host when the mosquito feeds, thus re-initiating the life cycle (Figure 1.1).

1.3 The pathogenesis of *P. falciparum* infection

The pathology associated with malaria is largely a consequence of the erythrocyte stage since the hepatic stage is mostly asymptomatic (Paul *et al*., 2004). The intermittent fever paroxysms are due to the synchronous lysis of the infected erythrocytes that occurs when merozoites are released (Bousema *et al*., 2014). The bursting of erythrocytes results in the release of proteins into the blood stream, which in turn stimulate an immune response. The immune response to the antigenic parasite proteins stimulates the release of proinflammatory cytokines such as tumour necrosis factor (TNF) which is responsible for periodic fevers (Bannister *et al*., 2000; Geleta *et al*., 2016).

P. falciparum infection is characterized by the sequestration of parasite-infected erythrocytes in various organs, which include the lungs, brain and placenta. By so doing, *P. falciparum* avoids clearance by the spleen (Soni *et al*., 2016). Sequestration of infected erythrocytes results from adhesive interactions that occur between parasite proteins displayed on infected erythrocyte surfaces and several molecules on host surfaces such as uninfected erythrocytes, endothelial cells, and placental cells (Rowe

et al., 2009). As a result, when the infected erythrocytes lodge in the brain, they block the capillaries in the brain thereby causing complications such as cerebral malaria.

1.4 Invasion of the host erythrocyte cells by *P. falciparum* merozoites

The ability of *P. falciparum* merozoites to recognize and invade erythrocytes is an essential step for parasite survival. The overall process of erythrocyte invasion is complex but it is extremely rapid (Olshina *et al*., 2015). It is important for the invasion time to be short since the merozoite is one of the few stages of the *Plasmodium* life cycle in which the parasite is extracellular and directly exposed to immunological attack (Olshina *et al*., 2015). Invasion is initiated when the merozoites released from hepatic schizonts make primary contacts and attach to the erythrocytes (Figure 1.2; Crick *et al*., 2014). One of the proteins implicated in the formation of a primary contact is the merozoite surface protein 1 (MSP1) (Kadekoppala *et al*., 2008). Upon attachment, merozoites then undergo a series of adhesive interactions with the erythrocyte receptors.

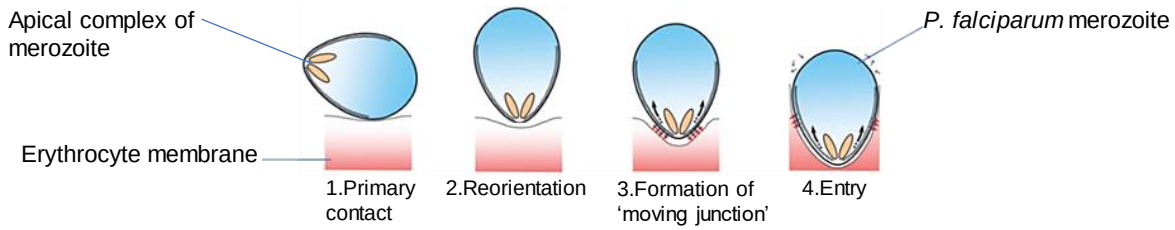

Figure 1.2. *P. falciparum* host erythrocyte cell invasion process

Erythrocyte invasion is a complex multistep process which involves contact, re-orientation of the merozoite, moving junction formation and entry. (Adapted from Koch and Baum, 2016).

Primary contact and attachment of merozoites to erythrocytes is generally governed by two classes of proteins, which include adhesins and invasins (Wright and Rayner, 2014). *P. falciparum* adhesins bind directly to specific receptors on the erythrocyte. The main adhesins involved in erythrocyte invasion belong to the erythrocyte binding-like domains (EBL) and reticulocyte binding-like homologues (PfRh) families (Cowman *et al*., 2012). Different members of these adhesins bind to specific receptors, for instance, erythrocyte binding antigen-175 (EBA-175), erythrocyte binding ligand 1

(Ebl1), and erythrocyte binding antigen-140 (EBA-140) bind to the erythrocyte receptors glycophorin A, B, and C, respectively (Baum *et al*., 2008). The PfRh and EBL protein families play an important role in phenotypic variation that provide the different strains of *P. falciparum* with options to invade via alternative host receptors (Sim *et al*., 1990; Duraisingh *et al*., 2003). Invasins, anchored on merozoite surface, indirectly facilitate erythrocyte invasion since they do not necessarily bind to erythrocyte receptors (Cowman *et al*., 2012). In addition, invasins, such as the apical membrane antigen-1 (AMA1), are thought to be essential for merozoite invasion (Cowman *et al*., 2012).

Primary contact and attachment of the merozoites is then quickly followed by AMA1-mediated reorientation of the polar merozoite such that its apical end is adjacent to the erythrocyte membrane (Figure 1.2; Thera *et al*., 2011). This allows the parasite to deploy an arsenal of apically located secretory organelles which include rhoptries, micronemes and dense granules (Baum *et al*., 2008). These organelles then discharge EBLs in a regulated and ordered manner at the site of contact (Baum *et al*., 2008). The ligands released then interact with erythrocyte surface receptors to form an electron dense thickening of the erythrocyte membrane at the tight junction of erythrocyte-merozoite contact (Olshina *et al*., 2015). The moving junction is passed around the merozoite's surface in a belt-like structure that is thought to be driven by an actin-myosin motor anchored to the merozoite's inner membrane complex (IMC) (Baum *et al*., 2008). This process facilitates the internalization of the merozoite into the erythrocyte.

Once inside the erythrocytes, the parasites are enclosed in a compartment called the parasitophorous vacuole (PV) (Lingelbach and Joiner, 1998; Weiss *et al*., 2015). The PV functions as a transit compartment for proteins destined for the erythrocyte cytosol (Charpian and Przyborski, 2008). The parasitophorous vacuole membrane (PVM) forms a structural border that surrounds the PV. It also acts as a physical barrier that separates the parasites from the erythrocyte cytosol (Grüring *et al*., 2012). Upon parasite maturation Maurer's clefts develop within the erythrocyte cytosol (Sherling *et al*., 2016). Maurer's clefts are parasite-induced secretory organelles, or sack-like

structures in the erythrocyte cytosol, in which parasite proteins that are destined for the erythrocyte accumulate (Mundwiler-Pachlatiko and Beck, 2013).

1.5 *P. falciparum* mediated host cell remodelling

Mature erythrocytes are terminally differentiated and therefore do not facilitate *de-novo* protein synthesis (Bull and Hermamen, 2010). As such, to meet their metabolic requirements, the parasites mostly rely on the extracellular milieu of the erythrocyte in order to survive and develop (Desai, 2014). *P. falciparum* trophozoites engulf a portion of the erythrocyte cytoplasm in large vacuoles called 'cytosmes' (Elliott *et al*., 2007; Wendt *et al.,* 2016). It is during this process that parasite proteases within the acidic digestive vacuole lyse haemoglobin to release amino acids that are utilized by the parasite for protein synthesis (Goldberg, 2005; Abu Bakar *et al*., 2010). However, haemoglobin hydrolysis does not provide the parasite with all the amino acids that are necessary for synthesis of all members of its proteome (Mbengue *et al*., 2012). As such, the parasite re-models the host erythrocyte membrane in order to increase its permeability to organic solutes in the extracellular milleu containing the amino acids isoleucine, glutamate, methionine, cysteine and proline. These solutes together with anions and cations such as sodium (Na^+) and potassium (K^+) are all important for parasite survival (Desai, 2014; Soni *et al*., 2016). *P. falciparum* infected erythrocytes consume approximately a 100-fold more glucose than non-infected erythrocytes since the parasite continuously metabolizes sugars to support its growth and replication (Srivastava *et al.,* 2016; Althoff and Abramson, 2020). The parasite protein, *P. falciparum* hexose transporter 1 (PfHT1) is a scavenger protein that has recently been implicated in facilitating the transport of D-glucose/D-fructose from an infected erythrocyte (Althoff and Abramson, 2020). These adaptations help to improve the parasite's chances of survival in erythrocytes.

Parasite proteins that are exported to the erythrocyte facilitate remodelling of the host erythrocyte to make it conducive for parasite survival and development (Mbengue *et al*., 2012; Soni *et al*., 2016). It is thought that *P. falciparum* exports approximately 8-10 % of its proteome into the infected erythrocyte (Grüring *et al*., 2012; Przyborski *et al*., 2015; Soni *et al*., 2016). As such, the host erythrocyte then undergoes several

alterations that are important for parasite survival (Koch and Baum 2016). The exported parasite proteins have been reported to perform various functions to facilitate the survival of *P. falciparum* during its life cycle. For instance, the parasite protein ring-infected erythrocyte surface antigen (RESA) has been reported to bind β-spectrin and increase membrane stability in order to maintain the structural integrity of the erythrocyte (Silva *et al*., 2005; Goel *et al*., 2014). Another parasite protein, mature-parasite-infected erythrocyte surface antigen (MESA) binds to the membrane skeleton protein 4.1 to ensure parasite survival (Kilili and LaCount, 2011). It has been established that protein 4.1 (PlasmoDB accession # PF3D7_0410300) is important in maintaining the structural and mechanical integrity of the erythrocyte membrane through its interaction with spectrin and actin (Bennett *et al*., 1997). The anchoring of MESA onto protein 4.1 is thought to be essential for parasite survival (Contreras-Puentes, 2019).

Parasite proteins are also thought to play an important role in the destabilization of the erythrocyte membrane to allow for the egress of merozoites from infected erythrocytes. The protein *Plasmodium falciparum* erythrocyte membrane protein 1 (PfEMP-3) binds α-spectrin to destabilize the spectrin-protein 4.1-actin complex and thus compromise the mechanical stability of the erythrocyte membrane (Mohandas and An, 2012). This results in the bursting of the erythrocyte to release merozoites (Figure 1.1). The rupture of the erythrocyte and subsequent egress of merozoites is also regulated by a cascade of proteases (Thomas *et al*., 2018) . A few minutes prior to egress, the serine protease *P. falciparum* subtilisin-like protease 1 (PfSUB1) is discharged into the PV where it cleaves multiple substrates including SERA and MERA (Withers-Martinez *et al*., 2012). These events subsequently trigger disassembly of the erythrocyte cytoskeleton, culminating into rupture. As such, *P. falciparum* survival highly depends on a robust network of proteins, in order to remodel the host cell to facilitate survival within erythrocytes. Therefore, the parasite requires an efficient protein folding machinery for its development and pathogenicity.

1.6 Heat shock proteins: key drivers of proteostasis in *P. falciparum* survival

The development of *P. falciparum* within the mosquito vector and the human host exposes it to various stress conditions such as temperature and pH variations, oxidative stress as well as attack from the host's immune system (Silva *et al*., 2019). The parasite cells therefore need to adapt to the constantly changing physiological environments in order to maintain cellular viability during the different stress conditions. As such, *P. falciparum* possesses a robust heat shock response system (HSR) in which heat shock proteins (Hsps) are upregulated to ensure proteostasis (Shonhai *et al*., 2007; Shonhai, 2010; Daniyan *et al*., 2019).

Hsps are a class of molecular chaperones that perform a myriad of housekeeping and stress-protective roles in cells in order to maintain cellular proteostasis (Table 1.1; Lindquist, 1986). Approximately 2% of the parasite proteome is comprised of hsps, which are expressed at various stages of the parasite's life cycle (Acharya *et al*., 2007). Hsps broadly function to facilitate the correct folding and assembly of polypeptides, thus preventing the formation of misfolded or incorrectly assembled proteins (Zugel and Kaufmann, 1999).

Approximately 30% of the parasite proteome is characterized by aggregation-prone proteins that are rich in glutamate/asparagine repeat segments (Singh *et al*., 2004; Pallarès *et al*., 2018). Hsps play an important role in the suppression or inhibition of polypeptide aggregation (Muralidaran *et al*., 2012; Zininga *et al*., 2015b). When a nascent polypeptide chain exits the ribosome or an organellar import pore, or when a labile native protein becomes transiently heat denatured, it exposes hydrophobic segments to the aqueous environment (Mattoo *et al*., 2013). Depending on the intensity and duration of the stress, the misfolded segments may clamp together through intermolecular hydrophobic associations to form aggregates (Marinko *et al*., 2019). Hsps of the 'holdase' class can bind to the exposed hydrophobic segments on the surface of misfolded polypeptides thus preventing the formation of aggregates

(Mattoo *et al*., 2014; Mogk *et al*., 2017. *P. falciparum* Hsps are generally classified into seven major families which are distinguished from each other based on molecular weight and functions (Table 1.1; Shonhai, 2010). Hsps function cooperatively by forming an intricate molecular network which acts synergistically to maintain cellular proteostasis (Acharya *et al*., 2007).

Table 1.1 Summary of *P. falciparum* heat shock protein family properties

Protein Family	Function	Predicted Localization	Size (kDa)	Reference
Hsp110	Protein aggregation suppression; Possess holdase function	cytosol, ER	100	Muralidharan *et al*., 2012 Zininga *et al*., 2016
Hsp100	Dis-assembly of quaternary structure of polypeptide complexes and are required for thermotolerance	apicoplast, PV, mitochondrium	80-110	Rathore et al., 2011 de Koning Ward, 2009 El Bakkouri *et al*., 2013
Hsp90	Involved in cell cycle control, cell survival and other cell signalling pathways	cytosol, ER mitochondria Apicoplast	82-96	Acharya *et al*., 2007 Shahinas *et al*., 2013 Reviewed in Zininga and Shonhai, 2019
Hsp70	Folding of nascent polypeptides, protein translocation	cytosol, ER, nucleus, PV, mitochondria, apicoplast, J dots	73-76	Shonhai, 2008 Kulzer et al., 2012 Mabate *et al*., 2018
Hsp60	Ensure correct folding of newly synthesized or stress denatured proteins	apicoplast, mitochondria	58-65	Polson *et al*., 2018 Yeo *et al*., 2015
Hsp40	Co-chaperone of Hsp70-1; Host cell modifications	cytosol, membranes, J-dots, Maurer's cleft ER	40-100	Botha *et al*., 2007; Kulzer et al., 2010; Njunge *et al*., 2013
sHsps	Aggregation suppression	Cytosol, nucleus	12-43	Montagna et al., 2012

1.6.1 Heat shock protein 40 (Hsp40)

Hsp40 (DnaJ in prokaryotes) are homodimeric proteins that are localized in the cytoplasm of prokaryotes (Caplan *et al*., 1993). In eukaryotes, Hsp40s are localized in the cytosol and various subcellular compartments or the extracellular milieu (Carrigan *et al*., 2006; Kulzer *et al*., 2012). Hsp40 homologs are well represented in both prokaryotes and eukaryotes. For instance, in *Escherichia coli*, six DnaJ homologues have been identified, while a total of 22 have been identified in *Saccharomyces cerevisiae* (Walsh *et al*., 2004; Qui *et al*., 2006). Hsp40s play important roles in gene expression and translation initiation, folding and unfolding as well as translocation and degradation of proteins (Qui *et al*., 2006). Hsp40s are also known to form functional partnerships with Hsp70s to facilitate the folding of nascent proteins (Botha *et al*., 2007; Alderson *et al.*, 2016) and the refolding of misfolded proteins that accumulate in response to stress conditions (Fan *et al*., 2003; Mattoo *et al*., 2013).

Based on their domain organization, Hsp40s can be broadly classified into 4 types which are types I, II, III and IV (Figure 1.3; Szabo *et al*., 1996). Hsp40s are typically characterised by the J-domain which is present in all four types. The J-domain harbours a highly conserved HPD motif which is important for the functional interaction of Hsp40s with Hsp70s (Kityk *et al*., 2018). Type I Hsp40s are marked by the presence of a J-domain, GF-rich region, cysteine rich region and a C-terminal domain which is important for substrate binding (Figure 1.3; Hennesy *et al*., 2005). Type II Hsp40s generally possess a similar domain architecture to type I Hsp40s with the exception that type II Hsp40s lack a cysteine rich region domain (Figure 1.3; Szabo *et al*., 1996; Behl and Mishra, 2018). Both type I and II Hsp40s are known to act as substrate scanners for Hsp70 by binding to unfolded or near-native polypeptides and delivering them to Hsp70 for folding (Fan *et al*., 2003; Cryr and Ramos, 2015). Type I and type II Hsp40s also function as holdases that bind hydrophobic regions on proteins in order to prevent their aggregation (Cryr and Ramos, 2015). Type III and IV Hsp40s possess a J-domain although they typically lack the zinc finger and cysteine rich domains (Figure 1.3). Type IV Hsp40s possess a less conserved J-domain which lacks an HPD motif (Figure 1.3; Botha *et al*. 2007).

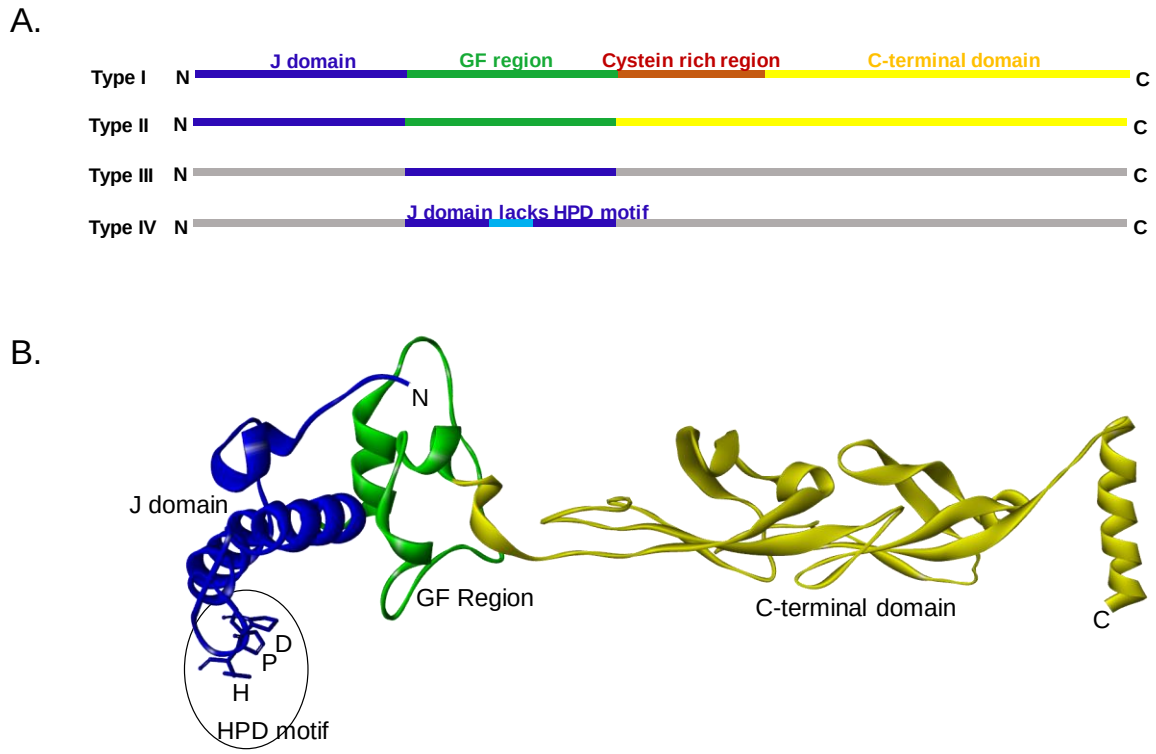

Figure 1.3. Subtypes of the Hsp40 group

(A). Type I contains all 3 domains (J, G/F and ZN), type II has 2 while types III and IV have 1 domain each. (B). Typical type II Hsp40 showing major domains and HPD motif important for Hsp70 binding.

The *P. falciparum* genome encodes 49 Hsp40s (Pesce *et al*., 2014). Of these Hsp40s, two are classified under type I, eight are type II, 26 are type III and 13 are type IV. Type I and II *P. falciparum* Hsp40s function primarily as co-chaperones for *P. falciparum* Hsp70s (Botha *et al*., 2007; Section 1. 7. 4). In addition, Hsp40s regulate specificity of substrate recognition apart from stimulating the ATPase activity of Hsp70 (Botha *et al*., 2012; Pesce *et al*., 2014; Section 1.7.4). Interestingly, approximately half of the parasite's complement of *P. falciparum* Hsp40s are exported outside the erythrocyte (Sargeant *et al*., 2006; Botha *et al*., 2007). The exported Hsp40s have been implicated in host cell modification, including biogenesis of knob structures under the surface of the erythrocyte, insertion of PfEMP1 into the knob structures as well as alteration of erythrocyte deformability (Pasternak *et al*., 2009). This erythrocyte modification is thought to have a direct effect on pathogenicity of parasites in the human host (Maier *et al*., 2008).

1.6.2 Heat shock protein 90

Heat shock protein 90 (Hsp90) is a highly abundant chaperone which plays an important role in cell growth and development (Acharya *et al*, 2007). Hsp90 is distinguished from other molecular chaperones in that it has the ability to bind target proteins that are in a near native state thus facilitating the final stages of protein folding and activation (Luengo *et al*., 2018). The Hsp90 clientome is large, spanning across over 200 proteins (Picard, 2002; Zhao *et al*., 2005; Schopf *et al*., 2017). For example, Hsp90 is implicated in the folding, assembly and stabilization of protein kinases, steroid hormone receptors, toll like receptors (TLRs) for innate immunity, RNA polymerases and PI3-kinase-related kinases (PIKKs) (Kakihary and Houry, 2012; Pal *et al*., 2014). Hsp90 modulates cell signalling, genome maintenance and assembly of transcriptional and translational factors (Buchner *et al*., 2013). In addition, Hsp90 plays an active role in protein quality control by directing misfolded proteins towards the ubiquitin-proteosome system (UPS) for degradation (Gamerdinger *et al*., 2009).

The *P. falciparum* genome encodes for four Hsp90 genes which express PfHsp90 (PF3D7_0708400; cytosol-localised), PfGrp94 (PF3D7_1222300; ER localised) and PfTRAP1 (PF3D7_1118200; mitochondrium-localised) (P3D7_1443900; apicoplast-localized) (Acharya *et al*., 2007; Zininga and Shonhai, 2019). Extensive research has however focused on the stress-inducible cytosolic isoform, PfHsp90 (PF3D7_0708400) (Seraphim *et al*., 2019). PfHsp90 plays an important role in the folding, assembly and activation of several proteins involved in cellular processes such as signal transduction, growth and developmental regulation (Wang *et al*., 2016). In *P. falciparum*, Hsp90 is expressed in all stages of the parasite's life cycle although it is upregulated in the early ring stage of the erythrocytic cycle (Kumar *et al*., 2003). Inhibition of PfHsp90 blocks the erythrocytic stage of the parasites life cycle and has also been shown to result in parasitaemia clearing in mouse malaria models (Banumathy *et al*., 2003; Shahinas *et al*., 2013).

It has been established through structural and biochemical studies, that PfHsp90 is a nucleotide dependent chaperone that functionally operates as a homodimer *in vivo*

(Pallavi *et al*., 2010; Wang *et al*., 2016). PfHsp90 is characterised by an N-terminal domain (NTD) for ATP binding, a middle domain (MD) which possesses ATPase activity and a C-terminal domain (CTD) that is responsible for dimerization (Figure 1.4; Pallavi *et al*., 2010). The CTD also harbours a C-terminal Met-Glu-Glu-Val-Asp (MEEVD) motif which facilitates Hsp90 interaction with tetratricopeptide repeat (TPR) domain containing co-chaperones such as Hsp70-Hsp90 organising protein (Hop) (Figure 1.4; Gitau *et al*., 2012). PfHsp90 NTD and the MD are connected by a long, flexible, charged linker that modulates NTD/MD contacts dictating Hsp90 function (Tsutsumi *et al*., 2012).

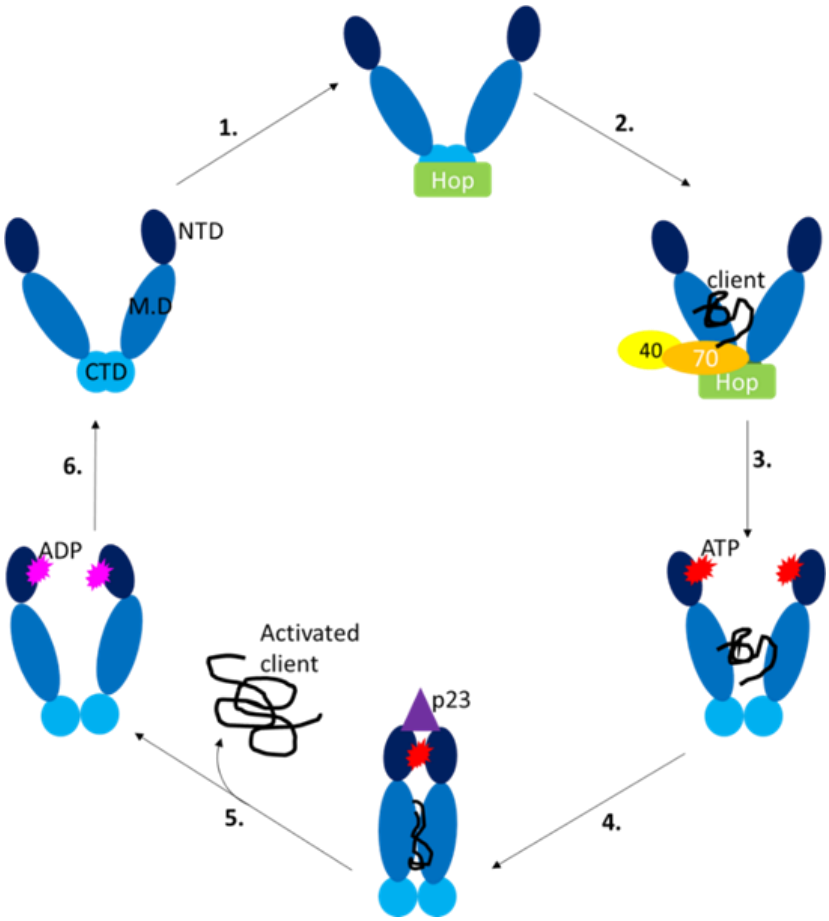

Figure 1.4. Co-operation of co-chaperones during the functional cycle of PfHsp90

(1) PfHop binds to Hsp90-CTD to facilitate the further binding of PfHsp70-1. (2) The client is recruited to Hsp90 by the PfHsp70-1/PfHsp40 complex. (3) ATP binds to PfHsp90 NTD resulting in a closed conformation of Hsp90. (4) p23 binds to the NTD activating ATP hydrolysis and (5) subsequent client release. (6) PfHsp90 assumes an open conformation to repeat the cycle.

Hsp90 associates with various co-chaperones during protein folding and the specific co-chaperones involved depend on the client protein being activated. Previous studies identified more than 10 co-chaperones of PfHsp90 involved in protein folding (Chua *et al*., 2012). While some of these co-chaperones, such as p23 function as ATP hydrolysis modulators in the functional cycle (Felts *et al*., 2003), others such as Hop) act as adaptors which couple client proteins for recruitment (Figure 1.4; Lyons and Johnson, 1998).

1.6.3 Hsp70-Hsp90 organising protein (Hop)

Hop, also known as Sti1 (Stress inducible protein 1), is a protein that forms part of the foldosome complex formed by the cytosolic Hsp70 and Hsp90 chaperones (Rohl *et al*., 2015). Mechanistically, Hop acts as an adaptor upon which both Hsp70 and Hsp90 dock to facilitate client substrate transfer from Hsp70 for complete folding by Hsp90 (Gitau *et al*., 2012; Zininga *et al*., 2015a). However, it has recently been demonstrated that some Hsp70 and Hsp90 homologs can directly form functional partnerships in the absence of Hop (Sun *et al*., 2019). Furthermore, in prokaryotes, where Hop homologues are absent, the bacterial Hsp70/Hsp90 (DnaK/HtpG) directly form a functional folding partnership (Genest *et al*., 2013; Nakamoto *et al*., 2014). This suggests the possibility of direct Hsp70/Hsp90 co-operation in the absence of Hop.

P. falciparum Hop (PfHop) is approximately 68 kDa in size and is upregulated under stress conditions (Gitau *et al*., 2012; Zininga *et al*., 2015a). The low resolution structure of PfHop has recently been solved via small angle x-ray scattering (SAXS) analysis and the chaperone is reported to exist in the form of elongated homodimers in solution (Makumire *et al*., 2019). PfHop possesses three major tetracopeptide repeat domains (TPR1, TPR2A and TPR2B) and two Pro-Asp dipeptide repeat domains (DP1 and DP2) (Zininga *et al*., 2015a; Figure 1.5).

During client protein folding, PfHsp90, PfHop and PfHsp70-1 form a foldosome complex in which PfHop serves as an adaptor protein that bridges the interaction between PfHsp70-1 and PfHsp90 (Gitau *et al*., 2012; Zininga *et al*., 2015a; Silva *et al*

2019). TPR1 domain binds the EEVD motifs of PfHsp70-1 resulting in conformational changes which facilitate PfHsp90 binding to TPR2A (Figure 1.5; Rohl *et al*., 2015; Zininga *et al*., 2015a). PfHsp90 docks onto the TPR2A domain of PfHop through its MEEVD motif on its C-terminus (Figure 1.5). Upon PfHsp90 binding, PfHsp70-1 then shifts from TPR1 to TPR2B domain resulting in client substrate transfer from PfHsp70-1 to PfHsp90 (Rohl *et al*., 2015; Zininga *et al*., 2015a).

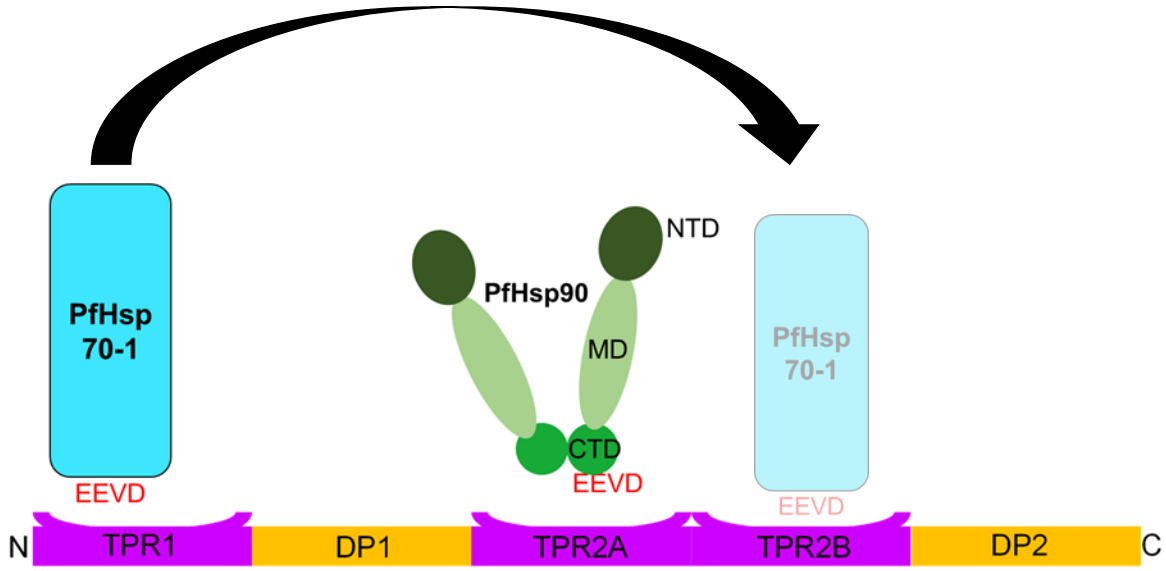

Figure.1.5. PfHop structure

PfHop has 3 TPR domains labelled in purple and 2 DP domains shown in yellow. PfHsp70-1 binds to the TPR-1 domain of Hop through the EEVD motif. PfHsp90 also binds to the TPR2A domain through the EEVD motif to facilitate further protein folding.

1.6.4 Heat shock protein 70

The Hsp70 (DnaK in prokaryotes) family of molecular chaperones is a central hub for the maintenance of proteostasis in cells (Calloni *et al*., 2012). Hsp70s are actively involved in almost every stage of a protein's life course. Thus, Hsp70s facilitate folding of nascent peptides emerging at the ribosomes (Szabo *et al*., 1994), protein trafficking and translocation across membranes (Rosenzweig *et al*., 2017). In addition, Hsp70s facilitate the refolding of misfolded protein (Mattoo *et al*., 2014; Goloubinoff and De Los Rios, 2007) and also channelling misfolded proteins which are beyond repair towards degradation (Kampinga *et al*., 2010; Shiber and Ravid, 2014). Hsp70s are some of the most conserved proteins found in all kingdoms of life (Zhang, 2014).

Furthermore, Hsp70s are ubiquitous, accounting for approximately 1-2% of the cellular proteome (Dhamad *et al*., 2016). Although most Hsp70s are expressed in response to stress, some Hsp70s are constitutively expressed (also referred as heat shock cognate 70, Hsc70) to perform housekeeping roles (Mayer and Kityk 2015; Jacob *et al*., 2017).

Structurally, Hsp70s are generally comprised of two domains; a conserved N-terminal nucleotide binding domain (NBD) and a less conserved C-terminal substrate binding domain (SBD) which are connected by a linker (Figure 1.6). The NBD of Hsp70 is characterised by an 'actin-like' fold composed of 4 lobes denoted as IA, IB, IIA and IIB which form two subdomains (I and II) (Figure 1.6). These in turn form a hydrophilic nucleotide binding cleft at the interface between lobes IB and IIB (Zhuravleva and Gierasch, 2011). The SBD is composed of a two layered twisted β-sandwich (SBDβ) and an α-helical segment (SBDα) (Figure 1.6). The SBDβ is responsible for binding substrates, whilst the SBDα functions as a lid which stabilizes substrate binding (Figure 1.6). The SBD of Hsp70 is functionally promiscuous as it allows for the binding of short degenerate hydrophobic motifs which occur after approximately 30 residues in most proteins within peptide substrates (Rosenzweig *et al.*, 2017). This technically provides Hsp70 with the capability to bind to virtually all proteins.

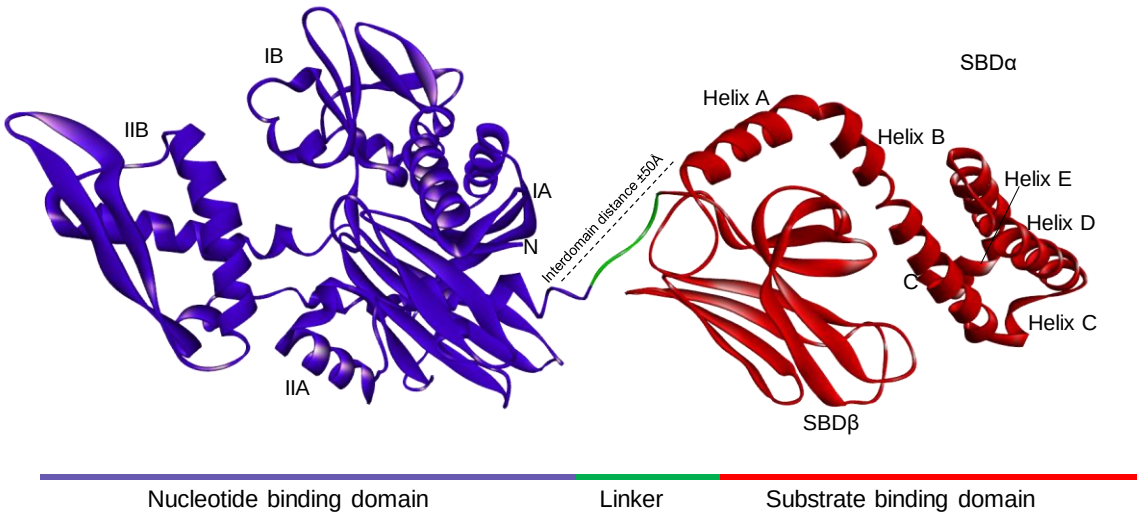

Figure 1.6. Structural organization of Hsp70

The NBD (blue) is comprised of lobes IA, IIA, IB and IIB. The SBD (red) is constituted by SBD-β and SBD-α subunits of which the latter is subdivided into 5 helices A-E. The NBD and SBD are adjoined by a highly conserved linker (green).

The Hsp70 family is generally classified into two main subgroups which include the canonical and non-canonical Hsp70s (Dragovic *et al*., 2006). Canonical Hsp70s structurally resemble *E. coli* Hsp70 (DnaK) while their non-canonical counterparts, the Hsp110s and their ER homologues Glucose regulated protein 170 (Grp170), mostly occur in eukaryotes (Easton *et al*., 2000). Hsp110 occurs in high concentration in mammalian cells and has also been reported to be the third most abundant Hsp after Hsp70 and Hsp90 (Easton *et al*., 2000; Young and Heikkila, 2010). Like their canonical Hsp70 counterparts, members of the Hsp110 subfamily are able to bind misfolding polypeptides and also hydrolyse ATP (Mattoo *et al*., 2013; Zininga *et al*., 2016).

Structurally, Hsp110s are marked by extended acidic insertions located within their SDB-β and SBD-α subunits (Oh *et al*., 1999; Figure 1.7). Additionally, Hsp110s also possess linker segments that are distinct from canonical Hsp70s (Zininga *et al*., 2016; Chakafana *et al*., 2019a). While Hsp110s are predicted to exhibit seven β strands in its SBD, canonical Hsp70s possess eight β strands in the SBD (Figure 1.7). However, the NBDs of both canonical Hsp70s and their Hsp110 counterparts are highly conserved (Figure 1.7; Chakafana *et al*., 2019a). Hsp110s function as 'holdases' and are thus capable of suppressing substrate aggregation (Dragovic *et al*., 2006; Zininga *et al*., 2016; Velasco *et al*., 2019). This is thought to maintain denatured protein substrates in a soluble, folding-competent state for hand over to canonical Hsp70 for folding (Mattoo *et al*., 2014; Mogk *et al*., 2015). In addition to their role as holdases, Hsp110s serve as nucleotide exchange factors (NEFs) of their canonical Hsp70 counterparts (Pollier *et al*., 2008; Garcia *et al*., 2017).

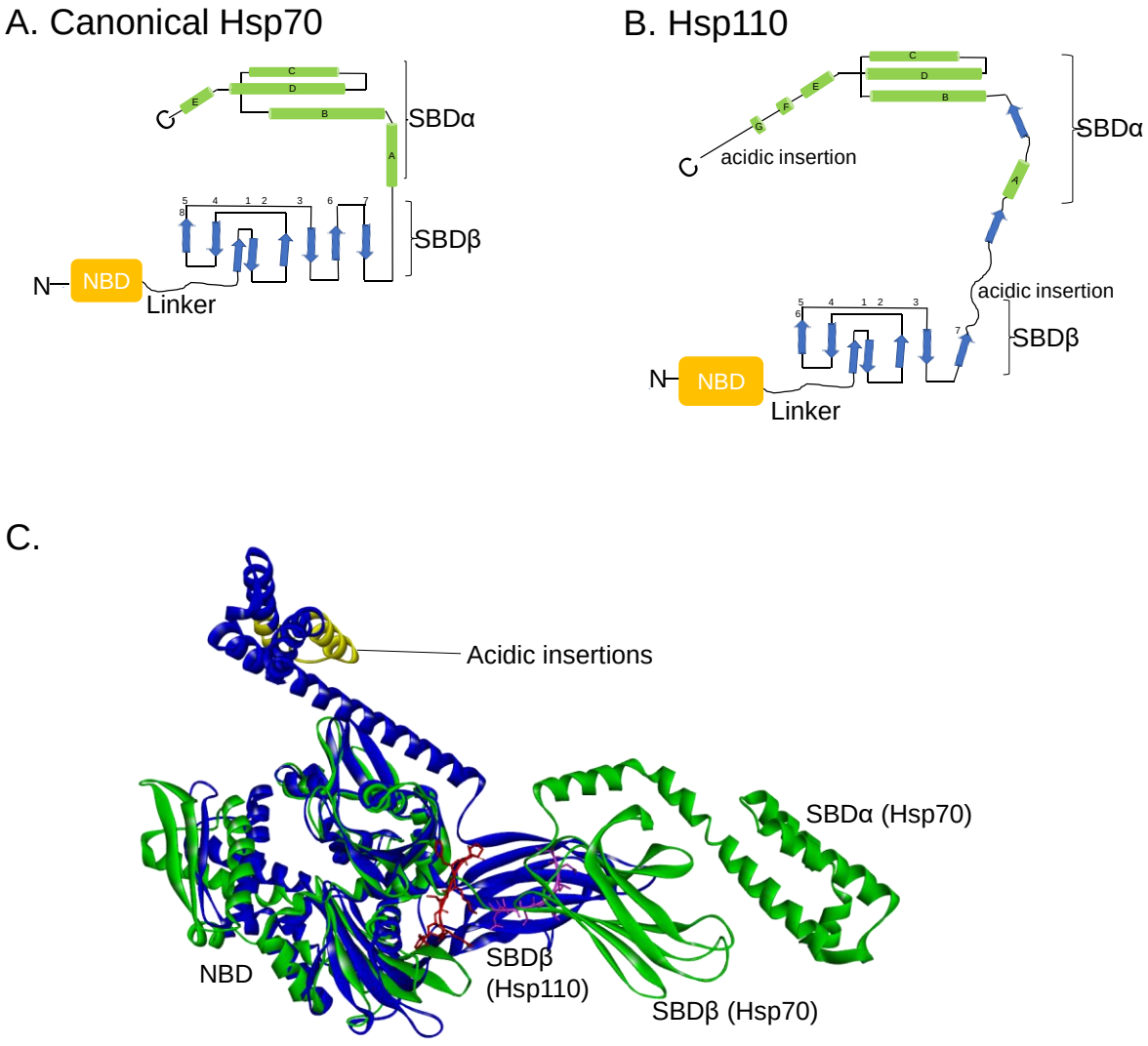

Figure 1.7. Structural comparison of canonical Hsp70s and Hsp110

The schematic represents canonical and non-canonical Hsp70 structures.(A) The SBDα is constituted by helices A-E while SBD_{β} of canonical Hsp70 is composed of 8 sheets. (B) Hsp110s possess insertions in SBDα and towards the lid segment.(C) The three-dimensional model of a canonical Hsp70 (based on template 2KHO; green; Bertelsen *et al*., 2009) was superimposed against that of Hsp110 (based on template 32DF; blue; Pollier *et al*., 2008) whose linker (red) and acidic insertions (yellow) are highlighted (C). Figure adapted from Oh *et al*., 1999.

Despite the high structural conservation of the NBDs from canonical Hsp70s and Hsp110s their SBDs exhibit structural variation (Easton *et al*., 2000; Chakafana *et al*., 2019a). As such, Hsp110s are thought to exhibit unique substrate preferences from canonical Hsp70s (Xu *et al*., 2012). The Hsp70 substrate binding cleft is located within the loops $L_{1,2}$ and $L_{3,4}$ in SBDβ. These loops are thought to be responsible for imparting substrate specificity (Xu *et al*., 2012; Zininga 2016). It is therefore plausible that, variations within these loops potentially account for the varied substrate preferences

between canonical and non-canonical Hsp70 types. It was recently reported that most variations in the SBDs of Hsp70s occur in the loop regions of the substrate binding cleft in addition to the helical lid sections (Chakafana *et al*., 2019a). This suggests that the lid may have additional influence in modulating functional specificity of Hsp70 (Mabate *et al*., 2018).

1.6.4.1 Co-operation of Hsp70 with co-chaperones

In order for Hsp70s to function efficiently, they depend on assistance from functional networks formed with members of several co-chaperones (Figure 1.8). The most common Hsp70 co-chaperones are Hsp40 (Alderson *et al*., 2016), Hsp90 (Genest *et al*., 2018), Hsp100 (Mogk *et al*., 2015), Hsp110 (Andreasson *et al*., 2008) and Hop (Lyons and Johnson, 1998). Protein folding by Hsp70 is tightly controlled by J-domain proteins (Hsp40) and nucleotide exchange factors (NEFs) such as Hsp110 (Pollier *et al*., 2008). Hsp70 members are also known to co-operate with sHsps and Hsp100 to form chaperone systems that facilitate the degradation of misfolded proteins (Mogk *et al*., 2015).

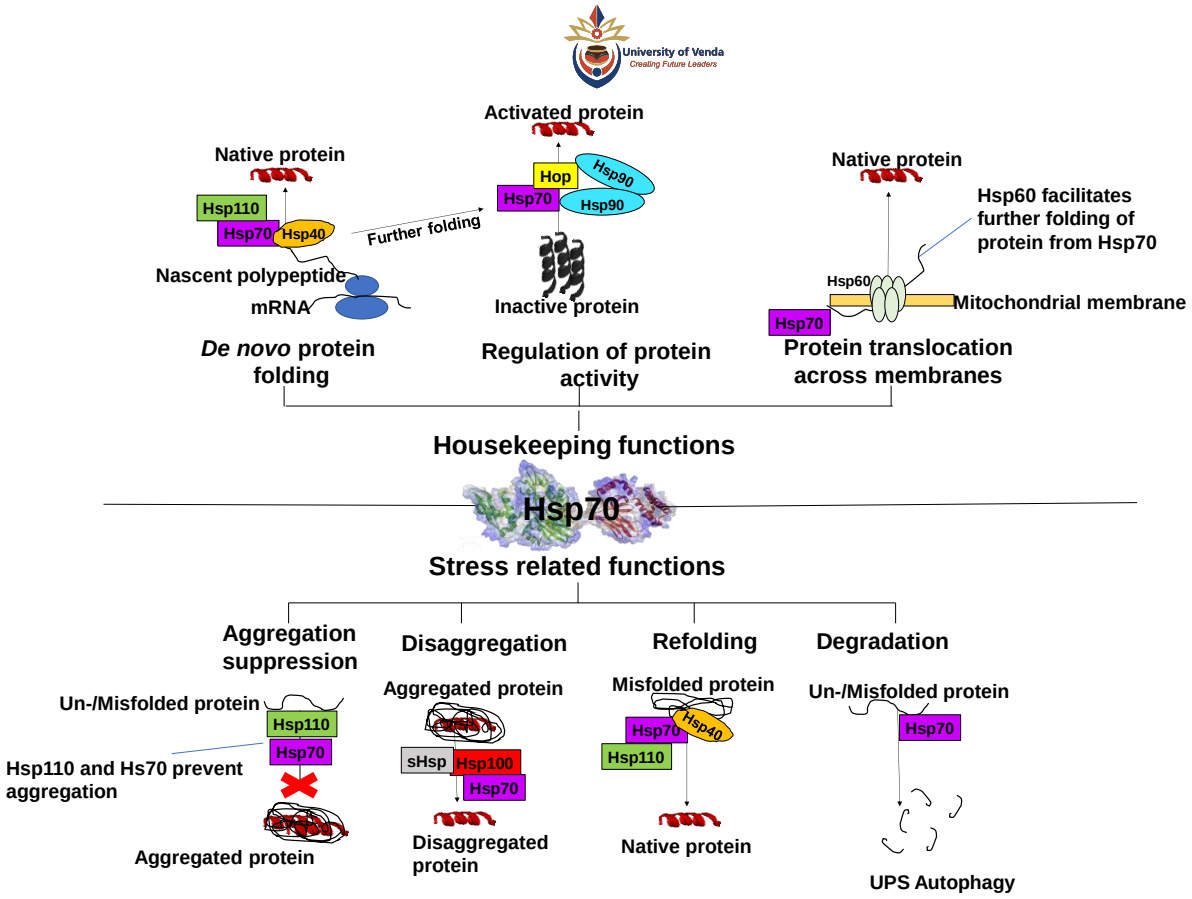

Figure 1.8. Co-operation of Hsp70 with various co-chaperones

In cells, Hsp70s perform both housekeeping and stress response related roles. Hsp70s co-operate with various co-chaperones such as Hsp40 and Hsp110 to facilitate the de novo folding of polypeptides from the ribosome to facilitate their folding into their native conformations (Botha *et al*., 2007). Hsp70s also co-operate with Hsp90 and Hop to activate proteins (Zininga *et al*., 2015). Hsp70s also form partnerships with Hsp60 to facilitate the translocation of proteins across membranes (Yeo *et al*., 2015). Under stress conditions, Hsp70s prevent the formation of aggregates and also facilitate the degradation of misfolded/unfolded proteins.

Hsp70 co-operates with Hsp90 to fold select substrate proteins (Section 1.3.2). In this process, Hsp70 which is bound to a partially folded substrate interacts with Hop via the TPR1 domain and this allows the TPR2A domain of Hop to access Hsp90 (Zininga *et al*., 2015a). The concomitant conformational changes associated with this leads to the migration of Hsp70 from TPR1 domain to the TPR2B domain of Hop (Rohl *et al*., 2015). The transition of Hsp70 to the TPR2B domain is linked to substrate transfer from Hsp70 to Hsp90 for further folding (Rohl *et al*., 2015). In this association, the conformational re-orientation of Hsp70 to allow substrate handover to Hsp90 is nucleotide dependent and dependent on Hsp70 interdomain allostery.

In addition, Hsp70 also associates with NEFs, during protein folding. In eukaryotes, nucleotide exchange function is facilitated by NEFs belonging to the Hsp110/Grp170, Bcl2-associated athanagene (Bag) and heat shock protein binding protein 1 (HspBP1) families (Patury *et al*., 2009; Rosenzweig *et al*., 2017). In prokaryotes, nucleotide exchange is facilitated by GroP-like gene E (GrpE) (Packschies *et al*., 1997). Generally, NEFs facilitate the opening of the nucleotide binding cleft of Hsp70 to allow for ADP release (Brodsky, 2007; Benhke *et al*., 2015). The release of ADP and P_i then allows the rebinding of ATP onto the nucleotide binding cleft and this in turn stimulates substrate release from Hsp70 (Clerico *et al*., 2015; Chen *et al*., 2018). The crystal structure of Hsp70 interaction with Hsp110 revealed that the proteins make contacts via their NBDs which facilitate the association (Pollier *et al*., 2008). The NBD of Hsp110 is thought to make contacts with subdomain IIB of Hsp70 resulting in the opening of the nucleotide binding cleft (Andreasson *et al*., 2008). The opening of the nucleotide binding cleft then lowers the affinity for nucleotide binding at Hsp70's NBD. Furthermore it has been reported that ATP binding is important for Hsp110 to assume a favourable conformation for its interaction with canonical Hsp70 (Dragovic *et al*., 2006).

The interaction of Hsp70 with Hsp40 is important for protein folding. During the interaction of Hsp40 and Hsp70, the HPD motif, located in the J-domain of Hsp40, docks onto the Hsp70 linker binding cleft between the NBD lobes IA and IIA (Jiang *et al*, 2007). The binding of the J-domain on Hsp70 then disrupts the direct association of the NBD and the SBD. This allows the SBD to flip freely allowing it to capture substrates recruited by Hsp40 (Alderson *et al*., 2016). The C-terminal EEVD motif of Hsp70 has also been reported as an additional Hsp40 interaction site (Yu *et al*., 2015). The CTD of Hsp40 is thought to interact through electrostatic interactions with the EEVD motif of Hsp70 (Yu *et al*., 2015).

Generally, protein folding relies on conformational structural changes which occur between the NBD and SBD upon ATP or ADP binding (Mayer *et al*., 2001; Kityk *et al*., 2015). The binding of ATP at the NBD reduces substrate binding affinity at the SBD by 2 to 3 orders of magnitude (Gassler *et al*., 1998). ATP hydrolysis at the NBD is thus

a rate limiting state in the functional cycle of protein folding as it causes the locking of substrates into the substrate binding cavity of Hsp70s. The control of substrate binding or release (at SBD) by nucleotides (at NBD) requires interdomain communication between the NBD and the SBD (Figure 1.9).

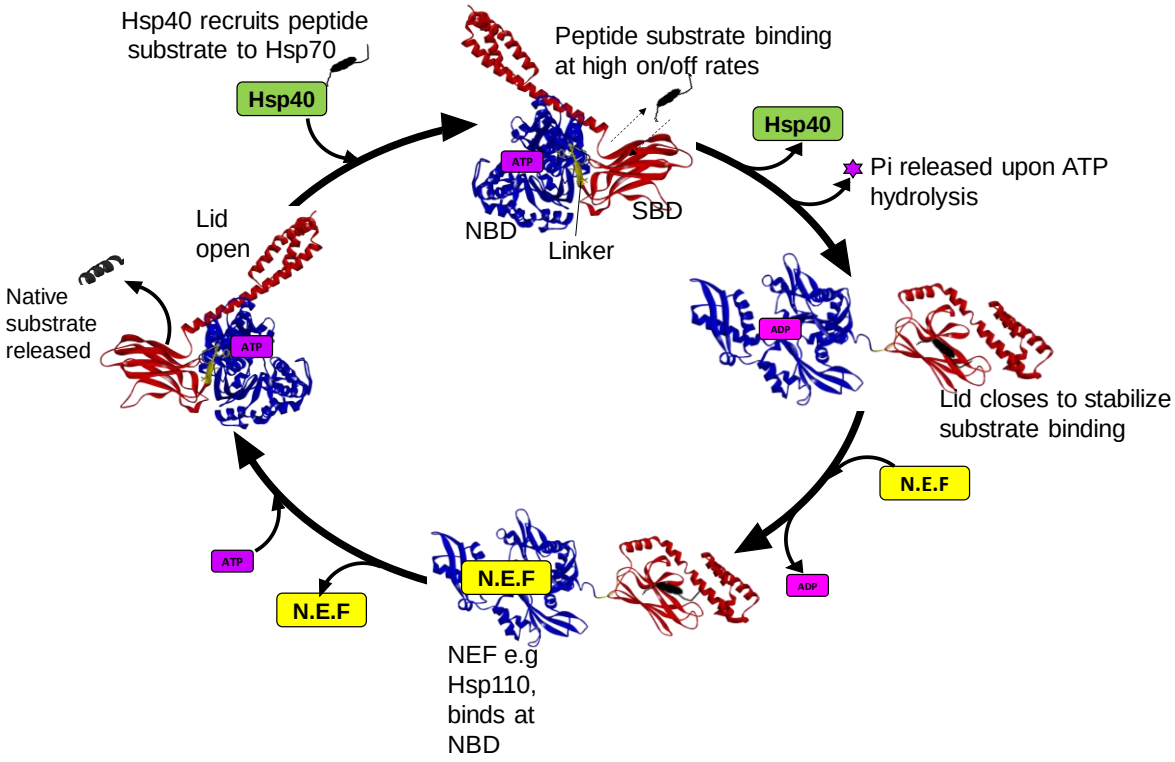

Figure 1.9. Hsp70 functional cycle

The Hsp40 coupled-protein substrate is delivered to the SBD of the ATP-bound Hsp70. ATP is hydrolyzed and Hsp40 is released from the chaperone complex. Upon Hsp70 binding to ADP, its lid closes to tightly clamp the substrate within the SBD. A nucleotide exchange factor (NEF) facilitates the exchange of ADP for ATP. In the Hsp70-ATP conformation, the lid is open, and the chaperone possesses lower affinity for peptide. This results in the release of the peptide substrate from Hsp70. The fully folded protein is subsequently released. (Figure adapted from Chakafana *et al*., 2019b).

1.6.4.2 Allosteric function of Hsp70

Mechanistically, the folding function of canonical Hsp70s is regulated by allostery through nucleotide binding at the N-terminal NBD, which in turn influences affinity for substrate at the SBD (Figure 1.9; English *et al*., 2017). The conformational changes which occur within the NBD on ATP binding are subsequently transmitted to the SBD modulating the substrate binding affinity (Sharma and Masison, 2009; Stetz *et al*.,

2015). Inversely, substrate binding at the SBD also influences ATP hydrolysis on the NBD (Zhuravleva and Gierasch, 2011).

Upon ATP binding, lobe I of the NBD rotates towards lobe II resulting in the closure of the nucleotide binding crevice (Figure 1.10; Liu and Hendrickson, 2007). This results in the opening of the lower lobes IA and IIA, forcing them to make direct contacts with the linker (Zhuravleva and Gierasch, 2011). The SBDα and SBDβ subdomains are then separated from each causing SBDβ to interact with the NBD (Mayer *et al*., 2013). This rearrangement causes the substrate binding pocket to open, thus subsequently leading to approximately 5-50-fold increase in the rate of substrate dissociation at the SBD (Zuiderweg *et al*., 2012). SBDβ then undergoes additional conformational changes that are triggered by SBDβ interaction with the NBD. This causes a shearing movement in the β- sandwich, which causes β8 to relocate from the lower β-sheet to the upper β-sheet thus opening the substrate binding channel (Clerico *et al*., 2015). These events give rise to ATP-induced peptide release from the SBD with concomitant hydrolysis of ATP (Vogel *et al*., 2006; Kumar *et al*., 2011; Kityk *et al*., 2012).

On the other hand, in the ADP-bound state Hsp70 exhibits a high peptide substrate affinity (K_D = 0.1-1 µM) at the SBD, which is coupled with slow on-off rates (Liberek *et al*., 1991; Kampinga and Craig, 2010). The binding of ADP triggers the undocking of SBDβ from the NBD and this is also accompanied by the undocking of the linker from the linker binding cleft (Mayer and Kityk, 2015). As such, in the ADP state, Hsp70s domains are separated from each other by the linker domain (Figure 1.10).

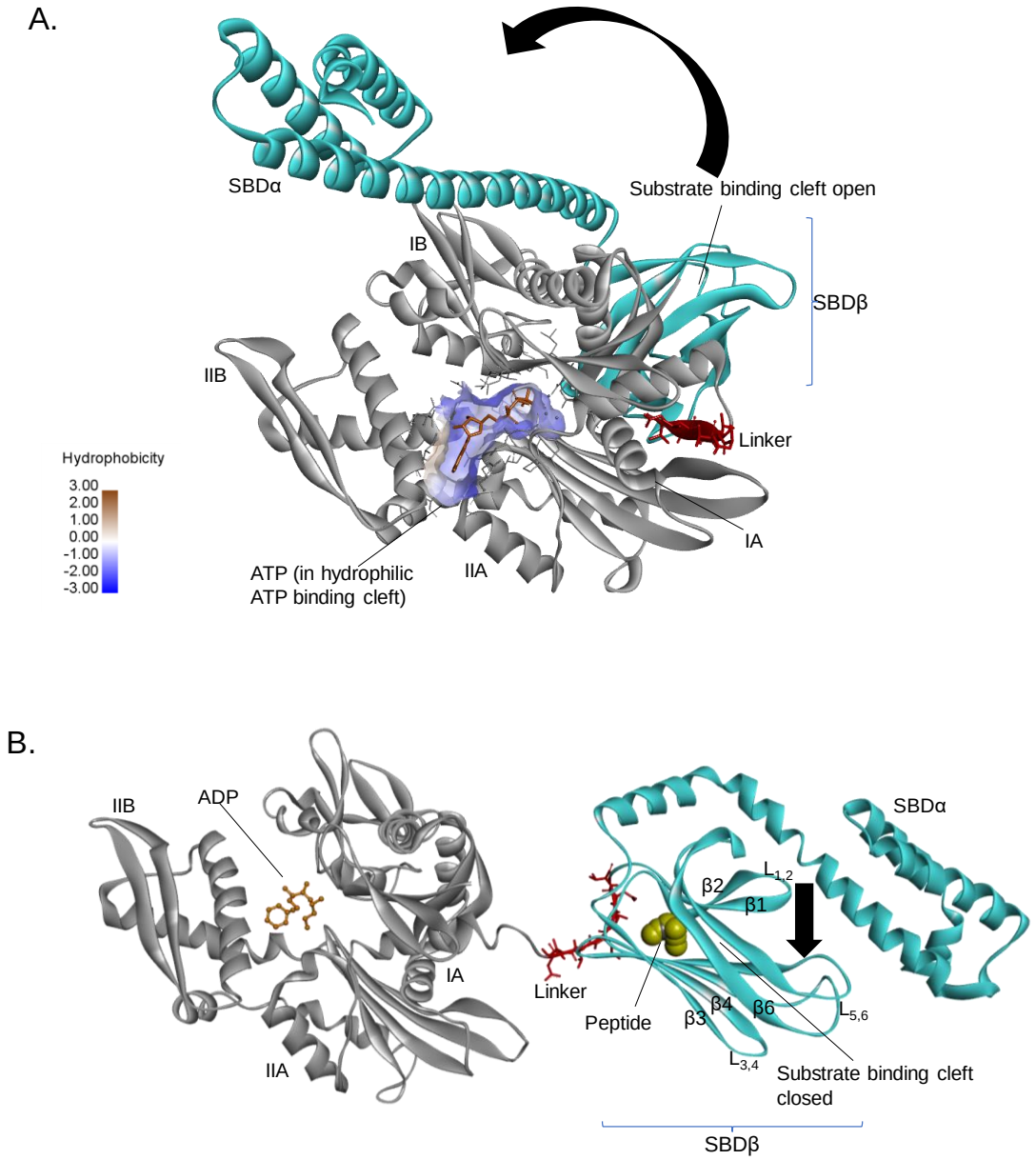

Figure 1.10. Allosteric conformations of canonical Hsp70 during protein folding

(A) ATP binds in the hydrophilic nucleotide binding cleft. In the ATP bound state, Hsp70 assumes an open conformation and exhibits low substrate affinity. (B) ADP induces a closed conformation which has a high substrate binding affinity. In the closed state, SBDα docks over SBDβ as shown by the black arrow.

The substrate binding cleft of Hsp70 is composed of a unique hydrophobic two layered twisted β-sandwich onto which the hydrophobic patches on the peptide substrate bind (Flaherty *et al*., 1990; Kityk *et al*., 2012). Subdomains β1, β3 and β4 of the SBDβ bind onto hydrophobic patches of the substrate that are recognised by Hsp70 (Figure 1.10; Mayer, 2013). The bound substrate backbone is then stabilised by β1 and β2 with further reinforcement from loops $L_{1,2}$; $L_{3,4}$; $L_{4,5}$ and $L_{5,6}$ (Figure 1.10; Kityk *et al*., 2012;

Mayer, 2013). Subsequently, the bound substrate is trapped by the 'closing in' of SBDα when it undergoes conformational changes to associate with SBDβ (Kityk *et al*., 2012; Zhang *et al*., 2014). This ensures substrate binding stabilization through cooperation of the SBDβ-SBDα subdomains (Stetz *et al*., 2015). Although most available Hsp70 structures reveal a single substrate binding site (Bertelsen *et al*., 2009; Qi *et al*., 2013), a novel peptide binding site in Hsp70 has recently been described (Li *et al*., 2019). This novel site denoted as P2, is located in the vicinity of $L_{5,6}$ of the SBD and is thought to be essential for peptide binding (Li *et al*., 2019).

1.6.5 *Plasmodium falciparum* Hsp70s

P. falciparum expresses six Hsp70 members which are located in various subcellular compartments: PfHsp70-1 and PfHsp70-z (cytosol), PfHsp70-2 and PfHsp70-y (ER), PfHsp70-3 (mitochondrium) as well as PfHsp70-x (parasitophorous vacuole/ exported to the infected erythrocyte) (Table 1.2; Shonhai 2007; Kulzer *et al*., 2012; Chen *et al*., 2018). PfHsp70-1, PfHsp70-2 and PfHsp70-3 constitute the canonical Hsp70 isoforms of *P. falciparum*. PfHsp70-z and PfHsp70-y belong to the Hsp110 and Grp170 families, respectively (Shonhai, 2007; Kampinga *et al*., 2009). In *P. falciparum* cells, Hsp70s have manifold roles which include the folding and assembly of nascent polypeptides, refolding of kinetically trapped misfolded and aggregated proteins, membrane translocation of organellar and secretory proteins as well as control of the activity of regulatory proteins (Table 1.2; Shonhai, 2014; Zininga *et al*., 2015b; Chakafana *et al*, 2019a). *P. falciparum* Hsp70s are also implicated in signal transduction and DNA replication (Shonhai *et al*., 2008).

Table 1.2 Characteristic features of *P. falciparum* Hsp70s

PfHsp70 (PlasmoDB accession number)	Size (kDa)	Localization	Functions	References
PfHsp70-1 (PF3D7_0818900)	74	nucleus and cytosol	protein folding/ translocation/ aggregation suppression	Misra and Ramachandran, 2009 Shonhai *et al*., 2007 Matambo *et al*., 2004
PfHsp70-z (PF3D7_0708800)	100	cytosol	predicted NEF of PfHsp70-1; aggregation suppression	Muralidharan *et al*., 2012 Zininga *et al*., 2016
PfHsp70-2 (PF3D7_0917900)	73	ER	protein import and folding in the ER, retrograde translocation of proteins for degradation	Chen *et al*., 2018 Kumar et al., 1991
PfHsp70-y (PF3D7_1344200)	108	ER	thought to be NEF for PfHsp70-2	Njunge *et al*., 2013, Kudyba *et al*., 2019
PfHsp70-3 (PF3D7_1134000)	73	mitochondrium	protein translocation into the mitochondria	Sargeant *et al*., 2006
PfHsp70-x (PF3D7_0831700)	76	PV and exported to parasite infected erythrocyte, J dots	protein export and subsequent protein folding of exported proteins in the infected erythrocytes	Kulzer *et al*., 2012 Charnaud *et al*., 2017 Cobb *et al.,* 2017 Day *et al*., 2019

1.6.5.1 Cytosolic Hsp70s of *P. falciparum*

The cytosol localised parasite proteins, PfHsp70-1 and PfHsp70-z play important roles in maintaining cellular proteostasis. PfHsp70-1 is a stress inducible canonical Hsp70 which is expressed at all stages of the parasites' life cycle (Acharya *et al*., 2007; Shonhai *et al*., 2007). Furthermore, PfHsp70-1 is induced and translocated from the cytosol to the nucleus upon heat-shock at 41 °C (Acharya *et al*., 2007). Structurally, PfHsp70-1 is characterised by the same domain architecture for canonical Hsp70s (Figure 1.11). PfHsp70-1 possesses an electronegative C-terminal EEVD motif which facilitates its interaction with PfHop to form a foldosome (Figure 1.5; Zininga *et al*., 2015a). The C-terminal TVEEVD motif of the *S. cerevisiae* canonical Hsp70, Ssa1, has recently been reported to function as a SUMO-interacting motif (Gong *et al*., 2018). It is plausible that PfHsp70-1 may also be involved in SUMOylation, since it possess the conserved EEVD motif. SUMOylation is essential for normal cell function and a potential target of small molecule inhibitors against *P. falciparum* (Reiter and Matunis 2016). PfHsp70-1 also possess a distinct set of GGMP repeat motifs positioned towards its C-terminal in the lid segment. In *Toxoplasma gondii*, the GGMP repeat motif of Hsp70 was reported to be associated with parasite virulence (Lyons and Johnson 1998). This possibly implicates the GGMP motif of PfHsp70-1 in parasite virulence.

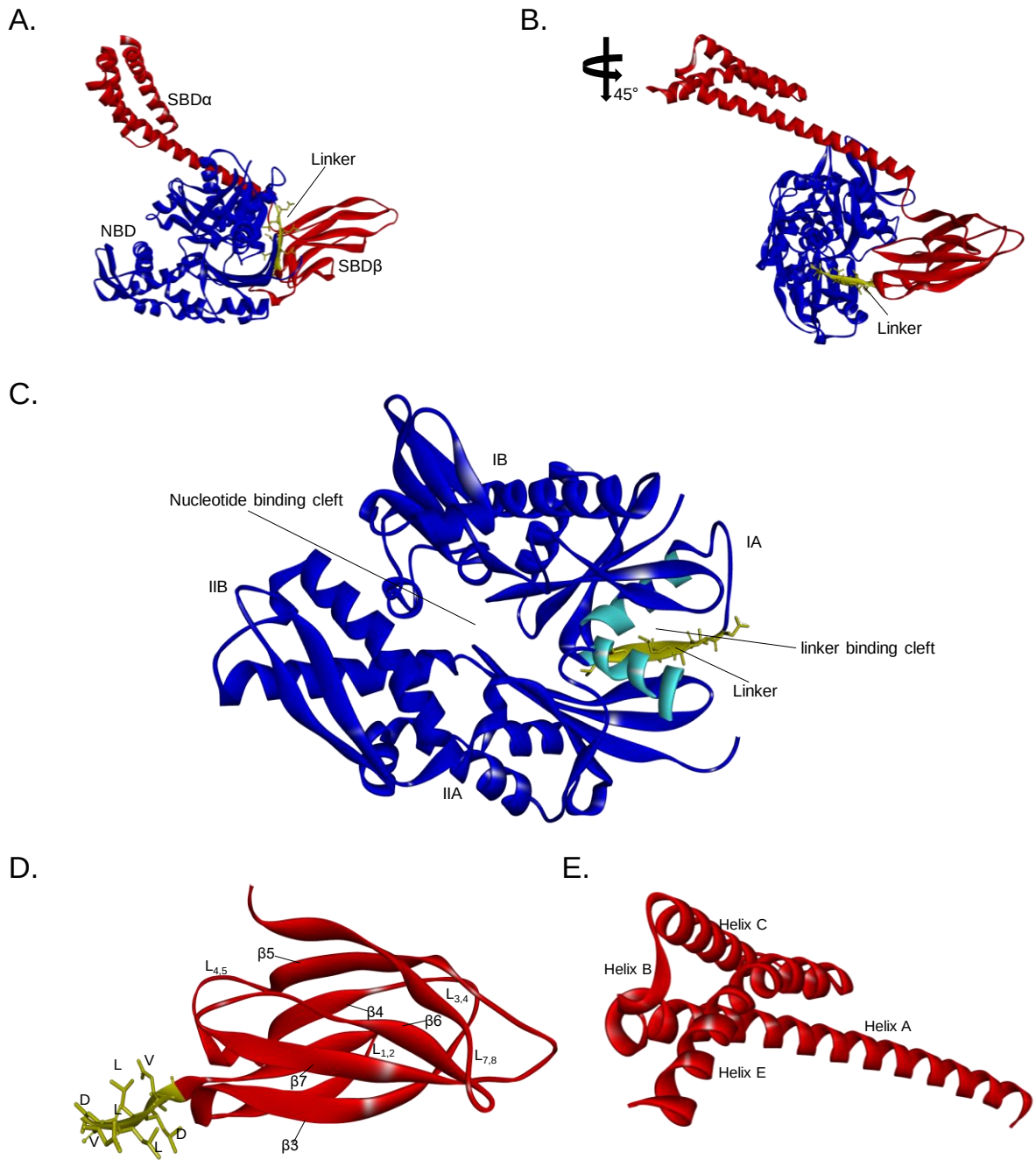

Figure 1.11. Structural organization of PfHsp70-1

(A) PfHsp70-1 possesses an NBD (blue) and an SBD (red) adjoined by a linker (yellow). (B) The position of the linker is shown between NBD and SBDβ. (C) The NBD of PfHsp70-1 and the linker docked on the linker binding cleft. (D) The SDBβ and linker motif delineated by the residues DLLLLDV. (E) The SBDα (lid) of PfHsp70-1 with helices A-E.

PfHsp70-1 is thought to confer cytoprotection to the parasite as evidenced by an *in cellulo* study conducted using *E. coli* with a functionally compromised DnaK (Shonhai, 2005). Using the recombinant form of PfHsp70-1, the C-terminal domain was shown to stabilize the overall conformation of the protein (Misra and Ramachandran, 2009). This may partly explain the reported thermostability of PfHsp70-1 (Gitau *et al*., 2012; Zininga *et al*., 2016). Furthermore, PfHsp70-1 is thought to be essential for parasite survival as inhibition of PfHsp70-1 has been shown to result in parasite death implying that the chaperone may pose as a potential drug target (Chiang *et al*., 2009).

PfHsp70-z is a member of the Hsp110 protein family that exhibits thermal resilience (Shonhai *et al*., 2007; Zininga *et al*., 2016). Based on *in vitro* studies, PfHsp70-z has been shown to exhibit holdase function, supressing the heat induced aggregation of model substrates (Zininga *et al*., 2016). Structurally, PfHsp70-z is characterised by an N-terminal NBD of approximately 45 kDa, which exhibits ATPase activity, as well as a C-terminus SBD of approximately 55 kDa. The NBD of PfHsp70-z is highly conserved while the C-terminal substrate binding domain (SBD) is less conserved. These two domains are connected to each other by a unique linker fragment defined by the amino acids ^{421}EYECVEK^{427} (Figure1.12). PfHsp70-z possesses a unique SBD that has extra acidic insertions in its SBDα as well as a recently described highly charged 18meric EKEK motif on position ^{810}EKEK--K^{827} (Chakafana *et al*., 2019a). This motif could potentially facilitate electrostatic interactions between PfHsp70-z and its functional partners. It may also influence the stability of the molecule, since C-terminal segments of Hsp70 have previously been reported to confer stability (Misra and Ramachandran 2009; Mabate *et al*. 2018).

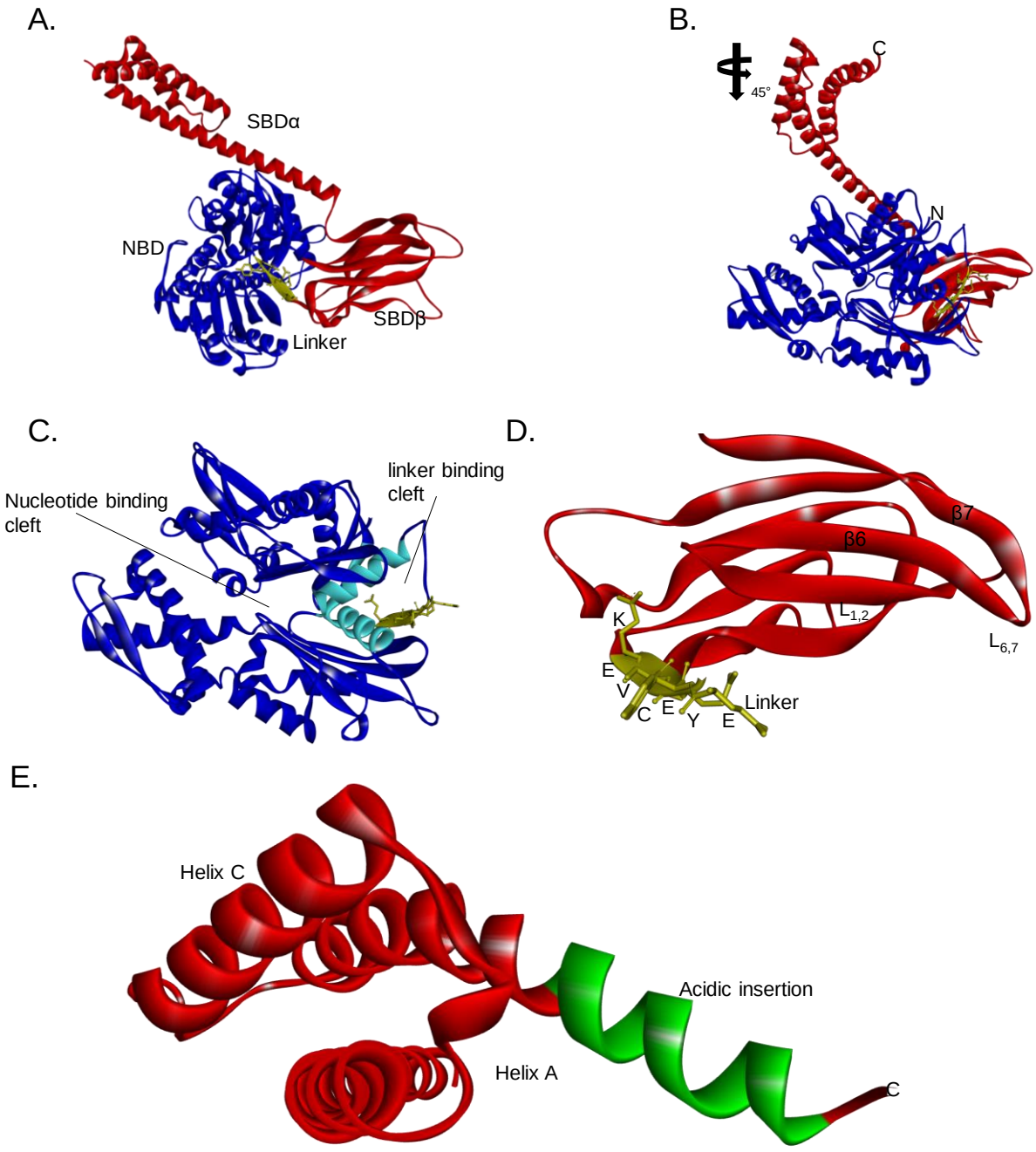

Figure1.12. The structural domains of PfHsp70-z

(A) PfHsp70-z possesses an NBD (blue) and an SBD (red) adjoined by a linker (yellow). (B) The structure of PfHsp70-z rotated at 45° to show the position of the linker between the NBD and SBDβ. (C) The NBD of PfHsp70-z and the linker (yellow) docked on the linker binding cleft (light blue). (D) The SDBβ and linker motif delineated by the residues EYECVEK. (E) The SBDα (lid) of PfHsp70-z showing helices A and E as well as the acidic insertions (green) towards the C-terminal.

Previously, PfHsp70-z has been proposed to function as a nucleotide exchange factor (NEF) for PfHsp70-1 during protein folding (Shonhai *et al*., 2007; Zininga *et al*., 2015b; Zininga *et al*., 2016). PfHsp70-z is an essential protein in parasite survival as knockout of the PfHsp70-z gene has been shown to result in parasite death (Muralidharan *et al*., 2012). PfHsp70-z is thought to prevent the aggregation of asparagine rich proteins of the parasite under stress conditions (Muralidharan *et al*., 2012). Furthermore, PfHsp70-z is a heat stable molecule which is thought to play an important role in cytoprotection of malaria parasites during febrile conditions in the human host (Zininga *et al*., 2016).

Although both PfHsp70-1 and PfHsp70-z possess some overlapping functions such as aggregation suppression, PfHsp70-z has been demonstrated to be more effective at inhibiting protein aggregation than PfHsp70-1 (Zininga *et al*., 2016). Furthermore, unlike its canonical Hsp70 (PfHsp70-1) isoform, PfHsp70-z function has been shown to be independent of nucleotides (Zininga *et al*., 2016). As such, PfHsp70-z is thought to act as a buffer against misfolding of the aggregation-prone asparagine-rich proteins of the malaria parasite. This implies that structural variations in the signature motifs of these proteins may account for the functional specializations.

1.7 The linkers of Hsps

Linkers are short peptide sequences (2-13 residues in length) that connect two protein domains (Ruiz *et al*., 2016). In most proteins, linkers either serve as covalent connectors between domains or alternatively as regulators of cooperative function of the domains (Gokhale and Khosla, 2000). Generally, linkers can be classified as flexible or rigid based on their amino acid composition (Chen *et al*., 2013). In protein structures, linker flexibility or rigidity is an important feature which can modulate functional specialization (Chen *et al*., 2013). While flexible linkers are thought to be important when adjoined domains require a certain degree of movement to allow for their interaction, (Chichili *et al*., 2013) rigid linkers mostly act as tethers or 'molecular rulers' which provide spatial separation of the domains (Wriggers *et al*., 2005). Linker

flexibility is determined by the rotational freedom of the individual amino acid moieties which constitute the linker segment (Chichili *et al*., 2013).

It has previously been reported that flexible linkers are typically constituted of small/polar residues which provide stability due to their capability to form hydrogen bonds with water (Chen *et al*., 2013). Rigid linkers, however, often contain proline residues where the presence of a cyclic side chain restricts movements and lack of an amide group also prevents hydrogen bonding with joined domains (Chen *et al*., 2013). Previously, the charged PfHsp90 linker has been demonstrated to direct various functional properties of the protein which include ATPase activity and *in vivo* chaperone function (Tsutsumi *et al*., 2012). In addition, the PfHsp90 linker was shown to enhance the overall flexibility of Hsp90 to facilitate domain rearrangements and subsequently, protein function. In another study, the charged linker of the *S. cerevisiae* Hsp90 (Hsp82) was demonstrated to be a dispensable motif (Shiau *et al*., 2006). These studies suggest that linkers differentially modulate protein function.

Canonical Hsp70s generally possess conserved linkers, while Hsp110s are marked by unique linker motifs. While the allosteric role of the linker of canonical Hsp70s have previously been proposed in DnaK and Hsc70 (Swain *et al*., 2007; Zhuravlvela and Gierasch, 2011; English *et al*., 2017), the other functional specifications which the linker potentially regulates in canonical Hsp70 are unknown. In view of the fact that PfHsp70-1 and PfHsp70-z are marked by unique linker motifs, it is important to explore the role of this motif in modulating the structure and functions of the respective proteins.

1.8 Problem Statement, Aim and Objectives

1.8.1 Problem Statement

The Hsp70 family of molecular chaperones are important for the survival and pathogenicity of the main agent of malaria, *P. falciparum*. In *P. falciparum*, Hsp70s play central roles in maintaining cellular proteostasis. Structurally, Hsp70s are characterised by a nucleotide binding domain (NBD) which exhibits ATPase activity and a substrate binding domain (SBD). These two domains are connected by a linker motif. Hsp70s form two main subgroups, canonical Hsp70 and the enlarged relatives Hsp110s. Canonical Hsp70 members suppress protein misfolding and are also capable of refolding misfolded proteins. Hsp110 members are characterised by an extended lid segment and their function tends to be largely restricted to suppression of protein aggregation. In addition, the latter serve as nucleotide exchange factors (NEFs) of canonical Hsp70s. The cytosolic Hsp70s from *P. falciparum*, PfHsp70-1 and PfHsp70-z are essential chaperones (Chiang *et al*., 2009; Muralidharan *et al*., 2012). The distinct functions of these two groups of Hsp70s are thought to be defined at least in part by their respective signature motifs. Notably, the linkers of the plasmodial Hsp110, PfHsp70-z, exhibits less conservation across species as compared to that of the canonical PfHsp70-1 chaperone. The linker could thus potentially define structural and functional features of the two proteins. Therefore, the current study explored the role of the unique linker segments of both the canonical Hsp70 and Hsp110 of *P. falciparum* in their structural and functional specialisation.

1.8.2 Study Aim

To characterize the roles of the linker motifs of PfHsp70-1 and PfHsp70-z on the structure and function of the proteins.

1.8.3 Objectives

The objectives of this study were as follows:

1. Predict the structural features of linker substitution mutants of PfHsp70-1, PfHsp70-z and DnaK using bioinformatics

Experimental approaches

(i) Multiple sequence alignments were used to determine the level of conservation between the linkers of PfHsp70-1/DnaK with other canonical Hsp70s as well as in the linkers of PfHsp70-z with other Hsp110s.

(ii) Three dimensional protein structure models of wild type PfHsp70-1, PfHsp70-z, DnaK and their respective linker substitution mutants were generated and compared using Biovia™ Discovery Studio Visualizer software (Dassault Systèmes BIOVIA, San Diego, USA) and Chimera (Pettersen *et al*., 2004).

(iii) STRING analysis was used to predict interaction partners of PfHsp70-1 and PfHsp70-z.

2. Characterize the secondary and tertiary structural organization of linker substitution mutants of PfHsp70-1, PfHsp70-z and DnaK

Experimental approaches

(i) The recombinant forms of PfHsp70-1, PfHsp70-z, DnaK and their linker substitution mutants were expressed in *E. coli* and purified using nickel affinity chromatography.

(ii) The secondary structures of the linker substitution mutants of PfHsp70-1, PfHsp70-z, DnaK were determined via far-UV circular dichroism (CD) spectroscopy analysis.

(iii) Tertiary structural conformation of the recombinant linker substitution mutants of PfHsp70-1, PfHsp70-z and DnaK was analysed by intrinsic (tryptophan) and extrinsic (1-Anilino-8-Naphthalene Sulfonate, ANS) fluorescence spectroscopy.

3. Determine the role of the linkers of PfHsp70-1, DnaK and PfHsp70-z in modulating the chaperone functions of the proteins

Experimental approaches

(i) Surface plasmon resonance (SPR) analysis was used to determine the nucleotide binding affinity of the recombinant linker substitution mutants of PfHsp70-1, PfHsp70-z and DnaK.

(ii) The ATPase activity of the recombinant linker substitution mutants of PfHsp70-1, PfHsp70-z and DnaK was determined using colorimetric ATP hydrolysis activity assays.

(ii) The peptide binding affinity of the recombinant linker substitution mutants of PfHsp70-1, PfHsp70-z and DnaK was determined in the presence and absence of nucleotides via SPR analysis.

(iv) Malate dehydrogenase and luciferase aggregation suppression activity assays were conducted to determine the suppression of heat induced aggregation by the linker substitution mutants.

(v) The refolding capability of the linker substitution mutants relative to their wild type versions was investigated by conducting luciferase refolding assays.

4. Explore the role of the linkers of PfHsp70-z, PfHsp70-1 and DnaK in modulating interactions of the respective proteins with select co-chaperones

Experimental approaches

(i) The protein-protein interaction kinetics of the linker substitution mutant of PfHsp70-1 with its respective co-chaperones, PfHop, PfHsp40 and PfHsp70-z were evaluated using SPR and ELISA .

(ii) SPR and ELISA were also used to investigate the interaction of the linker substitution mutant of PfHsp70-z with its respective co-chaperone PfHsp70-1.

(iii) The self-association interaction kinetics of PfHsp70-1, PfHsp70-z and DnaK were also analysed using SPR and ELISA.

5. Investigate of the effect of the PfHsp70-z linker insertion on DnaK *in cellulo* function

Experimental approach

(i) Complementation assays to investigate the effect of the PfHsp70-z linker on DnaK *in cellulo* function

CHAPTER 2

Bioinformatics analysis of the linker motifs of PfHsp70-z, PfHsp70-1 and DnaK

2.1 Introduction

Homology modelling is an important tool for predicting protein structure. Such analyses are especially useful in cases where the crystal structure data is unavailable. In view of the fact that the crystal structures of PfHsp70-1 and PfHsp70-z are yet to be solved, homology modelling provides important insights on the structural features of these proteins. Several three-dimensional viewing software such as Chimera (Pettersen *et al*., 2004) and Biovia™ Discovery Studio Visualizer (Dassault Systèmes BIOVIA, San Diego, USA) are appropriate for modelling and rendering three-dimensional images of proteins. Features that includes protein hydrophobicity level, formation of ionic contacts as well as hydrogen bonds can be deciphered this way. The Hsp70 linker motif is located at the interface of the NBD and SBD (Figure 1.6). It is therefore possible that the biochemical features of this motif may potentially influence overall Hsp70 structure and function. For example, the hydrophobic composition of linker segments is thought to regulate overall protein fold and function (Agros, 1991; Chichili *et al*., 2013).

Sequence analysis tools such as JALVIEW (Waterhouse *et al*., 2009) and MAFFT (https://mafft.cbrc.jp/alignment/server/index.html) are used for the comparative analysis of amino acid sequences of proteins. Comparative multiple sequence analyses can form a basis for the identification of functional features in protein structures. The amino acid composition of linker motifs is an important determinant for flexibility or rigidity (Gokhale *et al*., 2012). Flexible linkers are typically constituted by small/non-polar residues whose small sizes provide stability due to formation of hydrogen bonds with water (Chen *et al*., 2013). On the other hand, rigid linkers may contain residues with cyclic side chains that restrict movements between adjoined domains (Chen *et al*., 2013). Restricted or more enhanced allosteric communication between protein domains may potentially alter the functional specifications of a protein (Tsutsumi *et al*., 2012). In the current study, bioinformatics tools were used to predict and analyse the effects of swapping linker motifs of canonical Hsp70s (PfHsp70-1/DnaK) and Hsp110. Comparative *in silico* analysis of the linker domain swap mutants were also conducted to predict the impact of the linkers on overall protein structure.

The objectives of this study were to:

(i) design linker swap (LS) chimeric mutants of PfHsp70-z, PfHsp70-1 and DnaK *in silico*;

(ii) investigate the possible functional and structural changes upon introducing linker motifs of a non-canonical Hsp70 (PfHsp70-z) into canonical Hsp70s (PfHsp70-1/ DnaK);

(ii) identify the allosteric hotspots of PfHsp70-1 and PfHsp70-z.

2.2 Experimental Procedures

2.2.1 Multiple sequence analysis of Hsp70s

Multiple sequence alignments were conducted to determine the level of conservation of the linkers of canonical Hsp70 homologues and those from Hsp110 homologues. Initially, the amino acid sequence of PfHsp70-1 (PDB accession #: PF3D7_0818900), which represents a canonical Hsp70, was retrieved from the PlasmoDB database (www.PlasmoDB.org). The retrieved sequence was then aligned to approximately 500 sequences of other Hsp70 homologues using MAFFT database (https://mafft.cbrc.jp/alignment/server/index.html) and JALVIEW software (Waterhouse *et al*., 2009). In JALVIEW, the percentage residue conservation in the respective linkers were also calculated using the 'autocalculated annotation' tool. The amino acid sequence of PfHsp70-z (PlasmoDB accession # PF3D77_0708800) was also retrieved in a similar manner from PlasmoDB and aligned with 500 other homologues in MAFFT database (https://mafft.cbrc.jp/alignment/server/index.html) and JALVIEW software (Waterhouse *et al*., 2009).

2.2.2 Design of linker substitution mutants of PfHsp70-1, PfHsp70-z and DnaK

Linker mutant versions of PfHsp70-1, PfHsp70-z and DnaK, denoted as PfHsp70-1_{LS}, PfHsp70-z_{LS} and $DnaK_{LS}$, were designed by swapping the linker residues of PfHsp70-1/DnaK with those of PfHsp70-z (Figure 2.1). PfHsp70-1_{LS} and $DnaK_{LS}$ were created by replacing the linker residues ^{388}DVLLLDV^{394} of PfHsp70-1 and ^{403}DLLLLDV^{409} of DnaK with the PfHsp70-z linker residues EYECVEK (Figure 2.1). PfHsp70-z_{LS} was created by replacement of the linker ^{421}EYECVEK^{427} residues of PfHsp70-z with the PfHsp70-1 linker residues to ^{421}DVLLLDV^{427} (Figure 2.1).

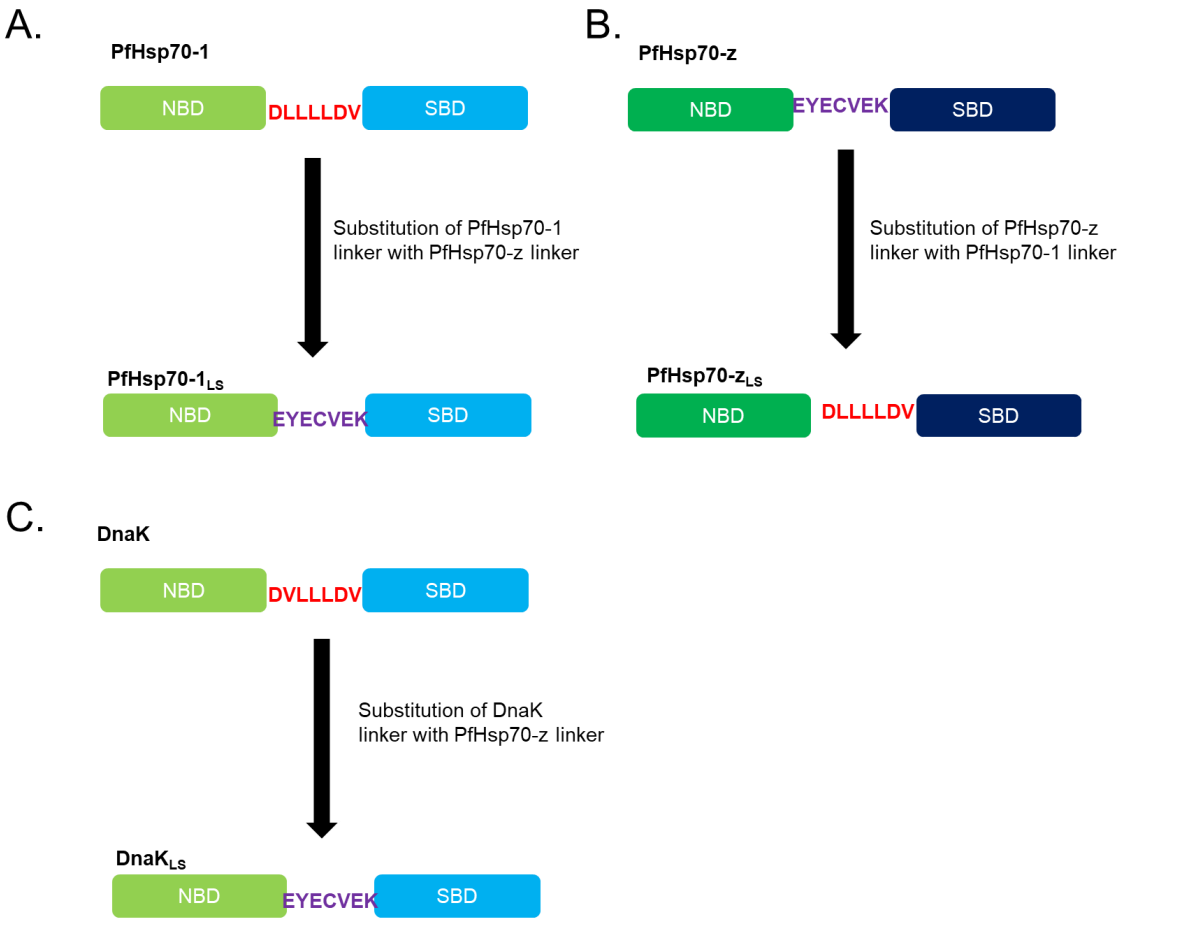

Figure 2.1. Design of linker mutants

(A) PfHsp70-1$_{LS}$ was designed by substitution of the linker residues ^{388}DVLLLDV^{394} with the residues EYECVEK from PfHsp70-z. (B) PfHsp70-z$_{LS}$ was constructed by replacement of the linker residues ^{421}EYECVEK^{427} with the PfHsp70-1 linker residues DVLLLDV. (C) DnaK$_{LS}$ was created by replacing the linker residues ^{403}DLLLLDV^{409}, with the PfHsp70-z linker residues EYECVEK. (D) Sequence alignments to show new linker residues in respective proteins. Replaced residues in PfHsp70-1 are shown in red, DnaK residues in blue and PfHsp70-z in green.

2.2.3 Comparative analysis of three-dimensional models of PfHsp70-1, PfHsp70-z, DnaK relative to their linker mutants

The secondary structures and three dimensional models of the wild type and linker mutant versions of canonical Hsp70s (PfHsp70-1 and DnaK) and the Hsp110 (PfHsp70-z), were generated by depositing the respective amino acid sequences on the online tool PHYRE^2 (http://www.sbg.bio.ic.ac.uk/phyre2; Kelly *et al*., 2015). In order to evaluate structural variations induced by the linker mutations, the predicted secondary structures of the wild type proteins were compared to those of their linker mutants. Additionally, the three-dimensional models of the respective proteins were retrieved from PHYRE^2 as PDB files. The three-dimensional models were visualised using Chimera version 1.9 (Pettersen *et al*., 2004). The three-dimensional models of wild type proteins and their respective linker mutants were compared using the SuperPose tool (http://wishart.biology.ualberta.ca/Superpose/; Maiti *et al*., 2004). In SuperPose, the superimposed proteins are scored based on structural similarities using root mean square deviation (RMSD) statistics. The intra protein contact site distances were measured using Chimera (Pettersen *et al*., 2004). The biochemical features (hydrophobicity, charges and hydrogen bonding) of the linker segments of each protein were determined using Biovia Discovery Studio (Dassault Systèmes BIOVIA, San Diego, USA).

2.2.5 Comparative analysis of predicted interactomes of PfHsp70-1 and PfHsp70-z

The interactomes of PfHsp70-1 and PfHsp70-z were retrieved from the STRING 10.5 database (http://string-db.org/, Szklarczyk *et al.,* 2017). STRING functions as a meta-database which collects and integrates data from various sources such as text mining, experiments, co-expression and gene neighbourhood to predict likelihood for association (Jensen *et al*., 2009; Szklarczyk *et al.,* 2017). In total, fifty interacting partners for each protein were selected at a high confidence score of 0.7. The confidence score gives an estimated measure of the likelihood that the interaction is biologically meaningful and a score of 1 is assigned as the highest confidence score (Szklarczyk *et al.,* 2017). Upon identification of the specific interaction partners, the

proteins were then manually screened based on subcellular localization. This was done in order to filter only proteins which are localized within the same cell compartment as PfHsp70-z and PfHsp70-1 to make biologically valid predictions. Both PfHsp70-1 and PfHsp70-z localize in the cytosol (Shonhai *et al*., 2007; Muralidharan *et al*., 2012) and therefore, only interacting partners predicted to localize in the cytosol were considered. The network partners were then grouped according to both known and predicted functions using data obtained from PlasmoDB (http://plasmodb.org/plasmo/).

2.3 Results

2.3.1 Linker residues of Hsp110 members are distinct from those of canonical Hsp70s

Multiple sequence alignments were conducted to determine the degree of conservation of residues that constitute linkers of canonical Hsp70s and Hsp110s. Initially, alignments were conducted for the six *P. falciparum* Hsp70s in order to establish linker conservation levels within the parasite. Notably, linkers of *P. falciparum* Hsp70s exhibited high conservation across the canonical Hsp70 members while the Grp170 (PfHsp70-y) and Hsp110 (PfHsp70-z) members possessed distinct linkers (Figure 2.2 A). However, it was noted that, across the six *P. falciparum* Hsp70s, there was high conservation (83%) in the aspartate residues D^{403} and D^{408} (numbering based on PfHsp70-1) (Figure 2.2 A). In contrast, PfHsp70-z possesses glutamate (E) residues in the same positions (Figure 2.2 A). This substitution is conserved as both aspartate (D) and glutamate (E) are polar, negatively charged and hydrophilic in nature (Appendix B, Table 1).

Multiple sequence alignment of 500 canonical Hsp70s revealed that the linker residues of these proteins are highly conserved as previously documented (Kityk *et al*., 2018; Chakafana *et al*., 2019b; Figure 2.2 B). Canonical Hsp70s possessed high conservation in the C-terminal residues ^{390}LLDV^{394} (numbering based on PfHsp70-1) of their respective linkers (Figure 2.2 A,B). In view of the fact that the Grp170 and Hsp110 members of *P. falciparum*, (PfHsp70-y and PfHsp70-z) lack these residues (Figure 2.2 A) it suggests that the conserved -LLDV- residues that characterise canonical Hsp70s are important for functional specificity.

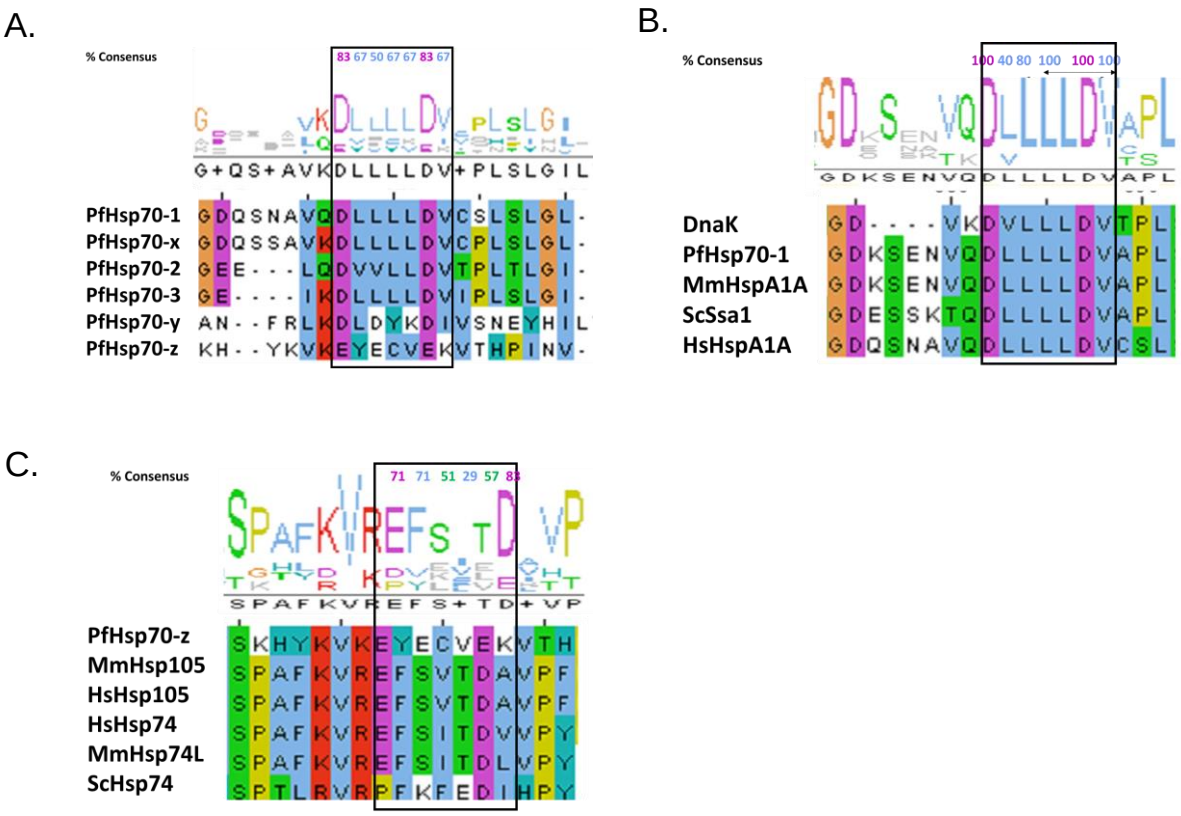

Figure 2.2. Sequence conservation in linkers of *P. falciparum* Hsp70s
Sequence alignments of PfHsp70s were analysed using JALVIEW to determine residue conservation. The sequences shown are representatives from 500 sequences retrieved and analysed via JALVIEW. (A) Representative multiple sequence analysis of linkers the *P. falciparum* Hsp70 and Hsp110s. (B) representative sequence alignments of canonical Hsp70 linkers from 500 sequences using JALVIEW. MmHspA1A, HsHspA1A and ScSsa1 represent Hsp70 homologues from mouse, human and yeast respectively. (C) Multiple sequence analysis of Hsp110s. MmHsp105,HsHsp74, ScHsp74 represent Hsp110 homologues from mouse, human and yeast species. Full length sequences in Appendix B 4 and B5.

The linkers of Hsp110s were, however, shown to exhibit low sequence conservation across 193 various species (Figure 2.2 C). In addition, it was also observed that the linker residues from Hsp110 generally fell into three specific clades, denoted by the linker residues -EYECVE/IK- (plasmodial), -PFKFEDI- (yeast) and -EFSVTDA- (mammalian) (Figure 2.2 C). Although the linkers of Hsp110s are not conserved across species, they seem to exhibit conservation in the same group of organisms. For instance, PfHsp70-z is marked by a glutamate residue E^{426}, while the rest of the Hsp110s possess an Isoleucine residue in the same position. This suggests that the EYECVE linker is a signature motif of PfHsp70-z which possibly carries out specialized function since it is distinct from those of other Hsp110s.

2.3.2 PfHsp70-z linker displays distinct charge and hydrophobicity character

Given that linker residues of canonical Hsp70s were previously shown to exhibit low conservation from the Hsp110 (PfHsp70-z) linker (Figure 2.2), it was necessary to explore the properties of the respective linker segments of the Hsp70s. This study analysed local changes within the linker motifs of PfHsp70-1, PfHsp70-z and DnaK after substitution mutations. The predicted biochemical properties of the linkers were analysed using Biovia Discovery Studio software (Dassault Systèmes BIOVIA, San Diego, USA). In general, the respective linker substitution mutations induced local changes in hydrophobicity, ionic charges and hydrogen bond acceptors/donors on the linker motifs (Figure 2.3; Appendix B1-3). The PfHsp70-z linker residues (EYECVEK) form a hydrophilic interface between the respective NBDs and SBDs (Figure 2.3 A; Appendix B1-3). On the other hand, the canonical linker residues form a hydrophobic interface that connects the NBD and SBD (Figure 2.3 B; Appendix B1-3). This change in hydrophobicity possibly suggests that the linker causes the respective proteins to behave differently in aqueous environments.

The PfHsp70-z linker displays a distinct charged character in comparison to the canonical Hsp70 linker (Figure 2.3 C,D). The 3 glutamate residues E^{421}, E^{423} and E^{426} of the PfHsp70-z linker confer a strong negative charge onto the linker (Figure 2.3 C). In contrast, the canonical Hsp70 linker is mostly neutral as it possesses four uncharged leucine residues (^{422}LLLL^{425}). However, both the canonical (PfHsp70-1/DnaK) and Hsp110 (PfHsp70-z) linkers were predicted to each possess three hydrogen bond acceptors (Figure 2.3 E,F; Appendix B3). In PfHsp70-z, the 3 glutamate residues (E^{421},E^{423} and E^{426}) are predicted to act as hydrogen bond acceptors. In the canonical Hsp70 linker, the aspartate (D^{403} and D^{408}) and valine (V^{409}) residues are predicted to act as hydrogen acceptors (Appendix B1-3). Hydrogen bonding may help stabilize the linker during nucleotide, substrate or co-chaperone binding.

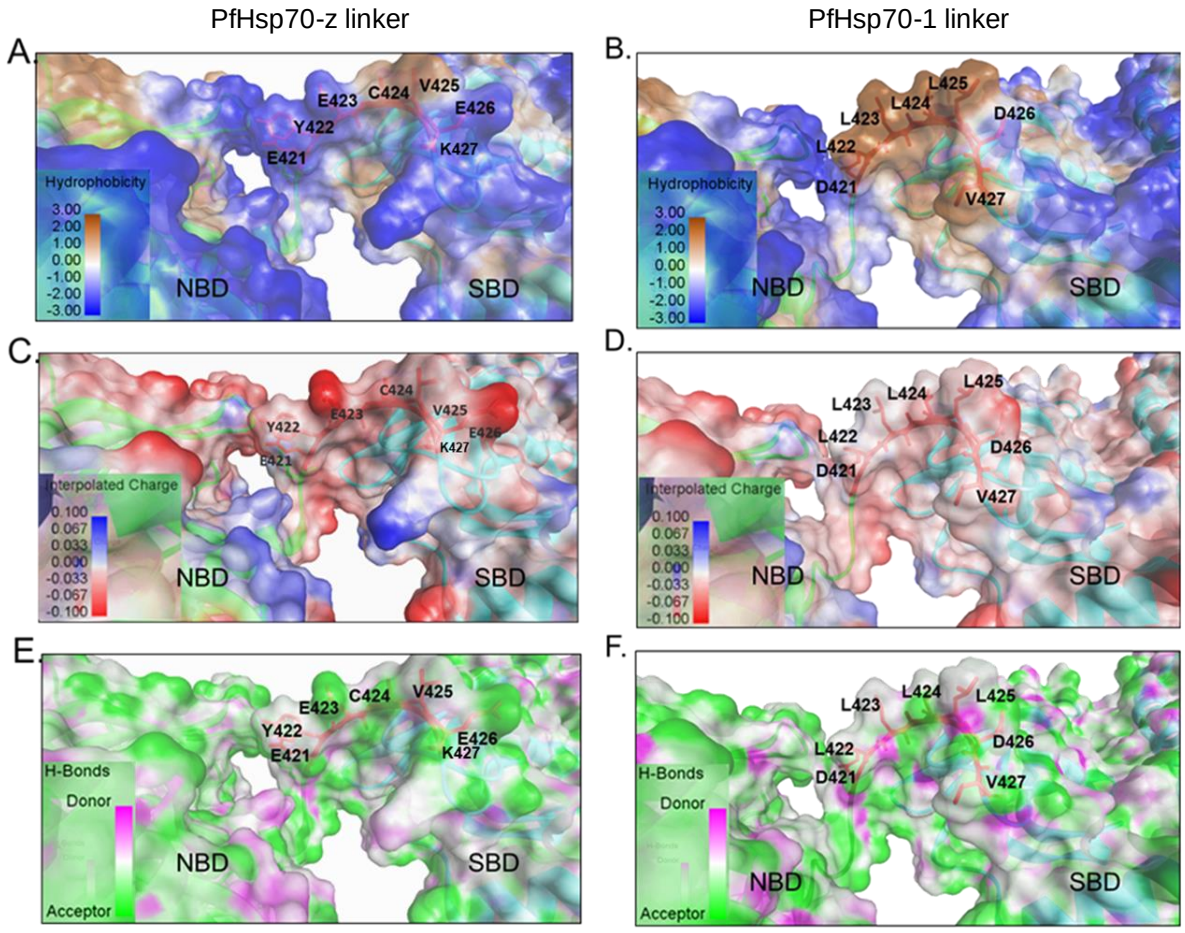

Figure 2.3. Properties of linker motifs of PfHsp70-z and PfHsp70-1
(A) The linker surface of PfHsp70-z is characteristically hydrophilic in nature as opposed to that of PfHsp70-1 (B) which is characterised by hydrophobic residues that create a hydrophobic interface around the linker. (C) PfHsp70-z has a relatively more negatively charged linker as opposed to the PfHsp70-1 linker (D) which is mostly neutral. (E) PfHsp70-z possesses fewer hydrogen acceptors during hydrogen bond formation as opposed to PfHsp70-1 (F) which is predicted to form more hydrogen bonds.

In Hsp70s, hydrogen bonding is thought to stabilize linker docking into the linker binding cleft in the ATP bound state (English *et al*., 2017). The current study explored the predicted effects of linker domain swapping on docking in the ATP bound state (open state). In the ATP state, PfHsp70-1_{LS} possess unique H-bonds that are predicted to be absent in PfHsp70-1 (Figure 2.6; Table 2.3). While PfHsp70-1_{LS} linker residues at positions E^{405} and V^{407} are predicted to form 4 H-bonds with the SBD, the PfHsp70-1 linker residue D^{408} forms only 2 H-bonds with the SBD (Table 2.3). This suggests that upon ATP binding, linker docking is relative more stabilized in PfHsp70-1_{LS} than in PfHsp70-1.

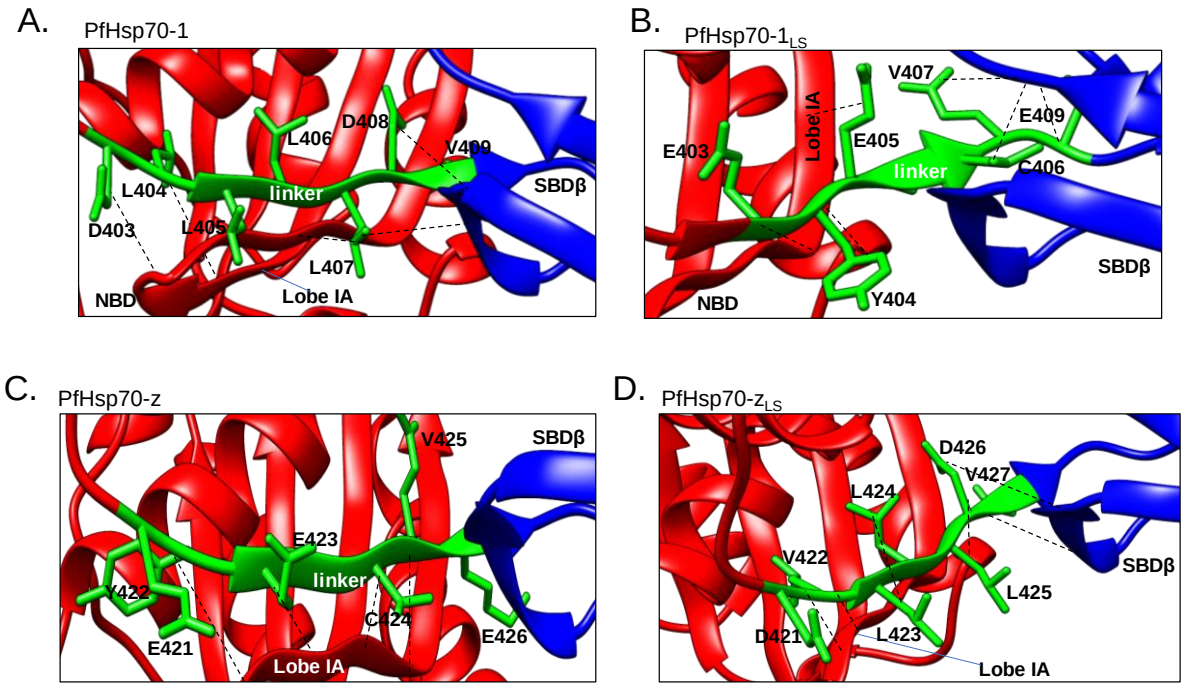

Figure 2.4. The linker dictates differential hydrogen bonding between its residues and the NBD/SBD resulting in varied stability of the docked state.

(A) The linker of PfHsp70-1_{LS} is predicted to form four H-bonds with the SBDβ residues when in the open state as compared to PfHsp70-1 (B) which is predicted to form only two SBD contacts. (C) PfHsp70-z possesses four hydrogen bonds with lobe IA of the NBD and one hydrogen bond with SBDβ. (D) PfHsp70-z_{LS} possesses four hydrogen bonds with lobe IA and two bonds with SBDβ.

Generally, there were marginal differences in hydrogen bonds predicted to form between the linkers of either PfHsp70-z or PfHsp70-z_{LS}, with the NBD (Figure 2.6; Table 2.3). However, the linker of PfHsp70-z_{LS} is predicted to possess two SBD contacts at D^{426} as opposed to one contact in the PfHsp70-z linker at position E^{426} implying differential stabilization of linker docking at the SBD. Overall, the linker mutations across the different Hsp70s modulate stabilization of the linker motif by H-bonding in the open state. This could potentially affect Hsp70 function. The three-dimensional model of $DnaK_{LS}$ in the ATP state could not be rendered on both Chimera (Pettersen *et al*., 2004) and Discovery studio (Dassault Systèmes BIOVIA, San Diego, USA). PDB files derived from Phyre2 are modelled from sequences via a combination of multiple template modeling and simplified ab initio folding simulation (Kelly et al., 2015). This means that there was no reliable template on the database to construct a model for $DnaK_{LS}$. As such, hydrogen bonds in the docked state of $DnaK_{LS}$ could not be mapped and analysed.

Table 2.3 Predicted Hydrogen bond formation in Hsp70 linker residues in the ATP-bound state

Protein	Linker residue	Contact	Length/Å
PfHsp70-1$_{LS}$	Glu 402 (O)	Phe 229 (N) NBD	3.110
	Tyr 404 (N)	Phe 229 (O) NBD	3.028
	Tyr 404 (O)	Val 231 (N) NBD	2.985
	Glu 405 (N)	Ile 432 (O) SBD	3.176
	Glu 405 (O)	Ile 432 (N) SBD	2.918
	Val 407 (N)	Thr 430 (O) SBD	2.822
	Val 407 (O)	Asn 429 (N) SBD	2.797
PfHsp70-1	Leu 405 (N)	Gly 227 (O) NBD	2.914
	Leu 405 (O)	Phe 229 (N) NBD	3.110
	Leu 407 (N)	Phe 229 (O) NBD	3.028
	Leu 407 (O)	Val 231 (O) NBD	2.985
	Asp 408 (N)	Ile 433 (O) SBD	3.176
	Asp 408 (O)	Ile 433 (N) SBD	2.918
PfHsp70-z$_{LS}$	Leu 423 (N)	Asn 217 (O) NBD	2.914
	Leu 423 (O)	Cys 219 (N) NBD	3.110
	Leu 425 (O)	Cys 219 (O) NBD	3.028
	Leu 425 (O)	Ile 221 (O) NBD	2.985
	Asp 426 (N)	Lys 458 (O) SBD	3.176
	Asp 426 (O)	Lys 458 (N) SBD	2.918
PfHsp70-z	Glu 423 (N)	Asn 217 (O) NBD	2.914
	Glu 423 (O)	Cys 219 (N) NBD	3.110
	Val 425 (N)	Cys 219 (O) NBD	3.038
	Val 425 (O)	Ile 221 (O) NBD	2.985
	Glu 426 (O)	Lys 457 (N) SBD	3.176
DnaK	ND	ND	ND
DnaK$_{LS}$	ND	ND	ND

*ND: Not determined

2.3.3 Linker motif swapping is predicted to induce structural changes in PfHsp70-1 and PfHsp70-z

The predicted three-dimensional models of wild type Hsp70s and their linker mutants were analysed to identify structural variations induced by linker motif swapping. The three-dimensional models of PfHsp70-z and PfHsp70-z_{LS} reveal slight variations in the loop preceding lobe IA which forms part of the linker binding cleft of PfHsp70-z/PfHsp70-z_{LS} (Figure 2.5 A,B). In addition, the SBD of PfHsp70-z_{LS} possesses a protrusion due to re-orientation of the Phe189 residue in the loop that connects lobe IA to the linker binding cleft (Figure 2.5 A, B, C). The hydrogen bonds stabilizing the loop that precedes the linker binding cleft are also predicted to be affected by the linker mutation (Figure 2.5 C). Furthermore, the linker mutation abrogated the hydrogen bonds formed in the wild type model between Phe189 with Ser216 at a 2.935Å distance and Glu188 with Phe214, respectively (Figure 2.5 C). This suggests that the linker mutation had an impact on the linker binding cleft of PfHsp70-z.

The linker mutation in PfHsp70-z caused a positional reorientation of the tyrosine residue (Y^{686}) residue located in the TEDWLYEE motif (Figure 2.5 E-G). Interestingly, a helix in the TEDWYLEE motif was changed into a loop when the linker was mutated (Figure 2.5 E-F). This suggests that the replacement of the PfHsp70-z linker with the PfHsp70-1 linker has far reaching effects on the three-dimensional structure of the protein.

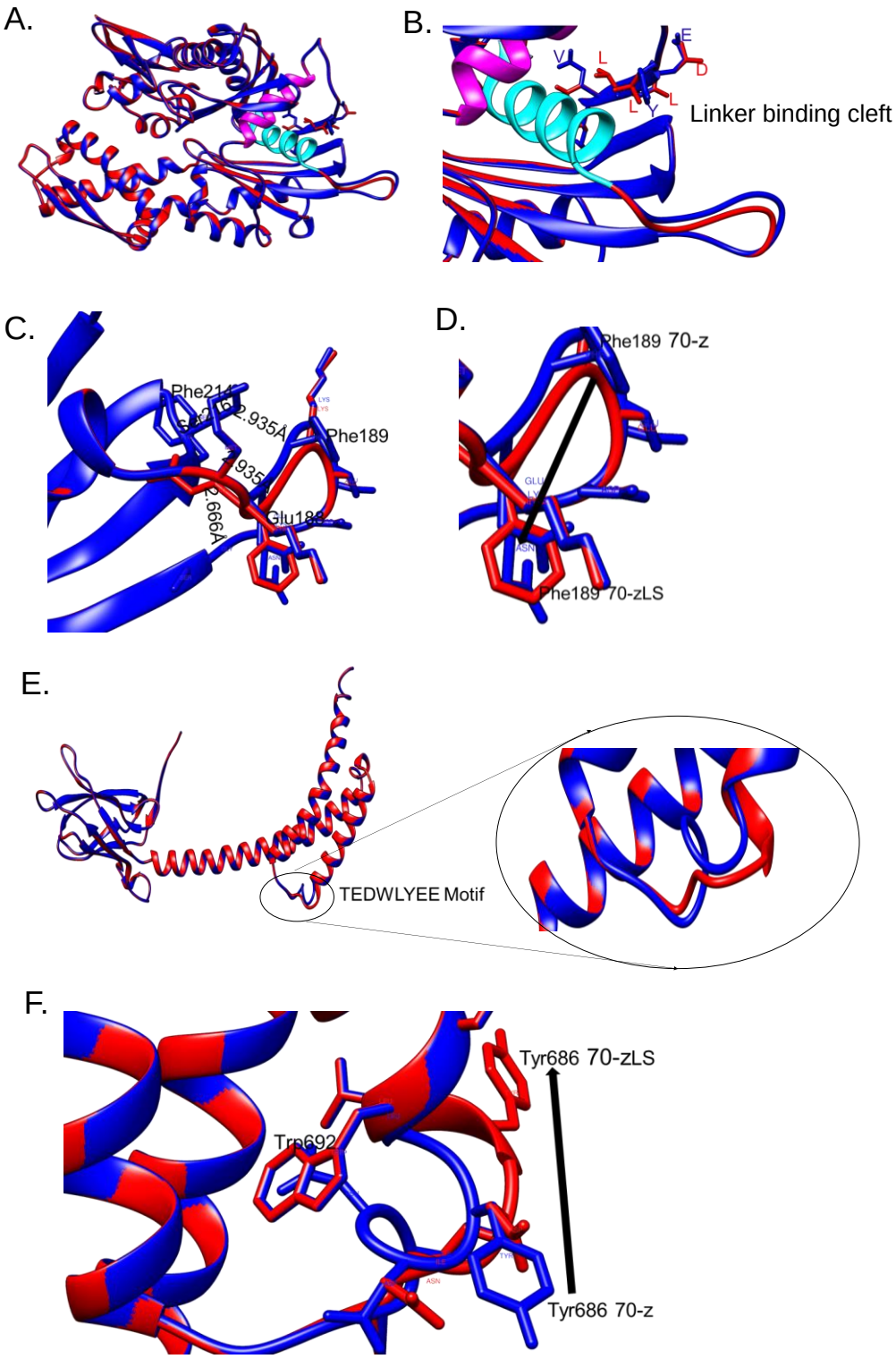

Figure 2.5. Predicted differences between PfHsp70-z and PfHsp70-z$_{LS}$ structural features
(A). Superimposed NBDs of PfHsp70-z (blue) and PfHsp70-z$_{LS}$ (red), showing helices of lobe IA (cyan) and lobe IIA (magenta) which form the linker binding cleft. (B) The loops preceding lobe IA of the linker binding cleft exhibit structural differences between PfHsp70-z (blue) and PfHsp70-z$_{LS}$ (red). (C) The residues Phe189 and Glu188 of PfHsp70-z form hydrogen bonds with Ser216 and Phe214, respectively. These bonds are absent in PfHsp70-z$_{LS}$. (D) Phe189 is predicted to reorient in PfHsp70-z$_{LS}$ (red). (E) PfHsp70-z (blue) and PfHsp70-z$_{LS}$ (red) are predicted to possess structural differences within their TEDWLYEE motifs. The insert represents the zoomed TEDWLYEE motif showing the structural differences within the proteins. (F) Tyr686 is reoriented between PfHsp70-z (blue) and PfHsp70-z$_{LS}$ (red).

Variations between the structures of PfHsp70-1 and PfHsp70-1_{LS} were mostly observed in SBDβ (Figure 2.6). Variations were also noted in $L_{1,2}$ connecting β_1 and β_2 of the SBD (Figure 2.6). It is conceivable that this variation possibly affects substrate binding since β_1 and β_2 subdomains are thought to be stabilized by $L_{1,2}$ during substrate binding (Kityk *et al*., 2012). In addition, a unique protrusion within the residues ^{415}LETAGGV^{421} was formed in PfHsp70-1_{LS} (Figure 2.6 C). Furthermore, Thr407 formed a hydrogen bond with Thr441 in the β4 unit of the PfHsp70-1_{LS} substrate binding cleft (Figure 2.6 C). This bond was predicted to be absent in the wild type form of the protein. These findings suggest that in PfHsp70-1, the linker mutation affects the structure of the SBD which might translate into possible differences in substrate binding between the two proteins.

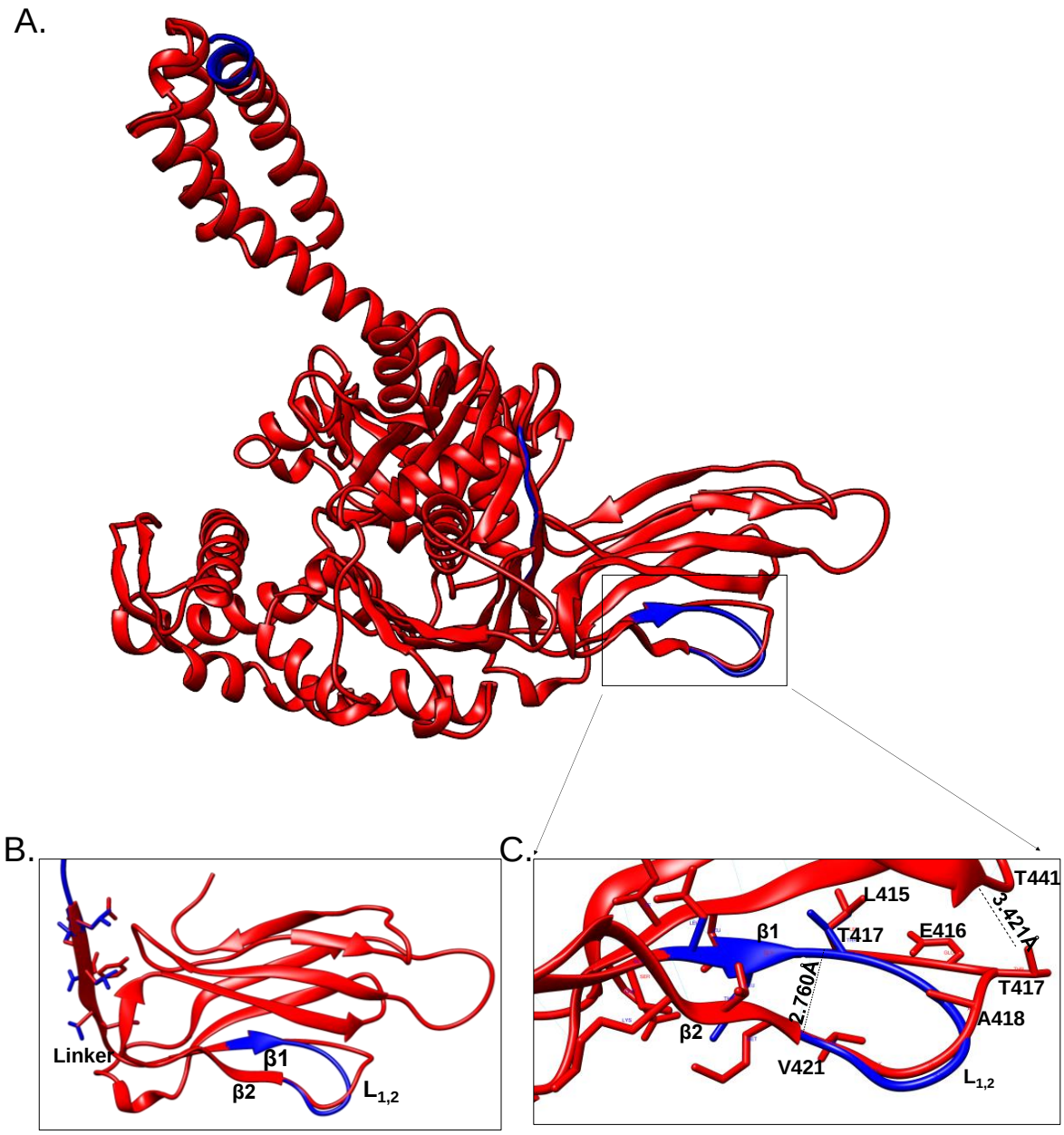

Figure 2.6. Predicted structural differences between PfHsp70-1 and PfHsp70-1_{LS}
(A) PfHsp70-1_{LS} structure (red) superimposed onto PfHsp70-1 (blue) showing minor structural differences in SBDβ. (B) PfHsp70-1_{LS} (red) exhibit more protruded loops in SBDβ as opposed to that of PfHsp70-1 (blue). (C) Zoomed $L_{1,2}$ protrusion shows differences arising in the PfHsp70-1_{LS} residues Glu416, Thr417 and Ala418 as compared to those in PfHsp70-1 (blue).

2.3.4 Comparative analysis of the NBD:SBD interfaces of PfHsp70-1, PfHsp70-z and DnaK

Interdomain communication between the NBD and SBD is important in the Hsp70 functional cycle. This study sought to identify conservation levels of amino acid residues that are crucial for the NBD:SBD interfaces of DnaK, PfHsp70-1 and

PfHsp70-z. Residues (R^{151}, R^{169}, D^{326}, K^{414}, D^{481}) which act as essential allosteric hotspots for signal transmission between the domains were previously described in DnaK (Kityk *et al*., 2015). It has been proposed that since the linker adjoins the NBD and SBD, it possibly modulates the formation of the NBD:SBD interface which is important for allostery (Chakafana *et al*., 2019b). DnaK, PfHsp70-z and PfHsp70-1 displayed variations within their respective allosteric hotspots (Figure 2.7 A,B). The most conserved residue was R^{167} on DnaK, which corresponded to R^{183} and R^{169} in PfHsp70-1 and PfHsp70-z, respectively (Figure 2.7 A,B). Additionally, it was also observed that PfHsp70-1 generally possessed most of the allosteric hotspots found in DnaK such as R^{151}, D^{326} and D^{481} (Figure 2.7). However, PfHsp70-1 lacks a lysine residue (K^{414} in DnaK) which is replaced by an arginine residue (R^{429}) (Figure 2.7). The substitution of lysine for arginine is however a conservative substitution, since both residues are positively charged.

On the other hand, PfHsp70-z was observed to possess only two out of the five allosteric hotspots that are important in the formation of the NBD:SBD interface. This suggests that PfHsp70-z possibly derives allostery from mechanisms that are different form the canonical Hsp70s. Although PfHsp70-z possesses R^{169} and R^{453} which correspond to the allosteric hotspots R^{167} and K^{414} (numbering based on DnaK), it lacks the aspartate residues (corresponding to D^{326} and D^{481}) which are both replaced with threonine residues, T^{353} and T^{521}, respectively. Interestingly, it was observed that the plasmodial chaperones PfHsp70-z and PfHsp70-1 both possess arginine residues at the allosteric hotspot corresponding to K^{414} in DnaK. This suggests that this residue modulates functional specialization of *P. falciparum* Hsp70s. Since the linker is thought to be important in allostery, it was therefore important to predict and analyse the effects of linker domain swapping on the allosteric functions of the respective Hsp70s.

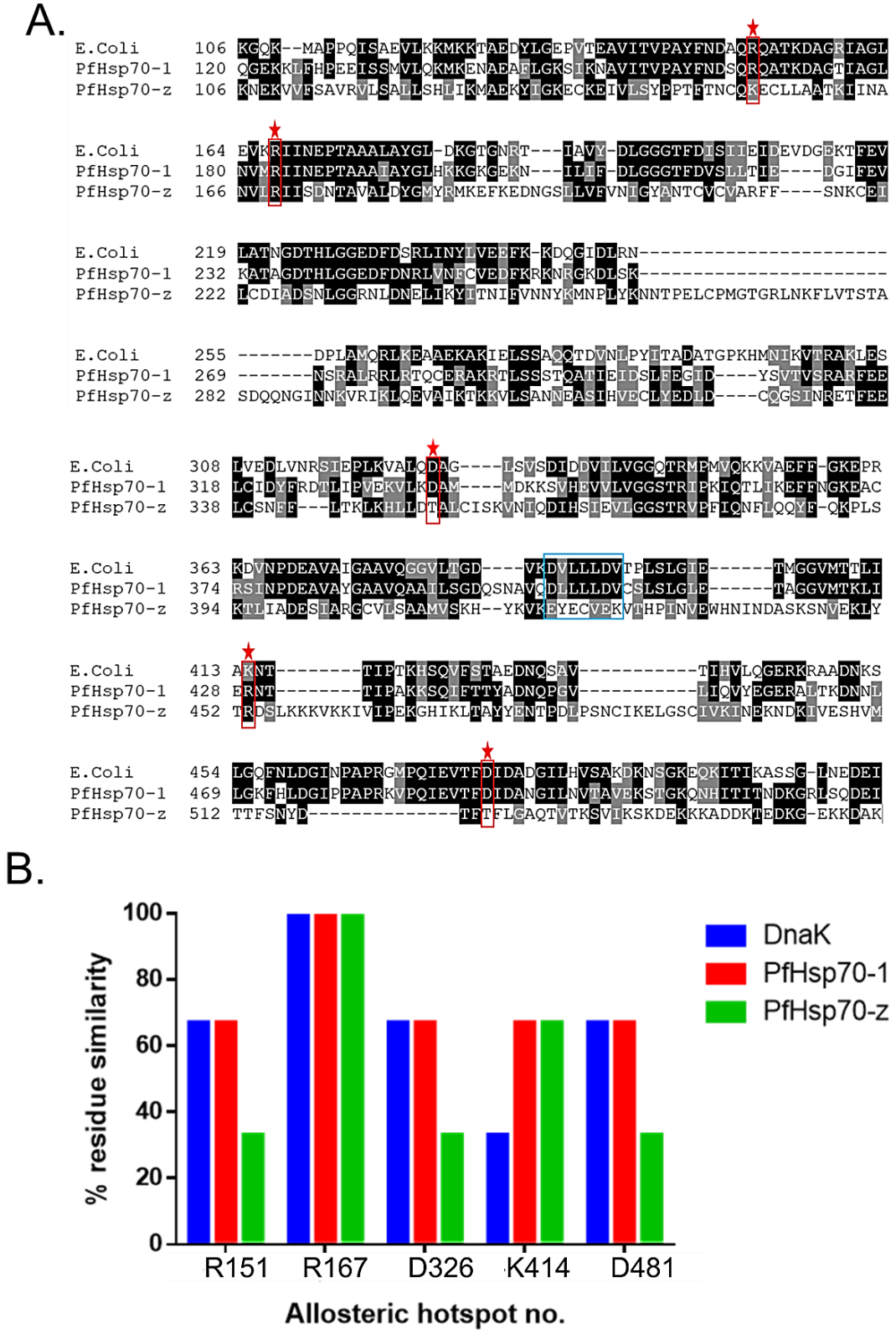

Figure 2.7. Allosteric hotspots of DnaK, PfHsp70-1 and PfHsp70-z
(A) The allosteric hotspots (R^{151}, R^{167}, D^{326}, K^{414}, D^{481}) re shown in red boxes marked with stars and the linker is shown in a blue box. The starred residues are important for NBD:SBD interface formation. (B) The percentage similarity of allosteric residues of DnaK, PfHsp70-1 and PfHsp70-z was analysed using JALVIEW software via sequence alignment. Allosteric hotspots were numbered as follows (based on DnaK residue numbering).

2.3.5 PfHsp70-1 and PfHsp70-z are predicted to exhibit distinct interaction partners

Hsp70s generally possess a conserved structural architecture which is marked by less conserved linker and SBD segments. Having successfully established the differences within the linker segments of PfHsp70-1 and PfHsp70-z (Figure 2.2 A), the study then sought to compare the predicted interactomes of the respective proteins. Based on STRING analysis (http://string-db.org/, Szklarczyk *et al.,* 2017), PfHsp70-z and PfHsp70-1 are predicted to share overlapping but distinct interactors (Figure 2.8 A; Appendix B; Table B2). For instance, PfHsp70-1 likely co-operates with a greater complement of J-domain proteins as compared to PfHsp70-z (Figure 2.8; Appendix B; Table B2). While PfHsp70-1 is predicted to interact Hsp40, Hsp60,Hsp90 and Hop, PfHsp70-z was mostly predicted to interact with Hsp90, Hsp100 and sHsps of the Hsp20 family (Figure 2.8 A; Appendix B; Table B3).

Furthermore, PfHsp70-1 was predicted to interact with a relatively larger complement of proteins involved in RNA metabolism and biosynthesis than PfHsp70-z (Figure 2.8). Notably, PfHsp70-z is predicted to interact with plasmepsin III. Plasmepsin III is a haemoglobinase which facilitates the hydrolysis of haemoglobin during the intra-erythrocytic stage of the parasites life cycle (LoesbanluechaI *et al*., 2019). This suggests that PfHsp70-z plays an important role in facilitating nutrient uptake by parasites in the erythrocytes. Additionally, it was predicted that PfHsp70-z interacts with a putative asparagine/aspartate rich protein (PlasmoDB Accession # PF 3D7_1233600). This implies that PfHsp70-z possibly possesses high affinity towards peptide substrates harbouring asparagine residues. It is therefore conceivable that, since the two proteins are delineated from each other by the linker segment, this motif may possibly dictate functional specialization within the proteins.

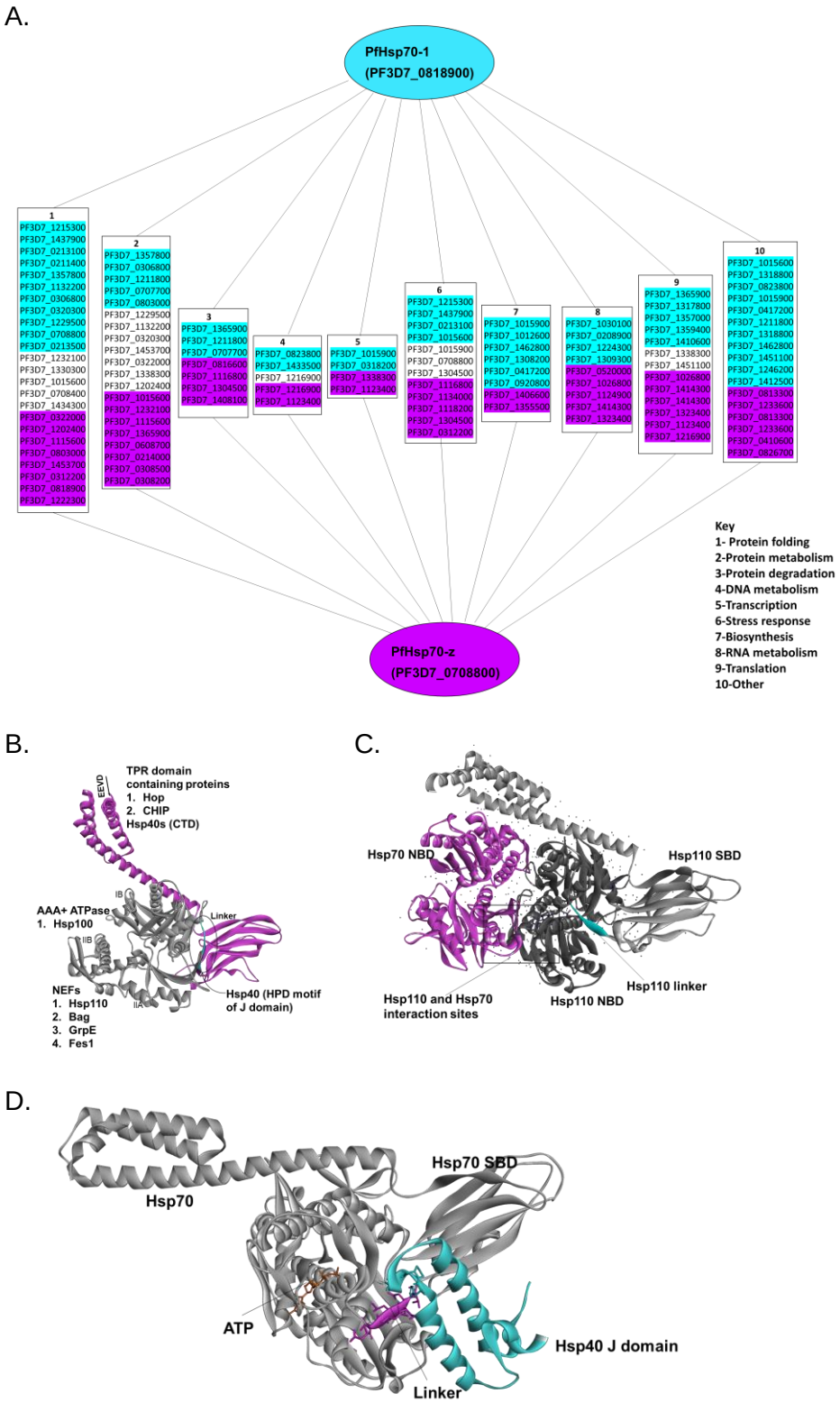

Figure 2.8. Interactome of PfHsp70-1 and PfHsp70-z
(A) The interactomes of PfHsp70-1 and PfHsp70-z were constructed from STRING database hits. Proteins shown in cyan represent exclusive interactors of PfHsp70-1 while those in purple represent interaction partners of PfHsp70-z. Proteins that are not highlighted represent network partners that are shared by the two proteins. (B) Model for interaction partners of Hsp70 at various sites of the protein. (C) Hsp70 and Hsp110 interaction via the NBD from crystal structure solved by Polier *et al*., 2008. (D) Interaction of Hsp70 with Hsp40 J domain at the linker binding cleft of Hsp70.

2.4 Discussion

The amino acid residues that constitute linkers regulate inter-domain orientations and protein function (van Leeuwen *et al*., 1997; Robinson and Sauer, 1998). Using bioinformatics, the current study sought to predict the effect of linker substitution mutations in PfHsp70-1, PfHsp70-z and DnaK. Based on multiple sequence alignments, linkers of plasmodial Hsp70 family members were observed to be divergent (Figure 2.2). Both PfHsp70-z and PfHsp70-y, which represent the Hsp110 and Grp170 members within the parasite, are marked by linkers that are unique from those of their canonical Hsp70 counterparts. Furthermore, since the parasite Hsp70s perform unique roles within cells, it is plausible that the differences arising within their respective linkers of the proteins delineate their functional capabilities. The two cytosolic proteins, PfHsp70-1 and PfHsp70-z, are generally characterised by distinct interaction partners (Figure 2.8A). Since the two proteins are marked by unique linkers, this motif possibly modulates the differential association of the proteins with respective functional network partners thus dictating their functional specialization in cells. For example, PfHsp70-z has previously been demonstrated to be a more effective holdase than PfHsp70-1 (Zininga *et al*., 2016).

The C-terminal linker residues (-LLLDV-) of canonical Hsp70s generally exhibit high conservation with a 100% consensus across 500 canonical Hsp70 species (Figure 2.2C). Leucine residues allow for increased rotational freedom between the αC-N and the C-C bond in peptides (Argos, 1990). This could possibly enhance flexibility within the linkers of canonical Hsp70s harbouring leucine repeats. The highly conserved leucine residues have also been previously implicated in modulating interdomain allostery and interaction with Hsp40 in the *E. coli* chaperone, DnaK (Kumar *et al*., 2011). On the other hand, Hsp110 linkers are characterized by divergent sequences from canonical Hsp70 members (Figure 2.2 D). Recently, it was reported that Hsp110 linkers generally cluster into three distinct clades constituted by the residues; -EFSVTDA, PFKFEDI and EYECVIE/K (Chakafana *et al*., 2019b). The PfHsp70-z linker (EYECVEK) is unique in that it harbours more charged residues compared to that of most studied Hsp110, yeast Sse1 (EFSVTDA).

The properties of the linker regions of PfHsp70-1$_{LS}$, PfHsp70-z$_{LS}$, DnaK$_{LS}$ relative to their wild type forms were then analysed using Biovia Discovery studio. The canonical Hsp70 (PfHsp70-1/DnaK) linker was predicted to possess a hydrophobic, neutral linker while the Hsp110 (PfHsp70-z) linker was hydrophilic and charged (Figure 2.4). In a previous study by Argos (1990), small, polar and hydrophilic amino acids such as Ser, Thr and Asp were noted as desirable linker constituents for achieving an extended conformationally stable oligopeptide. This suggests that the Hsp110 linker is more stable than that of canonical Hsp70s. This is in line with a previous report that PfHsp70-z is more stable that PfHsp70-1 (Zininga *et al*., 2016). Canonical Hsp70s, are however constituted of a hydrophobic linker, which is thought to enhance their flexibility (Zuiderweg *et al*., 2014; Chiappori *et al*., 2016). The linker motifs are thought to act as a 'potentiometer' which helps Hsp70s to sense physiological changes in the cellular environment (Swain *et al*., 2007; Chakafana *et al*., 2019b). This possibly implicates the linker in dictating the overall structural conformation of the proteins (Figure 2.5).

In the open conformation, the linker docks into the linker binding cleft to facilitate ATP hydrolysis (Gassler *et al*., 1998; Qi *et al*., 2013). This docking is thought to be stabilized by hydrogen bonding between linker residues and some NBD or SBD residues (Chiaporri *et al*., 2016; Chakafana *et al*., 2019b). The linkers of wild type PfHsp70-1, PfHsp70-z and DnaK and their mutant versions were predicted to form different hydrogen bonds in the docked state (Figure 2.6). PfHsp70-1$_{LS}$ forms more hydrogen bonds than wild type PfHsp70-1 (Table 2.2). This observation implies that the presence of the EYECVEK linker sequence in PfHsp70-1$_{LS}$ confers a more stable docked state as compared to PfHsp70-1. The increased stability possibly implies that PfHsp70-1$_{LS}$ requires relatively more energy to undock than in wild type protein. Upon analysis of the conservation levels of allosteric hotspots it was noted that PfHsp70-1 possess four out of the five residues that are thought to be important in allosteric regulation (Figure 2.8). On the other hand, PfHsp70-z lacks most of the allosteric hotspots as Hsp110s are generally thought to exhibit atypical allosteric communication between their domains (Kumar *et al*., 2019). In conclusion, the findings from this study noted that the linker substitution mutations have far reaching consequences on the structures of PfHsp70-1, PfHsp70-z and DnaK. As such, it is imperative to validate

whether the recombinant proteins would exhibit secondary and tertiary structural differences *in vitro*.

CHAPTER 3

Biophysical analyses of linker swap variants of PfHsp70-1, PfHsp70-z and DnaK

3.1 Introduction

Canonical Hsp70s and their Hsp110 counterparts, generally share a highly conserved structural organisation comprised of an NBD and SBD adjoined by a linker segment. Although the linkers of canonical Hsp70s are highly conserved across species, Hsp110 linkers generally exhibit low sequence conservation (Figure 2.2; Chakafana *et al*., 2019b). Linkers serve as covalent connectors which tether separate domains of proteins from one another. Alternatively, linkers may also regulate or restrict cooperative interdomain interactions in proteins (Gokhale and Khosla, 2000). In this way, linkers can dictate the overall structural conformation of a protein. Altering the amino acid residue compositions within the linker has previously been demonstrated to affect overall stability, folding rates and allostery of *E. coli* DnaK (Robinson and Sauer, 1998; Swain *et al*., 2011).

The amino acid composition of the linker constitutes an important determinant of protein structure and function since the amino acid moieties within its vicinity influence the biophysical and chemical properties of the protein (Chichili *et al*., 2013; Chakafana *et al*., 2019b). The rotational freedom that linker residues enjoy influence the flexibility or rigidity of the linker. The flexibility or rigidity of the linker may in turn impact on the secondary and tertiary structural orientations of the proteins. Following *in silico* predictions on the structures of PfHsp70-1, PfHsp70-z and DnaK upon linker motif swapping, it was necessary to characterise the biophysical properties of the proteins *in vitro*. This study sought to investigate changes in secondary and tertiary structural conformations of wild type Hsp70s relative to their linker mutants.

The objectives of this study were to:

i. heterologously express and purify recombinant PfHsp70-1_{LS}, PfHsp70-1, PfHsp70-z_{LS}, PfHsp70-z, $DnaK_{LS}$ and DnaK;

ii. determine the secondary and tertiary structural conformations of PfHsp70-1_{LS}, PfHsp70-z_{LS} and $DnaK_{LS}$ in comparison to their wild type forms as well as;

iii. investigate the effect of the linker substitution mutations on overall secondary and tertiary structure stability of the Hsp70 proteins in the presence of denaturants.

3.2 Materials and Methods

3.2.1 Materials

The list of reagents used in this study is presented in the Appendix C. The following antibodies were used for protein validation by immunoblotting; rabbit raised α-PfHsp70-1 antibody (Shonhai *et al.,* 2008), rabbit raised α-PfHsp70-z antibody and HRP conjugated α-rabbit (Zininga *et al*., 2015a), mouse raised α-DnaK antibody (Sigma-Aldrich, U.S.A), HRP conjugated α-mouse secondary antibodies (Sigma-Aldrich, U.S.A) and an HRP-conjugated α-His antibody (Sigma-Aldrich, U.S.A). The plasmid constructs and bacterial strains used for recombinant protein production are listed in Table 3.1.

Table 3. 1: List of plasmids and *E. coli* strains used for protein expression

Strains and Constructs	Description	Supplier/Reference
Construct		
pQE30/PfHsp70-1	pQE30 encoding full length PfHsp70-1, Amp^r	Shonhai *et al*., 2008
pQE30/PfHsp70-1_{LS}	pQE30 encoding PfHsp70-1_{LS}, Amp^r	Genscript, This study
pQE30/PfHsp70-z	pQE30 encoding PfHsp70-z, AmpR	Zininga *et al*., 2015b
pQE30/PfHsp70-z_{LS}	pQE30 encoding PfHsp70-z_{LS}, AmpR	Genscript, This study
pQE30/DnaK	pQE30 encoding *E. coli* DnaK, AmpR	Genscript, This study
pQE30/$DnaK_{LS}$	pQE30 encoding *E. coli* $DnaK_{LS}$ mutannt, AmpR	Genscript, This study
***E. coli* strains used for protein expression**		
E. coli XL1 Blue	*rec*A1 *end*A1 *gyr*A96 *thi*1 *hsd*R17 supE44 *rel*A1 *lac* (*F´proAB lacIqZM15 Tn10 (Tetr*)	Thermofisher scientific, (USA)
E. coli JM109	*e14– (McrA–) recA1 endA1 gyrA96 thi-1 hsdR17* (*rK – mK +) supE44 relA1 Δ(lac-proAB) (F´ traD36 proAB lacIq ZΔM15*)	Thermofisher scientific, (USA)

3.2.2 Methods

3.2.2.1 Design and production of plasmid constructs for expression of PfHsp70-1_{LS}, PfHsp70-z_{LS}, and $DnaK_{LS}$

The pQE30/PfHsp70-1_{LS}, pQE30/PfHsp70-z_{LS} and pQE30/$DnaK_{LS}$ plasmid constructs were designed as previously described in Section 2.2.1. The DNA sequences for the linker mutants were individually cloned into pQE30 (Qiagen, USA) vectors between *Bam*HI and *Kpn*I restriction sites. The constructs were produced by GenScript (USA).Plasmid DNA for the respective constructs was then extracted (Appendix A1) and verified by restriction analysis (Appendix A2). The resultant restriction fragments were then resolved on 0.8 % agarose gel electrophoresis (Appendix A3). The constructs were further verified by DNA sequencing (Appendix A4).

3.2.2.3 Recombinant protein production

The recombinant proteins were expressed in *E.coli* XL1 Blue cells (Thermofisher scientific, USA). Chemically competent *E. coli* XL1 Blue cells were transformed with respective constructs coding for PfHsp70-1, PfHsp70-1_{LS}, PfHsp70-z, PfHsp70-z_{LS}, DnaK, and $DnaK_{LS}$ (Appendix 5). Protein expression was conducted as previously described by Zininga *et al*. (2015a). Briefly, Transformed cells were grown in 2YT broth (Yeast extract, 1.0 %; Tryptone, 1.6 % and sodium chloride, 0.5 %) supplemented with 100 µg/ml ampicillin at 30 °C. Induction of protein expression was initiated by the addition of 1 mM isopropyl β- d-1-thiogalactopyranoside (IPTG). Post induction expression was allowed for 6 hrs during which samples were collected at 1 hr intervals for sodium dodecyl sulphate-polyacrylamide gel electrophoresis (SDS-PAGE) analysis (Appendix A6).

Upon successful protein expression, the respective recombinant Hsp70s (PfHsp70-1/PfHsp70-1_{LS}, PfHsp70-z/PfHsp70-z_{LS}, DnaK/$DnaK_{LS}$) were purified using Nickel affinity chromatography as previously described (Zininga *et al*., 2015a). The buffers used for purification were prepared as follows: lysis buffer (10 mM Tris-HCl, pH 7.5, 300 mM NaCl, 10 mM Imidazole, 1X Sigmafast Protease Inhibitor, 1 mM 2-β-

mercaptoethanol and 1 mg/ml lysozyme), Wash buffer I was modified by supplementing imidazole to a final concentration of 25 mM into the lysis buffer. Wash buffer II consisted of lysis buffer supplemented with 50 mM imidazole. Elution buffer I was comprised of lysis buffer supplemented with 250 mM Imidazole, while Elution buffer II was comprised of lysis buffer with 500 mM Imidazole. At each purification stage, samples were collected for SDS PAGE analysis to assess the protein purity. Purified recombinant proteins were then extensively dialysed in dialysis buffer (20 mM Tris-HCl, pH 7.5, 10 mM NaCl, 5 % (v/v) glycerol, containing 1 mM 2-β-mercaptoethanol) using Amicon® centrifugal filter units according to a protocol from the manufacturer (Merck, USA).

3.2.2.4 Secondary structure determination of Hsp70 linker mutants

The secondary structures of the recombinant Hsp70s were determined using far-UV CD spectroscopy. The relative secondary structures and structural stability of the Hsp70s and their linker mutant forms were determined following a previously described method (Zininga *et al*., 2016) using a JASCO far-UV J-1500 CD spectrometer (JASCO Ltd, UK). Briefly, Spectra measurements were recorded at 100 nm/min scan speed, 1 nm bandwidth and averaged for 7 accumulations after subtraction of baseline (buffer only). The Dichroweb server (http://dichroweb.cryst.bbk.ac.uk) was subsequently used for deconvolution of derived spectra to determine α-helix, β-sheet, β-turn and unordered regions in the proteins.

To determine the role of the linkers in stabilizing the secondary structures of the Hsp70s, the relative stability of the proteins in the presence of thermal and chaotropic denaturants was investigated. Comparative thermal melts for wild type and linker substitution mutant proteins were determined by subjecting the proteins to monotonical temperature increments at a rate of 0.5 °C per min from 20 - 90 °C and spectra measurements were recorded at a fixed wavelength 222 nm as previously described (Zininga *et al*., 2015b). The folded state of the proteins at the respective temperature was determined using the equation 1:

((θ)t – (θ)h) / ((θ)l – (θ)h)……(1)

where (θ)t represents the molar ellipticity at a given temperature (or urea concentration), (θ)h the highest temperature (or urea concentration) and (θ)l the lowest temperature (or urea concentration), respectively (Zininga *et al*., 2015a).

The folded states of Hsp70s and their linker mutants were monitored by assessing the molar residue ellipticity at 222 nm in the presence of variable (0 - 8 M) urea concentration. The folded state of the proteins exposed to various urea levels was then calculated using equation 1 as previously described (Zininga *et al*., 2015b).

3.2.2.5 Tertiary structure determination

The tertiary structures of PfHsp70-1_{LS}, PfHsp70-z_{LS} , $DnaK_{LS}$ and their wild type forms were analysed using intrinsic (tryptophan) and extrinsic (1-Anilino-8-Naphthalene Sulfonate- ANS) fluorescence spectroscopic assays. Tryptophan fluorescence spectroscopy assays were conducted as previously described (Zininga *et al*., 2016). The generated fluorescence spectra were analysed after initial excitation at 295 nm using a JASCO FP-6300 spectrofluorometer (JASCO Ltd, UK). The emission spectra were monitored between 280 to 450 nm at a scan speed of 500 nm/min. Furthermore, the effect of nucleotides on the tertiary structure of each protein was determined by exposing the proteins to nucleotides (5 mM ADP/ATP) for 15 mins before taking fluorescence readings as previously described by Zininga *et al* (2016). To further validate the changes observed upon nucleotide binding, the effect of chemical denaturants on the tertiary structures of the respective proteins was investigated. Briefly, the recombinant proteins were allowed to sit for 30 mins in the presence of varying concentrations of urea (0 - 8 M) and guanidine hydrochloride (0 - 6 M) before spectral measurements were taken. Urea is a chaotropic denaturant which can unravel the tertiary structure of a proteins by either directly destabilizing internal, non-covalent bonds between peptide groups or by altering the hydrodynamics of the protein structure (Dunbar *et al*., 1997). Spectra generated from the readings made using denaturation buffers (with either guanidine hydrochloride or urea) were used for baseline subtraction.

The tertiary structures of the recombinant Hsp70s were further validated by extrinsic fluorescence using an ANS assay as previously described (Achilonu *et al*., 2014). ANS is a small amphipathic dye that is used as a probe to detect hydrophobic pockets on protein surfaces (Tiwari *et al*., 2009). Briefly, 200 µM ANS was incubated together with 2 µM of the respective Hsp70 for a total of 30 min at 25 °C in the dark. ANS binding to the respective Hsp70s was determined by monitoring the fluorescence spectra recorded between 400 to 500 nm after initial excitation at 390 nm. A total of 7 scans were collected and averaged for each sample. In addition, the fluorescence spectra of free ANS was also monitored as a negative control.

3.3 Results

3.3.1 Confirmation of DNA plasmid constructs

The pQE30/PfHsp70-1$_{LS}$, pQE30/PfHsp70-z$_{LS}$ and pQE30/DnaK$_{LS}$ plasmid constructs were each verified by restriction digestion using *Kpn*I and *Hind*III and sequencing (Appendix B10). Restriction digestion of the pQE30/PfHsp70-1$_{LS}$ plasmid construct with either *Kpn*I or *Hind*III, produced a band of approximately 5504 bp which corresponds to the size of the pQE30 vector (3461 bp) plus the PfHsp70-1$_{LS}$ insert (2043 bp) (Appendix B10 A). Similarly, pQE30/PfHsp70-z$_{LS}$ and pQE30/DnaK$_{LS}$ plasmid constructs were successfully confirmed by restriction analysis and sequencing (Appendix B10 B, C). In addition to these, the pQE30/PfHsp70-1, pQE30/PfHsp70-z and pQE30/DnaK plasmid constructs were each verified by restriction digestion with *Bam*HI and *Hind*III restriction enzymes (Appendix B10).

3.3.2 Expression and purification of recombinant Hsp70s

Recombinant PfHsp70-1, PfHsp70-z, DnaK and their linker swap versions were successfully expressed and purified as observed upon SDS PAGE and Western blot analysis (Figure 3.2; Appendix B13-14). PfHsp70-1 and PfHsp70-1$_{LS}$ migrated as bands resolving at approximately 74 kDa (Figure 3.1; Appendix B10-11) which is in line with previous reports (Matambo *et al*., 2004; Shonhai *et al*., 2008).

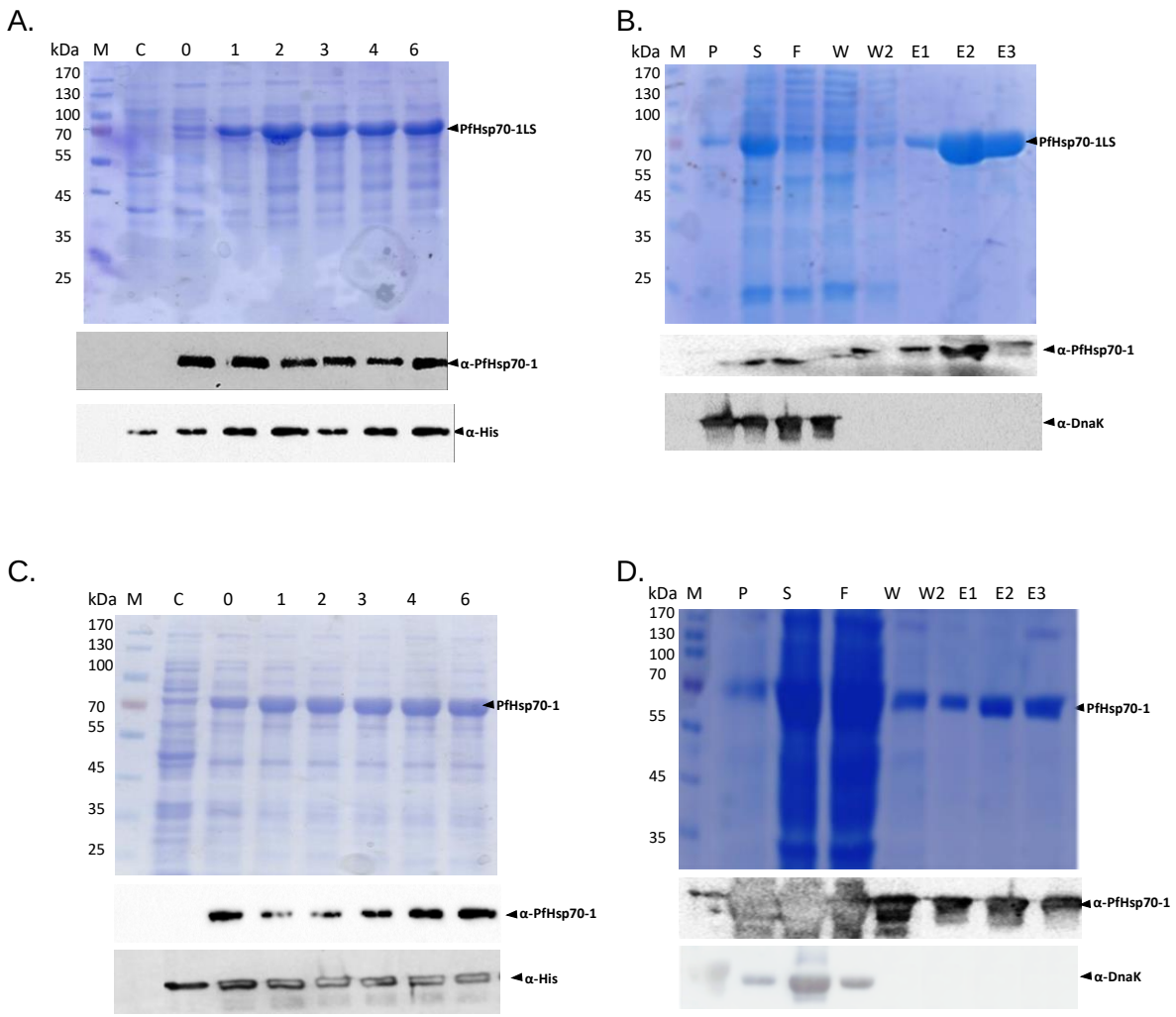

Figure 3.1. Expression and purification of PfHsp70-1_{LS} and PfHsp70-1

PfHsp70-1_{LS} and PfHsp70-1 were expressed in *E. coli* XL1 Blue cells transformed with pQE30/PfHsp70-1_{LS} and pQE30/PfHsp70-1, respectively. (A) SDS-PAGE analysis for the expression of PfHsp70-1_{LS}. M: molecular weight marker (in kDa), C: total extract for the cells transformed with a neat pQE30 vector control and 0: pre-induction sample. Lanes 1-6 represent hourly samples that were each collected at the respective hour after IPTG induction. (B) Purification of PfHsp70-1_{LS}. P: pellet fraction, S: supernatant, F: flowthrough, W: washes, E: elutions. Panels (C) and (D) represent expression and purification of PfHsp70-1, respectively. Lower panels represent the respective immunoblots generated using α-PfHsp70-1 and α-His antibodies. Full blots are presented in Appendix B11-12.

The protein band representing PfHsp70-z_{LS} migrated at approximately 100 kDa as previously reported for the wild type form of the protein (Figure 3.2; Zininga *et al*., 2016). PfHsp70-z/PfHsp70-z_{LS} expression and purification was confirmed by immunoblotting using either α-PfHsp70-z or α-His antibodies (Figure 3.2). Furthermore, the absence of endogenous DnaK contamination in the purified PfHsp70-z/PfHsp70-z_{LS} was validated using α-DnaK antibodies (Figure 3.2).

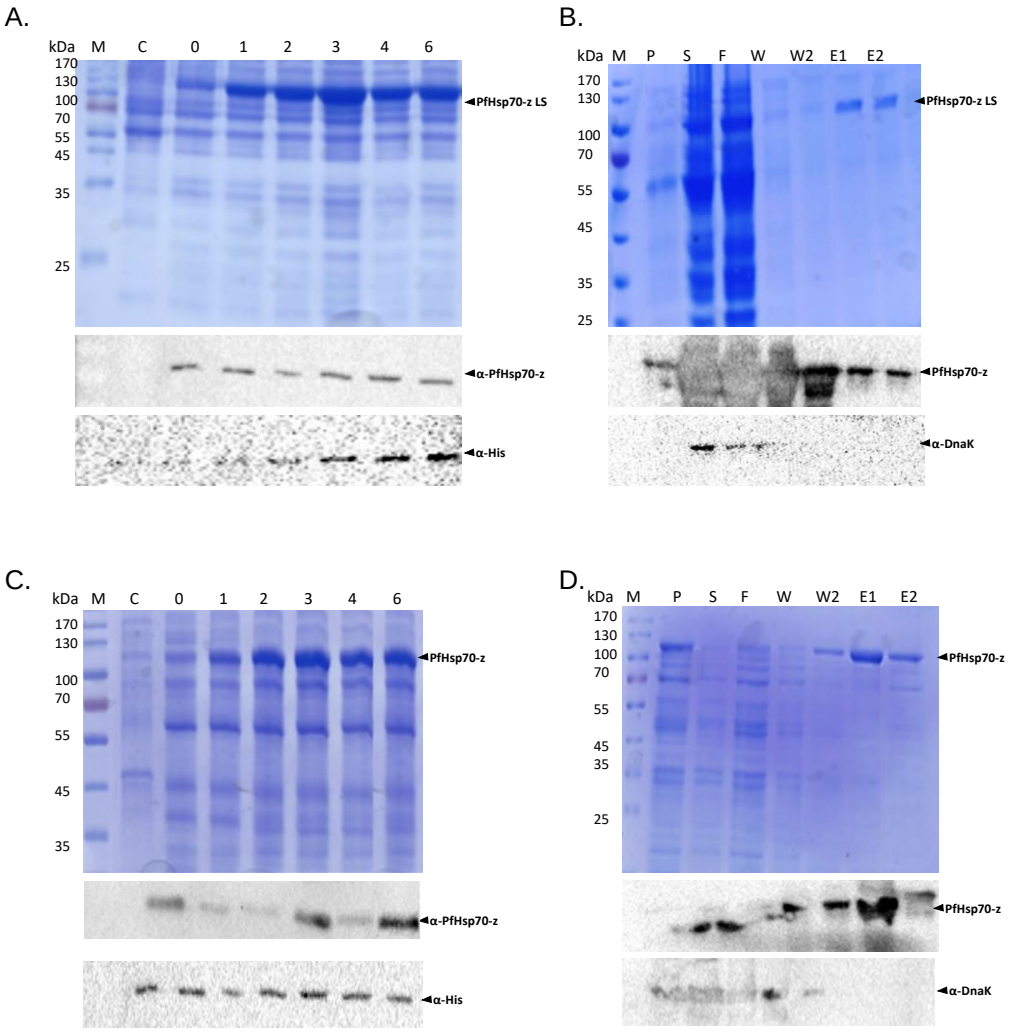

Figure 3.2. Expression and purification of PfHsp70-z_{LS} and PfHsp70-z

PfHsp70-z_{LS} and PfHsp70-z were expressed in *E. coli* XL1 Blue cells transformed with pQE30/PfHsp70-z_{LS} and pQE30/PfHsp70-z, respectively. (A) SDS-PAGE analysis for the expression of PfHsp70-1_{LS}. M: molecular weight marker (in kDa); C: total extract for the cells transformed with a neat pQE30 vector control; 0: pre-induction samples. Lanes 1-6 represent samples that were collected at the respective hour after IPTG induction. (B) Purification of PfHsp70-z_{LS}; P: pellet fraction, S: supernatant, F: flowthrough, W: washes; E: elution fractions. Panels (C) and (D) represent expression and purification of PfHsp70-z, respectively. Lower panels represent respective immunoblots for expression using α-PfHsp70-z and α-His antibodies. Full blots are presented in Appendix B13-14.

Recombinant DnaK and $DnaK_{LS}$ were similarly expressed and purified (Figure 3.3; Appendix B15-16). The recombinant $DnaK_{LS}$ band migrated at approximately 70 kDa as previously observed for its wild type form (Figure 3.3; Kim *et al*., 1998; Makhoba *et al*., 2016). Expression and purification of DnaK/$DnaK_{LS}$ were confirmed by immunoblotting using α-DnaK and α-His antibodies (Figure 3.3).

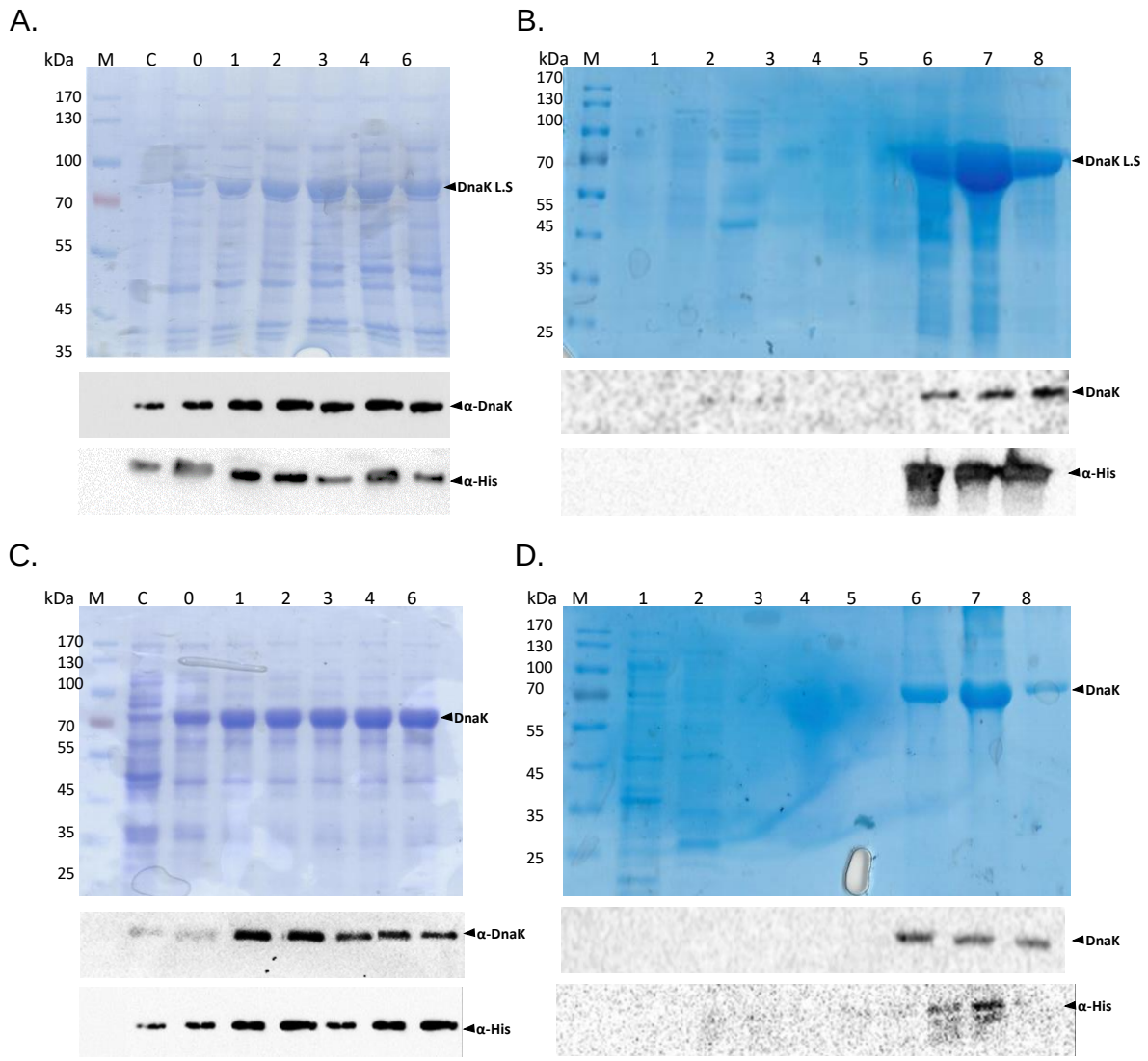

Figure 3.3. Expression and purification of DnaK and $DnaK_{LS}$

SDS-PAGE analysis and immunoblots for the expression and purification of $DnaK_{LS}$ (A, B) and DnaK (C, D) in *E. coli* XL1 Blue cell line. Left panels (A and C) represent protein expression; lane M: molecular weight marker (in kDa); Lane C: total extract of cells transformed with pQE30 plasmid, Lane 0: total extract of cells transformed with expression construct before IPTG induction and lane 6: total extract of cells 6 hr after induction. Right panels (B and D) represent purification of $DnaK_{LS}$ (B) and DnaK (D). Full blots are available in Appendix B15-16.

3.3.3 The linker of PfHsp70-z confers stability on the chaperone's secondary structure

The secondary structures of PfHsp70-1, PfHsp70-z and DnaK and their linker mutants were determined by far UV CD spectroscopy. The respective CD spectra for all the recombinant Hsp70s were characterised by a positive peak at approximately 195 nm as well as two negative troughs at approximately 208 nm and 222 nm, respectively (Figure 3.4 A-C). Generally, this suggests that the secondary structures of the recombinant Hsp70s were predominantly α-helical. Furthermore, deconvolution of the structures using Dichroweb confirmed that all the Hsp70s generally possessed over 50% α-helical content (Table 3.2). A similar observation was made during a previous study in which PfHsp70-z was reported to be predominantly α-helical (Zininga *et al*., 2015b). All the structural values derived upon deconvolution were quality checked with RMSD values less than 1 suggesting that the data were reliable (Table 3.2). There were no significant differences that were observed between the secondary structures of the wild type forms of the Hsp70s and their respective linker mutants (Table 3.2; *p>0.01*). This suggests that the global secondary structures of the Hsp70s were not largely perturbed by the linker mutations as previously predicted by *in silico* studies (Appendix B 4-9). However, DnaK$_{LS}$ and PfHsp70-1$_{LS}$ exhibited enhanced proportions of unordered regions relative to their wild type forms. Furthermore, the introduction of the canonical Hsp70 linker into PfHsp70-z resulted in a gain of α-helical content coupled to the loss of unordered segments (Table 3.2) as backed up by *in silico* predictions (Figure 2.5 E).

Table 3.2 Comparative secondary structures of Hsp70s and their LS mutants

	α-helix	β-sheet	β-turns	Unordered*	RMSD
PfHsp70-1	59	17	11	09	0.14527
PfHsp70-1$_{LS}$	56	16	14	14	0.18471
DnaK	59	18	11	13	0.43310
DnaK$_{LS}$	54	17	12	17	0.13936
PfHsp70-z	59	18	10	14	0.73097
PfHsp70z$_{LS}$	62	17	10	11	0.14209

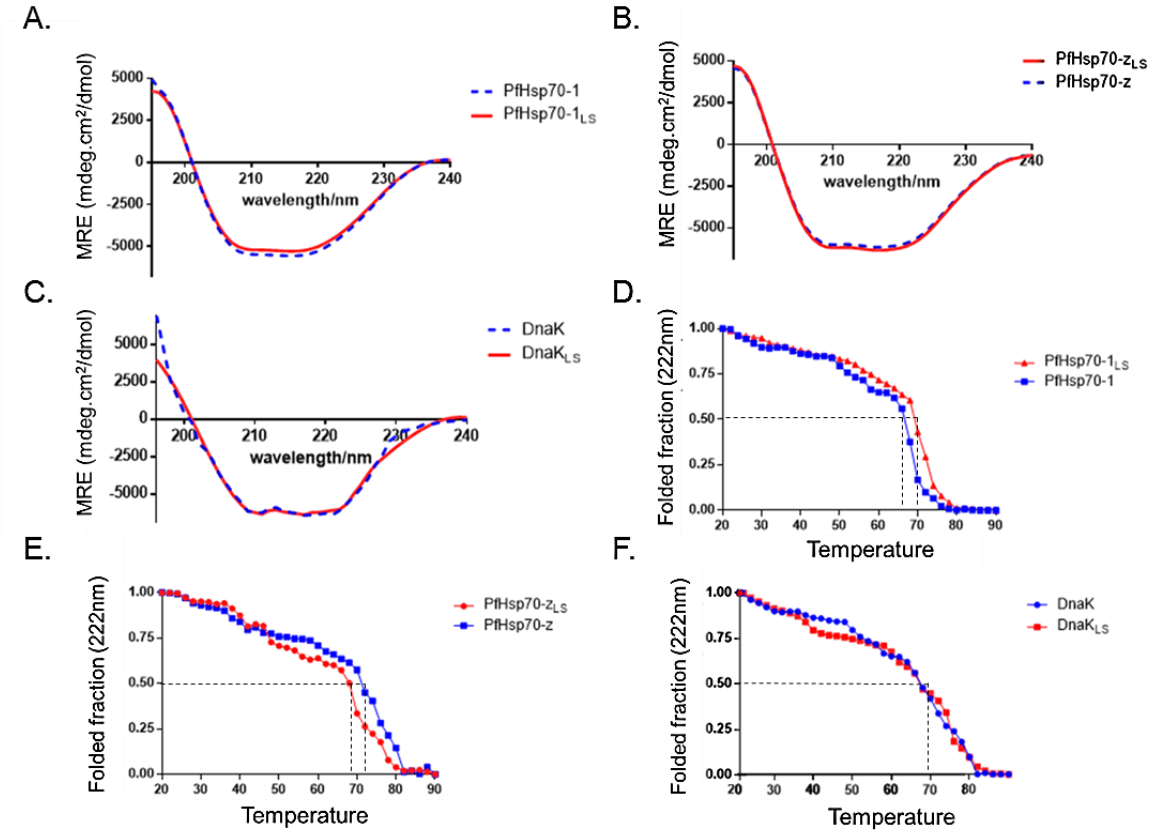

Figure 3.4. Hsp70 linker regulates thermal stability of the chaperone

CD Spectra of PfHsp70-1 and PfHsp70-1_{LS} (A); PfHsp70-z and PfHsp70-z_{LS} (B); as well as DnaK and DnaK$_{LS}$ are shown. Thermal stability of the following proteins are shown; PfHsp70-1/PfHsp70-1_{LS} (D); PfHsp70-z/PfHsp70-z_{LS} (E) and DnaK/DnaK$_{LS}$ (F).

The effects of the respective linkers in modulating the stability of the secondary structures of PfHsp70-1, PfHsp70-z and DnaK were determined. The wild type and linker mutant versions of the recombinant proteins were subjected to thermal and chaotropic denaturation to assess their stability. The recombinant proteins generally exhibited thermal resilience up to temperatures above 50 °C as they maintained 50 % of their folded structure (Figure 3.4 D-F). However, PfHsp70-1_{LS} lost 50 % of its secondary structure at a higher temperature of approximately 73 °C in comparison to 68 °C observed in PfHsp70-1 (Figure 3.4 D). This suggests that PfHsp70-1_{LS} possesses relatively higher thermal stability as compared to its wild type form, PfHsp70-1 (Figure 3.4 D). Thus it seems the PfHsp70-z linker plays an important role in enhancing the secondary structure of PfHsp70-1_{LS} under thermal stress. On the other hand, PfHsp70-z_{LS} lost 50 % of its secondary structure at a much lower temperature of 69°C in comparison to PfHsp70-z which required a higher temperature

of approximately 74 °C to attain the same conformation (Figure 3.4 E). These findings further suggest that the linker of PfHsp70-z is important for its stability. It is plausible that PfHsp70-z possesses a rigid linker which overally confers the protein with enhanced heat stability. DnaK and $DnaK_{LS}$ did not show marked differences as both proteins maintained approximately 50 % of their secondary structures at approximately 65 °C (Figure 3.4 F). This suggests that the introduction of the PfHsp70-z linker into DnaK did not significantly improve the stability of DnaK in contrast to the influence of the same motif in PfHsp70-1. It is therefore conceivable that motifs which are unique to plasmodial proteins, such as the GGMP and EKEK repeat motifs of PfHsp70-1 and PfHsp70-z (Section 1.6.5.1), respectively, possibly also play important roles in stabilizing the plasmodial Hsp70s.

To further validate the role of the linker in influencing structural stability of the Hsp70s, chemical denaturation was conducted using urea. Similar to findings from thermal denaturation studies, $PfHsp70\text{-}1_{LS}$ exhibits a more stable secondary structure than its wild type isoform upon chemical denaturation with urea (Appendix B17). Furthermore DnaK, exhibited greater stability than $DnaK_{LS}$ (Appendix B17). This suggests that the introduction of the linker of PfHsp70-z into the *E. coli* Hsp70, DnaK, reduced the protein's stability. $PfHsp70\text{-}z_{LS}$ was more susceptible to urea denaturation, as it lost approximately 50 % of its folded state at a urea concentration of 3 M in comparison to 4.5 M urea observed in PfHsp70-z (Fig 3.4 H). Taken together, these studies further demonstrated that the PfHsp70-z linker confers enhanced structural stability to both PfHsp70-z and PfHsp70-1.

3.3.4 Linker mutations induce tertiary structure perturbations in PfHsp70-1, PfHsp70-z and DnaK

To determine the effects of the linker mutations on the tertiary structures of the Hsp70s, intrinsic and extrinsic fluorescence analyses were conducted using tryptophan and ANS fluorescence spectroscopy, respectively. DnaK harbours one tryptophan residue (W^{102}) located in its NBD while PfHsp70-1 possesses a total of

three tryptophan residues located in the NBD (W^{32} and W^{101}) and the SBD (W^{593}). PfHsp70-z harbours only two tryptophan residues within its SBD at positions W^{436} and W^{692}. Generally, it was noted that all the Hsp70s possessed maxima in the range of 330-345 nm (Appendix B18; Figure 3.5). This is consistent with previous reports which demonstrated that in its native form, PfHsp70-1 exhibits fluorescence maxima of approximately 340 nm (Misra and Ramachandran, 2009), PfHsp70-z a maxima of approximately 340 nm (Zininga *et al*., 2016) and DnaK a maxima of 345 nm(Lebepe *et al.*, 2020). Fluorescence spectra derived from this study showed that linker mutant versions of the canonical Hsp70s ($DnaK_{LS}$ and $PfHsp70\text{-}1_{LS}$) exhibited red shifts relative to their wild type forms (Figure 3.5A). This suggests that the tryptophan residues in both $PfHsp70\text{-}1_{LS}$ and $DnaK_{LS}$ were in a more exposed microenvironment than those in the wild type forms of the respective proteins. However, $PfHsp70\text{-}z_{LS}$ displayed a blue shift of approximately 5.5 nm relative to its wild type form (Appendix B18; Figure 3.5A). The findings suggest that the linker mutations induced tertiary structural changes in all three Hsp70s (Figure 3.5; Appendix B18).

To further validate the tertiary structural changes in the Hsp70 linker mutants, ANS fluorescence spectroscopy was conducted. ANS was used as an extrinsic probe to determine the exposed hydrophobic sites on the protein structures. The free ANS control exhibited a fluorescence emission maxima at approximately 520 nm as expected (Appendix B18; Tiwari *et al*., 2009). Generally, for all the three proteins and their mutants, the respective fluorescence spectra exhibited increased quantum which was accompanied by corresponding blue shifts relative to free ANS (Appendix B18; Figure 3.5B). $DnaK_{LS}$ and $PfHsp70\text{-}1_{LS}$ were characterised by relatively higher quantum yields in comparison to their wild type versions (Appendix B18). This suggests that the presence of the PfHsp70-z linker in the canonical Hsp70s (PfHsp70-1 and DnaK) induced more ANS binding events. Furthermore, it implies that $PfHsp70\text{-}1_{LS}$ and $DnaK_{LS}$ were relatively less folded as they possessed more exposed hydrophobic patches than their wild type forms. However, $PfHsp70\text{-}z_{LS}$ possessed lower fluorescence quantum yields than wild type PfHsp70-z, suggesting that the mutant had less exposed hydrophobic regions (Figure 3.5B).

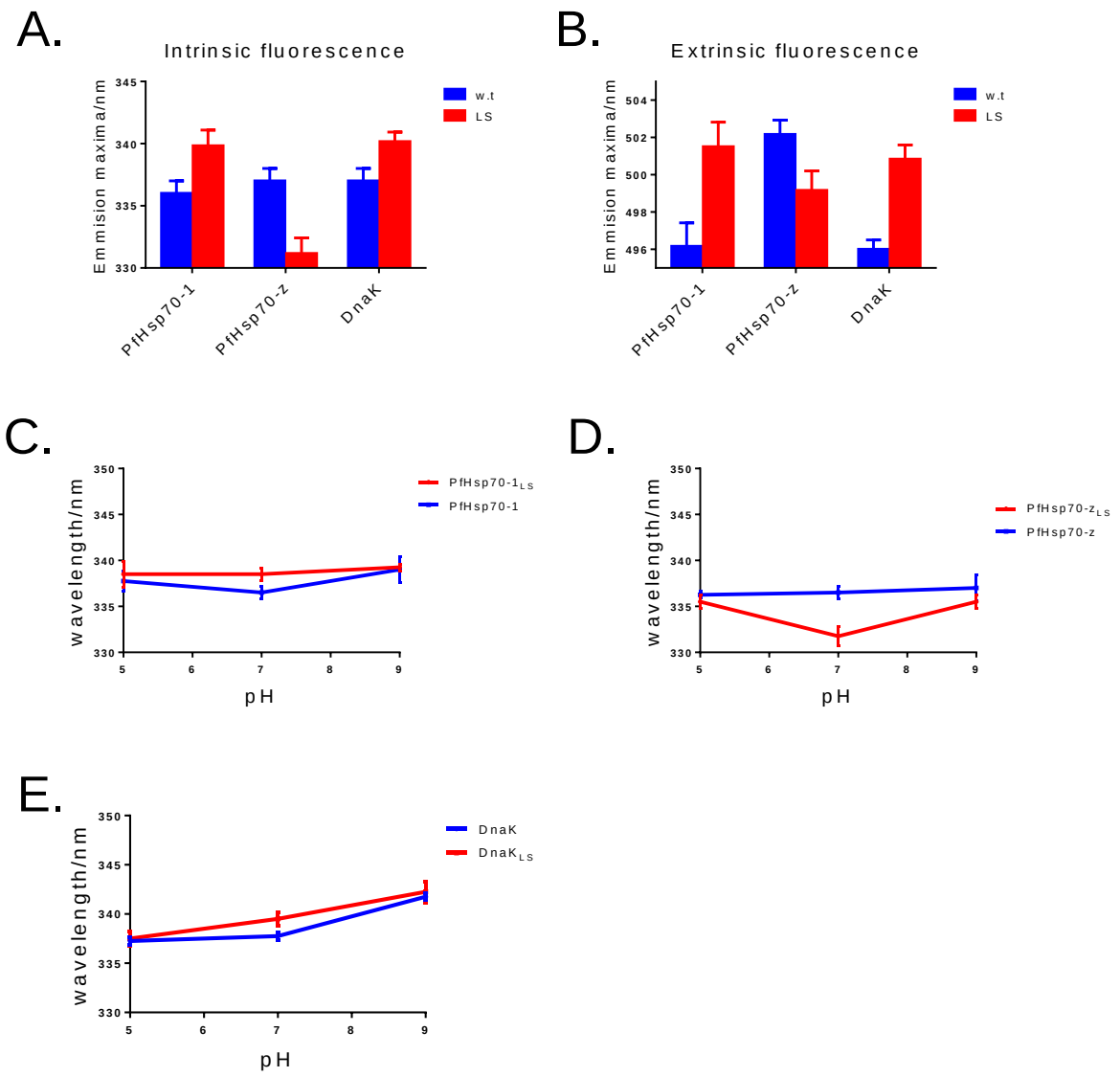

Figure 3.5. Hsp70 linker mutants exhibit unique tertiary structures from their wild type forms

Graphical representation of shifts in maximum emission upon tryptophan fluorescence spectroscopy for the Hsp70s (A). The graphs show ANS fluorescence spectroscopy analysis of recombinant Hsp70s showing spectral shifts (B). Conformational shifts in PfHsp70-1/PfHsp70-1_{LS} (C); PfHsp70-z/PfHsp70-z_{LS} (D) and DnaK/DnaKLS (E) structures upon exposure to a pH range of 5-9 are shown.

The stability of the tertiary structures of the respective Hsp70s was then analysed at pH 5-9. During its development, *P. falciparum* is exposed to pH fluctuations in the range of 4.5-7.4 (Goldberg, 2005; Kuhn *et al*., 2007; Ragheb *et al*., 2009). The PV is thought to maintain an acidic environment (pH 4.5 - 5.0) which corresponds with the optimum pH for proteases involved in haemoglobin degradation (Goldberg, 2005). Based on current findings, at pH 7.4, which corresponds to the pH of the *P. falciparum* cytosol (Ragheb *et al*., 2009), PfHsp70-1 and PfHsp70-1$_{LS}$ had emission maxima of 333 and 337 nm, respectively (Figure 3.5C; Appendix B19). It was however observed that both proteins exhibited red shifts upon any deviation in pH from pH 7.4 (Figure 3.5C). Under the varying pH conditions PfHsp70-1$_{LS}$ exhibited relatively reduced red shifts of approximately ±0.5 nm than its wild type form which had a red shift of approximately ±2 nm. This suggests that PfHsp70-1$_{LS}$ possessed a relatively more stable tertiary structure than PfHsp70-1 under varying pH conditions (Figure 3.5C). This further confirms that the PfHsp70-z linker acted as a module which enhanced the tertiary structural stability of PfHsp70-1.

Under acidic (pH=5) and basic pH (pH=9) conditions, PfHsp70-z $_{LS}$ exhibited a marked red shift of ±4.5 nm compared to its wild type form (Figure 3.5D). This further implies that PfHsp70-z possessed a more stable tertiary structure than PfHsp70-z$_{LS}$. Similarly, both DnaK and its linker mutant were both highly responsive to pH shifts (Figure 3.5E). Both DnaK and DnaK$_{LS}$ exhibited red shifts of approximately 6.5 nm and 3 nm, respectively, upon exposure to alkaline pH (Figure 3.5E). The reduced red shift in DnaK$_{LS}$ suggests stabilization in the protein, possibly due to the presence of the PfHsp70-z linker segment. In addition, under acidic conditions, both DnaK and DnaK$_{LS}$ exhibited blue shifts, signifying that both proteins assumed similar conformations. This difference noted between PfHsp70-1$_{LS}$ and DnaK$_{LS}$ could imply that the plasmodial Hsp70 is functionally specialized and distinguishable from the *E. coli* canonical Hsp70.

3.3.5 Linker mutants of PfHsp70-1 and DnaK exhibit unique tertiary structure conformations upon nucleotide binding

It has been established that Hsp70s are nucleotide dependent chaperones (Zhuravlevela et al., 2013; Zininga *et al*., 2016). Hsp70s undergo conformational changes upon binding and hydrolysing ATP which in turn drives the functional cycle of the chaperones. As such this study sought to explore the effects of linker mutations on nucleotide binding induced conformational changes of Hsp70s. Upon exposure to nucleotides, Hsp70s and their linker mutants assumed unique tertiary structural conformations (Figure 3.6; Appendix B20). In the ATP state, both canonical Hsp70 wild type forms (PfHsp70-1 and DnaK) exhibited blue shifts (Figure 3.6) as previously observed (Qi *et al*., 2013). However, both PfHsp70-1_{LS} and $DnaK_{LS}$ displayed marginal blue shifts of approximately 1 nm upon ATP binding (Figure 3.6). This suggests that, PfHsP70-1_{LS} and $DnaK_{LS}$ both assume unique structural conformations relative to their wild type forms in the ATP bound state. Insertion of the PfHsp70-z linker into the canonical Hsp70s (DnaK and PfHsp70-1) possibly causes the proteins to assume unique conformations upon ATP binding relative to their wild type forms. As expected, the spectra for the canonical Hsp70s (PfHsp70-1 and DnaK) exhibited no significant shift in the ADP state (Figure 3.6). The emission maximum of $DnaK_{LS}$ blue shifted by 1 nm in both the ATP and ADP states, respectively. This suggests that the introduction of the PfHsp70-z linker into DnaK resulted in limited interdomain movement upon nucleotide binding. This phenomenon has previously been reported for PfHsp70-z (Zininga *et al.,* 2016), thus implying that the PfHsp70-z linker is responsible for reduced conformational shifts in response to ATP binding.

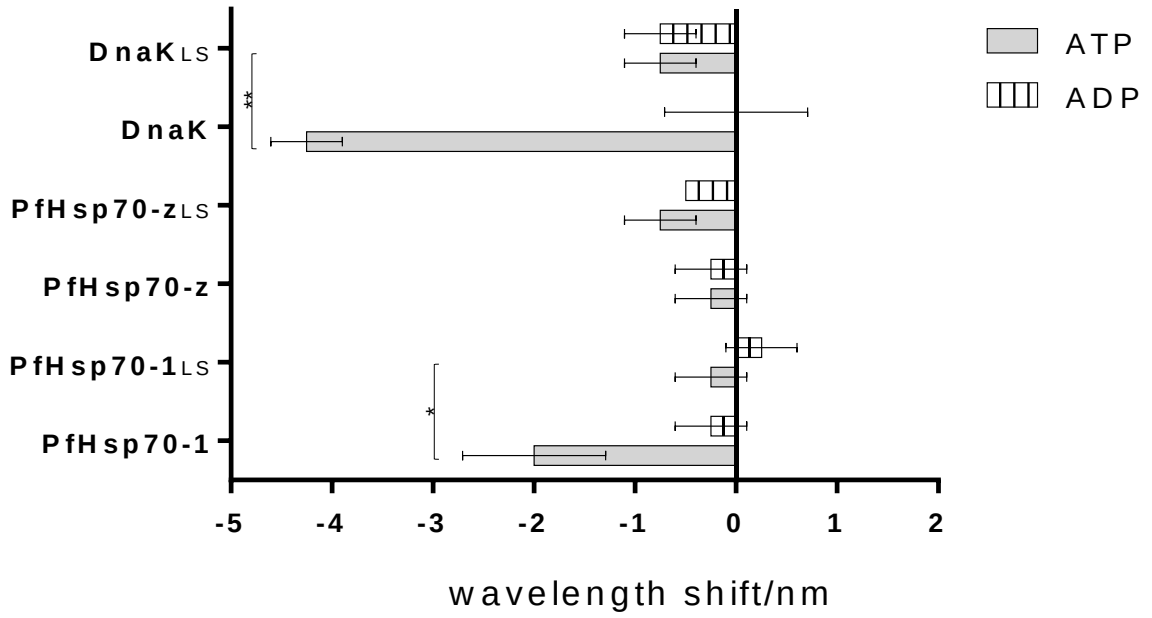

Figure 3.6. Nucleotide induced conformational changes in Hsp70s

The shifts in emission maxima wavelengths in the ATP or ADP states were calculated and plotted for each protein. The results are an average of 2 independent runs. PfHsp70-1 was shown to be possess a significant blue shift in the ATP state, as compared to PfHsp70-1. Statistical analysis was conducted using a One-way ANOVA at *p<0.05*; p<0.01**;p<0.001*** .

As previously demonstrated, PfHsp70-z did not exhibit significant spectral shifts in both the ATP and ADP states (Zininga *et al*., 2016). However, PfHsp70-z$_{LS}$ exhibited marginal spectral variation between the ATP and ADP states (Figure 3.6). In the ATP state, PfHsp70-z$_{LS}$ exhibited a blue shift of approximately 1.5 nm as opposed to PfHsp70-z which had a blue shift of approximately 0.5 nm (Figure 3.6). These findings suggest that PfHsp70-z$_{LS}$ slightly responded to ATP binding as opposed to the largely unresponsive wild type form of the protein.

In order to validate that fluorescence spectral shifts were due to conformational changes on the protein tertiary structure, chaotropic denaturants were used. As expected all the recombinant Hsp70s generally had maxima between 330-345 nm at 0 M urea/ guanidine HCl (Figure 3.7; Ramachandran *et al*., 2011). This suggests that the proteins initially assumed a folded state before the denaturants were introduced (Figure 3.7). Upon incubating the individual proteins at increasing denaturant

concentrations (urea/guanidine HCl), fluorescence intensity decreased (Appendix B21-22). This observation suggests that there was quenching of tryptophan fluorescence intensity possibly caused by increased exposure of charged amino acid residues within the more unfolded structure (Vivian and Callis, 2001). An interesting observation was that PfHsp70-z was more resilient to chaotropic denaturants than its linker mutant version (Figure 3.7). As previously observed in thermal denaturation experiments (Figure 3.4 C-F), the PfHsp70-z linker seemed to confer structural stability to canonical Hsp70s (PfHsp70-1 and DnaK). In contrast, the canonical Hsp70 linker reduced the stability of PfHsp70-z. Taken together, this suggests that the linker of PfHsp70-z enhances the stability of the chaperone.

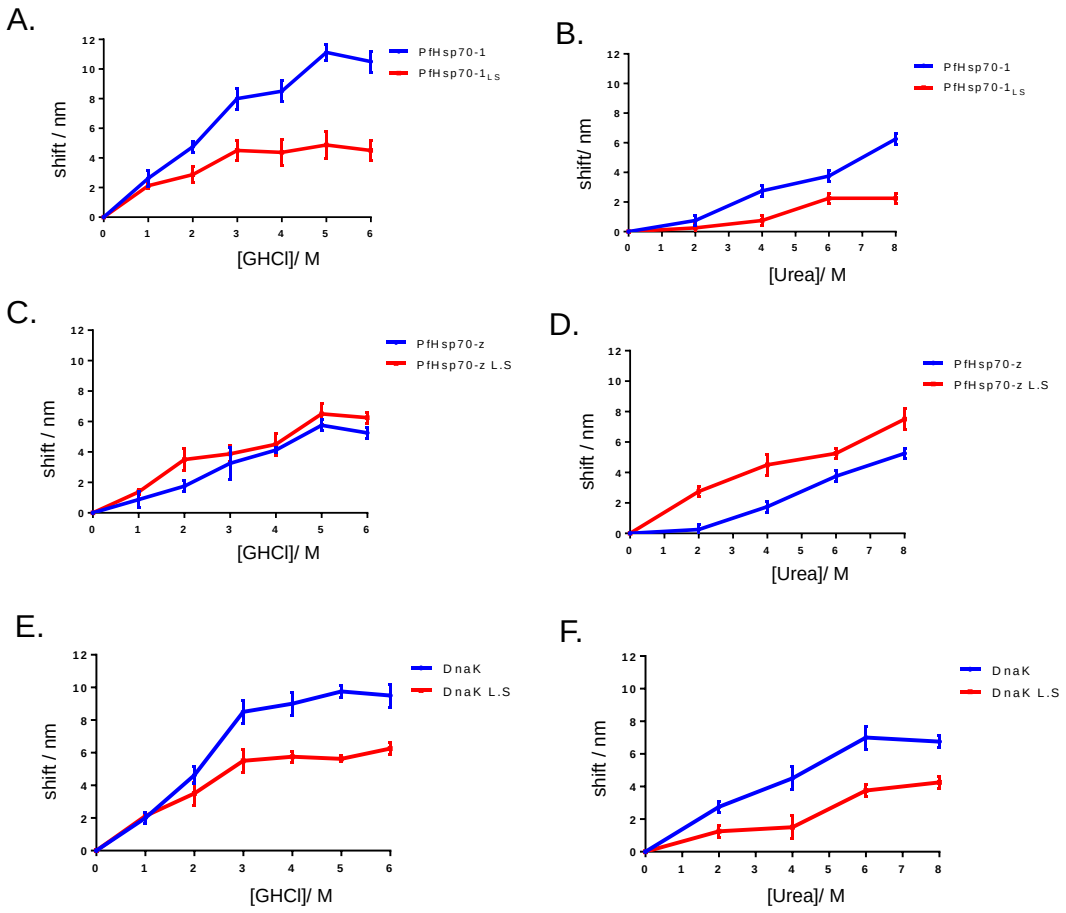

Figure 3.7. PfHsp70-z linker enhances stability of the tertiary structure of the protein in the presence of chemical denaturants

The stability of PfHsp70-1 and PfHsp70-1$_{LS}$ in the presence of a range of 0-6M guanidine HCl (A) and 0-8M urea (B). Inserts show fluorescence graphs. Wavelength shifts were calculated from the 0M denaturant concentration and the red shift intensity was determined. (C) Denaturation of PfHsp70-z and PfHsp70-z$_{LS}$ by guanidine HCl and (D) urea denaturation. (E) DnaK and DnaK$_{LS}$ denaturation by 0-6M guanidine HCl and (D) 0-8M urea.

3.3.6 Hsp70 linker regulates interaction of the chaperone with substrate

The role of the linkers of PfHsp70-1, PfHsp70-z and DnaK in modulating conformational changes upon peptide substrate binding was investigated using tryptophan fluorescence. Since the linker is located at the interface of the NBD and the SBD, it was important to determine the role of this motif in regulating peptide substrate binding. The peptide substrate, NRLLTG, a well-known Hsp70 substrate (Gragerov and Gottesman, 1994; Kabani *et al*., 2003; Mabate *et al*., 2018), induced conformational changes in all the Hsp70 proteins (Figure 3.8).

Upon NRLLTG peptide binding, marginal shifts in emission maxima were recorded in both DnaK and $DnaK_{LS}$ (Figure 3.8). When the NRLLTG peptide concentration was increased from 0 nM to 125 nM, both DnaK and its linker mutant exhibited blue shifts of approximately 1 nm. It has been previously reported that substrate binding only induces intradomain perturbations within the SBD (Swain *et al*., 2007). Since the sole tryptophan residue (W^{102}) of DnaK is located in the NBD, peptide binding at the SBD could have resulted in the observed marginal shift in conformation as substrate binding occurs in the undocked state. PfHsp70-1 also exhibited a blue shift of approximately 2 nm at 125 nM NRLLTG peptide concentration (Figure 3.8). At the same concentration (125 nM) of NRLLTG, PfHsp70-1_{LS} only exhibited a marginal blue shift of approximately 0.5 nm. This suggests that PfHsp70-1 and PfHsp70-1_{LS} assume unique tertiary structure conformations upon peptide substrate binding. PfHsp70-z and PfHsp70-z_{LS} exhibited marginal shifts in their emission maxima in the presence of varying peptide concentrations (Figure 3.8). These findings generally suggest minimal tertiary structural conformational changes in both PfHsp70-z and PfHsp70-z_{LS} upon peptide substrate binding.

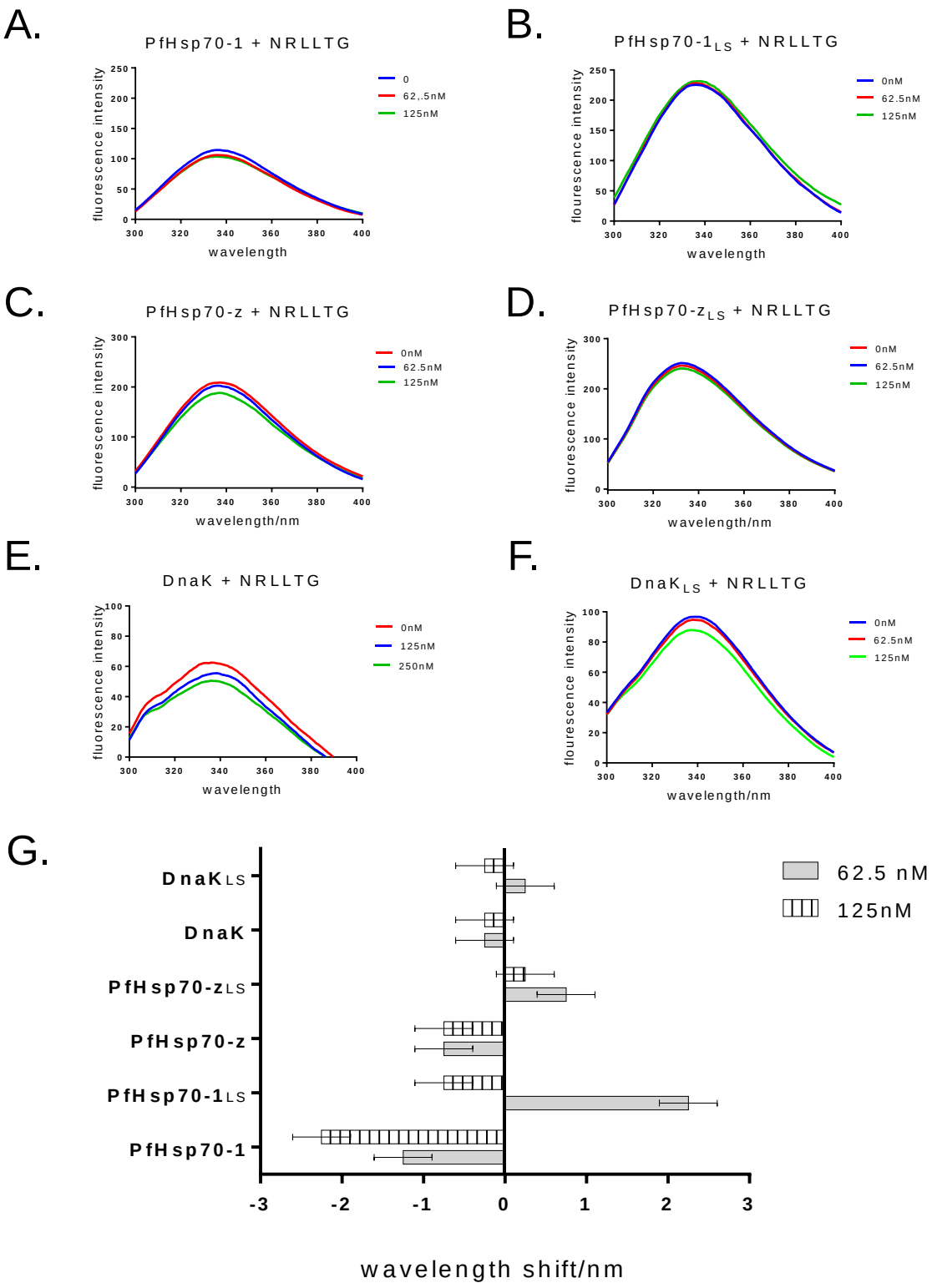

Figure 3.8. Tertiary structure conformational changes of Hsp70s in the presence of peptide NRLLTG

The shifts in emission maxima upon incubation with either 62.5 nM or 125 nM NRLLTG peptide where measured. All the recombinant Hsp70s exhibited marginal shifts within ±2 nm**.**

3.4 Discussion

The current study sought to determine the roles of the linkers of the respective Hsp70s in dictating the secondary and tertiary structural conformations of the proteins. Based on bioinformatics data, the linker swap mutations were predicted to induce conformational changes to PfHsp70-1 and PfHsp70-z (Figure 2.5-7). Although marginal differences were observed in the secondary structure compositions of the wild type Hsp70s relative to their linker mutants (Figure 3.4; Table 3.2), the linker mutations altered the heat stability of the individual proteins. While the PfHsp70-z linker seemed to have a stabilizing effect on PfHsp70-1_{LS} structure in the presence of both thermal and chemical denaturants, the canonical (PfHsp70-1) linker seemed to significantly destabilize PfHsp70-z_{LS} secondary structure (Figure 3.4). The canonical Hsp70 linker has previously been implicated in conferring structural stability (Swain *et al*., 2007). Findings from the current study suggest that the PfHsp70-z linker enhances the stability of Hsp70s under temperature and pH variations. It is therefore conceivable that the linker of PfHsp70-z enhances the stability of the chaperone in parasite cells under thermal stress which is experienced during malaria febrile episodes. In light of the fact that *P. falciparum* is exposed to pH fluctuations in the range of 4.5-7.4 during its development (Goldberg, 2005; Kuhn *et al*., 2007; Ragheb *et al*., 2009), the linker possibly plays an important role in stabilizing PfHsp70-z structure.

The tertiary structural conformation of Hsp70s is an important determinant ensuring their functional capability. This study demonstrated that switching the linkers of canonical Hsp70s (PfHsp70-1 and DnaK) and PfHsp70-z had implications on the overall tertiary structure conformations of the respective proteins (Figure 3.5). This corroborated with the predicted three-dimensional models of the proteins (Figure 2.4 - 6). The blue shift exhibited by PfHsp70-z_{LS} implies that PfHsp70-z_{LS} assumed a more compact conformation as a result of linker substitution. Inversely, PfHsp70-1_{LS} and $DnaK_{LS}$ assumed less compact conformations due to the linker mutations. Overally, these findings imply that the linkers of both canonical (PfHsp70-1 and DnaK) and non-canonical (PfHsp70-z) Hsp70s dictate the overall tertiary conformation of the respective proteins.

ATP binding and hydrolysis are important events for Hsp70 function (Kityk *et al*., 2015; Alderson *et al*., 2016). As such, the study sought to analyse linker-induced conformational changes arising upon nucleotide binding. In the presence of either ATP or ADP, the linker mutants of PfHsp70-1, PfHsp70-z and DnaK exhibited unique tertiary structural conformations relative to their wild type forms (Figure 3.6). In the ATP state, PfHsp70-1 and DnaK both exhibited blue shifts in their respective emission maxima (Figure 3.6). A previously solved crystal structure of DnaK in the ATP state demonstrated that the SBDα residues, L^{507} and M^{515}, make direct contacts with the sole tryptophan residue, W^{102}, in the NBD (Qi *et al*., 2013). In this state, the Trp102 residue becomes sequestrated from solvent as it is packed against SBDα (Swain *et al*., 2007) creating a more hydrophobic tryptophan microenvironment which results in a blue shift in the fluorescence spectrum (Qi *et al*., 2013). Collectively, these findings suggest that the ATP state induces interdomain allosteric coupling of the NBD and the SBD in canonical Hsp70s as previously described (Swain *et al*., 2007; Qi *et al*., 2013). However, PfHsp70-1_{LS} and $DnaK_{LS}$ were characterised by relatively lower blue shifts in the ATP states (Figure 3.6). This suggests that the linker mutants and wild type proteins assumed unique conformations upon ATP binding. Additionally, it also suggests that interdomain coupling was abrogated in both $DnaK_{LS}$ and PfHsp70-1_{LS}. This is in line with previous reports highlighting the role of the DnaK linker in facilitating interdomain coupling in the ATP state (Swain *et al*., 2007; Chiappori *et al*., 2016). Overall, this implies that the linker of PfHsp70-z possibly imposes some restrictions for interdomain communication. Inversely, the linker of canonical Hsp70s (PfHsp70-1 and DnaK) possibly confers flexibility to the protein allowing for enhanced interdomain communication.

Marginal conformational shifts were observed upon NRLLTG peptide substrate binding by all the Hsp70s (Figure 3.8). Binding of substrates at the SBD of canonical Hsp70s is thought to induce a tethered conformation where the individual domains are separated from one another (Zhuravleva and Gierasch, 2011). It is therefore possible that, upon peptide binding, the respective NBDs and SBDs of wild type and linker substitution versions of the Hsp70s, are possibly separated from each other by their linkers. However, it is also possible that, since PfHsp70-z/PfHsp70-z_{LS} harbour two tryptophan residues (W^{436} and W^{692}) located in the SBD, binding of the peptide could

have possibly induced local structural changes that maintained the hydrophobicity around the tryptophan residues. It was interesting to note that although binding of ATP at the NBD induced major shifts in tertiary structural conformation, substrate binding at the SBD only induced minor conformational shifts.

Overall findings from this study suggest that the linker motifs of both canonical Hsp70s and Hsp110 are important in modulating the structural conformations of the proteins. The findings also imply that the linker of PfHsp70-z is important in maintaining the structural integrity of the chaperone under stress conditions. It also suggests that the linkers of PfHsp70-1 and PfHsp70-z are important determinants in the function of the essential parasite chaperones during *P. falciparum* development. As such, there was need to further investigate how these conformational changes would impact on the chaperone functions of the respective proteins.

CHAPTER 4

Determination of the role of the linker motifs of PfHsp70-1 and PfHsp70-z in modulating the function of the chaperones

4.1 Introduction

The Hsp70 family of molecular chaperones are among some of the most conserved molecules (Zhang, 2014). The proteins constitute a central hub for cellular proteostasis under both physiological and stress conditions (Calloni *et al*., 2012). Hsp70s bind to a broad range of polypeptide substrates through their hydrophobic substrate binding cleft (Zuiderweg *et al*., 2014; Roseinzweig *et al*., 2017). The versatility of Hsp70 in substrate recognition allows it to suppress aggregation and facilitate the refolding of virtually all types of misfolded protein substrates (Xu *et al*., 2012; Clerico *et al*., 2015; Mayer *et al*., 2019). Hsp70 is a nucleotide dependent chaperone. During protein folding, ATP binding at the NBD induces intradomain re-orientations between subdomains I and II of the NBD which subsequently reduce substrate binding affinity at the SBD (Gassler *et al*., 1998). On the other hand, ATP hydrolysis results in closure of the SBDα thereby stabilizing substrate binding (Clerico *et al*., 2015; Stetz *et al*., 2015). ATP hydrolysis is thus a rate limiting step in the functional cycle of Hsp70. Hsp40 is known to enhance the rather low basal ATPase activity of Hsp70, thus improving the efficiency of the folding process (Mayer *et al*., 2015).

In view of the fact that the distance between the nucleotide binding cleft and the substrate binding cleft is approximately 50 Å, allosteric communication between the two domains is important for Hsp70 chaperone function (Zuiderweg *et al*., 2012). The linker of the *E. coli* canonical Hsp70, DnaK, has previously been implicated in facilitating allosteric coordination between the NBD and SBD (Mayer *et al*., 2015; English *et al.,* 2017). Apart from the linker, the NBD:SBD interface is also thought to constitute an important feature for allosteric regulation of Hsp70 function. Thus flexibility or rigidity of the linker segment influences allosteric function of Hsp70. In this way, the linker regulates Hsp70 chaperone function. The chaperone function of canonical Hsp70s thus largely relies on allosteric shifts between a high and low substrate affinity state at the SBD which occurs in response to nucleotide binding at the NBD (Clerico, 2015; Chiappori *et al*., 2016). In Hsp110s, allosteric regulation has generally been reported to be absent (Stetz *et al*., 2014; Kumar *et al*., 2019). However, since plasmodial Hsp110 (PfHsp70-z) possesses a linker that exhibits sequence divergence from that of the well studies yeast Hsp110 (Sse1) (Liu and Hendrickson,

2007; Pollier *et al*., 2008), its role in modulating the protein's chaperone function is unknown.

Unlike PfHsp70-1, PfHsp70-z chaperone function is nucleotide independent. This distinction is thought to be on account of the varied roles of the linkers of the two proteins in regulating nucleotide binding (Chakafana et al., 2019b). As such, PfHsp70-z is generally considered a more effective holdase than PfHsp70-z since its holdase function is less inhibited by ATP as is observed in PfHsp70-1 (Shonhai et al., 2008 ;Zininga et al., 2016). On the other hand, PfHsp70-1 though a less effective holdase than PfHsp70-z, is thought to be a more effective refolding chaperone, possibly through its possession of a flexible linker. Thus, PfHsp70-z and PfHsp70-1 linkers may account for delineation of the chaperone responsibilities of the two proteins. As established before (Section 2.3.5), although PfHsp70-1 and PfHsp70-z share some interactors, they also exhibit an array of functional interactors. This potentially highlights the specialised nature of their function. Hence, the current study explored the role of the PfHsp70-1 and PfHsp70-z linkers in regulating the chaperone functions of the proteins. To do this, linker swap mutants of the two proteins and a PfHsp70-z linker insertion mutant of DnaK were used in the study. The main import of the study was to establish how the linker of PfHsp70-z versus that of PfHsp70-1 regulate substrate binding and chaperone functions of the proteins.

The objectives of this study were to:

(i) determine the nucleotide binding affinities of PfHsp70-1_{LS}, PfHsp70-z_{LS} and $DnaK_{LS}$ relative to their respective wild type forms;

(ii) analyse the peptide binding affinities of PfHsp70-1_{LS} , PfHsp70-z_{LS}, $DnaK_{LS}$ relative to their respective wild type forms;

(iii) evaluate the relative ATPase activities of PfHsp70-1_{LS}, PfHsp70-z_{LS}, and $DnaK_{LS}$ and their respective wild type versions;

(iv) investigate the chaperone function of wild type PfHsp70-1, PfHsp70-z, DnaK relative to their linker mutants and to

(v) investigate the functional implications of inserting the linker of PfHsp70-z into *E. coli* DnaK.

4.2 Materials and methods

4.2.1 Materials

The reagents and materials used in this study are listed in Appendix C. The NBDs of PfHsp70-1 (PfHsp70-1$_{NBD}$) and PfHsp70-z (PfHsp70-z$_{NBD}$) were introduced in functional assays as controls. The NBD controls used were devoid of the respective linker motifs (Figure 4.1). The following model Hsp70 peptides were used to explore the substrate binding preference of the Hsp70s; NRLLTG, ALLLMYRR and GFRVLLMYRF. NRLLTG has previously been described as a model substrate for the *E. coli* canonical Hsp70 DnaK (Xu *et al*., 2012) while ALLLMYRR is a model substrate derived from chicken mitochondrial aspartate amino-transferase (Mayer and Bukau, 2005; Mabate *et al*., 2018). The third substrate peptide, GFRVVLMYRF, was originally derived from the firefly luciferase amino acids 256-268 (Han and Christen, 2004). These peptides representing typical Hsp70 substrates and their asparagine enriched versions (NRNNTG, ANNNMYRR, and GFTNNNMYRF) have previously been described (Mabate *et al*., 2018).

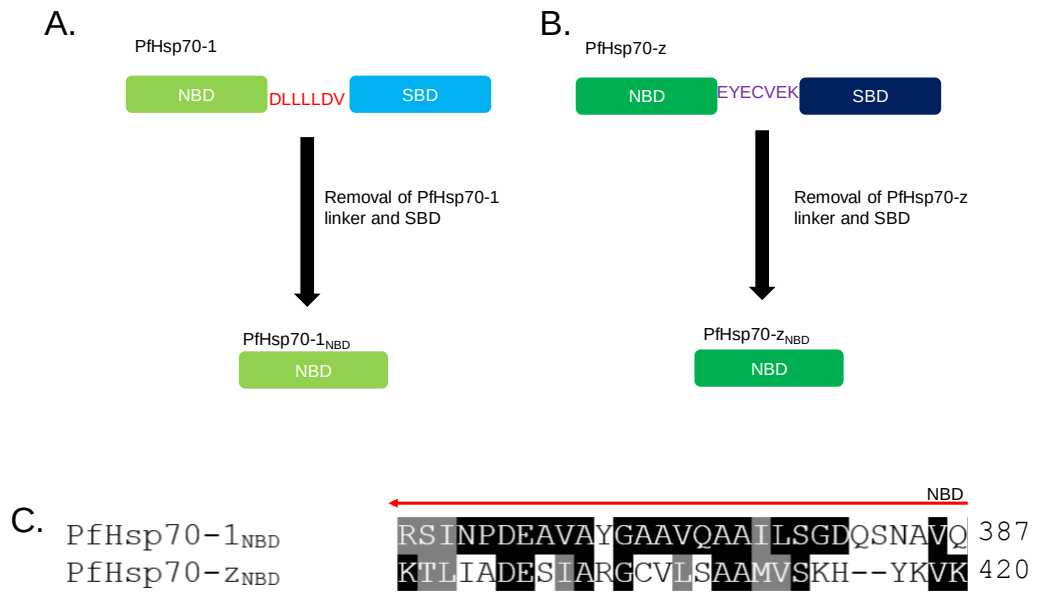

Figure 4.1. Design of PfHsp70-1$_{NBD}$ and PfHsp70-z$_{NBD}$

PfHsp70-1$_{NBD}$ (A) and PfHsp70-z$_{NBD}$ (B) lack the linker and SBD segments of PfHsp70-1 and PfHsp70-z, respectively. The NBD of PfHsp70-1 is represented by residues 1-387, while PfHsp70-z$_{NBD}$ consists of residues 1-420.

4.2.2 Determination of ATP binding affinity

The equilibrium nucleotide binding affinity assay of the proteins was conducted by SPR analysis using the BioNavis™ 420A ILVES MP SPR (BioNavis, Tampere, Finland) system at 25 °C. Degassed PBS-Tween 20 (4.3 mM Na_2HPO_4, 1.4 mM KH_2PO_4, 137 mM NaCl, 3 mM KCl, 0.005 % (v/v) Tween 20, and 20 mM EDTA; pH 7.4) was used as running buffer (Zininga *et al*., 2016; Mabate *et al*., 2018). The proteins (PfHsp70-1, PfHsp70-1_{LS}, PfHsp70-1_{NBD}, PfHsp70-z, PfHsp70-z_{LS}, PfHsp70-z_{NBD}, DnaK and $DnaK_{LS}$) were each immobilized in parallel as ligands onto gold functionalized three-dimensional carboxymethyl dextran sensors (CMD three-dimensional 500L) (BioNavis, Tampere, Finland). Individual proteins were each immobilized onto the CMD three-dimensional 500L sensor surfaces at a concentration of 100 µg/ml. Immobilization of ligands was achieved via activation of the chip surface by an equimolar mixture of 1-Ethyl-3-(3-dimethylaminopropyl)carbodiimide (EDC) and N-Hydroxy-succinimide (NHS) for amine coupling as described by the manufacturer (Bionavis, Tampere, Finland). Following immobilization, ATP was then injected in series in aliquots of 0, 1.25, 2.5, 5, 10, and 20 nM and at a flow rate of 50 µl/min into each flow channel. Association between ligand and analyte at a steady state was allowed for 2 min while dissociation was monitored for a total of 3 min. The steady-state equilibrium constant data were processed and analysed using TraceDrawer software version 1.8 (Ridgeview Instruments, Sweden). Kinetic evaluations were conducted on the sensograms after all five ATP concentrations were fitted using a 1:1 Langmuir model. This was followed by equilibrium affinity analysis. Statistical analyses were conducted using a One-way ANOVA at a 99% confidence interval ($p<0.01$).

4.2.3 ATPase activity assays

The ATPase activities of PfHsp70-1_{LS}, PfHsp70-z_{LS} and $DnaK_{LS}$ relative to their wild type forms were determined using a colorimetric ATPase activity assay as previously described (Zininga *et al*., 2016, Mabate *et al*., 2018). Initially, 0.4 µM of each Hsp70 was incubated for 5 hrs in HKMD buffer (10 mM HEPES-KOH pH 7.5, 100 mM KCl, 2 mM $MgCl_2$, 0.5 mM DTT) with ATP concentrations varying between 0 - 5 mM. Boiled samples of each Hsp70 were also used as non-enzymatic controls to monitor spontaneous hydrolysis of ATP. Three independent assay runs were conducted for

each protein, using different protein batches. To determine kinetics for the ATPase activity of the individual proteins, Michaelis-Menten plots were generated using GraphPad Prism 6.05.

4.2.4 Determination of peptide binding affinity

The peptide binding affinities of PfHsp70-1_{LS}, PfHsp70-z_{LS}, $DnaK_{LS}$ and their respective wild type forms were determined by SPR. Analyses were conducted with the BioNavis 420A ILVES MP SPR system at room 25 °C using degassed PBS-Tween (4.3 mM Na_2HPO_4, 1.4 mMKH_2PO_4, 137 mM NaCl, 3 mM KCl, 0.005 % (v/v) Tween 20, and 20 mM EDTA; pH 7.4) as running buffer. The following proteins were immobilized as ligands onto CMD three-dimensional chips as previously discussed (Section 4.2.1); PfHsp70-1, PfHsp70-1_{LS}, PfHsp70-z, PfHsp70-z_{LS}, DnaK and $DnaK_{LS}$. Aliquots of individual peptides (NRLLTG, NRNNTG, ALLLMYRR, ANNNMYRR, GFTVVLMYRF, and GFTNNNMYRF) were then injected as analytes at concentrations of 0, 1.25, 2.5, 5, 10, and 20 nM and a flow rate of 50 µl/min in each flow channel. Association between analyte and ligand was allowed for 3 min and dissociation was monitored for 5 min. Steady-state equilibrium constant data were processed and analysed using TraceDrawer software version 1.8 (Ridgeview Instruments, Sweden).

4.2.5 Aggregation suppression assays

The capability of PfHsp70-1_{LS}, PfHsp70-z_{LS} $DnaK_{LS}$ and their wild type forms to suppress heat-induced aggregation of malate dehydrogenase (MDH) from porcine heart (Sigma-Aldrich, USA) and firefly luciferase (VWR Life Sciences, USA) was investigated as previously described (Shonhai *et al*., 2008, Zininga *et al*., 2016) with minor adjustments. For each assay, 0.2 µM recombinant proteins (PfHsp70-1, PfHsp70-1_{LS}, PfHsp70-z, PfHsp70-z_{LS}, DnaK and $DnaK_{LS}$) were each incubated with equimolar MDH or luciferase concentrations. The respective reaction mixes were each incubated at 51 °C for 1 hr. Optical density (OD) readings were taken every 5 mins at 340 nm using a SpectraMax M3 spectrometer (Molecular Devices, USA). The resultant ODs were then converted to aggregation percentages relative

to aggregation level of MDH/luciferase (set as 100 %) and data was analysed using GraphPad Prism 6.05 software (San Diego, USA). To further determine the effect of nucleotides on the chaperone function of Hsp70s and linker mutants, the reaction was repeated in the presence of 5 mM ATP/ADP. A non-chaperone control, BSA, was also incubated with MDH/luciferase.

4.2.6 Luciferase refolding assay

To evaluate the capability of the recombinant Hsp70s to refold denatured luciferase, a refolding assay was conducted using a previously described protocol (Mattoo *et al*., 2013; Sarbeng *et al*., 2015) with minor modifications. Briefly, 100 nM luciferase was denatured in buffer A (25 mM HEPES-KOH, pH 7.5, 100 mM KOAc, 10 mM $Mg(OAc)_2$, 2 mM DTT, and 3 mM ATP) at 42 °C for 20 mins. To initiate luciferase refolding, chaperone combinations comprising 3 µM Hsp70 (PfHsp70-1/PfHsp70-1_{LS}), 0.5 µM Hsp40 (PfHsp40) and 3 µM Hsp110 (PfHsp70-z/PfHsp70-z_{LS}) were added to the heat denatured luciferase samples. The refolding reaction mix was then incubated at 25 °C for 30 mins to allow the chaperones to refold the previously denatured luciferase. The luciferase activity was determined by mixing one part of the refolding reaction components with twenty-five parts of the luciferin substrate. Luminescence was monitored at 526 nm using the SpectraMax M3 spectrometer (Molecular Devices, USA). Aliquots of native and denatured luciferase without suspended chaperones were used as positive and negative controls, respectively.

4.2.7 Complementation assays

Complementation assays were conducted to investigate the *in cellulo* functional capabilities of $DnaK_{LS}$ in conferring thermostability to *E. coli* cells as previously described by Shonhai *et al*. (2005). These assays were conducted using *E. coli* dnaK756 and *E. coli* BB2393 cells (Table 4.1). *E. coli* dnaK756 expresses a DnaK that has three glycine-to-aspartate substitutions at residues G32D, G455D, and G468D (Buchbeger *et al*., 1994). These mutations have been reported to cause defects in intrinsic and GrpE-stimulated ATPase activities of the protein (Buchbeger *et al*., 1994). The *E. coli* BB2393 strain expresses a truncated version of DnaK that is non-functional, thus making this strain sensitive to heat stress (Spence *et al*., 1990).

Complementation assays were conducted according to a protocol previously described by Shonhai *et al*., (2005). Individual cell lines were each transformed with pQE30/DnaK, pQE30/DnaK$_{LS}$ and pQE30 plasmids. Transformants were then inoculated and grown overnight at 37 °C in 2YT broth supplemented with respective antibiotics. Overnight cultures were then upscaled tenfold by transferring into fresh broth and cultures were allowed to mid-log phase (OD_{600} = 0.6) at 37 °C. The overexpression of the recombinant proteins was induced at mid log phase with 1 mM IPTG. Cells were then allowed to grow to an OD_{600} reading of 2 (post induction) before all the cultures were standardized to the same density of OD_{600}= 0.2. Serial dilutions were then made and cells were spotted onto 2YT agar plates supplemented with 100 µg/ml ampicillin and 50 µM IPTG. The plates were then incubated overnight at permissive and non-permissive growth temperatures, respectively (Table 4.1).

Table 4.1 *E. coli* strains used in complementation assays

Cell line	Antibiotics	PGT	NPGT	References
E. coli BB2393	Chloramphenicol, Tetracycline	30.0 °C	40.0 °C	Spence *et al*., 1990
E. coli dnak756	Kanamycin, Tetracycline	37.0 °C	43.5 °C	Buchbeger *et al*., 1994 Shonhai *et al*., 2005

*PGT: Permissive growth temperature; NPGT: Non permissive growth temperature

4.3 Results

4.3.1 The linkers of PfHsp70-z, PfHsp70-1 and DnaK influence the ATP binding affinities of the chaperones

Based on tryptophan spectroscopy based studies, the linker swap mutants of PfHsp70-1, PfHsp70-z, DnaK assumed unique tertiary structural conformations upon ATP binding (Section 3.3.7). As such, it was important to establish the role of the linker of Hsp70 in regulating the steady state ATP binding affinity. With the exception of PfHsp70-z, the Hsp70s managed to reach steady state at a concentration of 5 nM ATP (Figure 4.2 A). This suggests that PfHsp70-z possessed relatively lower ATP binding affinity than the other Hsp70s. This observation is in agreement with previous findings which reported that PfHsp70-z possesses lower ATP binding affinity than PfHsp70-1 (Zininga *et al*., 2016). On the other hand, PfHsp70-z_{LS} exhibited significantly higher ATP binding affinity (K_D= 0.42 µM) than its wild type form which had a K_D value of 2.41 µM (Figure 4.1 B; Table 4.2). This possibly suggests that the linker of canonical Hsp70 improved the ATP binding affinity of this chaperone. Interestingly, PfHsp70-1 (K_D= 0.174 µM) exhibited higher ATP binding affinity than its linker swap variant, PfHsp70-1_{LS} (K_D= 0.537 µM). However, there was no significant difference in the ATP binding affinities of PfHsp70-1_{NBD} and the full length proteins, PfHsp70-1 and PfHsp70-1_{LS} (Table 4.2). Notably, $DnaK_{LS}$ and its wild type form exhibited comparable ATP binding affinities (Table 4.2; Figure 4.2). This implies that ATP binding affinity in DnaK is not influenced by the linker but is possibly regulated by the nucleotide binding cleft itself. Furthermore, it may suggest that the linker mutation differentially modulates plasmodial and *E. coli* Hsp70s.

A.

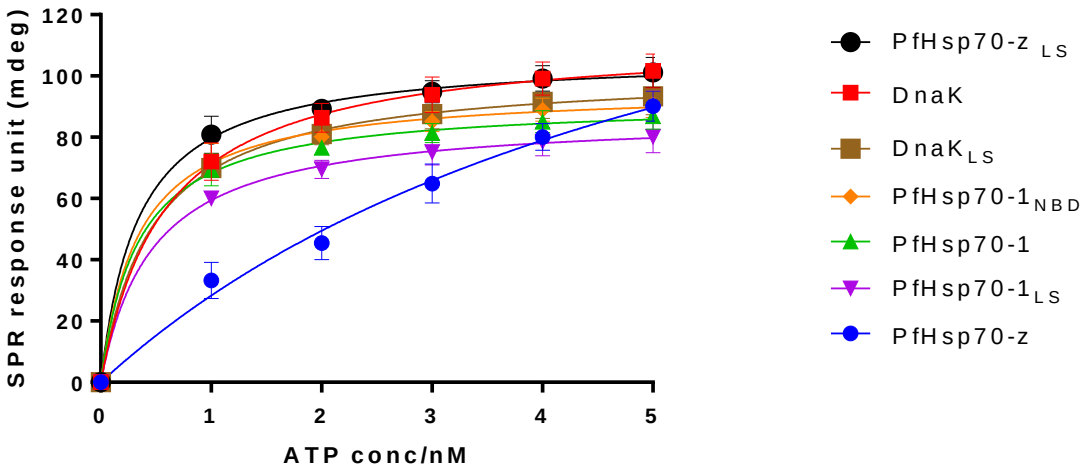

B.

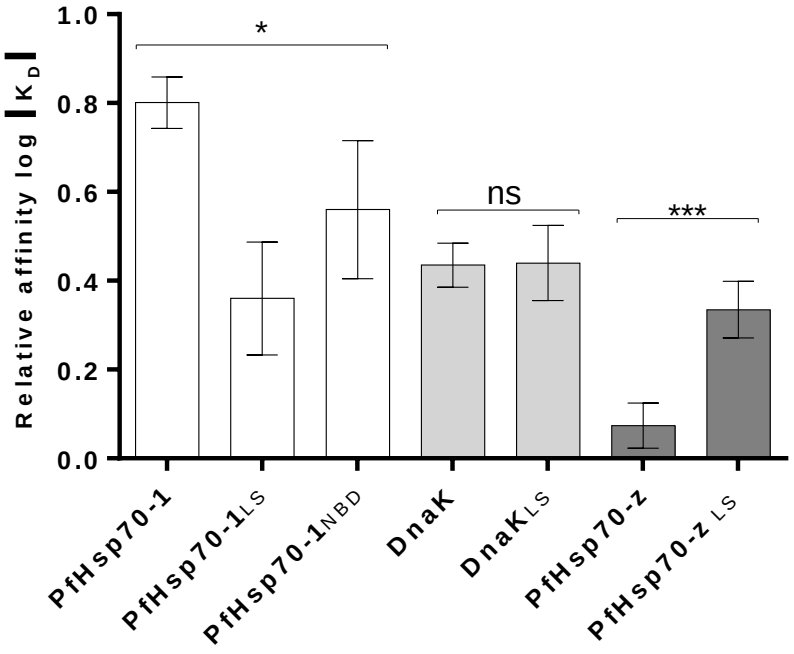

Figure 4.2. PfHsp70-z$_{LS}$ exhibits enhanced ATP binding affinity compared to its wild type form (A) Equilibrium binding affinity curve for wild type and linker mutants of PfHsp70-1, PfHsp70-z and DnaK at a concentration range of 0-5 nM. (B) The relative affinities for ATP binding exhibited by the Hsp70s were calculated from the reciprocal log of the K_D value of each protein. Statistical analysis was conducted using a One-Way ANOVA at p<0.05*; p<0.01**;p<0.001**.

Table 4.2. Comparative affinities for ATP of Hsp70 chaperones at equilibrium binding phase

	K_D (μM)	χ^2
PfHsp70-1	0.174 (±0.07)*	1.73
PfHsp70-1$_{LS}$	0.537 (±0.04)*	2.71
PfHsp70-1$_{NBD}$	0.351 (±0.01)	0.47
PfHsp70-z	2.410 (±0.01)***	2.57
PfHsp70-z$_{LS}$	0.442 (±0.02)***	1.12
DnaK	0.398 (±0.08)	1.38
DnaK$_{LS}$	0.314 (±0.04)	1.06

The K_D values for the individual proteins were derived from three independent analyses of the ATP binding affinity. Standard errors represent three independent assays conducted using independent protein batches. Statistical significance was conducted using a One-Way ANOVA at p<0.5*; *p<0.1***; *p<0.01****.

4.3.2 The linker of Hsp70 regulates ATP hydrolysis

ATPase activity assays were conducted to investigate the effect of the linker mutations on the hydrolysis of ATP by Hsp70s. The released inorganic phosphate was monitored upon ATP hydrolysis. PfHsp70-1 exhibited a K_m value of 26.29 nmol/min/mg (Table 4.3), which were comparable to those observed in previous studies (Matambo *et al*., 2004; Zininga *et al*., 2016). In general, it was observed that the linker mutations altered the basal ATPase activity of the respective Hsp70s (Figure 4.3). The catalytic efficiency of DnaK$_{LS}$ was reduced by half, relative to DnaK (Figure 4.3 B; Table 4.3). Similarly, PfHsp70-1$_{LS}$ possessed a significantly lower basal ATPase activity than its wild type form (Figure 4.3 C; Table 4.3). The lower ATP turnover rates exhibited by PfHsp70-1$_{LS}$ and DnaK$_{LS}$ imply that the linker motifs of canonical Hsp70s are important determinants of ATPase activity. On the other hand, PfHsp70-z$_{LS}$ exhibited a three-fold increase in basal ATPase activity relative to wild type PfHsp70-z (Figure 4.3 D; Table 4.3). Furthermore, the linker of PfHsp70-z suppressed the ATPase activity of both PfHsp70-1 and DnaK. This implies that the presence of the PfHsp70-1 linker in PfHsp70-z enhanced the catalytic efficiency of PfHsp70-z$_{LS}$.

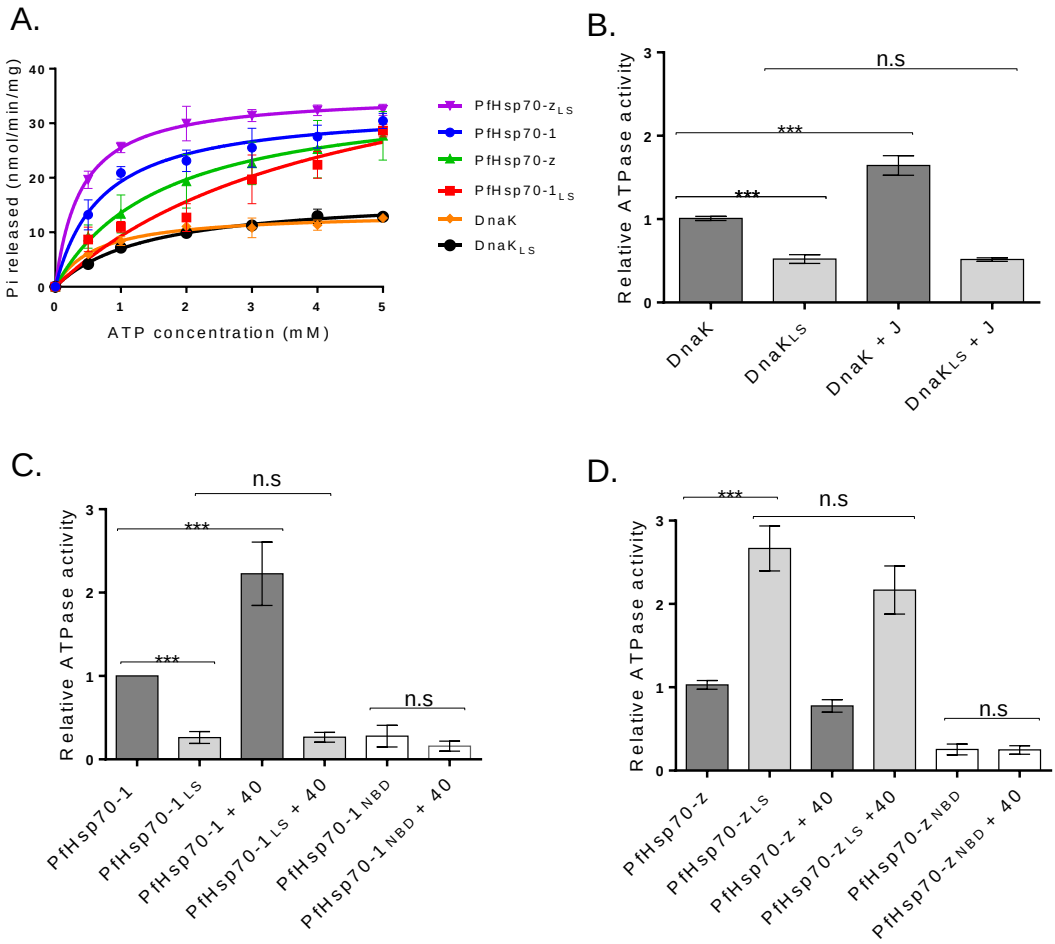

Figure 4.3. The linkers of Hsp70s regulate ATPase activity of the proteins
(A) Representative Michaelis-Menten curves for basal ATPase activity of PfHsp70-1, PfHs70-z, DnaK and their respective linker substitution mutant versions were plotted. (B) Basal and Hsp40-induced ATPase activity of DnaK and $DnaK_{LS}$. All ATPase activity rates were calculated based on catalytic efficiency. (C) Basal and PfHsp40-induced ATPase activity of full length PfHsp70-1 and $PfHsp70\text{-}1_{LS}$. (D) ATPase activity of PfHsp70-z/$PfHs70\text{-}z_{LS}$ with PfHsp40. Statistical analysis was conducted using a One-Way ANOVA at $p<0.05$*; $p<0.01$**;$p<0.001$**.

The stimulation of Hsp70 ATPase activity by the co-chaperone, Hsp40, was also investigated for the linker mutants and respective wild type Hsp70s. Canonical Hsp70s (PfHsp70-1 and DnaK) exhibited approximately two-fold increases in ATPase activity in the presence of Hsp40s (Table 4.3; Fig 4.3). The stimulation of the ATPase activities of both PfHsp70-1 and DnaK by PfHsp40 and DnaJ, respectively has been reported (Liberek *et al*., 1991; Botha *et al*., 2011; Alderson *et al*., 2016). Interestingly, PfHsp40 and DnaJ could not stimulate the ATPase activities of the linker variants of PfHsp70-1 and DnaK (Fig 4.3 B, C). This suggests that the linker of PfHsp70-z abrogated the stimulation of PfHsp70-1 and DnaK by their respective Hsp40 co-chaperones.

Table 4.3 ATPase activity kinetics for Hsp70s

Chaperones	K_m (µM)	V_{max} (nmol/min/mg)	K_{cat} /sec^{-1}	Catalytic efficiency ($M^{-1}sec^{-1}$)
DnaK	161.4 (±5.4)	13.09 (±7.3)	0.54	3.38e^3
$DnaK_{LS}$	314.9 (±8.1)	11.50 (± 3.2)	0.47	1.52e^3
DnaK + DnaJ	106.1 (±6.9)	14.83 (±7.2)	0.61	5.85e^3
$DnaK_{LS}$ + DnaJ	350.9 (±3.1)	10.29 (±2.9)	0.42	1.22e^3
PfHsp70-1	707.2 (±5.8)	26.29 (±6.6)	1.09	1.54e^3
PfHsp70-1_{LS}	1332 (±40.1)	15.02 (±4.7)	0.62	0.46e^3
PfHsp70-1 + PfHsp40	280.0 (±7.6)	29.31 (±5.3)	1.22	4.36e^3
PfHsp70-1_{LS} + PfHsp40	1417.2 (±9.6)	15.98 (±4.1)	0.66	0.47e^3
PfHsp70-1_{NBD}	1833.5 (±2.1)	23.24 (±7.4)	0.96	0.53e^3
PfHsp70-1_{NBD} + PfHsp40	1855.9 (±5.3)	26.30 (±4.3)	1.09	0.59e^3
PfHsp70-z	290.2 (±9.2)	23.03 (±2.9)	0.95	3.33e^3
PfHsp70-z_{LS}	97.7 (±3.9)	26.62 (±3.1)	1.10	11.35e^3
PfHsp70-z + PfHsp40	310.7 (±5.7)	15.74 (±5.5)	0.65	2.11e^3
PfHsp70-z_{LS} + PfHsp40	107.2 (±7.0)	16.58 (±6.3)	0.69	6.44e^3
PfHsp70-z_{NBD}	1214.4 (±8.1)	14.96 (±5.9)	0.62	0.513e^3
PfHsp70-z_{NBD} + PfHsp40	1260.3 (±9.8)	19.72 (±8.3)	0.82	0.65e^3

Km-is represents the substrate concentration at which the reaction rate is half its maximum speed. *Vmax*- represents the maximum rate of the catalysis reaction in nmol/mg/min. The data presented is from three independent assays with mean and standard deviations. K_{cat} represents the turnover number or the number of substrate molecules catalysed per unit time calculated as $V_{max}/[E_0]$. Catalytic efficiency was calculated as K_{cat}/K_M.

The Hsp70 linker is known to make contacts with the HPD motif located in the J domain of Hsp40 to facilitate ATP hydrolysis (Alderson *et al*., 2016). This suggests that the linker of Hsp70 is directly modulated by Hsp40. However, PfHsp40 did not stimulate the ATPase activity of PfHsp70-z and PfHsp70-z_{LS} (Fig 4.3B; Table 4.3). This suggests that the presence of the linker of canonical Hsp70 was not sufficient to facilitate modulation of the ATPase activity of this Hsp110 by Hsp40. This further suggests that stimulation by Hsp40 is dependent on contacts present in canonical Hsp70s but that are absent in Hsp110s. However, a previous study demonstrated that the ATPase activity of human Hsp110 (HspH1) was stimulated by Hsp40 (DnaJA1) (Mattoo *et al*., 2014). Since PfHsp40 failed to stimulate the ATPase activity of PfHsp70-z, this suggests that human Hsp110 is functionally distinguishable from

PfHsp70-z. Furthermore, the two proteins are marked by distinct linker segments which may account for their varied response to Hsp40 (Figure 2.2 C). To further validate the role of the linker in modulating the ATPase activity of PfHsp70-1 and PfHsp70-z, the assay was repeated using the NBDs of the proteins which lacked the linker motifs (Figure 4.1). It was observed that PfHsp40 failed to stimulate the ATPase activity of both PfHsp70-1_{NBD} and PfHsp70-z_{NBD} (Figure 4.3 B, C). The failure of PfHsp40 to stimulate the ATPase activity of PfHsp70-1_{NBD} highlights the role of both the linker and the SBD in regulating Hsp40-mediated ATP hydrolysis of Hsp70. This observation is in line with previous reports where Hsp40 failed to stimulate ATPase activity of the NBD of the human Hsp70, HscA (Alderson *et al*., 2014).

4.3.3 Hsp70 linker regulates substrate binding affinity and selectivity

The SBDs of Hsp70s are functionally promiscuous and allow for the binding of short degenerate hydrophobic peptide motifs of approximately seven residues (Rudiger *et al*., 1997; Rosenzweig *et al*., 2017). However, approximately 30% of the *P. falciparum* proteome is characterized by asparagine repeat segments (Pallares *et al*., 2018). As such, the study sought to investigate the roles of the linkers of PfHsp70-1, PfHsp70-z and DnaK in regulating substrate binding affinity and preference of the chaperones. The binding affinities for the model peptide substrates NRLLTG, ALLLMYRR, GFTVVLMYRF and their asparagine enriched versions (NRNNTG, ANNNMYRR, GFTNNNMYRF) were determined by SPR.

The canonical Hsp70s (PfHsp70 and DnaK) exhibited reduced affinity for peptide substrates in the ATP state as expected (Table 4.4; Liebscher and Roujeinikova, 2009; Mabate *et al*., 2018). Inversely, the ADP state increased the substrate binding affinity of the canonical Hsp70s as expected (Table 4.4; Kampinga and Craig, 2010). Interestingly, the peptide binding affinities for both PfHs70-1_{LS} and $DnaK_{LS}$ were largely independent of nucleotide states (Table 4.4). This suggests that the linker motif present in PfHsp70-1 and DnaK is important for allosteric communication between the NBD and SBD of the chaperones. This in turn makes binding of PfHsp70-1 and DnaK to substrate a nucleotide dependent process (Shonhai *et al*., 2008; Zininga *et al*., 2016; Mabate *et al*., 2018). The peptide binding affinities of PfHsp70-z for the various

peptide substrates were independent of the nucleotide states of the chaperone (Table 4.4). Although PfHsp70-z_{LS} possesses the canonical Hsp70 linker, there was no significant reduction in peptide binding affinity in the ATP state (Table 4.4). This suggests that PfHsp70-z possibly lacks allosteric regulation as previously proposed (Zininga et al., 2016). In support of this, the current study established that PfHsp70-z generally possesses fewer predicted allosteric hotspots in comparison to its' canonical counterpart, PfHsp70-1 (Figure 2.7).

Table 4.4 Comparative peptide binding affinities of Hsp70s and their linker switch mutants

Protein	Nucle-otide	KD (nM)					
		GFTVLLMYRF	GFRNNNMYRF	NRLLTG	NRNNTG	ALLLMYRR	ANNNMYRR
PfHsp70-1	NN	251 (±0.01)	26.7 (±0.07)	141 (±0.01)	85.4 (±0.04)	731(±0.01)	39.5(±0.05)
	ATP	146(±0.06)	139(±0.09)	181(±0.01)	296(±0.07)	140(±0.40)	45.4(±0.07)
	ADP	69.4(±0.04)	87.7(±0.07)	97.4(±0.04)	10.2(±0.02)	61.8(±0.08)	4.02(±0.02)
PfHsp70-1_{LS}	NN	259(±0.09)	520(±0.20)	337(±0.07)	161(±0.07)	105(±0.05)	29.8(±0.08)
	ATP	163(±0.03)	302(±0.02)	682(±0.02)	132(±0.02)	89.4(±0.04)	778(±0.08)
	ADP	204(±0.04)	158(±0.08)	174(±0.04)	466(±0.06)	99.3(±0.03)	977(±0.07)
PfHsp70-z	NN	37.0(±0.70)	9.16(±0.06)	293(±0.03)	8.08(±0.08)	41.6(±0.06)	33.1(±0.01)
	ATP	850(±0.50)	80.1(±0.01)	12.9(±0.09)	231(±0.01)	128(±0.08)	525(±0.05)
	ADP	232(±0.02)	10.6(±0.06)	4.31(±0.01)	237(±0.07)	45.3(±0.03)	241(±0.01)
PfHsp70-z_{LS}	NN	14.9(±0.09)	10.9(±0.09)	25.6(±0.06)	8.50(±0.50)	23.2(±0.02)	28.9(±0.09)
	ATP	120(±0.20)	11.2(±0.02)	36.5(±0.05)	2.00(±0.09)	207(±0.07)	595(±0.07)
	ADP	101(±0.01)	15.0(±0.50)	41.6(±0.06)	3.30(±0.30)	211(±0.01)	256(±0.06)
DnaK	NN	426(±0.06)	9650(±0.5)	85.6(±0.06)	644(±0.04)	101(±0.01)	830(±0.07)
	ATP	792(±0.02)	14100(±10)	2530(±30)	7310(±10)	4450 (±50)	8960(±60)
	ADP	90.3(±0.03)	2820(±8.0)	12.3(±0.03)	24.9(±0.09)	82.0(±0.02)	440(±4.0)
$DnaK_{LS}$	NN	218(±0.08)	405(±0.05)	1650(±5.0)	1150(±5.0)	2360(±6.0)	1420(±2.0)
	ATP	1920(±2.0)	1060(±6.0)	891(±1.0)	716(±6.00)	1950(±5.0)	1770(±7.0)
	ADP	2560(±6.0)	675(±5.00)	962(±5.00)	855(±5.00)	2440 (±4.0)	1690(±9.0)
PfHsp70-1_{NBD}	NN	ND	ND	ND	ND	ND	ND
	ATP	ND	ND	ND	ND	ND	ND
	ADP	ND	ND	ND	ND	ND	ND

ND: represents 'not detected' for SPR kinetics that were too low to detect by the SPR machine.

Plasmodial Hsp70s generally exhibited a propensity to bind asparagine enriched peptides as observed here (Table 4.4; Figure 4.4; Mabate *et al*., 2018). On the other hand, *E. coli* Hsp70 (DnaK) possessed higher binding affinities for the original hydrophobic peptides that were not enriched for asparagine (Table 4.4; Figure 4.4). This shows that DnaK is not predisposed to bind asparagine enriched peptides. Linker mutations in the canonical (PfHsp70-1 and DnaK) and non-canonical Hsp70s (PfHsp70-z) generally altered the substrate binding affinities and substrate preference exhibited by the proteins (Figure 4.4). Additionally, PfHsp70-z and its mutant version generally demonstrated high substrate binding affinities relative to its canonical counterpart. This can be attributed to the unique architecture of the SBDs of the two proteins (Section 1.6.4).

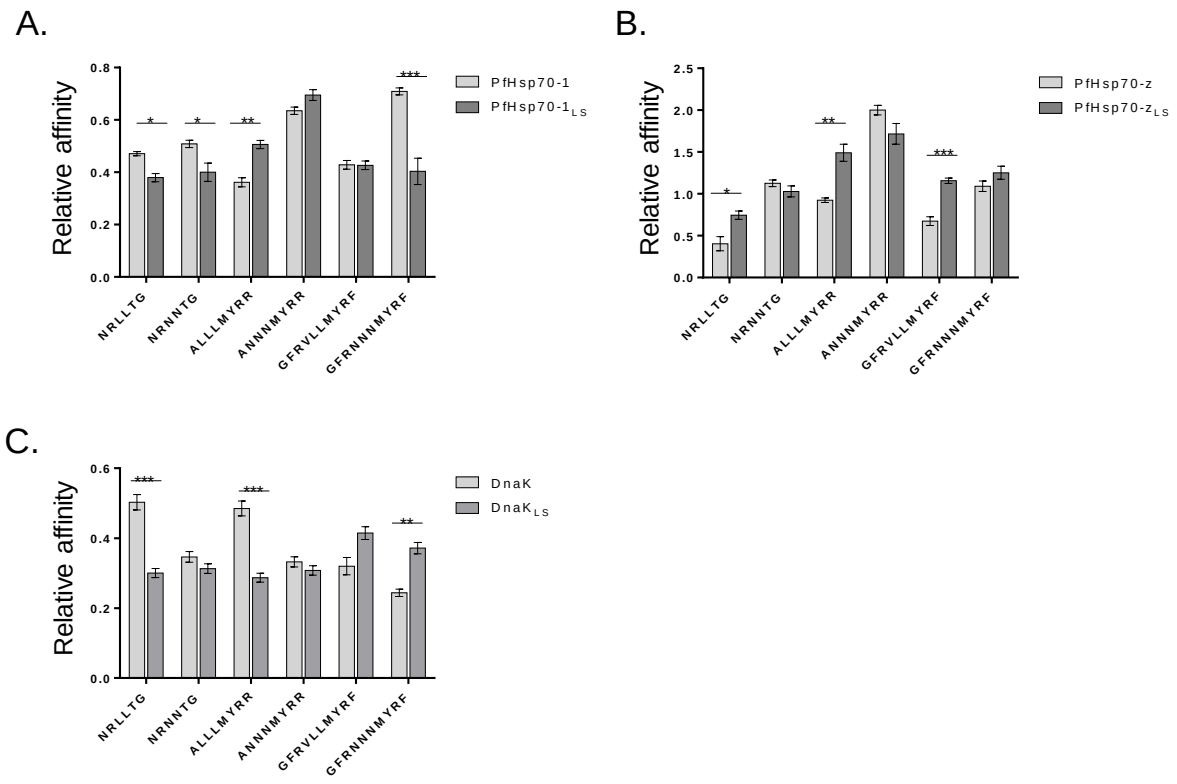

Figure 4.4. The linker regulates Hsp70 peptide binding affinity

Comparative affinities of Hsp70s and their linker mutants were established by SPR analysis. Presented here are binding affinity graphs for PfHsp70-1/PfHsp70-1LS (A), PfHsp70-z/PfHsp70-zLS (B) and DnaK/DnaKLS (C). SPR sensograms for these data are presented in Appendix B28. Statistical analysis was conductedat $p<0.05$*; $p<0.01$**;$p<0.001$**.

PfHsp70-z_{LS} exhibited unique peptide binding preferences from its wild type form (Figure 4.4; Table 4.4). While PfHsp70-z generally bound asparagine-enriched peptide substrates with a higher affinity than it exhibited for the original peptide substrates, PfHsp70-z_{LS} bound both the original and asparagine-enriched versions of the peptide substrates with comparable affinities (Table 4.4; Figure 4.4). For instance, PfHsp70-z bound the peptide substrate NRNNTG with a higher affinity (K_D = 8.08 nM) as compared to the peptide NRLLTG for which it exhibited a 36-fold decrease in binding affinity (K_D = 293 nM) (Table 4.3). PfHsp70-z_{LS} however exhibited a two-fold increase in affinity for the peptide substrate NRNNTG (K_D= 9 nM) than NRLLTG (K_D= 25.6 nM) (Table 4.4). This suggests that the linker of PfHsp70-z plays an important role in modulating substrate specificity of the chaperone.

$DnaK_{LS}$ generally possessed comparatively lower affinity for the peptides than its wild type version. DnaK possessed a higher affinity for the hydrophobic peptides as compared to their asparagine enriched versions. However, $DnaK_{LS}$ exhibited comparable affinities for both the hydrophobic and asparagine enriched peptides (Figure 4.4). Similarly, PfHsp70-1_{LS} did not exhibit substrate preference as was observed in PfHsp70-1 which had a higher affinity for asparagine enriched peptides. The findings suggests that the linker motif is important for Hsp70 substrate binding affinity and selectivity. Overall, it seems the PfHsp70-z linker in canonical Hsp70s abrogated substrate selectivity as the proteins bound both peptide classes with comparable affinities.

4.3.4 The linker modulates aggregation suppression activity of Hsp70s

Malate dehydrogenase (MDH) and firefly luciferase have previously been used as aggregation-prone protein models to demonstrate the aggregation suppression capabilities of DnaK, PfHsp70-z and PfHsp70-1 (Shonhai *et al*., 2008, Makhoba *et al*., 2016; Zininga *et al*., 2016, Mabate *et al*., 2018). Initially, it was shown that both wild type and the linker mutant versions of PfHsp70-1, PfHsp70-z and DnaK were thermally stable at 51°C making the chaperone preparations appropriate for use as aggregation suppressants (Appendix B26-27). As expected, both MDH and luciferase aggregated in response to heat stress at 51°C (Figure 4.5). Furthermore, the heat-

induced aggregation of MDH/luciferase could not be reversed by the non-chaperone control, BSA (Figure 4.5).

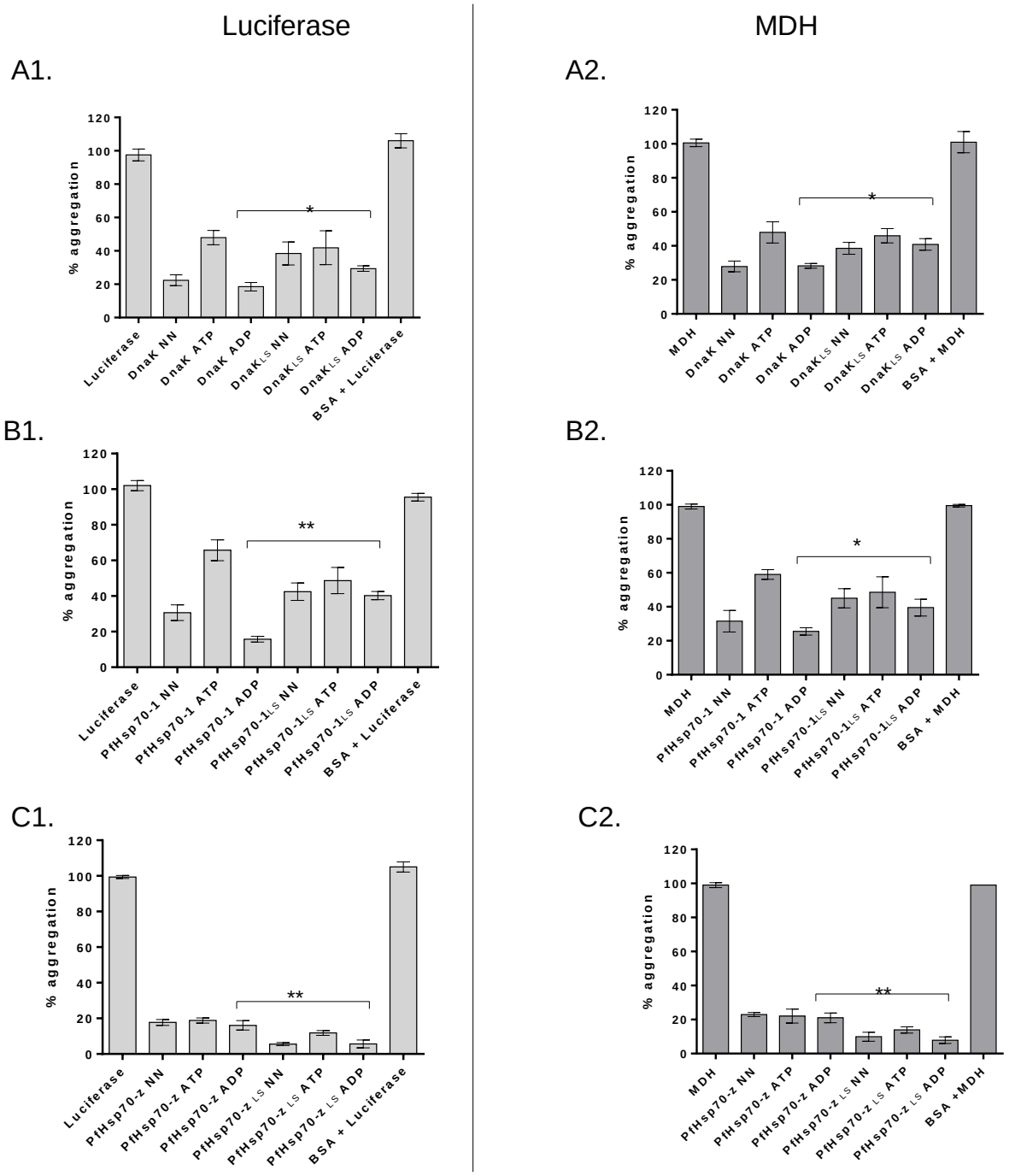

Figure 4.5. The linkers of Hsp70s modulate chaperone activity of Hsp70 *in vitro*

Heat induced aggregation of MDH or luciferase was investigated at 51 °C. The capability of each Hsp70 and its linker derivative to suppress luciferase/MDH aggregation was investigated. The assay was run in the absence or presence of 5 mM ATP/ADP. The bar graphs presented represent data obtained for aggregation of luciferase or MDH in the presence of DnaK/DnaKLS (A1, A2); PfHsp70-1/PfHsp70-1LS and PfHs70-z/PfHsp70-zLS. The data represents results from three independent repeats of the assay. Statistical analysis was conducted at $p<0.05$*; $p<0.01$**;$p<0.001$**.

Peptide substrate binding in Hsp70s is known to be enhanced in the ADP state (Kampinga and Craig, 2010). In the presence of ADP, $DnaK_{LS}$ exhibited a significantly lower aggregation suppression capability relative to its wild type form ($p<0.01$; Figure 4.5 A1-2). Similarly, PfHsp70-1 was more efficient at supressing heat-induced aggregation of MDH/luciferase in the ADP state (Figure 4.5 B1-2). However, $PfHsp70\text{-}z_{LS}$ exhibited higher aggregation suppression activity than wild type PfHsp70-z (Fig 4.5 C1-2). As expected, the presence of ATP reduced the aggregation suppression activity of both canonical Hsp70s (PfHsp70-1 and DnaK) as previously shown (Figure 4.4; Shonhai *et al*., 2008). Interestingly, the aggregation suppression activity of both $DnaK_{LS}$ and $PfHsp70\text{-}1_{LS}$ was not inhibited in the presence of ATP (Figure 4.5 A,B). Similarly, PfHsp70-z aggregation suppression activity was not inhibited in the ATP state (Figure 4.5 C1-2) as previously reported (Zininga *et al*., 2016; Smock *et al*., 2010). Hsp110s have previously been reported to be non-allosteric such that the NBD remains stably bound to ATP in a manner that does not affect substrate binding (Smock *et al*., 2010; Kumar *et al*., 2019). The introduction of the PfHsp70-z linker into canonical Hsp70s (PfHsp70-1 and DnaK) rendered them unresponsive to nucleotides during aggregation suppression activity suggesting that the linker motif is important for allosteric regulation in the chaperone.

4.3.5 The linker of PfHsp70-1 is important for the protein folding activity of the chaperone

Hsp70 functions in a network in tandem with co-chaperones to form a complex which facilitates protein folding. As part of its complex, Hsp70 co-operates with a NEF (Hsp110) and a co-chaperone, Hsp40 (Dragovic *et al*., 2006; Mattoo *et al*., 2011). Based on data from the ATPase activity assays, the PfHsp70-1 linker facilitated the enhanced ATPase activity of the chaperone in the presence of PfHsp40 (Figure 4.3). Increased ATPase activity acts as an important driver of protein folding by pushing Hsp70 into the ADP state thereby making it assume a higher substrate binding affinity status (Kityk *et al*., 2015). As such, luciferase refolding assays were conducted in order to determine the role of the linker in facilitating protein folding *in vitro*.

Upon exposure to heat stress, luciferase loses its activity rapidly although it is thought to become only partially unfolded (Dragovic *et al*., 2006). In the absence of either PfHsp40 or PfHsp70-z, PfHsp70-1 and PfHsp70-1_{LS} exhibited low refolding activities of 5.5% and 2.2% respectively (Figure 4.6). Furthermore, none of the Hsp110s (PfHsp70-z and PfHsp70-z_{LS}) were capable of refolding luciferase in the absence of PfHsp40 and PfHsp70-1 (Figure 4.6). These findings indicate that Hsp70s were incapable of individually refolding heat-denatured luciferase as previously reported (Shamer and Morano 2007). However a combination of PfHsp70-1 + PfHsp40 + PfHsp70-z exhibited the highest refolding capability (Figure 4.6). This suggests that the PfHsp70-1, PfHsp70-z and PfHsp40 chaperone complex facilitates efficient protein refolding in *P. falciparum* (Figure 1.9).

Linker substitutions resulted in significant reduction of the refolding capability of the PfHsp70-1+PfHsp70-z+PfHsp40 complex ($p<0.01$; Figure 4.6). The reduced refolding efficiency of PfHsp70-1_{LS} could have resulted from the reduced activation of PfHsp70-1_{LS} ATPase activity by PfHsp40 (Section 4.3.2). It therefore suggests that in the absence of the linker, PfHsp70-1 exhibits low basal ATPase activity which compromises the folding function if the protein. In addition, the Hsp70 linker has previously been reported to stabilize Hsp70+Hsp40 complexes (Kumar *et al*., 2011; Alderson *et al*., 2016). As such, in the absence of the PfHsp70-1 linker, PfHsp70-1_{LS} could have failed to form a stable complex with PfHsp40. Similarly, the linker mutation could have also compromised the formation of a stable PfHsp70-1+PfHsp70-z complex. It was also noted that when PfHsp70-z was replaced with PfHsp70-z_{LS} in the refolding complex, refolding efficiency was reduced by more than half (Figure 4.6). This implies that the linker mutation compromised the nucleotide exchange function of PfHsp70-z thereby lowering the overall refolding efficiency of PfHsp70-1.

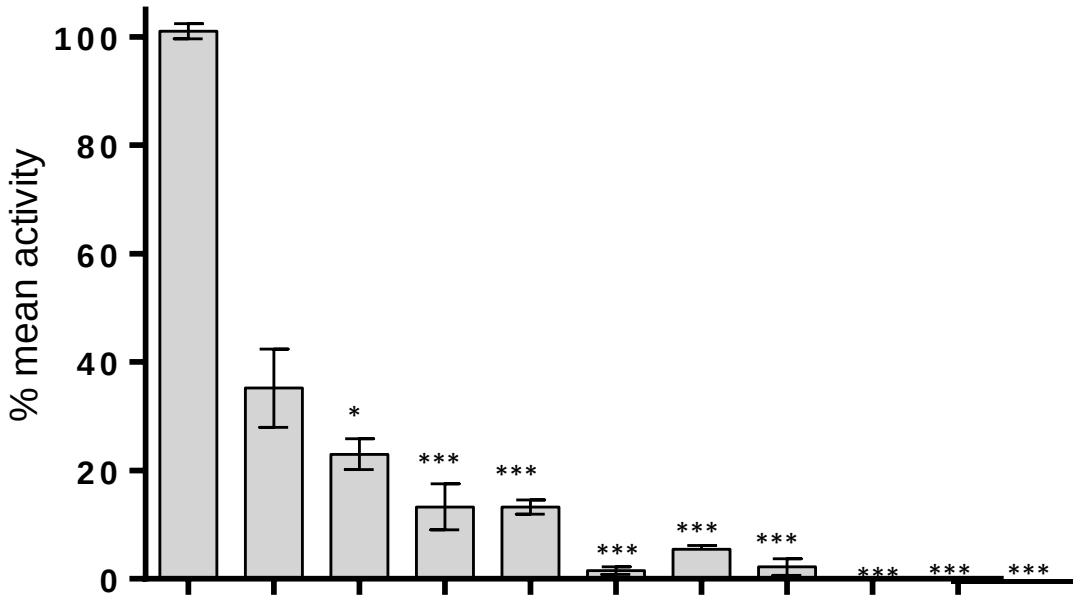

Luciferase (N/D)	N	D	D	D	D	D	D	D	D	D	D
PfHsp40	-	+	+	+	+	+	-	-	-	-	-
PfHsp70-z	-	+	+	-	-	-	-	-	+	-	-
PfHsp70-z_{LS}	-	-	-	+	+	-	-	-	-	+	-
PfHsp70-1	-	+	-	+	-	-	+	-	-	-	-
PfHsp70-1_{LS}	-	-	+	-	+	-	-	+	-	-	-
% mean activity	100	35.2	24.5	13.2	13.2	1.5	5.5	2.2	0.0	0.0	0.0

Figure. 4.6. Linker substitution mutations compromised protein refolding capability of the PfHsp70-1 complex

The bar graphs represent refolding of heat-denatured luciferase. The letters 'N' and 'D' represent native and denatured luciferase, respectively. The luminescence measured for the catalysis of luciferin by native luciferase was set at 100% luciferase activity. Denatured luciferase was exposed to various chaperone combinations and refolding activity was monitored. Statistical significance was conducted at p<0.5; p<0.01**; p<0.001***.

4.3.6 $DnaK_{LS}$ fails to confer cytoprotection on *E. coli* cells

To elucidate the role of the linker on the *in cellulo* chaperone function of DnaK, complementation assays were conducted. *E. coli* BB2393 and *E. coli* dnak756 cells were used to investigate whether $DnaK_{LS}$ conferred cytoprotection to cells subjected to a non-permissive growth temperature of >40 °C (Table 4.1). As expected, DnaK conferred cytoprotection to the *E. coli* cells under non-permissive growth temperatures (Figure 4.7; Shonhai *et al*., 2005). Furthermore, control cells transformed with the neat pQE30 plasmid failed to grow under non-permissive growth temperatures (Figure 4.7).

This shows that restoration of DnaK was responsible for growth of the cells at non-permissive growth temperature. *E .coli* BB2393 cells transformed with pQE30/DnaK$_{LS}$ plasmid failed to grow at both permissive and non-permissive growth temperature (Figure 4.7 A). This suggests that DnaK$_{LS}$ was toxic to these cells. On the other hand, *E. coli* dnaK756 cells heterologously expressing DnaK$_{LS}$ managed to grow at permissive growth temperature, although no cell growth was observed at non permissive temperature of 43.5 °C (Figure 4.7 B). This implies that, the replacement of the DnaK linker with the PfHsp70-z linker abrogated the cytoprotective function of DnaK *in cellulo*. Taken together, these findings suggest that the linker of DnaK is an important motif for its chaperone function. Furthermore, it suggests that the linker for PfHsp70-z is not functionally equivalent to that of PfHsp70-1 as previously observed through fluorescence spectroscopy studies (Figure 3.6).

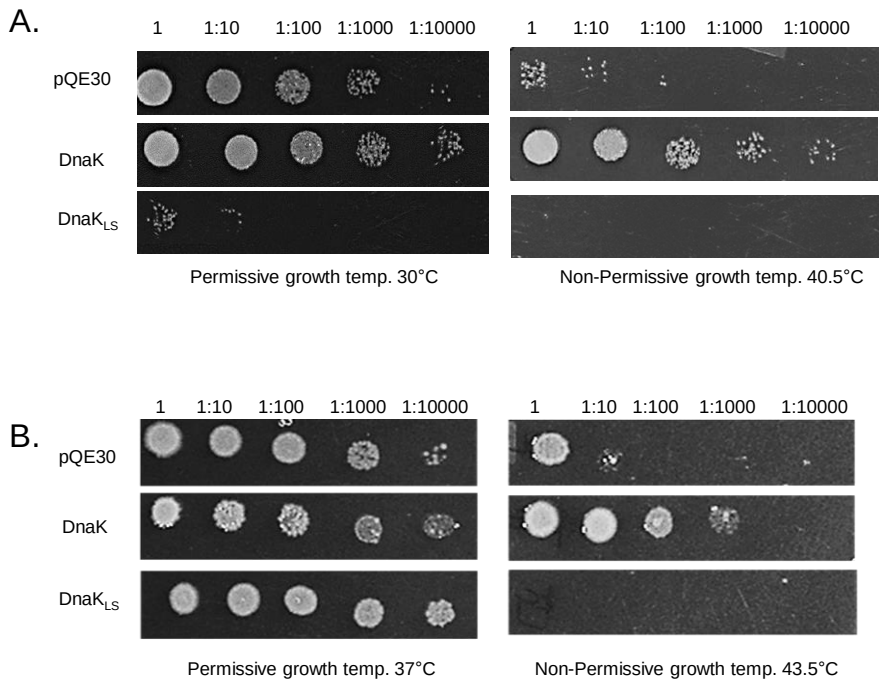

Figure 4.7. DnaK$_{LS}$ does not confer cytoprotection to *E. coli* cells

Complementation of *E. coli* BB2393 strain with DnaK and DnaK$_{LS}$ at permissive and non-permissive growth temperatures (A). Complementation of *E. coli* dnak756 at permissive and non-permissive growth temperatures (B).

4.4 Discussion

Both PfHsp70-1 and PfHsp70-z play important roles in the maintenance of cellular proteostasis during the parasites' development. While PfHsp70-z is an efficient holdase (Zininga *et al*., 2016), PfHsp70-1 is thought to serve both as a holdase and refoldase in parasite cells (Shonhai *et al*., 2007). Although these chaperones generally possess similar structural architecture, they are distinguished from each other by their linkers. The current study therefore sought to decipher the role of the linkers of PfHsp70-z and PfHsp70-1 in the chaperone function of the two proteins. Findings from the current study demonstrated that the linker of PfHsp70-1 and that of PfHsp70-z regulate several chaperone functions such as ATPase activities, holdase function and substrate binding.

PfHsp70-z_{LS} exhibited relatively higher ATP binding affinity than its wild type form. This suggests that the introduction of the PfHsp70-1 linker into PfHsp70-z_{LS} makes the latter to assume a conformation which is favourable for ATP binding. The three-dimensional model of PfHsp70-z_{LS} showed that the linker mutation introduced a protrusion on the loop connecting lobe IA to the linker binding cleft (Section 2.3.4). This variation in the NBD of PfHsp70-z may have modulated its affinity for ATP. Furthermore, the Hsp70 proteins harbouring the canonical Hsp70 linker (i.e. PfHsp70-1, DnaK and PfHsp70-z_{LS}) generally exhibited higher basal ATPase activity than those possessing the PfHsp70-z linker (i.e. PfHsp70-z, PfHsp70-1 $_{LS}$ and $DnaK_{LS}$) (Table 4.3; Figure 4.3). Collectively, these findings suggest that the canonical Hsp70 linker plays an important role in enhancing the basal ATPase activity of Hsp70s. On the other hand, the data suggest that the linker of PfHsp70-z is responsible for the suppressed ATPase activity of the protein.

Docking of the linker into the linker binding cleft as well as NBD re-orientation upon ATP binding are thought to be important determinants of Hsp70 ATPase activity (Bhattacharya *et al*., 2009; Zhuravleva and Gierasch, 2011; Chakafana *et al* ., 2019b). Two leucine residues (L^{390} and L^{392}) of the DnaK linker have previously been reported to play important roles in ATP hydrolysis since they form contacts with the NBD when the linker docks to the linker binding cleft (English *et al*., 2017). *In silico* analyses revealed that, PfHsp70-1_{LS} lacks some contacts for linker docking in the ATP state

that are present in the wild type form of the protein (Table 2.3). This underscores the importance of the leucine residues associated with canonical Hsp70 linkers in modulating the basal ATPase activities of these proteins. Interestingly, Hsp40s failed to stimulate the ATPase activities of PfHsp70-1$_{LS}$ and DnaK$_{LS}$ (Figure 4.3). The leucine residues in the DnaK linker (L^{391} and L^{392}) and the Hsc70 linker residues V^{388} and L^{393} have previously been implicated in facilitating Hsp40-induced stimulation of ATPase activity (Han and Cristen, 2001; Jiang, 2007). The absence of these residues in the linkers of PfHsp70-1$_{LS}$ and DnaK$_{LS}$ might have compromised the ATPase activity of the chaperones. The fact that PfHsp40 could not stimulate the ATPase activity of PfHsp70-1$_{NBD}$ further confirms the importance of the linker in the co-operation of this chaperone with its' co-chaperone, PfHsp40. This is supported by previous studies in which Hsp40 failed to stimulate the ATPase activity of human Hsp70 (Alderson *et al*., 2014).

The linkers of the canonical Hsp70s (PfHsp70-1 and DnaK) and Hsp110 (PfHsp70-z) are implicated in modulating substrate binding affinity (Figure 4.4; Table 4.4). Minor alterations in SBDβ have previously been reported to trigger unique allosteric coupling through regulation of the movement of the helical lid and the linker segments of Hsp70s (Liebscher and Roujeinikova, 2008). *In silico* predictions suggest that the linker mutations introduced structural variations within SBDβ and SBDα of PfHsp70-1 and PfHs70-z, respectively (Figure 2.4; Figure 2.5). This potentially altered the substrate binding preferences of the chaperones. While PfHsp70-z exhibited higher affinity for asparagine-enriched peptide substrates, PfHsp70-z$_{LS}$ bound both the original and asparagine-enriched peptides with comparable affinities (Figure 4.4; Table 4.4). The interactome of PfHsp70-z also suggested that the chaperone binds to a putative asparagine rich protein (Figure 2.9). This further suggests that Pfsp70-z exhibits preference for asparagine rich proteins as previously reported for another *P. falciparum* Hsp70 (PfHsp70-x) (Mabate *et al*., 2018). The hydrophobic linker of PfHsp70-1, that was inserted in PfHsp70-z$_{LS}$, possibly increased the linker flexibility allowing the SBD to assume a conformation favourable for enhanced substrate binding. Interestingly, PfHsp70-z$_{LS}$ suppressed heat-induced aggregation more effectively than PfHsp70-z (Figure 4.5), further suggesting that the linker possibly allows the SBD to bind to the substrate more appropriately. However, PfHsp70-1$_{LS}$ and DnaK$_{LS}$ were ineffective at suppressing heat-induced protein aggregation.

Altogether, these findings suggest that the linker of PfHsp70-1 is a module that facilitates effective substrate binding and hence chaperone activity.

The role of the linkers of PfHsp70-1 and PfHsp70-z in facilitating protein refolding *in vitro* was also explored. Based on the findings from this study, the linker mutation in PfHsp70-1 significantly reduced the refolding efficiency of the chaperone (Figure 4.6). ATP hydrolysis is a rate-determining step during protein folding (Section 1.3.4.1). As such, the low ATPase activity of PfHsp70-1_{LS} could be responsible for its' suppressed refolding capability. Interestingly, the PfHsp70-z linker inserted in PfHsp70-1 compromised the refolding function of PfHsp70-1_{LS} (Figure 4.6). The high ATPase activity of PfHsp70-z_{LS} (Figure 4.3) could have possibly compromised its NEF function to an extent where the refolding reaction became unproductive for substrate folding. In addition, the linker of canonical Hsp70s has previously been reported to stabilize the functional association between Hsp40 and Hsp70 (Han and Cristen, 2001; Jiang *et al*., 2007). As such, in the absence of the canonical linker, PfHsp70-1_{LS} might have failed to form a stable and functional complex with PfHsp40 to facilitate protein folding. In addition, the linker mutation in PfHsp70-1 could have also destabilized the protein's association with its NEF, PfHsp70-z.

The findings from the current study demonstrated that $DnaK_{LS}$ failed to confer cytoprotection to *E. coli* dnak756 cells (Figure 4.7). This observation was consistent with previous studies in which a linker mutant version of DnaK also failed to complement *E. coli* dnak756 cells (Kumar *et al*., 2011). Furthermore, a DnaK linker mutant version in which the leucine residues (L^{391}/L^{392}) were substituted with S^{391} and G^{392}, reportedly failed to co-operate with DnaJ and GrpE *in vitro* (Han and Cristen, 1998). It therefore implies that, the absence of the leucine residues in the $DnaK_{LS}$ linker possibly compromised the protein's interaction with GrpE, the NEF. Similarly, $DnaK_{LS}$ failed to suppress thermosensitivity in *E. coli* BB2393 but induced toxicity to the cells (Figure 4.7). Generally, findings from the current study suggest that the PfHsp70-z linker is not functionally equivalent to that of the canonical Hsp70. It also suggests that the linkers of PfHsp70-1 and PfHsp70-z play key roles in regulating the functions of the chaperones.

CHAPTER 5

Investigation of the role of the linkers of PfHsp70-z and PfHsp70-1 on interaction of the chaperones with co-chaperones

5.1. Introduction

Hsp70s are versatile chaperones that form functional complexes with a number of co-chaperones such as Hsp40, Hsp110 and Hop in maintaining cellular proteostasis (Jiang, 2007; Kampinga, 2011). The synergistic co-operation of canonical Hsp70s with co-chaperones is key to the chaperone's main function i.e. folding of client proteins. The linker alternates between the docked state in the presence of ATP and an undocked state in the presence of ADP (Chakafana *et al*., 2019b). Based on fluorescence spectroscopic analyses, the shifts between docked and undocked states of the linker are characterised by global conformational changes (Section 3.3.5). Thus, linker mutations modulate the interaction of Hsp70 with ligands such as nucleotides.

Binding of Hop to Hsp70 and Hsp90 facilitates substrate transfer to Hsp90 for further folding (Johnson *et al*., 1998; Gitau *et al*., 2012; Rohl *et al*., 2015). Hsp70's association with Hop occurs via the formers' strongly electronegative C-terminal EEVD motif that binds to the electropositive TPR domain of Hop (Johnson *et al*., 1998; Zininga *et al*., 2015; Mabate *et al*., 2018). PfHsp70-1 and PfHop have been shown to interact in a nucleotide dependent fashion (ADP enhances their association) (Zininga *et al*., 2015). Canonical Hsp70s also interact with Hsp40 (Botha *et al*., 2012) and Hsp110 (Cyr and Ramos, 2015). Interaction of canonical Hsp70 with Hsp40 is thought to occur through the EEVD motif located at the C-terminus of Hsp70 and the linker binding cleft at the NBD (Section 1.3.4.1; Yu *et al*., 2015; Alderson *et al*., 2016). On the other hand, Hsp70 interacts with Hsp110 through NBD:NBD contacts (Figure 2.8C; Pollier *et al*., 2008). The current study therefore sought to establish the role of the linker of PfHsp70-1 in modulating the interaction between PfHsp70-1 and its co-chaperones, PfHop and PfHsp40. In addition, the role of the PfHsp70-z linker in modulating the chaperone's interaction with PfHsp70-1 was elucidated. In view of the fact that linkers can dictate overall plasticity of Hsp70 protein structure (Section 3.3.4), it was necessary to validate whether the respective linkers also regulate the affinity for co-chaperone binding either in the presence or absence of nucleotides.

The objective of this study was to:

i. determine the role of the linkers of PfHsp70-1 and PfHsp70-z on the interaction of the chaperones with their respective co-chaperones *in vitro*

5.2 Methods

5.2.1 Surface plasmon resonance (SPR) analysis

In order to investigate the effect of the linker mutations on the interaction of PfHsp70-1, PfHsp70-z and DnaK with their co-chaperones, SPR analysis was conducted. SPR analyses were conducted using the Bionavis MP-SPR Navi 420A ILVES system as previously described in Section 4.2.2.The respective co-chaperones (PfHsp40, PfHop, DnaJ) were injected as analytes at concentrations of 0, 125, 250, 500, 1000 and 2000 nM and a flow rate of 50 µl/min onto the immobilised Hsp70 ligands. Data was analysed as previously described (Section 4.2.2).

5.3 Results

5.3.1 The linker of PfHsp70-1 regulates interaction of the chaperone with PfHop

Interaction of PfHsp70-1/PfHsp70-1_{LS} with PfHop was investigated using SPR analysis. The derived sensograms demonstrated that the interactions occurred in a dose dependent manner suggesting that the associations were specific (Figure 5.1). Results from this study confirmed that PfHsp70-1 interacts with PfHop at the nanomolar range (Table 5.1) as previously reported (Zininga *et al*., 2015a). In the absence of nucleotides, PfHsp70-1_{LS} exhibited significantly higher K_D values of 27.7 nM compared to a K_D value of 3.89 nM recorded for wild type PfHsp70-1. This suggests that PfHsp70-1_{LS} possessed reduced affinity for PfHop (Table 5.1). In the *apo* state, PfHsp70-1 exhibited comparable affinity for PfHop as in the presence of ADP as previously observed (Table 5.1; Zininga *et al*., 2015). Furthermore, upon introduction of ATP, the affinity of PfHsp70-1 for PfHop was reduced from a K_D value of 3.89 nm to 94.6 nm, in agreement with a previous independent study (Table 5.2; Zininga *et al*., 2015a). Interestingly, the affinity of PfHsp70-1_{LS} for PfHop interaction was marginally reduced in the ATP state. The K_D values recorded in all three nucleotide states were within the same order of magnitude (Table 5.1) implying that the interaction of PfHsp70-1_{LS} and PfHop was unaffected by nucleotides.

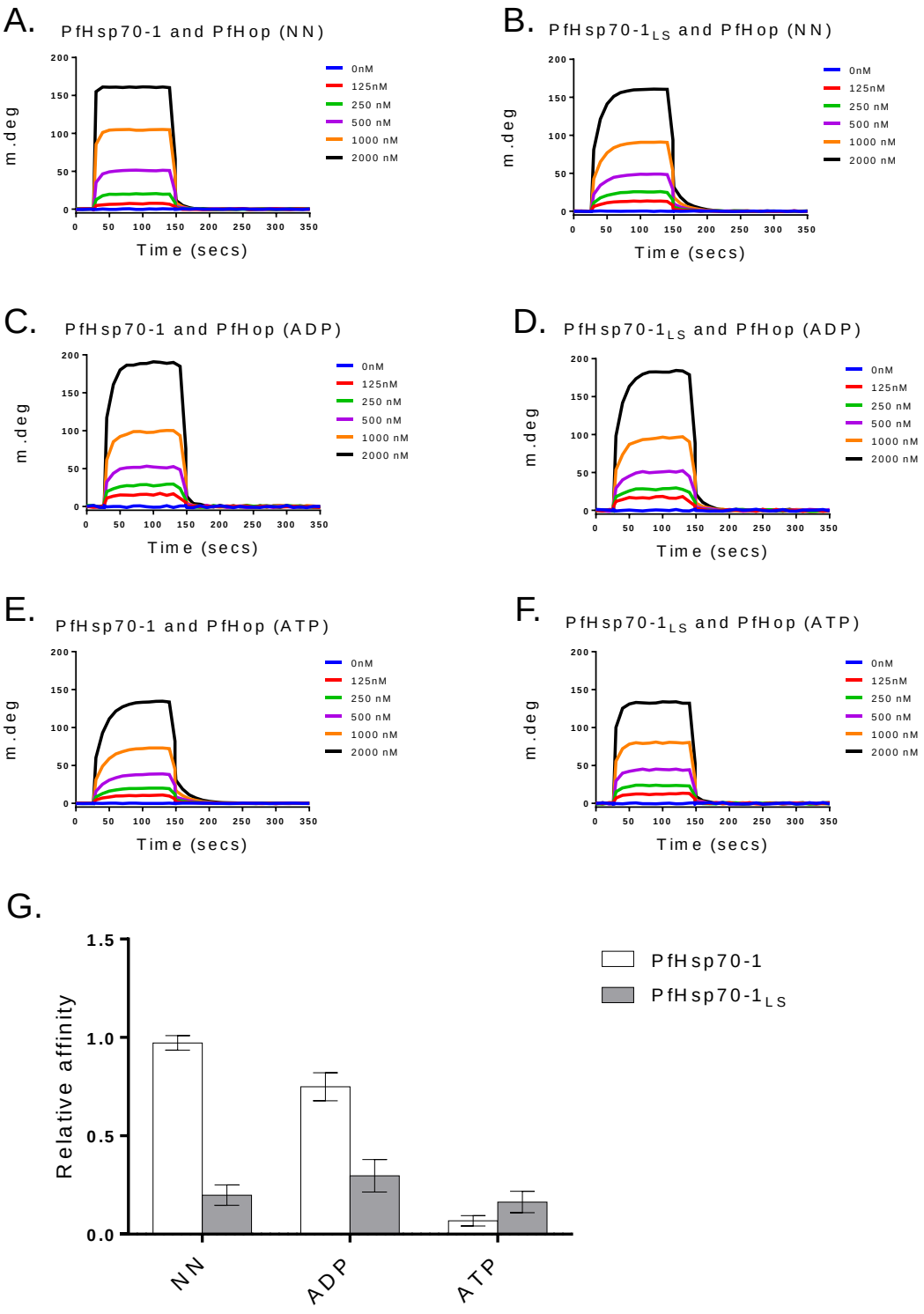

Figure 5.1. Interaction of PfHsp70-1$_{LS}$ and PfHop

Representative SPR sensograms demonstrating concentration dependent association between PfHsp70-1/PfHsp70-1$_{LS}$ immobilized on the chip and PfHop introduced in solution as an analyte. The assay was conducted in the absence of nucleotide (A)/(B); and repeated in the presence of 5 mM ADP (C)/(D), respectively. The assay was also repeated in the presence of 5 mM ATP (E)/(F). G The relative affinities for the interaction of PfHsp70-1$_{LS}$ and PfHop were calculated relative to the affinity of Pfsp70-1 for PfHop in the absence of nucleotides.

Table 5.1. Kinetics for the interaction of PfHsp70-1$_{LS}$ and PfHop

Ligand	Analyte	Ka (1/Ms)	Kd (1/s)	K_D (nM)	χ^2
PfHsp70-1	PfHop (NN)	3.54 (±0.04) e^3	1.38 (±0.08) e^{-5}	3.89 (±0.09)**	1.62
	PfHop (ADP)	6.45 (±0.05) e^4	4.99 (±0.09) e^{-4}	7.75 (±0.05)	1.26
	PfHop (ATP)	2.10 (±0.10) e^5	1.99 (±0.09) e^{-2}	94.6 (±0.06)	2.43
PfHsp70-1$_{LS}$	PfHop (NN)	4.82 (±0.02) e^5	1.34 (±0.04) e^{-2}	27.7 (±0.07)**	2.31
	PfHop (ADP)	1.00 (±0.09) e^5	1.00 (±0.09) e^{-3}	10.0 (±0.09)	2.07
	PfHop (ATP)	8.80 (±0.80) e^5	2.35 (±0.05) e^{-3}	37.6 (±0.06)	1.89
PfHsp70-1$_{NBD}$	PfHop (NN)	ND	ND	ND	-
	PfHop (ADP)	ND	ND	ND	-
	PfHop (ATP)	ND	ND	ND	-

Three independent analyses were conducted using SPR to elucidate PfHop interaction with PfHsp70-1/ PfHsp70-1$_{LS}$. Standard errors are shown in brackets. Chi^2 values indicate the score for the goodness of fit of the Langmuir fit model used to generate the kinetics. ND: represents 'not detected' for SPR kinetics that were too low to be detected. Statistical analysis was conducted using a One-Way ANOVA at p<0.05*; p<0.01**;p<0.001**.

5.3.2 The linker of PfHsp70-1 is important for its interaction with PfHsp40

The interaction between PfHsp70-1$_{LS}$ and PfHsp40 was also investigated by SPR. The SPR sensograms showed that the interactions occurred in a concentration dependent manner at 6 different concentrations (Figure 5.2). This suggests that the interactions between PfHsp70-1/PfHsp70-1$_{LS}$ and PfHsp40 were specific. The assay was then repeated in the presence of ADP (Figure 5.2 C,D), or ATP (Figure 5.2 E,F) and the associations occurred in a similar concentration dependent manner. Compared to its wild type form which had a K_D of 6.66 µM, PfHsp70-1$_{LS}$ generally possessed lower affinity for PfHsp40 with a higher K_D value of 15.8 µM (Table 5.2). In the absence of nucleotides, PfHsp70-1$_{LS}$ exhibited a two-fold reduction in affinity for PfHsp40 relative to its wild type form (Table 5.2). These findings suggest that the linker of PfHsp70-1 regulates the chaperone's affinity for PfHsp40. As expected, ATP enhanced PfHsp70-1 affinity for PfHsp40 by two orders of magnitude, from an initial K_D value of 6.66 µM

to 0.0526 µM (Table 5.2; Ahmad *et al*., 2011). However, for PfHsp70-1$_{LS}$, the ATP state only enhanced the chaperone's affinity for PfHsp40 interaction by one order of magnitude from an initial K_D value of 15.8 µM to 6.3 µM (Table 5.2). This suggests that, the substitution of PfHsp70-1's linker with the PfHsp70-z linker yielded a protein that was structurally compromised with respect to its capacity to engage PfHsp40.

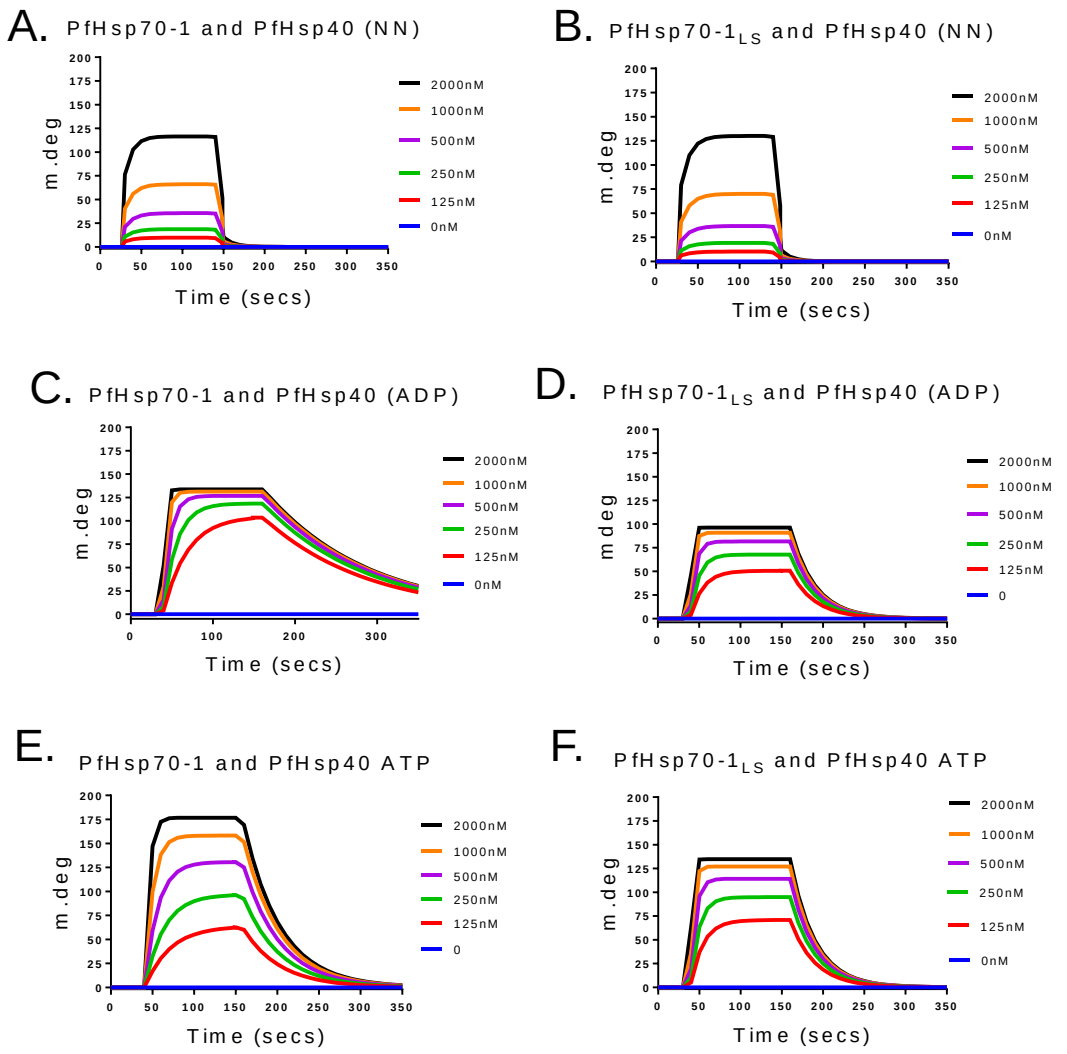

Figure 5.2. PfHsp70-1$_{LS}$ interaction with PfHsp40.

SPR sensograms for the interaction of PfHsp70-1/PfHsp70-1$_{LS}$ with PfHsp40. The interaction between PfHsp70-1 with PfHsp40 (A) and PfHsp70-1LS with PfHsp40 (B) in the absence of nucleotides occurred in a dose dependent manner at 6 different concentrations. The experiment was repeated in the presence of ADP for PfHsp70-1 and PfHsp40 (C) as well as for PfHsp70-1$_{LS}$ and PfHsp40 (D). The interaction of PfHsp70-1 and PfHsp40 (E) and that of PfHsp70-1$_{LS}$ and PfHsp40 (F) was then repeated in the presence of 5 mM ATP.

Table 5.2 Interaction of Hsp70s with co-chaperones (SPR analysis)

Ligand	Analyte	Ka (1/Ms)	Kd (1/s)	KD (M)	χ^2
DnaK	DnaJ (NN)	3.93 (±0.06)e^{4}	1.87 (±0.06)e^{-2}	4.76 (±0.06)e^{-7}**	3.91
	DnaJ (ADP)	1.19 (±0.06)e^{4}	2.71 (±0.06)e^{-3}	2.28 (±0.08)e^{-7}	4.87
	DnaJ (ATP)	6.01 (±0.06)e^{5}	4.09 (±0.06)e^{-3}	8.30 (±0.30)e^{-9}***	3.78
$DnaK_{LS}$	DnaJ (NN)	3.19 (±0.06)e^{4}	5.22 (±0.06)e^{-2}	1.64 (±0.04)e^{-6}**	0.19
	DnaJ (ADP)	2.11 (±0.06)e^{5}	6.76 (±0.06)e^{-2}	3.20 (±0.20)e^{-7}	0.03
	DnaJ (ATP)	4.17 (±0.06)e^{5}	7.32 (±0.06)e^{-2}	2.09 (±0.09)e^{-7}***	1.89
PfHsp70-1	PfHsp40 (NN)	1.23 (±0.06)e^{4}	8.15 (±0.06)e^{-2}	6.66 (±0.06)e^{-6}*	0.04
	PfHsp40 (ADP)	1.53 (±0.06)e^{3}	8.66 (±0.06)e^{-2}	3.98 (±0.08)e^{-5}	8.98
	PfHsp40 (ATP)	6.87 (±0.06)e^{5}	3.61 (±0.06)e^{-2}	5.26 (±0.06)e^{-8}***	9.09
$PfHsp70\text{-}1_{LS}$	PfHsp40 (NN)	6.04 (±0.06)e^{-3}	9.55 (±0.06)e^{-2}	1.58 (±0.08)e^{-5}*	0.78
	PfHsp40 (ADP)	2.20 (±0.06)e^{3}	1.18 (±0.06)e-^{2}	5.36 (±0.06)e^{-6}	0.01
	PfHsp40 (ATP)	6.14 (±0.06)e^{3}	3.87 (±0.06)e^{-2}	6.30 (±0.30)e^{-6}***	3.82
$PfHsp70\text{-}1_{NBD}$	PfHsp40 (NN)	ND	ND	ND	-
	PfHsp40 (ADP)	ND	ND	ND	-
	PfHsp40 (ATP)	ND	ND	ND	-

Three independent analyses were conducted using SPR to elucidate PfHsp40 interaction with PfHsp70-1/ $PfHsp70\text{-}1_{LS}$. Standard errors are shown in brackets. Chi^2 values indicate the score for the goodness of fit of the Langmuir fit model used to generate the kinetics. ND: represents 'not detected' for SPR kinetics that were too low to detect. Statistical analysis was conducted using a One-Way ANOVA at p<0.05*; p<0.01**;p<0.001**.

Hsp70 and Hsp40 interaction kinetics where further validated for the *E. coli* chaperones. The interaction between DnaK/$DnaK_{LS}$ with DnaJ was explored using SPR. Interactions for DnaK/$DnaK_{LS}$ with DnaJ occurred in a dose-dependent manner across the 6 different concentrations (Appendix B36). The derived findings mirrored previous observations made in the plasmodial chaperones, PfHsp70-1 and PfHsp40 (Table 5.2). DnaK generally exhibited higher affinity for DnaJ than its linker mutant

version, DnaK$_{LS}$ (Table 5.2). In the absence of nucleotides, DnaK exhibited a four-fold increase in affinity for DnaJ (K_D= 0.476 µM) as compared to DnaK$_{LS}$ (K_D= 1.64 µM). Furthermore, the presence of ATP significantly enhanced the interaction between DnaK and DnaJ by two orders of magnitude (Table 5.3). In the presence of ATP, DnaK exhibited a K_D value of 8 nM as opposed to an initial K_D value of 0.476 µM observed in the absence of nucleotides. However, DnaK$_{LS}$ and DnaJ interaction was only enhanced by one order of magnitude in the ATP state from a K_D value of 1.64 µM in the absence of nucleotides to a K_D value of 0.209 µM in the presence of ATP (Table 5.2). Taken together, these findings suggest that the linker of canonical Hsp70 plays an important role in modulating the interaction of Hsp70 with Hsp40. This reduced affinity of DnaK$_{LS}$ for DnaJ could have also been responsible for the observed toxicity of DnaK$_{LS}$ in *E. coli BB2393* cells upon complementation assays (Figure 4.7 B).

5.3.3 The linkers of PfHsp70-1 and PfHsp70-z modulate the interaction of the two proteins

PfHsp70-z is thought to be a nucleotide exchange factor (NEF) of PfHsp70-1 and has previously been demonstrated to interact with PfHsp70-1 (Zininga *et al*., 2016). The role of the linkers of PfHsp70-1 and PfHsp70-z in modulating interaction of the two chaperones was determined using SPR analysis. The derived SPR sensograms demonstrated that the interactions occurred in a concentration dependent manner at 6 different concentrations (Figure 5.3). Consistent with previous findings, PfHsp70-1 and PfHsp70-z interaction occurred with derived K_D values in the micromolar range (7.75 µM) (Table 5.4; Zininga *et al*., 2016). There was no significant difference observed in the affinity of PfHsp70-z for either PfHsp70-1$_{LS}$ or PfHsp70-1 (Table 5.4). Furthermore, both PfHsp70-z$_{LS}$ and PfHsp70-z exhibited comparable affinity for PfHsp70-1 with K_D values occurring within the same order of magnitude (Table 5.4). In addition, there was significantly reduced affinity between PfHsp70-1$_{LS}$ and PfHsp70-z$_{LS}$ which exhibited K_D values of 33.20 µM in comparison to K_D values of 7.75 µM observed for PfHsp70-z and PfHsp70-1 association. This implies that the mutation of the linkers of PfHsp70-1 and PfHsp70-z is detrimental to association of the two proteins.

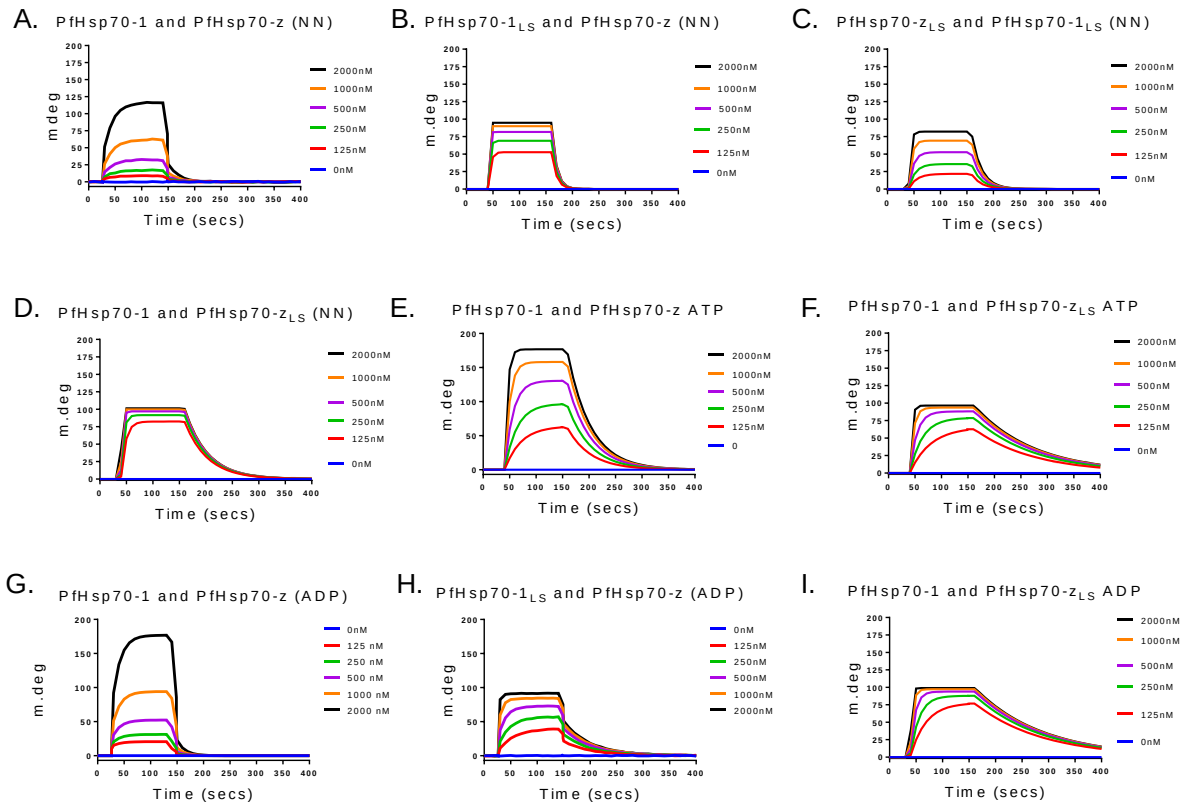

Figure 5.3. SPR sensograms for PfHsp70-1 and PfHsp70-z interaction

Representative sensograms for the interaction of wild type and linker switch mutant versions of PfHsp70-1 and PfHsp70-z. Sensograms show that interaction between wild type PfHsp70-1 and PfHsp70-z in the absence of nucleotides (A) occurred in a concentration dependent manner across the six different concentrations. Similarly, the interaction of PfHsp70-1_{LS} and PfHsp70-z (B), PfHsp70-z_{LS} and PfHsp70-1_{LS} (C) and PfHsp70-1 and PfHsp70-z_{LS} (D) in the absence of nucleotides occurred in a concentration dependent manner. Sensograms for the association between PfHsp70-1 with PfHsp70-z in the ATP state (E), PfHsp70-1 and PfHsp70-z_{LS} (F) in the ATP state also showed concentration dependence. In the ADP state, the interactions of PfHsp70-1 with PfHsp70-z (G), PfHsp70-1_{LS} with PfHsp70-z (H) and PfHsp70-1 and PfHsp70-z_{LS} occurred in a concentration dependent fashion.

Association of PfHsp70-1 with PfHsp70-z was shown to occur in a nucleotide dependent fashion as previously reported (Table 5.4; Zininga *et al*., 2016). In the ATP state, PfHsp70-1 exhibited increased affinity for PfHsp70-z with K_D values reduced by two orders of magnitude from an initial 7.75 µM to 94 nM (Table 5.4). However, the interaction of PfHsp70-1_{LS} with PfHsp70-z was only reduced by one order of magnitude in the ATP state (Table 5.4) suggesting that the interaction did not follow a typical Hsp70-Hsp110 interaction fashion. Thus, the linker substitution of PfHsp70-1 compromised its association with PfHsp70-z.

Table 5.4. SPR kinetics data of PfHsp70-1 and PfHsp70-z interaction kinetics

Ligand	Analyte	Ka (1/Ms)	Kd (1/s)	KD (M)	χ^2
PfHsp70-1	PfHsp70-z (NN)	6.45 (±0.05)e^{3}	4.99 (±0.09)e^{-2}	7.75 (±0.05)e^{-6}**	1.26
	PfHsp70-z (ADP)	3.54 (±0.04)e^{3}	1.38 (±0.08)e^{-3}	3.89 (±0.09)e^{-6}	2.43
	PfHsp70-z (ATP)	2.10 (±0.10)e^{5}	1.99 (±0.09)e^{-2}	9.46 (±0.06)e^{-8}	0.01
PfHsp70-1_{LS}	PfHsp70-z (NN)	1.70 (±0.70)e^{4}	2.35 (±0.05)e^{-2}	1.38 (±0.08)e^{-6}	3.46
	PfHsp70-z (ADP)	2.14 (±0.04)e^{4}	8.06 (±0.06)e^{-2}	3.76 (±0.06)e^{-6}	1.41
	PfHsp70-z (ATP)	2.61 (±0.01)e^{5}	5.99 (±0.09)e^{-2}	2.29 (±0.09)e^{-7}	2.64
PfHsp70-1	PfHsp70-z_{LS} (NN)	2.55 (±0.05)e^{3}	2.43 (±0.03)e^{-2}	9.54 (±0.04)e^{-6}	9.27
	PfHsp70-z_{LS} (ADP)	4.85 (±0.05)e^{3}	7.90 (±0.90)e^{-3}	1.63 (±0.03)e^{-6}	6.75
	PfHsp70-z_{LS} (ATP)	2.72 (±0.02)e^{4}	8.71 (±0.01)e^{-3}	3.20 (±0.20)e^{-7}	2.06
PfHsp70-1_{LS}	PfHsp70-z_{LS} (NN)	3.11 (±0.01)e^{3}	1.00 (±0.01)e^{-1}	3.32(±0.02)e^{-5}**	3.46
	PfHsp70-z_{LS} (ADP)	1.85 (±0.05)e^{3}	1.05 (±0.05)e^{-2}	5.65 (±0.05)e^{-6}	1.32
	PfHsp70-z_{LS} (ATP)	2.21 (±0.01)e^{3}	1.08 (±0.08)e^{-2}	4.89 (±0.09)e^{-6}	2.08
BSA	PfHsp70-1	ND	ND	ND	-
	PfHsp70-1_{LS}	ND	ND	ND	-
	PfHsp70-z	ND	ND	ND	-
	PfHsp70-z_{LS}	ND	ND	ND	-

Three independent analyses were conducted using SPR to elucidate PfHsp70-1/PfHsp70-1_{LS} interaction with PfHsp70-z/ PfHsp70-z_{LS}. Standard errors are shown in brackets. Chi^2 values indicate the score for the goodness of fit of the Langmuir fit model used to generate the kinetics. ND: represents 'not detected' for SPR kinetics that were too low to detect. Statistical analysis was conducted using a One-Way ANOVA at $p<0.05$*; $p<0.01$**;$p<0.001$**.

5.4 Discussion

In the current study, the role of the linkers of PfHsp70-1, PfHsp70-z and DnaK in modulating co-operation with respective co-chaperones was established. Compared to wild type PfHsp70-1, PfHsp70-1_{LS} exhibited much lower affinity for PfHsp40 (Table 5.2). Similarly, $DnaK_{LS}$ exhibited lower affinity for DnaJ (Table 5.2). This suggests that the linker present in canonical Hsp70 possibly has a stabilizing effect on the association between the chaperone and its co-chaperone, Hsp40. Previously, leucine residue mutations in the DnaK linker were demonstrated to induce a ten-fold reduction in DnaJ binding affinity (Kumar *et al*., 2011). Furthermore, the Hsp40 HPD motif has previously been reported to interact with Hsp70 through direct contact with the linker binding cleft (Alderson *et al*., 2016; Malinverni *et al*., 2016). It is therefore plausible that, the introduction of the PfHsp70-z linker into the canonical Hsp70 chaperones destabilized interaction with Hsp40.

Interestingly, interaction of PfHsp70-1_{LS} with either PfHsp40 or PfHop did not occur in a nucleotide dependent manner as observed in the wild type form (Figure 5.1; Figure 5.2; Table 5.1; Table 5.2). Similarly, $DnaK_{LS}$ interaction with DnaJ did not occur in a nucleotide dependent fashion as observed in wild type DnaK (Table 5.2). Previously, tertiary structure studies revealed that PfHsp70-1_{LS} is poorly conformationally responsive to ATP binding (Figure 3.7). It is conceivable that, binding of nucleotides at the NBD of either PfHsp70-1_{LS} or $DnaK_{LS}$ failed to induce efficient interdomain coupling essential for co-operation with the co-chaperones. As such, the linker of PfHsp70-z, possibly tethers the domains of PfHsp70-1_{LS} into a conformation that promotes co-operation with co-chaperones under varying nucleotide states.

Findings from this study further suggest that the linkers of PfHsp70-1 and PfHsp70-z play a crucial role in the co-operation between the two chaperones (Table 5.3). The interaction between the yeast Hsp110 (Sse1) and the canonical Hsp70 (Ssa1) has previously been established to occur through NBD: NBD contacts of the respective proteins (Pollier *et al*., 2008). Interestingly, the current findings suggest that the NBDs of PfHsp70-1 and PfHsp70-z are incapable of associating (Appendix B12). However,

PfHsp70-1$_{NBD}$ and PfHsp70-z$_{NBD}$ interacted with full length forms of PfHsp70-z or PfHsp70-1, respectively, with higher affinity (Appendix B 12). The findings suggest that minimally, at least one NBD of the two proteins is required to interact with a full length form of the other.

The current study demonstrated that the linker of PfHsp70-1 plays an important role in the association of the protein with its co-chaperones. Since Hsp70 is known to form co-operations with co-chaperones during its functional cycle, abrogating the linker may adversely impact on cellular proteostasis during the parasite development. The linker thus facilitates the engagement of PfHsp70-1 with co-chaperones and its NEF, PfHsp70-z.

CHAPTER 6

Conclusion and future perspectives

6.0 Conclusion and future perspectives

P. falciparum survives under physiologically diverse conditions during its life cycle (Figure 1.1). As such, the parasite relies on its robust network of Hsps to maintain cellular proteostasis. PfHsp70-1 and PfHsp70-z are essential chaperones that have previously been shown to play a key role in parasite survival (Chiang *et al*., 2007; Muralidharan *et al*., 2011). Although these cytosolic Hsp70 isoforms exhibit similar domain architecture, they are distinguished from each other by unique linker segments (Figure 2.2 A). Furthermore, plasmodial Hsp110s are marked a unique linker segment constituted by the residues -EYECVEK- (Figure 2.2). In view of the fact that PfHsp70-1 and PfHsp70-z are functionally distinguished from each other, signature motifs such as the linkers modulate functional features of the proteins.

While PfHsp70-1 function is largely dependent on nucleotides, the chaperone function of its Hsp110 counterpart, PfHsp70-z is independent of nucleotides (Figure 4.5; Zininga et al., 2016). The current study demonstrated for the first time that the variations in some functional capabilities exhibited by PfHsp70-1 and PfHsp70-z was on account of the differences existing between the linkers of the two proteins. For instance, the PfHsp70-1 linker exhibited flexibility which facilitated interdomain communication within the protein (Figure 3.6). Furthermore, in PfHsp70-1, ATP binding was coupled with concomitant release of bound substrate at the SBD (Figure 4.5). On the other hand, the rigid PfHsp70-z linker made PfHsp70-1_{LS} to remain bound to substrates in the ATP state. Thus, the PfHsp70-z linker possibly accounts for the increased efficiency of the protein's holdase function. Due to its linker, PfHsp70-z acts as a buffer that is capable of suppressing the otherwise aggregation prone *P. falciparum* proteome in a manner that is independent of nucleotide (Zininga et l., 2016; Chakafana et al., 2019b). This is of utmost importance, in view of the fact that approximately 30% of the parasite proteome consists of asparagine repeat-rich regions which are prone to aggregation under heat stress (Pallares et al., 2018).

The current study also demonstrated that PfHsp70-1 and PfHsp70-z linkers delineate the structural features of the proteins. *In silico* predictions and biophysical assays both revealed that linker swaps had far reaching consequences on the global conformations of the proteins. Notably, the rigid PfHsp70-z linker conferred stability to the protein upon exposure to thermal stress, pH shifts as well as chemical denaturants. Since the parasite is exposed to temperature and pH fluctuations during its development, the linker possibly plays a role in stabilizing PfHsp70-z structure under stress conditions. Previously, the DnaK linker was implicated in conferring increased sensitivity to pH (Swain *et al*., 2007). In a similar fashion, PfHsp70-1 and PfHsp70-z_{LS} were more responsive to thermal and pH shifts, suggesting that the PfHsp70-1 linker modulates the proteins' responsiveness to changes in the physiological environment. Overally, these findings suggest that, the PfHsp70-1 linker functions as a 'potentiometer' (Chakafana *et al*., 2019b) which makes the protein more sensitive to physiological changes.

The current study also demonstrated for the first time that, the PfHsp70-1 linker facilitates the protein's association with co-chaperones and peptides. As such, abrogating the linker reduces the interactome of Hsp70 and potentially impairs its cellular function. This was demonstrated by the lower refolding rates exhibited by the PfHsp70-1+PfHsp70-z+PfHsp40 complex upon linker mutations (Figure 4.5). Since both PfHsp70-z and PfHsp70-1 are expressed at the erythrocytic stage, the linkers of these chaperones may play a key role in the co-ordinated folding of *P. falciparum* invasion proteins (Joshi *et al*., 1992; Paul *et al*., 2004). As such, the linker could pose as a key determinant of erythrocyte invasion during infection. Complementation assays also revealed that the canonical linker cannot be functionally replaced by the PfHsp70-z linker. In view of the fact that PfHsp70-1 confers thermotolerance to cells (Shonhai *et al*., 2008), its linker may play a decisive role in cytoprotection of the parasite cells under thermal stress.

Overall, the linker residues of PfHsp70-1 and PfHsp70-z, are important for global protein structure and function. This study provided evidence that the linkers of PfHsp70-1 and PfHsp70-z modulate various functional specifications of the proteins which include ATP hydrolysis, chaperone function, refolding activity as well as substrate, nucleotide and co-chaperone binding. The linkers of PfHsp70-1 and PfHsp70-z therefore represent structural helms which modulates global conformation and functional capabilities of the respective proteins. Since PfHsp70-z is an essential protein for *P. falciparum* survival (Muralidharan *et al*., 2011), its unique linker motif may account for its unique function in comparison to its cytosolic Hsp70 counterpart, PfHsp70-1.

The flexibility of the PfHsp70-1 linker is crucial for the protein's function as it remotely facilitates the transmission of allosteric signals between the NBD and SBD. Small molecule inhibitors targeting the NBD of PfHsp70-1 have previously been shown to abrogate interaction of the protein with PfHop, which binds at the SBD (Zininga *et al*., 2017a,b). This implies that the PfHsp70-1 linker facilitates signal transmission between the proteins' domains thus perturbing the global conformation of the chaperone in response to inhibitor binding. Since the PfHsp70-z linker is rigid, it may imply that inhibitors targeting PfHsp70-1 are less effective on PfHsp70-z. As such, it is important to identify inhibitors that selectively target the linker and potentially modulate protein conformation. In light of the fact that linkers dictate structure, selected targeting potentially abrogates Hsp70 functional capabilities such as ATPase activity, chaperone function and association with co-chaperones/other chaperones. In light of the fact that the two essential chaperones are marked by distinct variations, it is important to determine the crystal structures of the proteins to further understand their structural conformations. Additionally, the role of the linkers in complex formation can be further investigated using more robust techniques such as Cryo-EM.

References

Absalon, S., Robbins, J. A, Drovin, J. (2016). An essential malaria protein defines the architecture of blood-stage and transmission-stage parasites. *Nat Comms,* **7:** 11449.

Abu Bakar, N.A., Klonis, N., Hanssen, E., Chan, C., Tilley, L. (2010). Digestive-vacuole genesis and endocytic processes in the early intraerythrocytic stages of *Plasmodium falciparum*. *J Cell Sci*, **123:** 441–50.

Achilonu, I., Siganunu, T.P., Dirr, H.W. (2014). Purification and characterisation of recombinant human eukaryotic elongation factor 1 gamma. *Protein Expr Purif*, **99:** 70-77.

Alderson, T.R., Kim, J.H., Cai, K., Frederick, R.O., Tonelli, M., Markley, J.L. (2014). The specialized Hsp70 (HscA) interdomain linker binds to its nucleotide-binding domain and stimulates ATP hydrolysis in both cis and trans configurations. *Biochem J*, **53:** 7148-7159.

Alderson, T. R., Kim, J., H., Markley, J. L. (2016). Dynamical Structures of Hsp70 and Hsp70-Hsp40 Complexes. *Structure,* **24:**1014-30.

Althoff, T., Abramson, J. (2020). Protein structure reveals how a malaria parasite imports a wide range of sugars. *Nat Struct Mol Biol*, doi: 10.1038/d41586-020-00148-8.

Alvarez, G., Pineros, J.G., Tobon, A., Rios, A., Maestre, A., Blair, S. and Carmona-Fonseca, J. (2006). Efficacy of three chloroquine–primaquine regimens for treatment of *Plasmodium vivax* malaria in Colombia. *Am J Trop Med Hyg,* **75:** 605-609.

Amino, R, Thiberge, S, Martin, B, Celli, S, Shorte, S, Frischknecht, F, Ménard, R. (2006). Quantitative imaging of *Plasmodium* transmission from mosquito to mammal. *Nat Med,* **12:** 220-4.

Andréasson, C., Fiaux, J., Rampelt, H., Druffel-Augustin, S., Bukau, B. (2008). Insights into the structural dynamics of the Hsp110-Hsp70 interaction reveal the mechanism for nucleotide exchange activity. *Proc Natl Acad Sci USA*, **105:**16519-16524.

Argos, P. (1990). An investigation of oligopeptides linking domains in protein tertiary structures and possible candidates for general gene fusion. *J Mol Biol*, **211:** 943-958.

Baer, K., Klotz, C., Kappe, S. H., Schneider, T., Frevert, U. (2007). Release of hepatic *Plasmodium yoelii* merozoites into the pulmonary microvasculature. *PLoS Path,* **3:** e171.

Banumathy, G., Singh, V., Pavithra, S.R., Tatu, U. (2003). Heat shock protein 90 function is essential for *Plasmodium falciparum* growth in human erythrocytes. *J Biol Chem*, **278:** 18336-18345.

Baum, J., Tonkin, C. J., Paul, A. S., Rug, M., Smith, B. J. *et al*. (2008). A malaria parasite formin regulates actin polymerization and localizes to the parasite-erythrocyte moving junction during invasion. *Cell Host Microbe*, **3:**188-98.

Behl, A., Mishra, P. C. (2018). Structural insights into the binding mechanism of *Plasmodium falciparum* exported Hsp40-Hsp70 chaperone pair. *Comput Biol Chem,* doi: 10.1016/j.compbiolchem.2019.107099

Behnke, M.S., Khan, A., Lauron, E.J., Jimah, J.R., Wang, Q., Tolia, N.H., Sibley, L.D. (2015). Rhoptry proteins ROP5 and ROP18 are major murine virulence factors in genetically divergent South American strains of *Toxoplasma gondii*. *PLoSGenet*, **11**: e1005434.

Bennett, B., Holz, R.C. (1997). Spectroscopically distinct cobalt (II) sites in heterodimetallic forms of the aminopeptidase from *Aeromonas proteolytica*: characterization of substrate binding. *Biochem J*, **36:** 9837-9846.

Billker, O., Lindo, V., Panico, M., Etienne, A. E., Paxton, T., Dell, A., Rogers, M., Sinden, R. E., Morries, H. R. (1998). Identification of xanthurenic acid as the putative inducer of malaria development in the mosquito. *Nature,* **392:** 289-92.

Billker, O., Miller, A. J., Sinden, R. E. (2000). Determination of mosquito bloodmeal pH in situ by ion-selective microelectrode measurement: implications for the regulation of malarial gametogenesis. *Parasitology,* **120:** 547-551

Botha, M., Pesce, E. R., Blatch, G. L. (2007). The Hsp40 proteins of *Plasmodium falciparum* and other Apicomplexa: regulating chaperone power in the parasite and the host. *Int J Biochem Cell Biol,* **39:** 1781-803.

Brodsky, J.L. (2007). The protective and destructive roles played by molecular chaperones during ERAD (endoplasmic reticulum associated degradation). *Biochem J,* **404:** 353-363.

Buchberger, A., Schröder,H., Büttner, M., Valencia, A., Bukau., B. (1994). A conserved loop in the ATPase domain of the DnaK chaperone is essential for stable binding of GrpE**.** *Nat Struct Biol,* **1:** 95-101

Bull, B.S., Herrmann, P.C. (2010). Morphology of the erythron. Chapter in Hematology**,** edited by Marshall A. Lichtman, Thomas J. Kipps, Uri Seligsohn, Kenneth Kaushansky, Josef T. Prchal. Copyright 2010, by The McGraw-Hill Companies.

Buchner, J., Li, J. (2013). Structure, function and regulation of the hsp90 machinery. *Biomed J*, **36:** 106.

Calloni, G., Chen, T., Schermann, S.M., Chang, H.C., Genevaux, P., Agostini, F., Tartaglia, G.G., Hayer-Hartl, M. and Hartl, F.U. (2012). DnaK functions as a central hub in the *E. coli* chaperone network. *Cell Rep*, **1:** 251-264.

Caplan, A. J, Cryr, D. M and Douglas, M. G.(1993). Eukaryotic homologues of *Escherichia coli* DnaJ: a diverse protein family that functions with Hsp70 stress proteins. *Mol Biol Cell*, **4:** 555-563.

Carrigan, P. E., Sikkink, L. A., Smith, D. F., Ramirez, A. (2006). Domain: domain interactions within Hop, the Hsp70/Hsp90 organizing protein, are required for protein stability and structure*. Prot Sci,* **15:** 522-532.

Chakafana, G., Zininga, T., Shonhai, A. (2019a). Comparative structure-function features of Hsp70s of *Plasmodium falciparum* and human origins. *Biophys Rev*, **11:** 1-12.

Chakafana, G., Zininga, T., Shonhai, A. (2019b). The link that binds: The linker of Hsp70 as a helm of the protein's function. *Biomolecules*, **9:** 543-563.

Charpian, S., Przyborski, J.M. (2008). Protein transport across the parasitophorous vacuole of *Plasmodium falciparum*: into the great wide open. *Traffic*, **9:** 157-165.

Chen, X., Zaro, J.L, Shen, W.C. (2013). Fusion protein linkers: property, design and functionality. *Adv Drug Deliv Rev*, **65:** 1357-1369.

Chen, Y., Murillo-Solano, C., Kirkpatrick, M., Antoshchenko, T., Park, T., Pizarro, J. (2018). Repurposing drugs to target the malaria parasite unfolding protein response. *Sci Rep,* **8:** 10333-10350.

Chiang, A.N., Valderramos, J.C., Balachandran, R., Chovatiya, R.J., Mead, B.P., Schneider, C. (2009). Select pyrimidinones inhibit the propagation of the malarial parasite *Plasmodium falciparum*. *Bioorg Med Chem,* **17:**1527-1533.

Chichili, V.P., Kumar, V., Sivaraman, J. (2013). Linkers in the structural biology of protein-protein interactions. *Prot Sci*, **22:** 153-167.

Chiappori, F., Merelli, I., Milanesi, L., Colombo, G., Morra, G. (2016). An atomistic view of Hsp70 allosteric crosstalk: from the nucleotide to the substrate binding domain and back. *Sci Rep*, **6:** 1-14.

Chua, C.S., Low, H., Lehming, N., Sim T.S. (2012). Molecular analysis of *Plasmodium falciparum* co-chaperone Aha1 supports its interaction with and regulation of Hsp90 in the malaria parasite*. Int J Biochem Cell Biol,* **44:**233-245.

Clerico, E.M., Tilitsky, J.M., Meng, W., Gierasch, L.M. (2015). How hsp70 molecular machines interact with their substrates to mediate diverse physiological functions. *J Mol Biol*, **427:** 1575-1588.

Cobb, D.W., Florentin, A., Fierro, M.A., Krakowiak, M., Moore, J.M., Muralidharan, V. (2017). The exported chaperone PfHsp70x is dispensable for the *Plasmodium falciparum* intraerythrocytic life cycle. *mSphere*, ***2*:** e00363-17.

Cowman, A. F., Crabb, B. S. (2006). Invasion of red blood cells by malaria parasites. *Cell,* **124:** 755-66.

Craig, A., Scherf, A. (2001). Molecules on the surface of the *Plasmodium falciparum* infected erythrocyte and their role in malaria pathogenesis and immune evasion. *Mol Biochem Parasitol*, **115:** 129-43.

Crick, A. J., Theron, M., Tiffert, T., Virgilio, L. L., Cicuta, P., Rayner, J. C. (2014). Quantitation of malaria parasite-erythrocyte cell-cell interactions using optical tweezers. *Biophys J*, **107:** 846-853.

Cryr, D. M., Ramos, C. H. (2015). Specification of Hsp70 function by Type I and Type II Hsp40. *Subcell Biochem,* **78:** 91-102.

Daniyan, M. O., Przyborski, J. M., Shonhai, A. (2019). Partners in mischief: Functional networks of heat shock proteins of *Plasmodium falciparum* and their influence on parasite virulence. *Biomolecules,* **9:** 295.

Desai, S. A. (2014). Why do malaria parasites increase host erythrocyte permeability? *Trends Parasitol*, **30:**151-159.

Dhamad, A.E., Zhou, Z., Zhou, J., Du, Y. (2016). Systematic proteomic identification of the heat shock proteins (Hsp) that interact with estrogen receptor alpha (ERα) and biochemical characterization of the ERα-Hsp70 interaction. *PLoS One*, **11**. e0160312

Dragovic, Z., Broadley, S.A., Shomura, Y., Bracher, A., Hartl, F.U. (2006). Molecular chaperones of the Hsp110 family act as nucleotide exchange factors of Hsp70s. *EMBO J*, **25:** 2519-2528.

Duhovny, D., Inbar, Y., Nussinov, R., Wolfson, H.J. (2005). PatchDock and SymmDock: servers for rigid and symmetric docking. *Nucl Acid Res*, **33:** 363-367.

Dunbar, J., Yennawar, H.P., Banerjee, S., Luo, J. and Farber, G.K. (1997). The effect of denaturants on protein structure. *Prot Sci*, **6:** 1727-1733.

Duraisingh, M. T., Maier, A. G., Triglia, T., Cowman, A. F. (2003). Erythrocyte-binding antigen 175 mediates invasion in *Plasmodium falciparum* utilizing sialic acid-dependent and independent pathways. *Proc Natl Acad Sci U S A,* **100:** 4796-4801

Easton, D.P., Kaneko, Y., Subjeck, J.R. (2000). The Hsp110 and Grp170 stress proteins: newly recognized relatives of the Hsp70s. *Cell Stress Chaperones*, **5:** 276.

Elliott, D. A., McIntosh, M. T., Hosgood, H. D., Chen, S., Zhang, G., Baevova, P., Joiner, K. A. (2007). Four distinct pathways of hemoglobin uptake in the malaria parasite *Plasmodium falciparum*. *Proc Natl Acad Sci U S A,* **105:** 2463-2468.

English, C.A., Sherman, W., Meng, W., Gierasch, L.M. (2017). The Hsp70 interdomain linker is a dynamic switch that enables allosteric communication between two structured domains. *J Biol Chem,* **292:** 14765-14774.

Fan, C. Y., Lee, S., Cryr, D. M. (2003). Mechanisms for regulation of Hsp70 function by Hsp40. *Cell Stress Chaperones*, **8:** 309-316.

Felts, S.J and Toft, D.O. (2003). p23, a simple protein with complex activities. *Cell Stress Chaperones*, **8:** 108.

Flaherty, K.M., DeLuca-Flaherty, C., McKay, D.B. (1990). Three-dimensional structure of the ATPase fragment of a 70K heat-shock cognate protein. *Nature*, **346:** 623-628.

Gamerdinger, M., Hajieva, P., Kaya, A.M., Wolfrum, U., Hartl, F.U., Behl, C. (2009). Protein quality control during aging involves recruitment of the macroautophagy pathway by BAG3. *EMBO J*, **28:** 889-901.

Gässler, C.S., Buchberger, A., Laufen, T., Mayer, M.P., Schröder, H., Valencia, A., Bukau, B. (1998). Mutations in the DnaK chaperone affecting interaction with the DnaJ cochaperone. *Proc Natl Acad Sci U S A*, **95:** 15229-15234.

Geleta, G., Ketema, T. (2016). Severe Malaria Associated with *Plasmodium falciparum* and *P. vivax* among Children in Pawe Hospital, Northwest Ethiopia. *Malar Res Treat*, doi: 10.1155/2016/1240962

Genest, O., Reidy, M., Street, T.O., Hoskins, J.R., Camberg, J.L., Agard, D.A., Masison, D.C., Wickner, S. (2013). Uncovering a region of heat shock protein 90 important for client binding in *E. coli* and chaperone function in yeast. *Mol cell*, **49:** 464-473.

Gitau, G.W., Mandal, P., Blatch, G.L., Przyborski, J., Shonhai, A. (2012). Characterisation of the *Plasmodium falciparum* Hsp70-Hsp90 organising protein (PfHop). *Cell Stress Chaperones*, **17:** 191-202.

Grüring, C., Heiber, A., Kruse, F., Flemming, S., Franci, G., Colombo, S.F., Fasana, S., Schoeler, H., Borgese, N., Stunnenberg, H.G., Przyborski, J.M., Gilberger, T.W., Spielmann, T. (2012). Uncovering common principles in protein export of malaria parasites. *Cell Host Microbe*, **12:** 71729.

Goel, S., Muthusamy, A., Miao, J., Cui, L., Salanti, A., Winzeler, E. A., Gowda, D. C. (2014). Targeted disruption of a ring-infected erythrocyte surface antigen (RESA)-like export protein gene in *Plasmodium falciparum* confers stable chondroitin 4-sulfate cytoadherence capacity. *J Biol Chem*, **289:** 34408-34421.

Gokhale, R.S., Khosla, C. (2000). Role of linkers in communication between protein modules. *Curr Opin Chem Biol*, **4:** 22-27.

Goldberg, D.E. (2005). Haemoglobin degradation. *Curr Top Microbiol Immunol*, **295:** 275-91.

Goloubinoff, P., De Los Rios, P. (2007). The mechanism of Hsp70 chaperones:(entropic) pulling the models together. *Trends Biochem Sci*, **32:** 372-380.

Gong, W., Hu, W., Xu, L., Wu, H., Wu, S., Zhang, H., Wang, J., Jones, G.W., Perrett, S. (2018). The C-terminal GGAP motif of Hsp70 mediates substrate recognition and stress response in yeast. *J Biol Chem*, **293:** 17663-17675.

Gragerov, A., Gottesman, M.E. (1994). Different peptide binding specificities of hsp70 family members. *J Mol Biol,* 241:133-5.

Han, W., Christen, P. (2004). cis-Effect of DnaJ on DnaK in ternary complexes with chimeric DnaK/DnaJ-binding peptides. *FEBS letters*, **563:** 146-150.

Hawking, F, Wilson, M. E, Gammage, K. Evidence for cyclic development and short-lived maturity in the gametocytes of *Plasmodium falciparum*. *Trans R Soc Trop Med Hyg*. **65:** 549-59.

Hennesy, F., Nicoll, W.S., Zimmermann, R., Cheetham, M. E., Blatch, G. L. Not all J domains are created equal: Implications for the specificity of Hsp40-Hsp70 interactions. *Prot Sci,* **14:** 1697-1709.

Hopp, C,S., Chiou, K., Ragheb, D. R. T., Salman, A. M., Khan, M. S., Liu, A. J., Sinnis, P. (2005). Longitudinal analysis of *Plasmodium* sporozoite motility in the dermis reveals component of blood vessel recognition. *eLife* 4: e07789

Jacob, P., Hirt, H., Bendahmane, A. (2017). The heat-shock protein/chaperone network and multiple stress resistance. *Plant Biotechnol J*, **15:** 405-414.

Jensen, L.J., Kuhn, M., Stark, M., Chaffron, S., Creevey, C., Muller, J., Doerks, T., Julien, P., Roth, A., Simonovic, M. and Bork, P. (2009). STRING 8- a global view on proteins and their functional interactions in 630 organisms. *Nucleic Acids Res*, **37:** 412-416.

Johnson, B.D., Schumacher, R.J., Ross, E.D. and Toft, D.O., 1998. Hop modulates Hsp70/Hsp90 interactions in protein folding. *J Biol Chem*, **273:** 3679-3686.

Kabani, M., Kelley, S.S., Morrow, M.W., Montgomery, D.L., Sivendran, R., Rose, M.D., Gierasch, L.M. and Brodsky, J.L. (2003). Dependence of endoplasmic reticulum-associated degradation on the peptide binding domain and concentration of BiP. *Mol Biol Cell*, **14:** 3437-3448.

Kadekoppala, M, O' Donnell, R. A, Grainger, M, Crabb, B, S, Holder, A. A. (2008). Deletion of the *Plasmodium falciparum* Merozoite Surface Protein 7 gene impairs parasite invasion of erythrocytes. *Eukaryot Cell*, **7:** 2123-2132

Kakihara, Y., Houry, W.A. (2012). The R2TP complex: discovery and functions. *BBA Mol Cell Res*, **1823:** 101-107.

Kampinga, H.H., Hageman, J., Vos, M.J., Kubota, H., Tanguay, R.M., Bruford, E.A., Cheetham, M.E., Chen, B. and Hightower, L.E. (2009). Guidelines for the nomenclature of the human heat shock proteins. *Cell Stress Chaperones*, **14:** 105-111.

Kampinga, H.H., Craig, E.A. (2010). The HSP70 chaperone machinery: J proteins as drivers of functional specificity. *Nat Rev Mol Cell Biol*, **11:** 579-592.

Khusmith, S, Sedegah, M., Hojman, S. L. (1994). Complete protection against *Plasmodium yoelii* by adoptive transfer of a CD8+ cytotoxic T-cell clone recognizing sporozoite surface protein 2. *Infect Immun,* **62:** 2979-2983.

Kilili, G. K., LaCount, D, J. (2011). An erythrocyte cytoskeleton-binding motif in exported *Plasmodium falciparum* Proteins. *Eukaryot Cell*, **11:** 1439-1447.

Kityk, R., Kopp, J., Sinning, I. and Mayer, M.P. (2012). Structure and dynamics of the ATP-bound open conformation of Hsp70 chaperones. *Mol Cell*, **48:** 863-874.

Kityk, R., Vogel, M., Schlecht, R., Bukau, B., Mayer, M.P. (2015). Pathways of allosteric regulation in Hsp70 chaperones. *Nat Commun,* **6:** 8308.

Kityk, R, Kopp, J, Mayer, M. P. (2018). Molecular mechanism of J-domain-triggered ATP hydrolysis by Hsp70 chaperones. *Mol Cell,* **69:** 227-237.

Koch, M., Baum, J. (2016). The mechanics of malaria parasite invasion of the human erythrocyte towards a reassessment of the host cell contribution. *Cell Microbiol,* **18:** 319-329

Kudyba, H.M., Cobb, D.W., Fierro, M.A., Florentin, A., Ljolje, D., Singh, B., Lucchi, N.W., Muralidharan, V. (2019). The endoplasmic reticulum chaperone PfGRP170 is essential for asexual development and is linked to stress response in malaria parasites. *Cell Microbiol*, **21:** p.e13042.

Kulzer, S, Charmaud, S, Dagan, T, Riedel, J, Mandal, P, Pesce, E. R, Blatch, G. L, Crabb, B. S and Gilson, P. R., Pryzyborski. (2012). *Plasmodium falciparum*-encoded exported Hsp70/Hsp40 chaperone/co-chaperone complexes within the host erythrocyte. *Cell Microbiol,* **14:** 1784-95.

Kumar, N., Koski, G., Harada, M., Aikawa, M., and Zheng, H. (1991). Induction and localization of *Plasmodium falciparum* stress proteins related to the heat shock protein 70 family. *Mol Biochem Parasitol*, **48:** 47–58.

Kumar, R., Musiyenko, A., Barik, S. (2003). The heat shock protein 90 of *Plasmodium falciparum* and antimalarial activity of its inhibitor, geldanamycin. *Malaria J,* **2:** 30.

Kumar, D.P., Vorvis, C., Sarbeng, E., Ledesma, V.C.C., Willis, J.E., Liu, Q. (2011). The four hydrophobic residues on the Hsp70 interdomain linker have two distinct roles. *J Mol Bio,* **4:** 1099-1113.

Kumar, V., Peter, J.J., Sagar, A., Ray, A., Jha, M.P., Rebeaud, M.E., Tiwari, S., Goloubinoff, P., Mapa, K. (2019). Interdomain communication suppressing high intrinsic ATPase activity of Sse1 is essential for its co-disaggregase activity with Ssa1. *FEBS J*, **287:** 681-694.

Lebepe, C.M., Matambanadzo, P.R., Makhoba, X.H., Achilonu, I., Zininga, T. and Shonhai, A. (2020). Comparative characterization of *Plasmodium falciparum* Hsp70-1 relative to *E. coli* DnaK reveals the functional specificity of the parasite chaperone. *Biomolecules*, **10:** 856.

Liberek, K., Marszalek, J., Ang, D., Georgopoulos, C., Zylicz M. (1991). *Escherichia coli* DnaJ and GrpE heat shock proteins jointly stimulate ATPase of DnaK. *Proc Natl Acad Sci USA,* **88:** 2874-2878.

Liebscher, M., Roujeinikova, A. (2009). Allosteric coupling between the lid and interdomain linker in DnaK revealed by inhibitor binding studies. *J Bacteriol*, **191:** 1456-1462.

Lindquist, S. (1986). The heat-shock response. *Annu Rev Biochem,* **55:** 1151-91.

Lim, L., McFadden, G.I. (2010). The evolution, metabolism and functions of the apicoplast. *Philos Trans R Soc Lond B Biol Sci*. **365:** 749-63.

Lingelbach, K., Joiner, K. A. (1998). The parasitophorous vacuole membrane surrounding *Plasmodium* and *Toxoplasma*: an unusual compartment in infected cells. *J Cell Sci,* **11:** 1467-75.

Liu, Q., Hendrickson, W.A. (2007). Insights into Hsp70 chaperone activity from a crystal structure of the yeast Hsp110 Sse1. *Cell*, **131:** 106-120.

Luengo, T.M., Kityk, R., Mayer, M.P., Rüdiger, S.G. (2018). Hsp90 breaks the deadlock of the Hsp70 chaperone system. *Mol Cell*, **70:** 545-552.

Lyons, R.E., Johnson, A.M. (1998). Gene sequence and transcription differences in 70 kDa heat shock protein correlate with murine virulence of *Toxoplasma gondii*. *Intl J Parasitol*, **28:** 1041-1051.

Maier, A.G., Rug, M., O'Neill, M.T., Brown, M., Chakravorty, S., Szestak, T., Chesson, J., Wu, Y., Hughes, K., Coppel, R.L., Newbold, C. (2008). Exported proteins required for virulence and rigidity of *Plasmodium falciparum*-infected human erythrocytes. *Cell*, **134:** 48-61.

Malinverni, D., Marsili, S., Barducci, A and De Los Rios, P. (2015). Large-scale conformational transitions and dimerization are encoded in the amino-acid sequences of Hsp70 chaperones. *PLoS Comput Biol*, **11**. e1004262.

Marinko, J.T., Huang, H., Penn, W.D., Capra, J.A., Schlebach, J.P., Sanders, C.R. (2019). Folding and misfolding of human membrane proteins in health and disease: from single molecules to cellular proteostasis. *Chem Rev,* **119:** 5537-5606.

Matambo, T.S., Odunuga, O.O., Boshoff, A., Blatch, G.L. (2004). Overproduction, purification and characterization of the *Plasmodium falciparum* heat shock protein 70. *Protein Expr Purif,* **33:** 214-222.

Mattoo, R. U., Sharma, S. K., Priya, S., Finka, A., Goloubinoff, P. (2013). Hsp110 is a bona fide chaperone using ATP to unfold stable misfolded polypeptides and reciprocally collaborate with Hsp70 to solubilize protein aggregates. *J Biol Chem,* **288:** 21399-411.

Mattoo, R. H., Goloubinoff, P. (2014). Molecular chaperones are nanomachines that catalytically unfold misfolded and alternatively folded proteins. *Cell Mol Life Sci,* **71:** 3311-3325.

Mayer, M.P., Brehmer, D., Gässler, C.S., Bukau, B. (2001). Hsp70 chaperone machines. *Adv Prot Chem*, **59:** 1-44.

Mayer, M.P., Bukau, B. (2005). Hsp70 chaperones: cellular functions and molecular mechanism. *Cell Mol Life Sci*, **62:** 670.

Mayer, M.P. (2013). Hsp70 chaperone dynamics and molecular mechanism. *Trends Biochem Sci*, **38:** 507-514.

Mayer, M.P., Kityk, R. (2015). Insights into the molecular mechanism of allostery in Hsp70s. *Front Mol Biosci*, **2:** 58.

Mayer, M.P., Gierasch, L.M. (2019). Recent advances in the structural and mechanistic aspects of Hsp70 molecular chaperones. *J Biol Chem,* **294:** 2085-2097.

Mbengue, A., Yam, X.Y., Braun-Breton, C. (2012). Human erythrocyte remodelling during *Plasmodium falciparum* malaria parasite growth and egress. *Br J Haematol*, **157:** 171-179.

Meibalan, E., Marti, M. 2017. Biology of Malaria Transmission. *Cold Spring Harb Perspect Med*, **7:** a025452

Meis, J. F., Wismans, P. G., Jap, P. H., Lensen, A. H., Ponnudurai, T. (1992). A scanning electron microscopic study of the sporogonic development of *Plasmodium falciparum* in *Anopheles stephensi*. *Acta Tropica,* **50:** 227-236.

Misra, G., Ramachandran, R. (2009). Hsp70-1 from *Plasmodium falciparum*: protein stability, domain analysis and chaperone activity. *Biophys Chem*, **142:** 55-64.

Mohandas, N., An, X. (2012). Malaria and human red blood cells. *Med Microbiol Immunol,* 201: 593-598.

Mogk, A., Kummer, E., Bukau, B. (2015). Cooperation of Hsp70 and Hsp100 chaperone machines in protein disaggregation. *Front Mol Biosci*, **2:** 22.

Mundwiler-Pachlatko, E., Beck, H. P. (2013). Maurer's clefts, the enigma of *Plasmodium falciparum. Proc Natl Acad Sci USA*, **110:** 19987-19994.

Nakamoto, N., Kanai, T. (2014). Role of toll-like receptors in immune activation and tolerance in the liver. *Front Immunol*, **5:** 221.

Njunge, J., Ludewig, M., Boshoff, A., Pesce, E.R., Blatch, G. (2013). Hsp70s and J proteins of *Plasmodium* parasites infecting rodents and primates: structure, function, clinical relevance, and drug targets. *Curr Phar Design*, **19:** 387-403.

Olshina, M. A., Angrisano, F., Marapana, D. S. *et al.* (2015). *Plasmodium falciparum* coronin organizes arrays of parallel actin filaments potentially guiding directional motility in invasive malaria parasites. *Malar J,* **14:** 280.

Oh, H.J., Easton, D., Murawski, M., Kaneko, Y., Subjeck, J.R. (1999). The chaperoning activity of Hsp110 identification of functional domains by use of targeted deletions. *J Biol Chem*, **274:** 15712-15718.

Packschies, L., Theyssen, H., Buchberger, A., Bukau, B., Goody, R.S., Reinstein, J. (1997). GrpE accelerates nucleotide exchange of the molecular chaperone DnaK with an associative displacement mechanism. *Biochem J*, **36:** 3417-3422.

Pal, M., Morgan, M., Phelps, S.E., Roe, S.M., Parry-Morris, S., Downs, J.A., Polier, S., Pearl, L.H., Prodromou, C. (2014). Structural basis for phosphorylation-dependent recruitment of Tel2 to Hsp90 by Pih1. *Structure*, **22:** 805-818.

Pallarès, I., de Groot, N. S., Iglesias, V., Sant'Anna, R., Biosca, A., Fernàndez-Busquets X., Ventura, S. (2018). Discovering putative prion-like proteins in *Plasmodium falciparum*: a computational and experimental analysis. *Front Microbiol,* **9:** 1737

Pallavi, R., Roy, N., Nageshan, R.K., Talukdar, P., Pavithra, S.R., Reddy, R., Tatu, U. (2010). Heat shock protein 90 as a drug target against protozoan infections: biochemical characterization of Hsp90 from *Plasmodium falciparum* and *Trypanosoma evansi* and evaluation of its inhibitor as a candidate drug. *J Biol Chem,* **285:** 37964-37975

Pasternak, N. D., Dzikowski, R. (2009). PfEMP1: an antigen that plays a key role in the pathogenicity and immune evasion of the malaria parasite *Plasmodium falciparum*. *Int J Biochem Cell Biol.* **41:**1463-6.

Pasvol, G. (2005). The treatment of complicated and severe malaria. *British Medical Bulletin*, **75:** 29-47

Paul, R. E., Diallo, M., Brey, P.T. (2004). Mosquitoes and transmission of malaria parasites-Not just vectors. *Malaria J,* **3:** 39

Priya, P. P., Grover, M., Tatu, U. S., Natarajan, V. (2015). Characterization of Precursor PfHsp60 in *Plasmodium falciparum* cytosol during its asexual development in human erythrocytes. *PLoS ONE,* **10:** e0136401

Pettersen, E.F., Goddard, T.D., Huang, C.C., Couch, G.S., Greenblatt, D.M et al. (2004). UCSF chimera-a visualization system for exploratory research and analysis. *J Comput Chem,* **25:**1605-1612

Picard, D. (2002). Heat-shock protein 90, a chaperone for folding and regulation. *Cell Mol Life Sci*, **59:** 1640-1648.

Polier, S., Dragovic, Z., Hartl, F.U., Bracher, A. (2008). Structural basis for the cooperation of Hsp70 and Hsp110 chaperones in protein folding. *Cell*, **133:** 1068-1079.

Przyborski, J. M., Diehl, M., Blatch, G.L. (2015). Plasmodial Hsp70s are functionally adapted to the malaria parasite life cycle. *Front Mol Biosci*, **2:** 34.

Qi, R., Sarbeng, E.B., Liu, Q., Le, K.Q., Xu, X., Xu, H., Yang, J., Wong, J.L., Vorvis, C., Hendrickson, W.A., Zhou, L. (2013). Allosteric opening of the polypeptide-binding site when an Hsp70 binds ATP. *Nat Struc Mol Biol*, **20:** 900.

Qui, X. B., Shao, Y. M., Miao, S., Wang, L. (2006). The diversity of the DnaJ/Hsp40 family, the crucial partners for Hsp70 chaperones. *Cell Mol Life Sci,* **63:** 2560-70.

Raviol, H., Sadlish, H., Rodriguez, F., Mayer, M.P., Bukau, B. (2006). Chaperone network in the yeast cytosol: Hsp110 is revealed as an Hsp70 nucleotide exchange factor. *EMBO J*, **25:** 2510-2518.

Reiter, K.H and Matunis, M.J. (2016). Detection of SUMOylation in *Plasmodium falciparum*. In *SUMO* (283-290). Humana Press, New York, NY.

Rinehart, M. T., Park, H. S., Walzer, K. A., Chi, J-T. A., Wax, A. (2016). Hemoglobin consumption by *P. falciparum* in individual erythrocytes imaged via quantitative phase spectroscopy. *Sci Rep,* **6:** 24461.

Robinson, C.R and Sauer, R.T. (1998). Optimizing the stability of single-chain proteins by linker length and composition mutagenesis. *Proc Natl Acad Sci U S A*, **95:** 5929-5934.

Rockabrand, D., Livers, K., Austin, T., Kaiser, R., Jensen, D., Burgess, R., Blum, P. (1998). Roles of DnaK and RpoS in starvation-induced thermotolerance of Escherichia coli. *J Bacteriol*, **180:** 846-854.

Röhl, A., Wengler, D., Madl, T., Lagleder, S., Tippel, F., Herrmann, M., Hendrix, J., Richter, K., Hack, G., Schmid, A.B., Kessler, H. (2015). Hsp90 regulates the dynamics of its cochaperone Sti1 and the transfer of Hsp70 between modules. *Nat Comms*, **6:** 6655.

Rosenzweig, R., Sekhar, A., Nagesh, J. and Kay, L.E. (2017). Promiscuous binding by Hsp70 results in conformational heterogeneity and fuzzy chaperone-substrate ensembles. *Elife*, **6:** e28030.

Rowe, J. A., Claessens, A., Corrigan, R.A., Arman, M. (2009). Adhesion of *Plasmodium falciparum*-infected erythrocytes to human cells: molecular mechanisms and therapeutic implications. *Expert Rev Mol Med*, doi:10.1017/S1462399409001082.

Rüdiger, S., Buchberger, A. and Bukau, B., 1997. Interaction of Hsp70 chaperones with substrates. *Nat Struct Mol Biol*, **4:** 342-349.

Ruiz, D.M., Turowski, V.R., Murakami, M.T. (2016). Effects of the linker region on the structure and function of modular GH5 cellulases. *Sci Rep*, **6:** 1-13.

Sarbeng, E.B., Liu, Q., Tian, X., Yang, J., Li, H., Wong, J.L., Zhou, L., Liu, Q. (2015). A functional DnaK dimer is essential for the efficient interaction with Hsp40 heat shock protein. *J Biol Chem*, **290:** 8849-8862.

Sargeant, T.J., Marti, M., Caler, E., Carlton, J.M., Simpson, K., Speed, T.P., and Cowman, A.F. (2006). Lineage-specific expansion of proteins exported to erythrocytes in malaria parasites. *Genome Biol,* **7:** R12

Sato, S., Wilson, R. J. (2004). The use of DsRED in single- and dual-color fluorescence labeling of mitochondrial and plastid organelles in *Plasmodium falciparum*. *Mol Biochem Parasitol*, **134:** 175-9

Schmitz, S, Schaap, I. A, Kleinjung, J, Harder, S, Grainger, M, Calder, L, Rosenthal, P. B, Holder, A. A., Veigel, C. (2010). Malaria parasite actin polymerization and filament structure. *J Biol Chem,* **285:** 36577-36585.

Schopf, F.H., Biebl, M.M., Buchner, J. (2017). The HSP90 chaperone machinery. *Nat Rev Mol Cell Biol*, **18:** 345.

Seraphim, T. V., Chakafana, G., Shonhai, A., Houry, W. A. (2019). *Plasmodium falciparum* R2TP complex: driver of parasite Hsp90 function. *Biophys Rev*, **11:** 1007-1015.

Shahinas, D., Folefoc, A., Pillai, D. A. (2013). Targeting *Plasmodium falciparum* Hsp90: Towards reversing antimalarial resistance. *Pathogens*, **2:** 33-54.

Sharma, D., Masison, D.C. (2009). Hsp70 structure, function, regulation and influence on yeast prions. *Prot Pept Lett*, **16:** 571-581.

Sherling, E and van Ooij. 2016. Host cell remodeling by pathogens: the exomembrane system in *Plasmodium*-infected erythrocytes. *FEMS Microbiol Rev*, **40:** 701-721.

Shiau, A.K., Harris, S.F., Southworth, D.R., Agard, D.A. (2006). Structural analysis of *E. coli* hsp90 reveals dramatic nucleotide-dependent conformational rearrangements. *Cell*, **127:** 329-340.

Shonhai, A., Boshoff, A., Blatch, G.L. (2005). *Plasmodium falciparum* heat shock protein 70 is able to suppress the thermosensitivity of an *Escherichia coli* DnaK mutant strain. *Molecular Genet Genom*, **274:** 70-78.

Shonhai, A., Boschoff, A., Blatch, G. L. (2007) .The structural and functional diversity of Hsp70s from *Plasmodium falciparum*. *Protein Sci,* **16:** 1803–1818

Shonhai, A., Botha, M., de Beer, T. A. P, Boshoff, A and Blatch, G. L. (2008). Structure-function study of *Plasmodium falciparum* Hsp70 using three-dimensional modelling and *in vitro* analyses. *Protein Pept Lett*, **15:** 1117-1125.

Silva, M.D., Cooke, B.M., Guillotte, M., Buckingham, D.W., Sauzet, J.P., Scanf, C.L., Contamin, H., David, P., Mercereau-Puijalon, O., Bonnefoy, S. (2005). A role for the *Plasmodium falciparum* RESA protein in resistance against heat shock demonstrated using gene disruption. *Mol Microbiol,* **56:** 990-1003.

Silva, N. S., Bertolino-Reis, D. E., Dores-Silva, P. R., Anneta, F. B., Seraphim, T. V., Barbosa, L. R. S., Borges, J.C. (2019). Structural studies of the Hsp70/Hsp90 organizing protein of Plasmodium falciparum and its modulation of Hsp70 and Hsp90 ATPase activities. *BBA Prot Proteome,* doi.org/10.1016/j.bbapap.

Sim, B. K., Orlandi, P. A., Haynes, J. D., et al. (1990). Primary structure of the 175K *Plasmodium falciparum* erythrocyte binding antigen and identification of a peptide which elicits antibodies that inhibit malaria merozoite invasion. *J Cell Biol,* **111:** 1877-1884.

Sinden, R.E. (1983). The cell biology of sexual development in *Plasmodium*. *Parasitol,* **4:** 7-28.

Sinden, R.E, Strong, K. (1978). An ultrastructural study of the sporogonic development of *Plasmodium falciparum* in *Anopheles gambiae*. *Trans R Soc Trop Med Hyg,* **72:** 477-491

Singh, G. P., Chandra, B. R., Bhattacharya, A., Akhouri, R. R., Singh, S. K., Sharma, A. (2004). Hyper-expansion of asparagines correlates with an abundance of proteins with prion-like domains in *Plasmodium falciparum*. *Mol Biochem Parasitol,* **137:** 307-319.

Sinnis, P., Kim Lee Sim, B. (1997). Cell invasion by the vertebrate stages of *Plasmodium*. *Trends Microbiol*, **5:** 52-58.

Soni, R, Sharma, D., Bhatt, T. K. (2016). *Plasmodium falciparum* secretome in erythrocyte and beyond. *Front Microbiol*, **7:** 194.

Spence, J., Cegielska, A., Georgopoulos, C. (1990). Role of *Escherichia coli* heat shock proteins DnaK and HtpG (C62. 5) in response to nutritional deprivation. *J Bacteriol,* **72:** 7157-7166.

Stetz, G., Verkhivker, G.M. (2015). Dancing through life: Molecular dynamics simulations and network-centric modelling of allosteric mechanisms in Hsp70 and Hsp110 chaperone proteins. *PLoS One*, ***10*****.** e0143752

Sun, M, Kotler, J. L. M.,Liu, S., Street, T.O. (2019). The endoplasmic reticulum (ER) chaperones BiP and Grp94 selectively associate when BiP is in the ADP conformation. *J Biol Chem,* **294**:6387-6396

Suppini, J.P., Amor, M., Alix, J.H., Ladjimi, M.M. (2004). Complementation of an *Escherichia coli* DnaK defect by Hsc70-DnaK chimeric proteins. *J Bacteriol*, **186:** 6248-6253.

Swain, J.F., Dinler, G., Sivendran, R., Montgomery, D.L., Stotz, M., Gierasch, L.M. (2007). Hsp70 chaperone ligands control domain association via an allosteric mechanism mediated by the interdomain linker. *Mol Cell*, **26:** 27-39.

Szabo, A., Langer, T., Schröder, H., Flanagan, J., Bukau, B., Hartl, F.U. (1994). The ATP hydrolysis-dependent reaction cycle of the Escherichia coli Hsp70 system DnaK, DnaJ, and GrpE. *Proc Natl Acad Sci U S A,* **91:** 10345-10349.

Szabo, A., Korszun, R., Hartl, F. U., Flanagan, J. (1996). A zinc finger-like domain of the molecular chaperone DnaJ is involved in binding to denatured protein substrates. *EMBO J,* **15:** 408-41

Szklarczyk, D., Morris, J.H., Cook, H., Kuhn, M., Wyder, S., Simonovic, M., Santos, A., Doncheva, N.T., Roth, A., Bork, P., Jensen, L.J. (2016). The STRING database in 2017: quality-controlled protein-protein association networks, made broadly accessible. *Nucl Acid Res*, 937.

Talman, A.M., Domarle, O., McKenzie, F.E. (2004). Gametocytogenesis : the puberty of *Plasmodium falciparum*. *Malar J,* **3:** 24.

Thera, M. A., Doumbo, O. K., Coulibaly, D., Laurens, M. B. *et al*. (2011). A field trial to assess a blood-stage malaria vaccine. *N Eng J Med,* **365:** 1004-13.

Tiwari, A., Liba, A., Sohn, S.H., Seetharaman, S.V., Bilsel, O., Matthews, C.R., Hart, P.J., Valentine, J.S., Hayward, L.J. (2009). Metal deficiency increases aberrant hydrophobicity of mutant superoxide dismutases that cause amyotrophic lateral sclerosis. *J Biol Chem,* **284:** 27746-27758.

Trcka, F., Durech, M., Vankova, P., Chmelik, P., Martinkova, V., Hausner, J., Kadek, A., Marcoux, J., Klumpler, T., Vojtesek, B., et al. (2019). Human stress inducible Hsp70 has a high propensity to form ATP-dependent antiparallel dimers that are differentially regulated by cochaperone binding. *Mol. Cell Proteomics*, **18:** 320–337.

Tsutsumi, S., Mollapour, M., Prodromou, C., Lee, C.T., Panaretou, B., Yoshida, S., Mayer, M.P., Neckers, L.M. (2012). Charged linker sequence modulates eukaryotic heat shock protein 90 (Hsp90) chaperone activity. *Proc Natl Acad Sci U S A*, **109:** 2937-2942.

Tuteja, R. (2007). Malaria- an overview. *FEBS*, 274: 4669-4941.

van Leeuwen, H.C., Strating, M.J., Rensen, M., de Laat, W. and van der Vliet, P.C. (1997). Linker length and composition influence the flexibility of DNA binding. *EMBO J,* **16:** 2043-2053.

Vivian, J.T., Callis, P.R. (2001). Mechanisms of tryptophan fluorescence shifts in proteins. *Biophys J*, **80:** 2093-2109.

Walsh, P., Bursac, D., Law, Y., C., Lithgow, T. (2004). The J-protein family: modulating protein assembly, disassembly and translocation. *EMBO Rep.* **5:** 567-71.

Wang, T., Mäser, P., Picard, D. (2016) Inhibition of *Plasmodium falciparum* Hsp90 contributes to the antimalarial activities of aminoalcohol-carbazoles. *J Med Chem* **59:** 6344-6352.23

Waterhouse, A.M., Procter, J.B., Martin, D.M., Clamp, M. and Barton, G.J. (2009). Jalview Version 2- a multiple sequence alignment editor and analysis workbench. *Bioinformatics*, **25:** 1189-1191.

Weiss, G.E., Gilson, P.R., Taechalertpaisarn, T., Tham, W-H., de Jong, N.W.M., Harvey, K.L., et al. (2015). Revealing the sequence and resulting cellular morphology of receptor-ligand interactions during *Plasmodium falciparum* invasion of erythrocytes. *PLoS Pathog*, **11:** e1004670.

Wendt, C., Rachid, R., Souza, W., Miranda, K. (2016). Electron tomography characterization of hemoglobin uptake in *Plasmodium chabaudi* reveals a stage-dependent mechanism for food vacuole morphogenesis. *J Struct Biol*, **194:** 171-9.

Wriggers, W., Chakravarty, S. and Jennings, P.A. (2005). Control of protein functional dynamics by peptide linkers. *Peptide Science: Biopolymers*, **80:** 736-746.

Wright, G., Rayner, J.C. (2014). *Plasmodium falciparum* erythrocyte invasion: combining function with immune evasion. *PLoS Path,* **10:** e1003943.

Xu, X., Sarbeng, E.B., Vorvis, C., Kumar, D.P., Zhou, L., et al. (2012). Unique peptide substrate binding properties of 110-kDa heat-shock protein (Hsp110) determine its distinct chaperone activity. *J Biol Chem,* **287:** 5661-5672.

Yahata, K., Treeck, M., Culleton, R., Gilberger, T.W. and Kaneko, O., 2012. Time-lapse imaging of red blood cell invasion by the rodent malaria parasite *Plasmodium yoelii*. *PloS One*, **7:** e50780.

Young, J.T., Heikkila, J.J. (2010). Proteasome inhibition induces hsp30 and hsp70 gene expression as well as the acquisition of thermotolerance in *Xenopus laevis* A6 cells. *Cell Stress Chaperones*, **15:** 323-334.

Yu, H.Y., Ziegelhoffer, T., Osipiuk, J., Ciesielski, S.J., Baranowski, M., Zhou, M., Joachimiak, A., Craig, E.A. (2015). Roles of intramolecular and intermolecular interactions in functional regulation of the Hsp70 J-protein co-chaperone Sis1. *J Mol Biol*, **427:** 1632-1643.

Zhang, Y.J., Jansen-West, K., Xu, Y.F., Gendron, T.F., Bieniek, K.F., Lin, W.L., Sasaguri, H., Caulfield, T., Hubbard, J., Daughrity, L. and Chew, J. (2014). Aggregation-prone c9FTD/ALS poly (GA) RAN-translated proteins cause neurotoxicity by inducing ER stress. *Acta neuropathologica*, **128:** 505-524.

Zhao, R., Houry, W.A. (2005). Hsp90: a chaperone for protein folding and gene regulation. *Biochem Cell Biol*, **83:** 703-710.

Zheng, H., Zhangping, T., Wenyue, X. (2014). Immune Evasion Strategies of Pre-Erythrocytic Malaria Parasites.*Mediat Inflamm*, doi.org/10.1155/2014/362605.

Zhuravleva, A., Gierasch, L.M. (2011). Allosteric signal transmission in the nucleotide-binding domain of 70-kDa heat shock protein (Hsp70) molecular chaperones. *Proc Nat Acad Sci*, **108:** 6987-6992.

Zininga, T., Shonhai, A. (2014). Are heat shock proteins druggable candidates? *Am J Biochem Biotech*, **10:** 211- 213.

Zininga, T., Makumire, S., Gitau, G. W., Njunge, J. M., Pooe, O. J., Klimek, H., Scheurr, R., Raifer, H., Prinsloo, E., Przyborski, J.M., Hoppe, H., Shonhai, A. (2015a). *Plasmodium falciparum* Hop (PfHop) interacts with the Hsp70 chaperone in a nucleotide-dependent fashion and exhibits ligand Selectivity. *PloS ONE*, **10:** e0135326.

Zininga, T., Achilonu, I., Hoppe, H., Prinsloo, E., Dirr, H. W., Shonhai, A. (2015b). Overexpression, Purification and Characterisation of the *Plasmodium falciparum* Hsp70-z (PfHsp70-z) Protein. *PloS One*, **10:** e0129445.

Zininga, T., Achilonu, I., Hoppe, H., Prinsloo, E., Dirr, H.W., Shonhai, A. (2016). *Plasmodium falciparum* Hsp70-z, an Hsp110 homologue, exhibits independent chaperone activity and interacts with Hsp70-1 in a nucleotide-dependent fashion. *Cell Stress Chaperones,* **21:** 499–513.

Zininga, T., Pooe, O.J., Makhado, P.B., Ramatsui, L., Prinsloo, E., Achilonu, I., Dirr, H., Shonhai, A. (2017a). Polymyxin B inhibits the chaperone activity of *Plasmodium falciparum* Hsp70. *Cell Stress Chaperones,* **22:** 707-715.

Zininga, T., Ramatsui, L., Makhado, P.B., Makumire, S., Achilinou, I., Hoppe, H., Dirr, H.W., Shonhai, A. (2017b). (-)-Epigallocatechin-3-Gallate inhibits the chaperone activity of *Plasmodium falciparum* Hsp70 chaperones and abrogates their association with functional partners. *Molecules,* **22:** 2139.

Zuiderweg, E.R., Bertelsen, E.B., Rousaki, A., Mayer, M.P., Gestwicki, J.E. and Ahmad, A. (2012). Allostery in the Hsp70 chaperone proteins. In *Molecular Chaperones*. Springer, Berlin, Heidelberg.

Appendix A: General experimental procedures

A1 Plasmid DNA extraction

Plasmid DNA was extracted using Thermo Scientific™ Plasmid Miniprep Kit according to the manufacturer's Protocol.

A2 Restriction digest analysis

Plasmid DNA was digested using the respective restriction enzymes (*Bam*HI and *Kpn*I for LS mutants, and *Bam*HI and *Hind*III for wild type versions) following the method described below. The reagents were set up as follows: Sterile deionized water (16 µl), 10x restriction buffer (2 µl) and DNA (100-200 ng) 2 µl. The reaction was initiated by addition of two units (2 µl) of restriction enzymes. The restriction was allowed to proceed for 2-3 hours at 37 °C. The reaction was stopped by addition of 4 µl of 10x DNA loading buffer (0.25 %) bromophenol blue and 30 % glycerol). The product was then analyzed by agarose gel electrophoresis as described in (Appendix A.3).

A3 Agarose gel electrophoresis

To prepare 0.8 % (w/v) agarose gel, the required amount of agarose was completely dissolved in 1x TAE buffer (40 mM, 20 mM acetic acid and 1 mM EDTA) by heating with frequent agitation. The agarose was then cooled to 55 ºC prior to addition of ethidium bromide (0.5 µg/ml). The agarose gel was allowed to polymerize for 15-30 minutes at room temperature. The gel was placed in the electrophoresis chamber and covered with 1x TAE buffer. A volume of 4 µl of 10x DNA loading buffer (0.25% bromophenol blue + 30% glycerol) was added to 20 µl of the sample followed by loading of the samples into the wells. Electrophoresis was conducted at 100 volts for one hour. The gel was then visualized using UV light (BioRad ChemiDoc Bioimaging System, USA).

A5 DNA Sequencing

PfHsp70-1 and PfHsp70-1$_{LS}$ plasmid DNA was sequenced using forward primers (5'CAGCTGCTATTGCATATGGTTT-3') which binds at position 718-740 and (5'CAAGAATTCCAAAAATCCAAACT-3') which binds at positions 1211-1233. The reverse primer (5'GAGTTCTGAGGTCATTACTGG-3') which binds at position 2243 to 2223 was used the reverse direction.

Reagent	Volume (µl)
Big dye 3.1	1
Sequencing buffer	1
Primer (3.2 pmol)	1
Plasmid (100ng)	X
Water (ultrapure)	10 –(3+x)

Appendix A5

Transformation A volume of 2 µl (equivalent to about 10 ng) of plasmid DNA was added into an aliquot of 100 µl of competent cell. The cells were then incubated on ice for 30 minutes followed by heat shock at 42 °C for 45 seconds and immediately placed on ice for 10 minutes. A volume of 900 µl of 2YT broth was added and then incubated at 37 °C for one hour with gentle agitation. The cells were transferred on 2YT plates containing the desired antibiotics followed by incubation at 37 °C overnight.

A6 SDS PAGE analysis

Proteins were treated by boiling in SDS sample buffer (0.25% Coomassie Brilliant blue (R250), 2% SDS, 10 % glycerol (v/v), 100 mM Tris, and 1 % β-mercaptoethanol) in a ratio of 4:1 for 5 mins at 95 °C and resolved using 12 % acrylamide resolving gel prepared as shown below (Table A.1). The gel is then transferred into the electrophoresis tank and electrophoresis buffer (25 mM Tris, pH 8.3 250 mM glycine and 0.1% (w/v) SDS) was added. The boiled samples were loaded in the respective wells and pre-stained protein molecular weight markers (ThermoFisher Scientific, USA) were also loaded. The electrophoresis was performed at 150 volts for one hour using the Bio-Rad Mini protein electrophoresis system (Biorad, U.S.A).

Table A1 Preparation of SDS-PAGE

Reagent (ml)	5 % Stacking Gel	12 % Separating Gel
30 % Bis/acrylamide	0.235	2.08
1.5 M Tris (pH 8.8)	-	1.25
1.0 M Tris (pH 6.8)	0.437	-
10 % SDS	0.0175	0.05
10 % Ammonium persulphate	0.00875	0.025
Distilled water	1.05	1.58
TEMED	0.03	0.0020

A7 Western blot analysis

Proteins were resolved in 12% acrylamide gel as described above (Appendix A.7). Removal of SDS-PAGE gel from the glass plates after completion of electrophoresis process and cutting off of the stacking gel was done. The Whatman filter papers, gel, two scotchbrite fibre pads, and nitrocellulose were immersed in the buffer and left to equilibrate at 8 °C for 30 minutes. Preparation of the gel for transfer was done as follows: filter paper was placed on a scotchbrite fibre pad; Gel was placed on the filter paper ensuring no air bubbles are trapped; nitrocellulose was placed over the gel; another filter paper was laid on top of the nitrocellulose, followed by another scotchbrite pad. The transfer of the protein on the nitrocellulose membrane was performed by running at 100 volts for one hour. The membrane was removed from the sandwich and rinsed using transfer buffer as well as removal of adhering gel on the nitrocellulose membrane using a cotton swab. The blot was stained with Ponceau stain to determine the success of the transfer followed by visualizing the band using chemiluminescence. The membrane was blocked in 10 ml of (5 % non-fat milk in TBS) for one hour on a rotary shaker set at 1 rpm. The membrane was washed three times in TBS-Tween for 10 minutes followed by incubation of the membrane with primary antibody for one hour. Unbound primary antibody was removed by washing of the membrane three times using TBS-Tween for 10 minutes each wash. The membrane was incubated with secondary antibody for one hour followed by washing of the membrane three times using TBS-Tween.

A8 Chemiluminescent detection

The Thermo Scientific Pierce ECL Western Blotting Substrate is a highly sensitive nonradioactive, enhanced luminol-based chemiluminescent substrate for the detection of horseradish peroxidase (HRP) on immunoblots.

1. Remove blot from the transfer apparatus and block nonspecific sites with Blocking Reagent for 60 minutes at room temperature (RT) with shaking. If desired, block overnight at 2-8 °C without shaking.

2. Remove the Blocking Reagent and add the primary antibody working dilution. Incubate blot for 1 hour at RT with shaking or overnight at 2-8 °C without shaking.

3. Briefly rinse membrane in Wash Buffer two times.

4. Wash membrane by suspending it in Wash Buffer and agitating for ≥ 5 minutes. Replace Wash Buffer at least 4-6 times. Increasing the Wash Buffer volume, the number of washes and wash duration may help minimize background signal.

5. Incubate blot with the HRP-conjugate working dilution for one hour at RT with shaking.

6. Repeat Steps 3 and 4 to remove non-bound HRP-conjugate. Note: Membrane MUST be thoroughly washed after incubation with the HRP-conjugate.

7. Prepare the substrate working solution by mixing equal parts of Detection Reagents 1 and 2. Use 0.125 mL Working Solution per cm^2 of the membrane. Note: For best results prepare working solution immediately before use. The working solution is stable for one hour at RT.

8. Incubate blot with a working solution for one minute at RT.

9. Remove blot from working solution and place it in a plastic sheet protector or clear plastic wrap. Use an absorbent tissue to remove excess liquid and to carefully press out any bubbles from between the blot and the membrane protector.

A9 Determination of protein concentration using Bradford assay

Protein concentration was determined by Bradford's method (Bradford, 1976). Bovine serum albumin (BSA) standards were prepared using concentration ranging from 0 to 1 mg/ml in 0.15 M NaCl. Bradfords reagent 200 µl (Sigma Aldrich, USA) was added to 10 µl of protein and the reaction incubated in the dark at room temperature for five minutes. Absorbance was read at 595 nm using a SpectraMax M3 (Molecular devices, USA). The recombinant protein was similarly treated and the protein concentration determined by extrapolation from the standard curve as indicated in (Appendix B3; Figure B1). The readings were prepared in triplicate and the average obtained.

A10 determination of CD molar residue ellipticity

The analysis of the CD spectrum was conducted by conversion of ellipticity units from the CD spectrometer to molar residue ellipticity. This was achieved using the following formula

$[\theta] = (100 \times \theta) / CMR \times l$…… ……Equation 3

Where [θ]: molar residue ellipticity (deg.cm^2.dmol-1) 100: constant converting path length in meters θ: ellipticity (mdeg) l: cuvette path length

CMR: mean residue concentration

$CMR = c \times N$ ……Equation 4

Where c: Protein concentration (mol)

N: number of amino acids on the protein

5.2.1 Enzyme Linked Immunosorbent Assays (ELISA)

The direct association of either PfHsp70-1 or PfHsp70-1$_{LS}$ with co-chaperones (PfHop, PfHsp40, PfHsp70-z and PfHsp70-z$_{LS}$) was assessed by enzyme linked immunosorbent assay (ELISA) as previously described (Mabate *et al*., 2018). PfHsp70-1$_{NBD}$, PfHsp70-z$_{NBD}$ and bovine serum albumin (BSA) were also included as negative controls (Mabate *et al*., 2018). Initially, as ligands, recombinant PfHsp70-

1/PfHsp70-1$_{LS}$ /PfHsp70-1$_{NBD}$ were each immobilized at a concentration of (5 µg/mL) by overnight incubation in 50 mM $NaHCO_3$ (pH 9) at 4° C to facilitate passive adsorption of the proteins onto the polystyrene surface of the wells. After blocking the wells with 1% BSA in TBST, the respective analyte recombinant proteins (PfHop, PfHsp40, PfHsp70-z, PfHsp70-z$_{LS}$, PfHsp70-z$_{NBD}$ or BSA) were each added in serial dilutions (0.137 nM - 300 nM) in the absence or presence of nucleotides (5 mM ATP/ADP) and incubated for 2 hours at 25 °C. Individual plates were then incubated with respective protein-specific antibodies for 1 hr. Next, HRP-conjugated secondary antibodies were added and reactants were incubated for 45 minutes. The substrate 5.5′-Tetramethylbenzidine (TMB) (Bio-Scientific, USA) was then added for colour development. Absorbance readings were then monitored at 370 nm using a SpectraMax M3 microplate reader (Molecular Devices, USA) every 5 minutes for 30 minutes. The derived data were then analysed using GraphPad prism 6.05 (GraphPad Software, USA).

Appendix B: Supplementary data

Table B1. Properties of residues used for linker substitution mutations

PfHsp70-1/DnaK linker residue	PfHsp70-z linker residue
Aspartate (Asp/D) MW:133 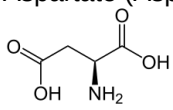 pI: 2.77 Side chain: polar and negative Hydrophilic (score -3.5)	Glutamate (Glu/E) MW: 89 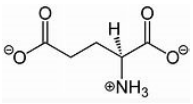 pI: 3.08 Side chain: polar and negative Hydrophilic (score -3.5)
Valine (Val/V) MW: 117.15 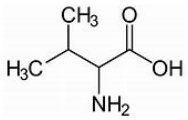 pI: 6.02 Side chain: non-polar and neutral Hydrophobic (score 4.2)	Tyrosine (Tyr/Y) MW: 181.19 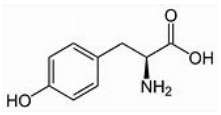 pI: 5.63 Side chain: polar and neutral Hydrophilic (score -1.3)
Leucine (Leu/L) MW: 131 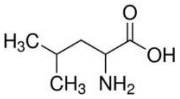 pI: 5.98 Side chain: non-polar and neutral Hydrophobic (score 3.8)	Cysteine (Cys/C) MW: 121.16 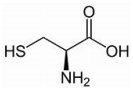 pI:5.02 Side chain: polar and neutral Hydrophilic (score -2.5)
	Valine (Val/V) MW: 117.15 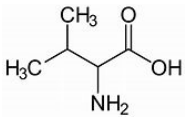 pI: 6.02 Side chain: non-polar and neutral Hydrophobic (score 4.2)
	Lysine (Lys/K) MW:146.19 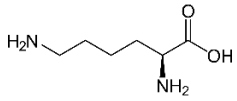 pI: 9.74 Side chain: polar and positive Hydrophobic (score -3.9)

B1. Properties of linker regions of PfHsp70-1 and PfHsp70-1$_{LS}$

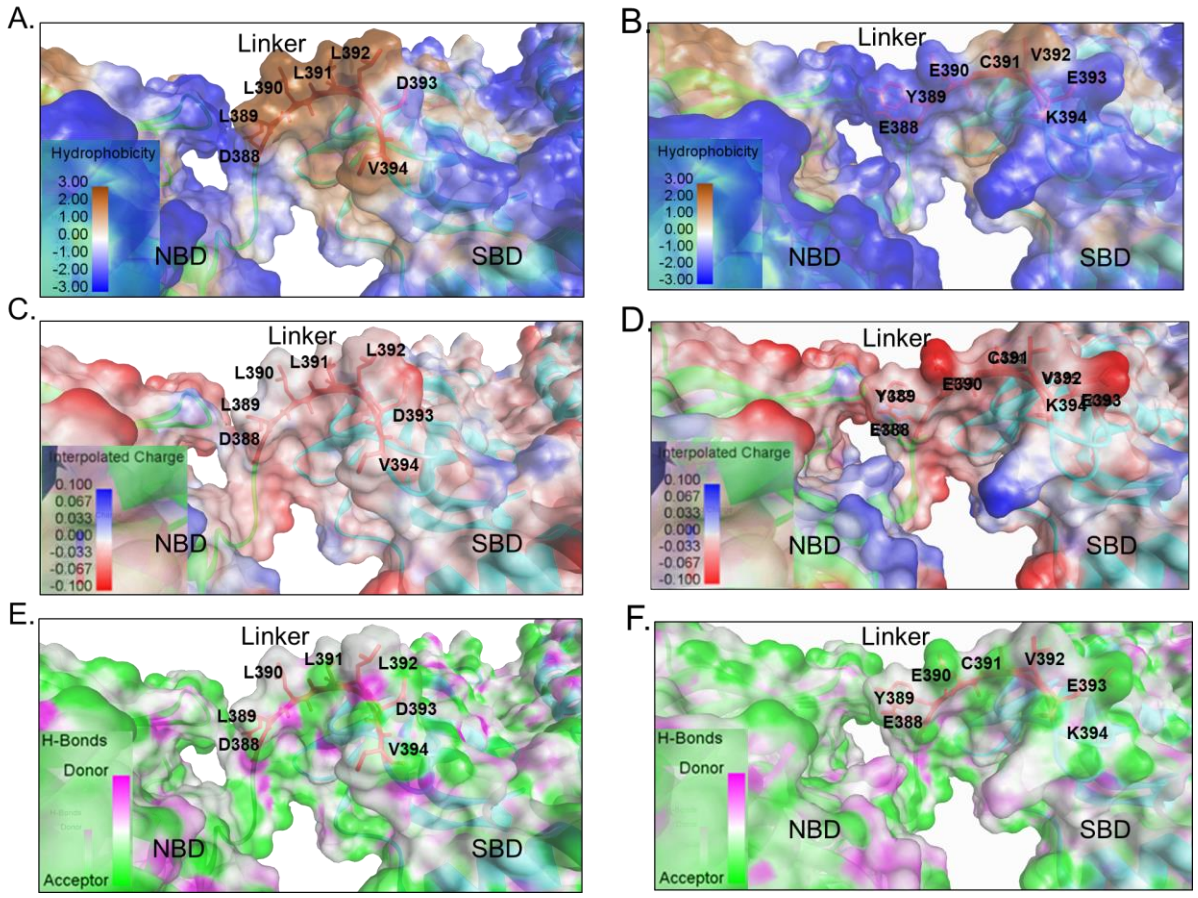

Figure B1 Properties of linker motifs of PfHsp70-1 and PfHsp70-1$_{LS}$
(A). The linker surface of PfHsp70-1 is characteristically hydrophobic in nature as opposed to that of PfHsp70-1$_{LS}$ (B) which is characterised by hydrophilic residues that create a hydrophilic interface around the linker. (C) PfHsp70-1 has a neutral linker as opposed to that of PfHsp70-1$_{LS}$ (D) which is charged. (E) PfHsp70-1$_{LS}$ possesses more hydrogen acceptors during hydrogen bond formation as opposed to PfHsp70-1 (F) which is predicted to form fewer hydrogen bonds.

B2. Properties of linker regions of PfHsp70-z and PfHsp70-z$_{LS}$

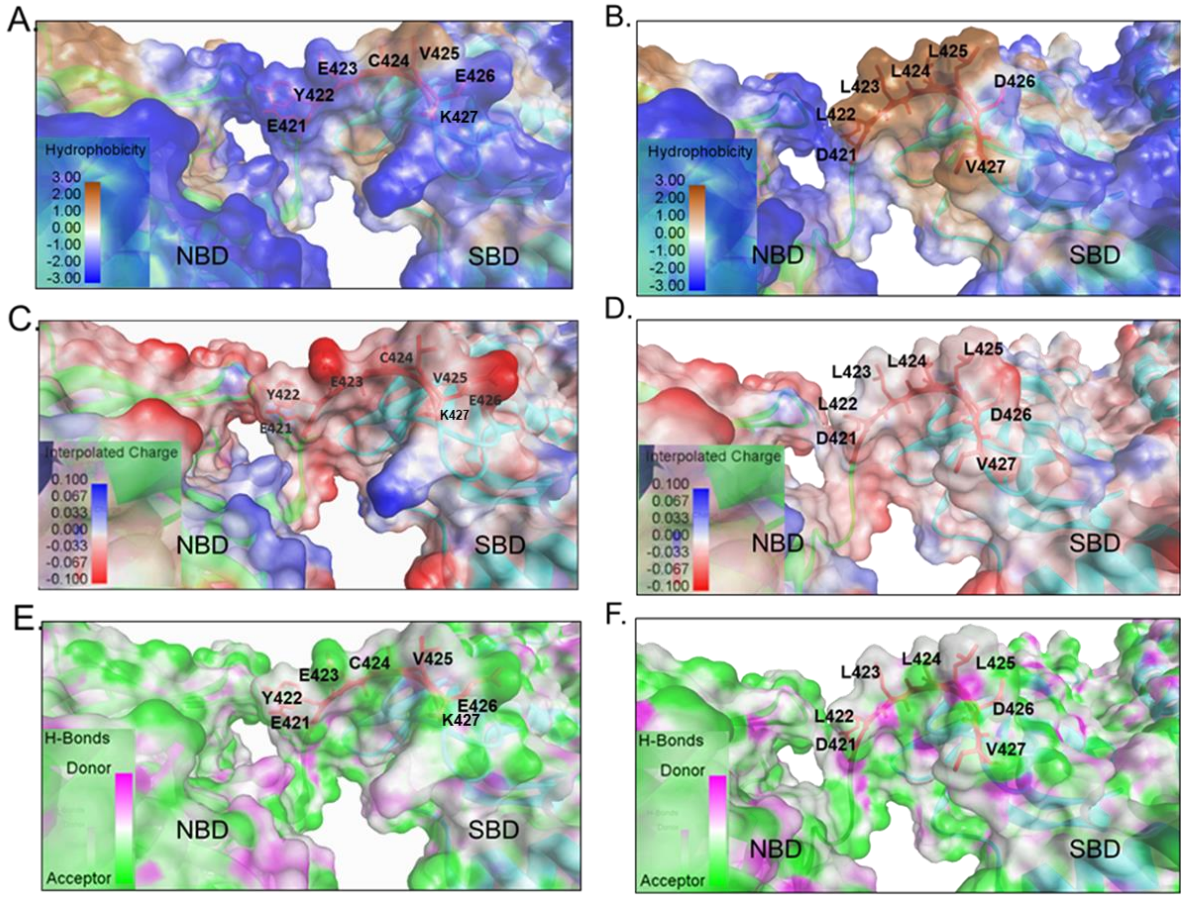

Figure B2 Properties of linker motifs of PfHsp70-z and PfHsp70-z$_{LS}$
(A). The linker surface of PfHsp70-z is characteristically hydrophilic in nature as opposed to that of PfHsp70-z$_{LS}$ (B) which is characterised by hydrophobic residues that create a hydrophobic interface around the linker. (C) PfHsp70-z has a relatively more negatively charged linker as opposed to that of PfHsp70-z (D) which is mostly neutral. (E) PfHsp70-z possesses fewer hydrogen acceptors during hydrogen bond formation as opposed to PfHsp70-z$_{LS}$ (F) which is predicted to form more hydrogen bonds.

B3. Properties of linker regions of DnaK and DnaK$_{LS}$

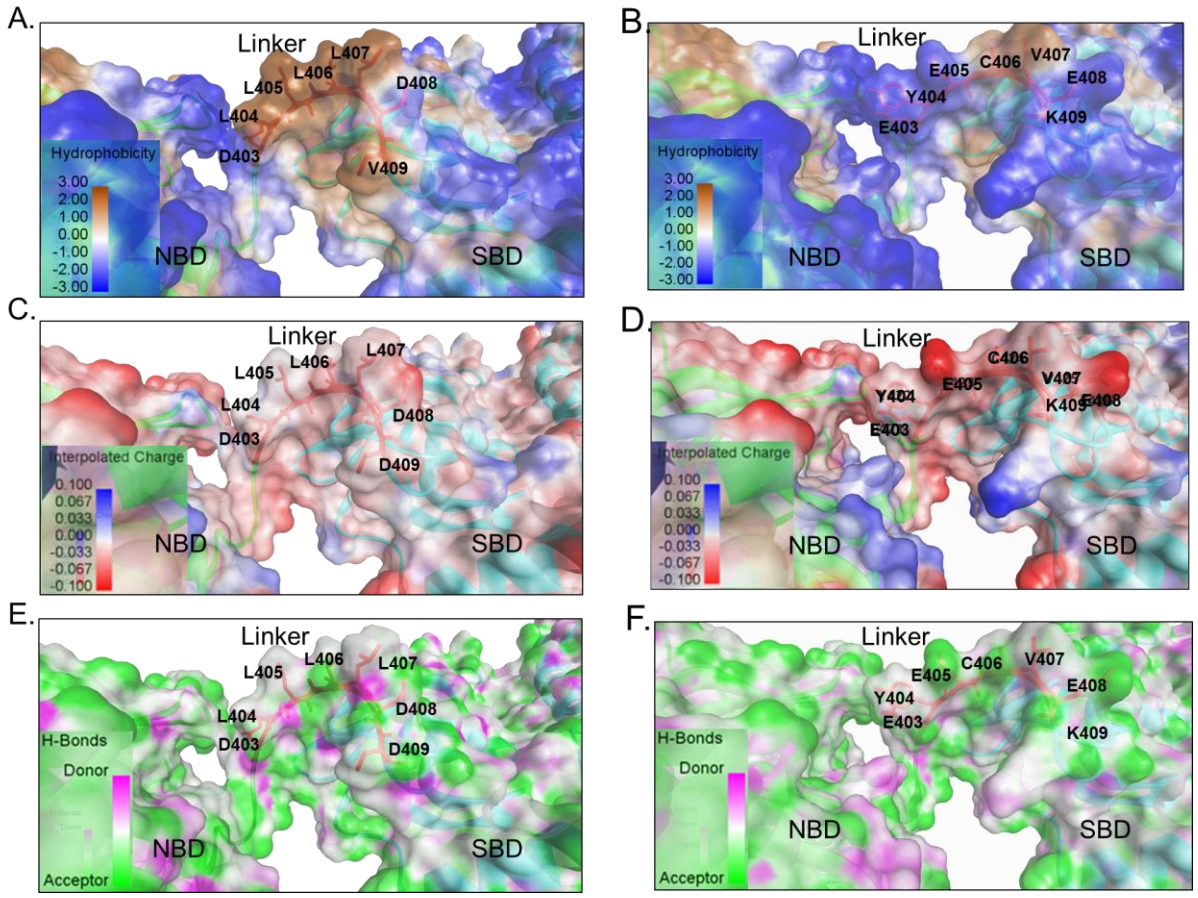

Figure B3 Properties of linker motifs of DnaK and DnaK$_{LS}$
(A). The linker surface of DnaK is characteristically hydrophobic in nature as opposed to that of DnaK$_{LS}$ (B) which is characterised by hydrophilic residues that create a hydrophilic interface around the linker. (C) DnaK has a neutral linker as opposed to that of DnaK$_{LS}$ (D) which is charged. (E) DnaK$_{LS}$ possesses more hydrogen acceptors during hydrogen bond formation as opposed to DnaK (F) which is predicted to form fewer hydrogen bonds.

B4: JALVIEW MSA of canonical Hsp70s

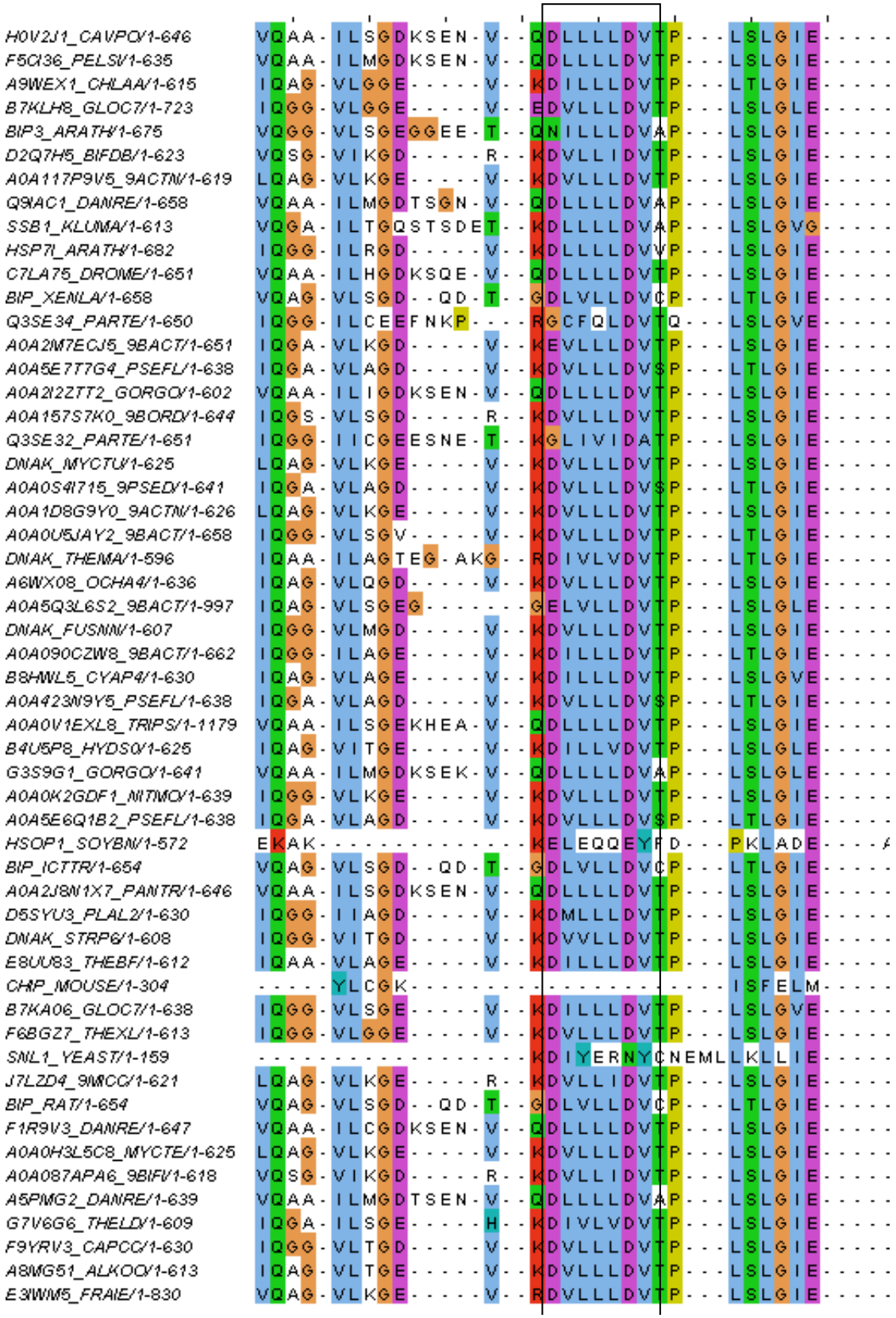

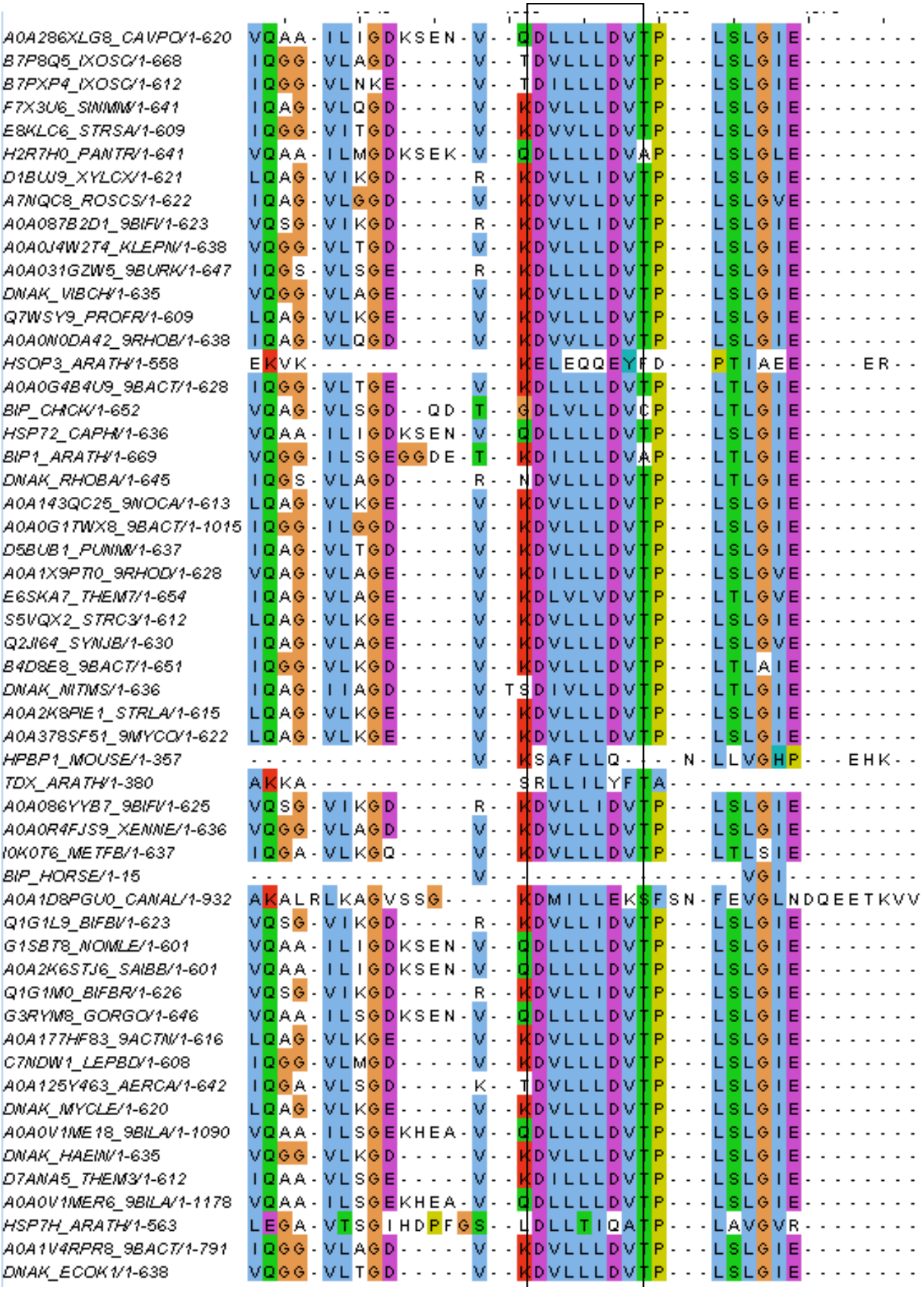

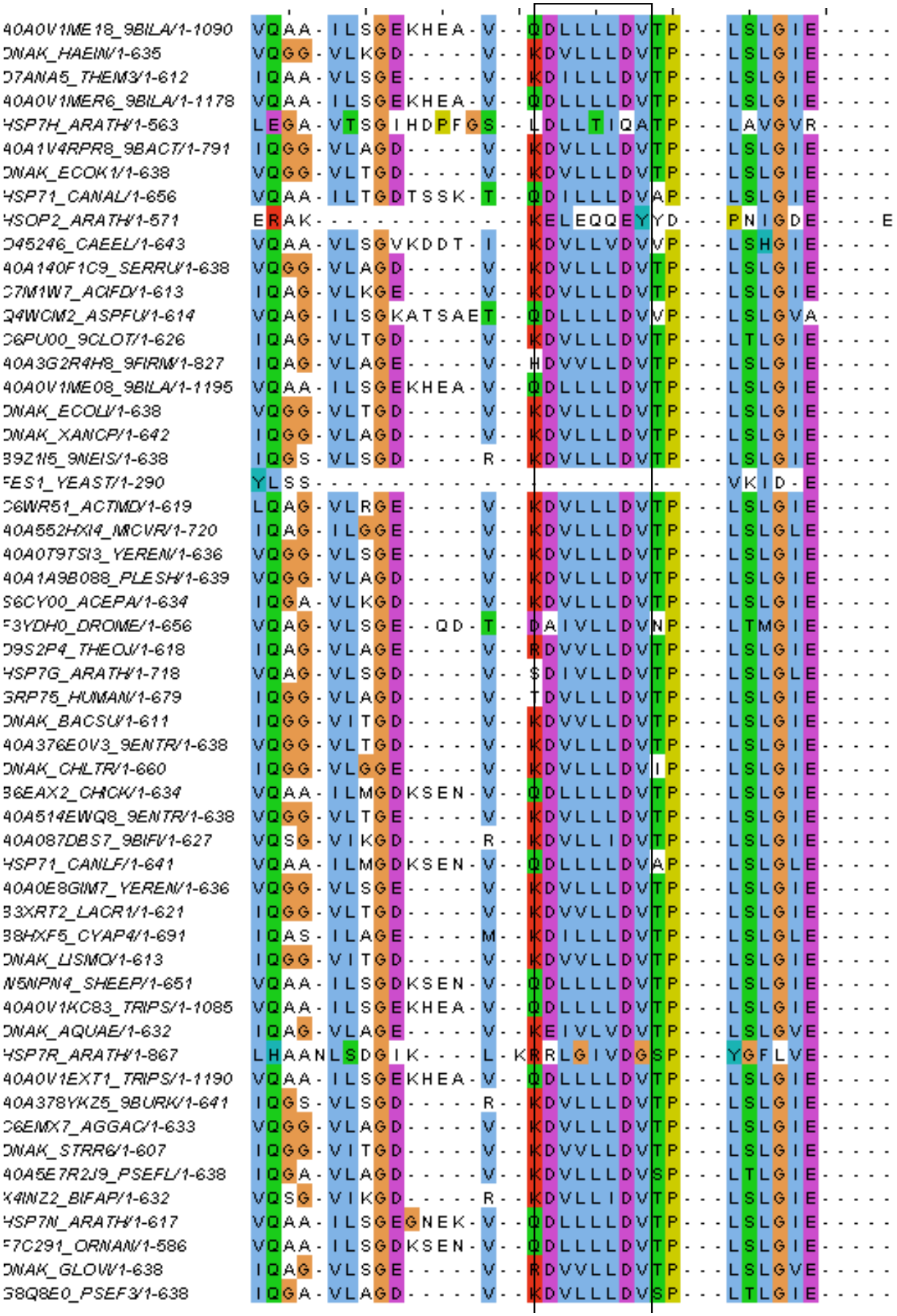

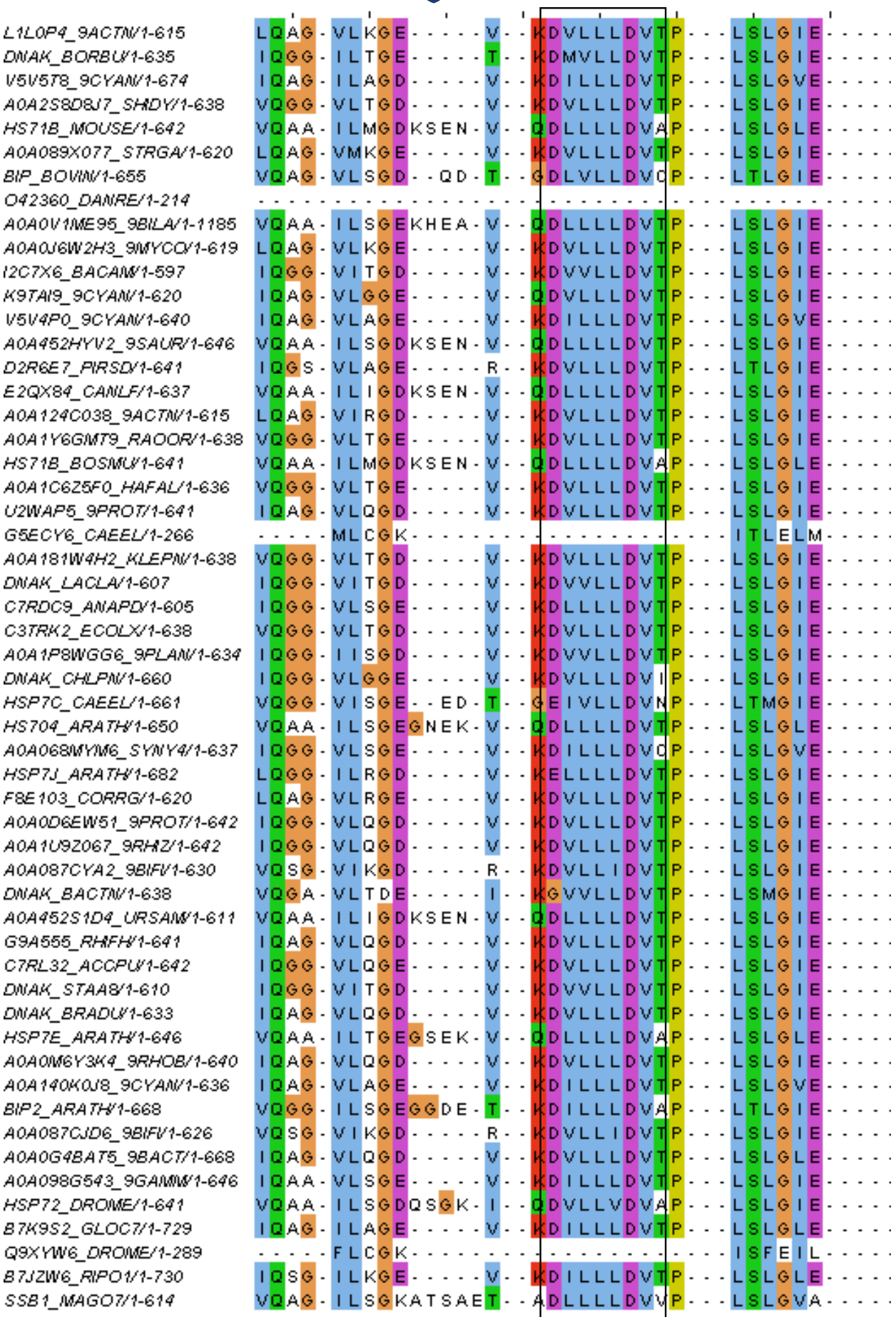

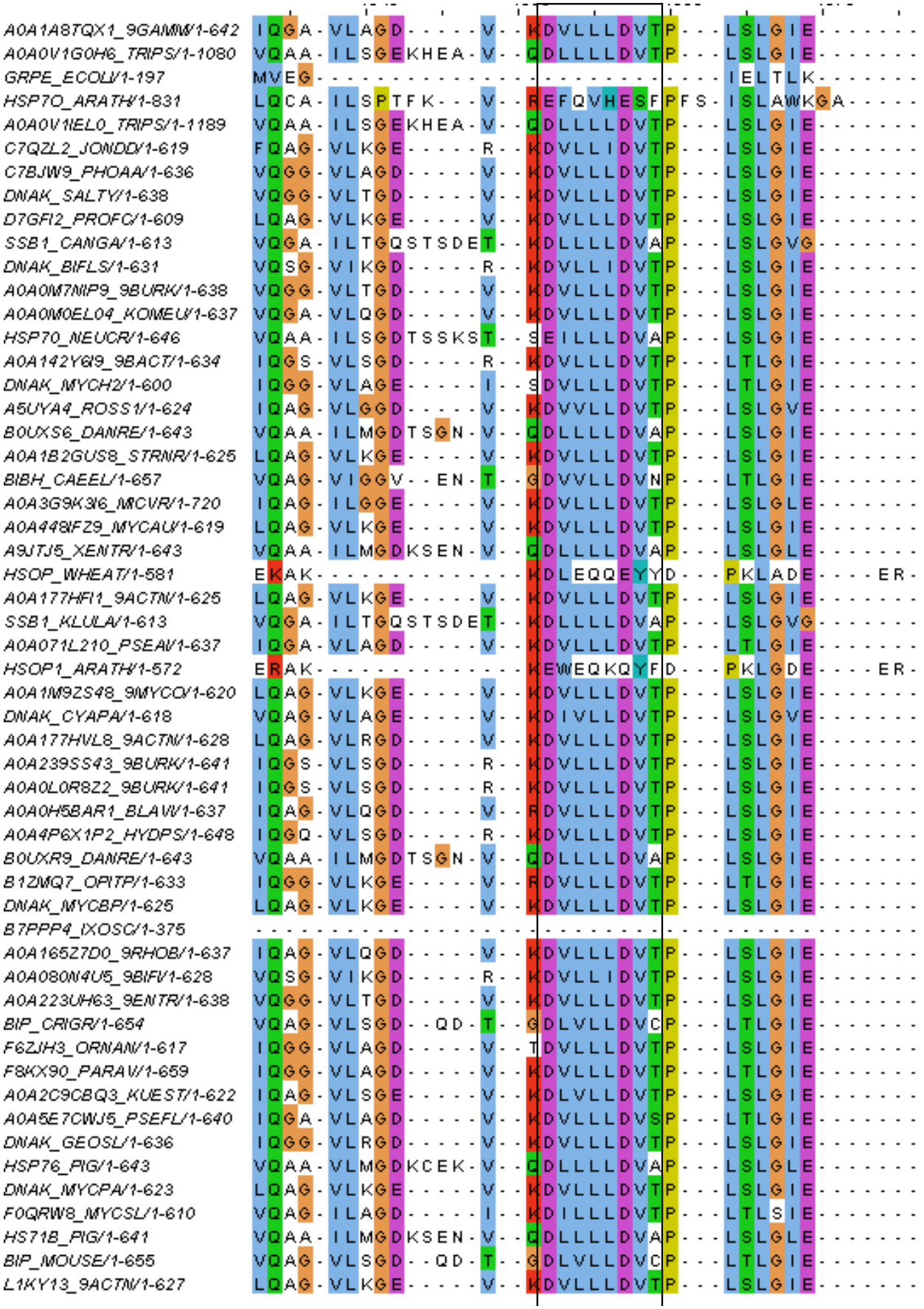

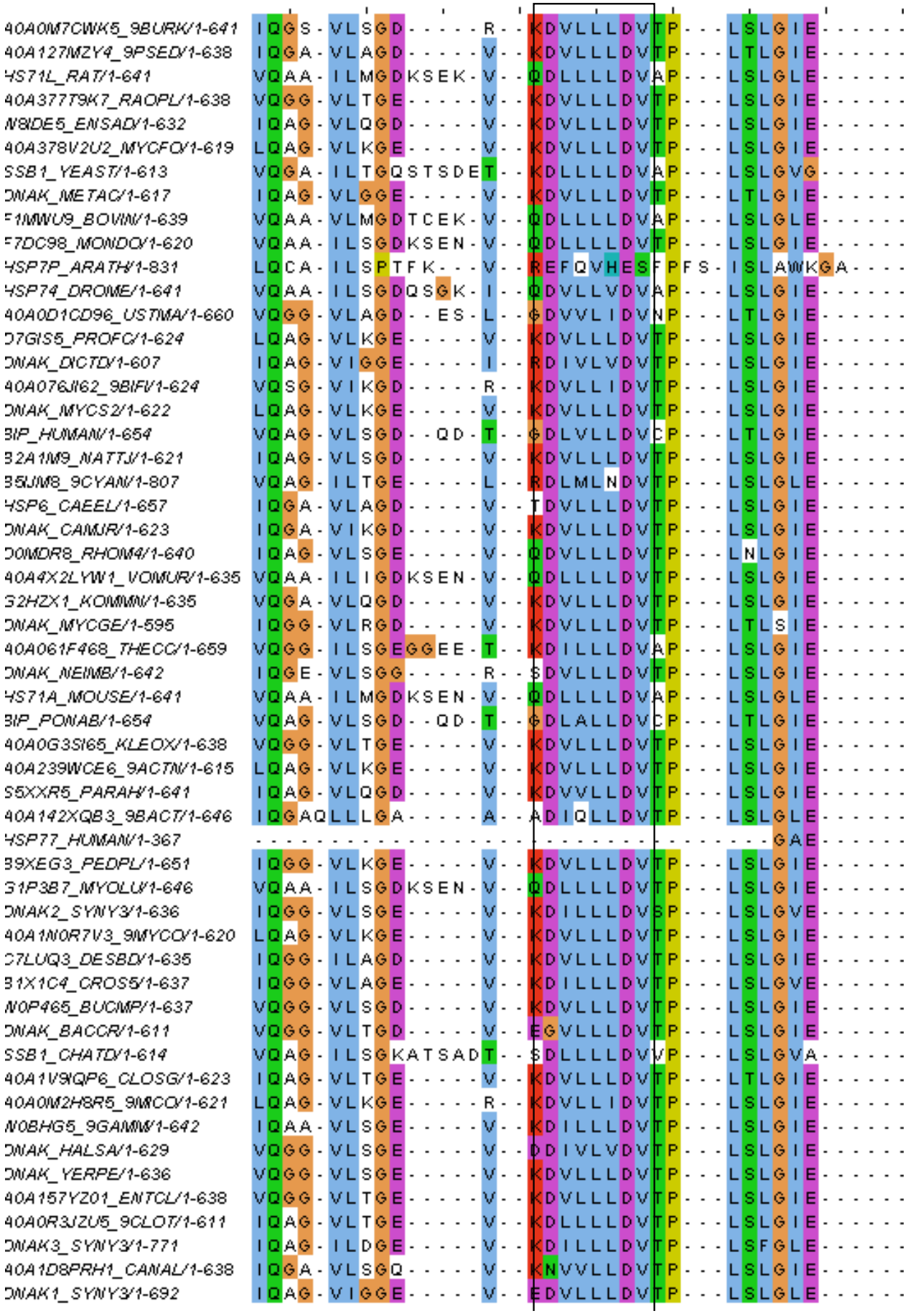

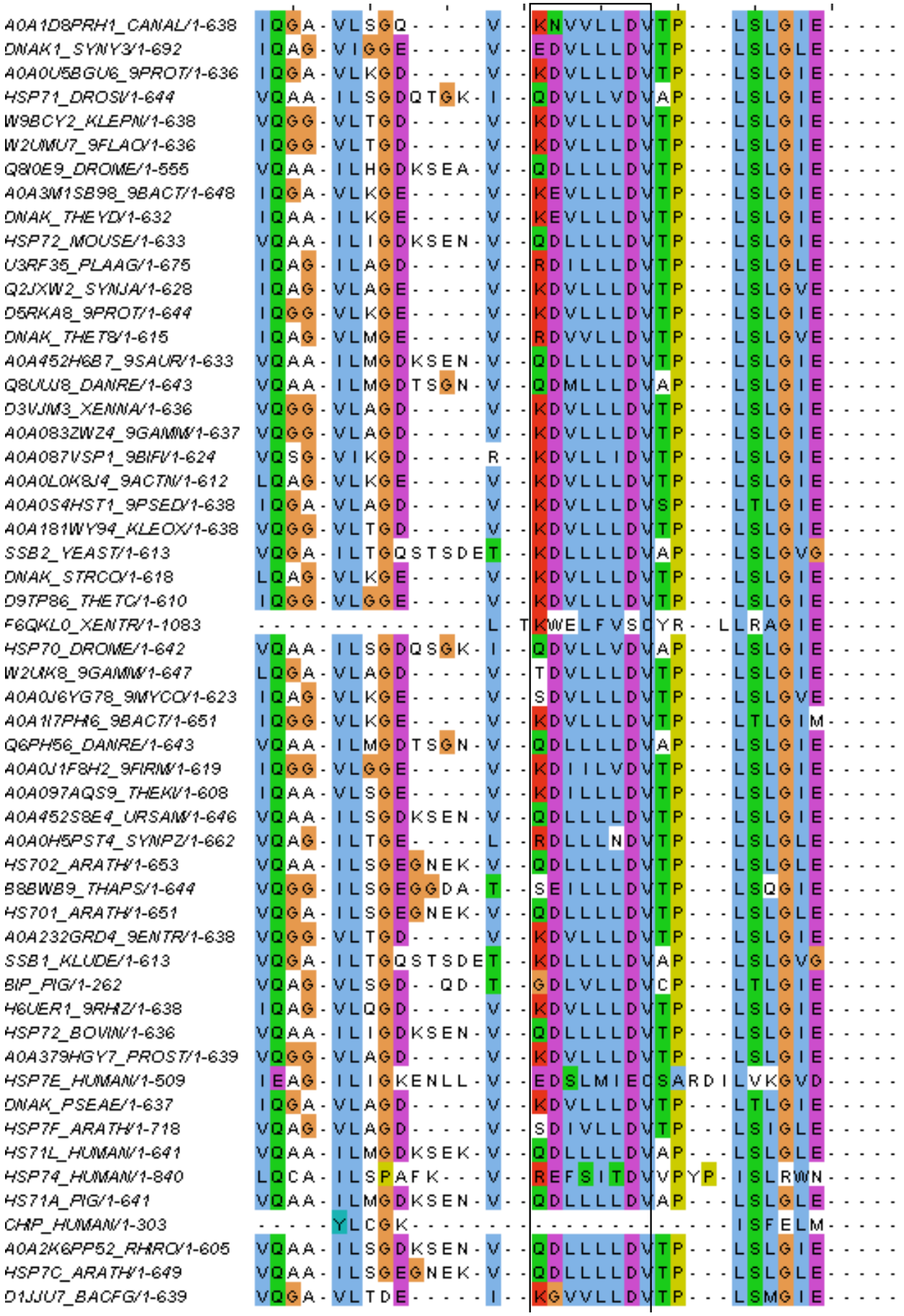

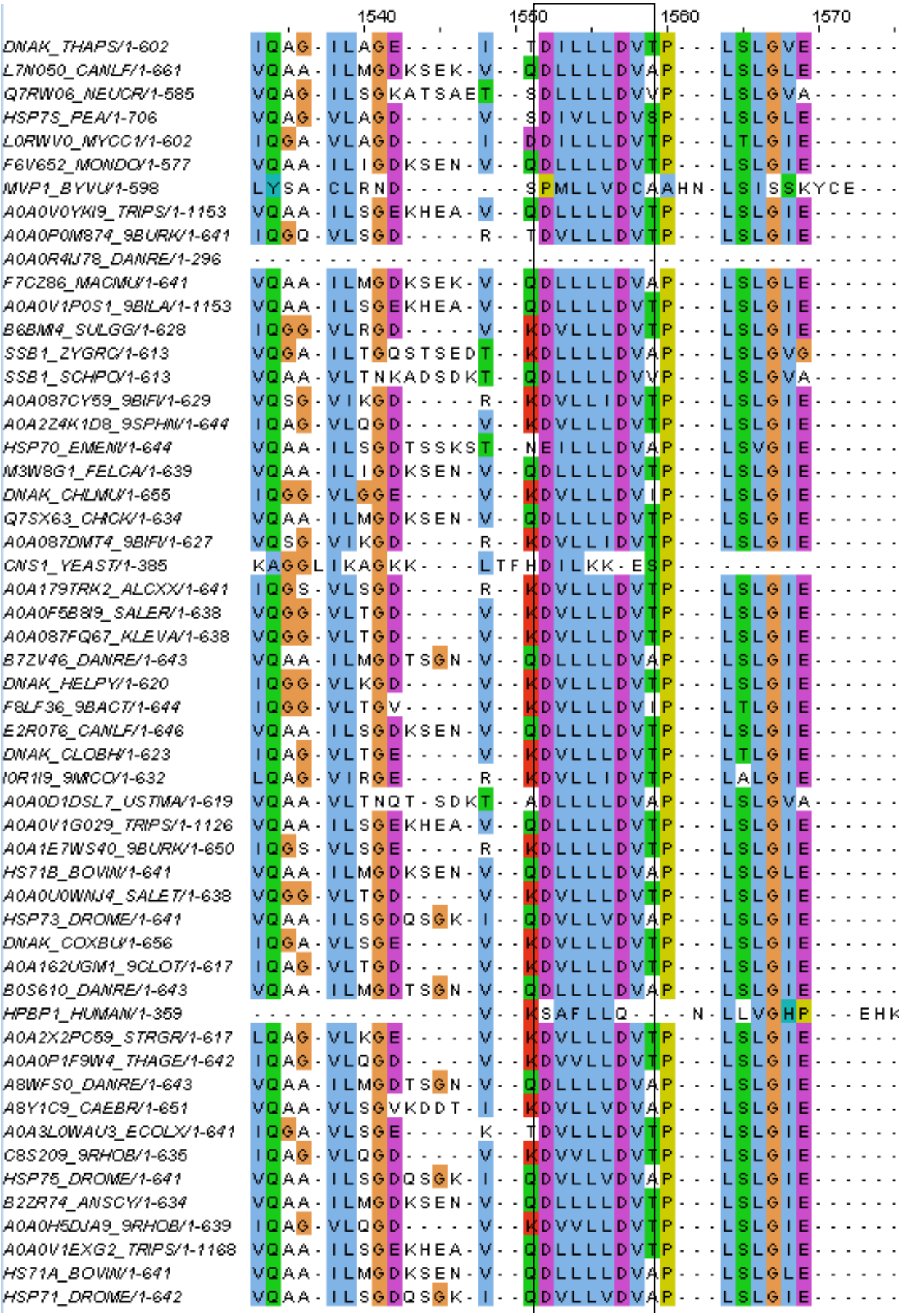

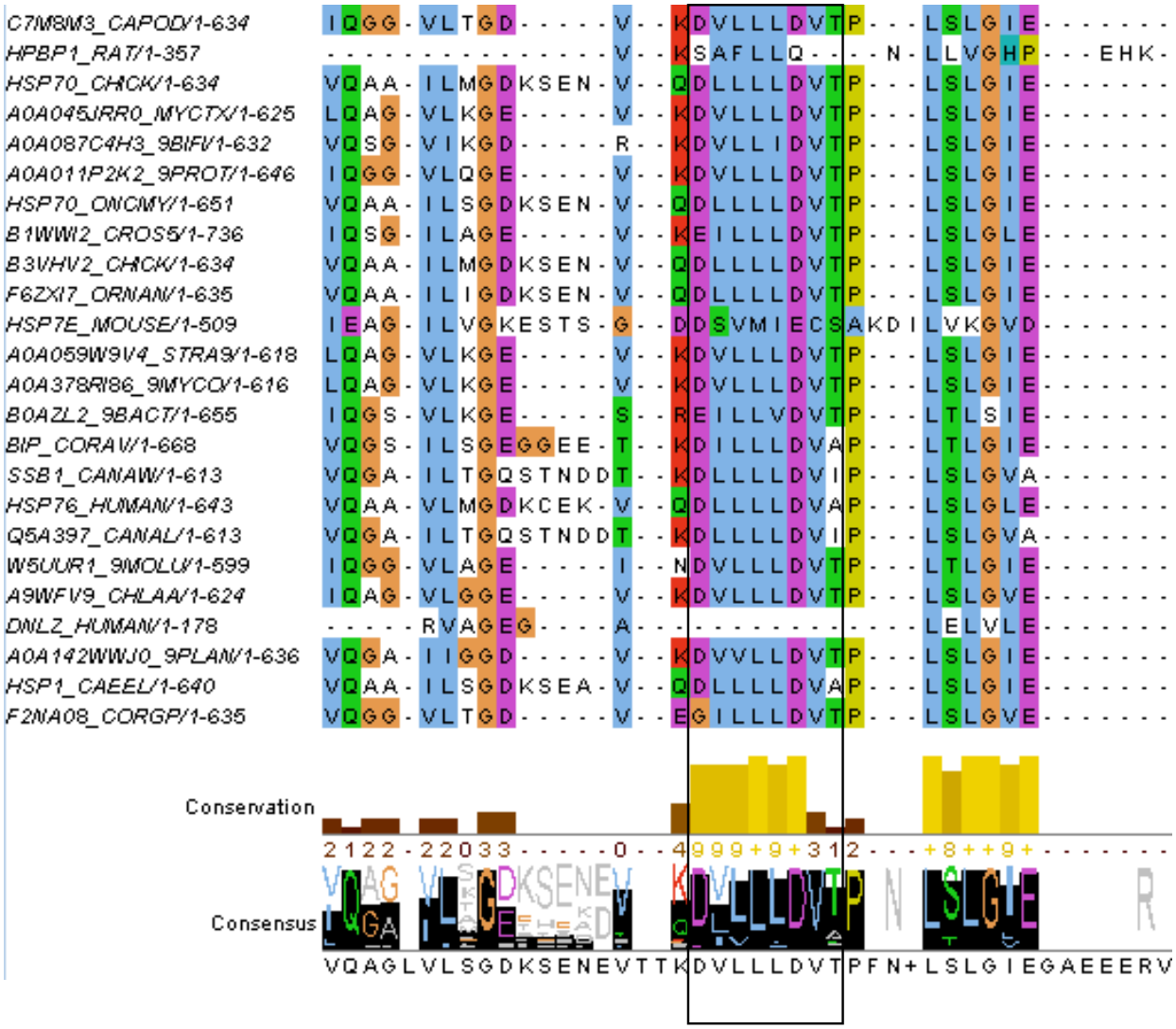

B5: JALVIEW Hsp110 sequence alignments

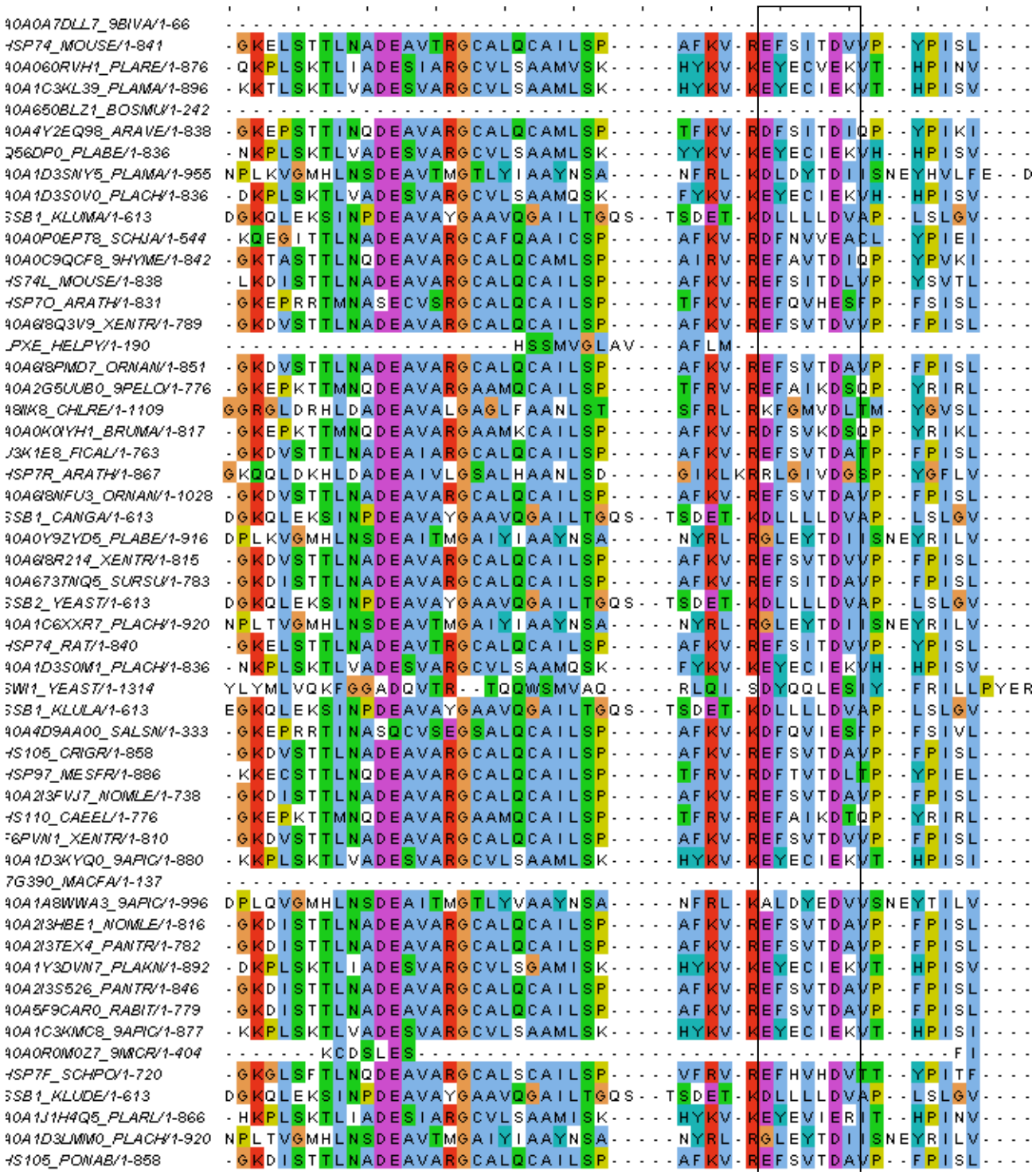

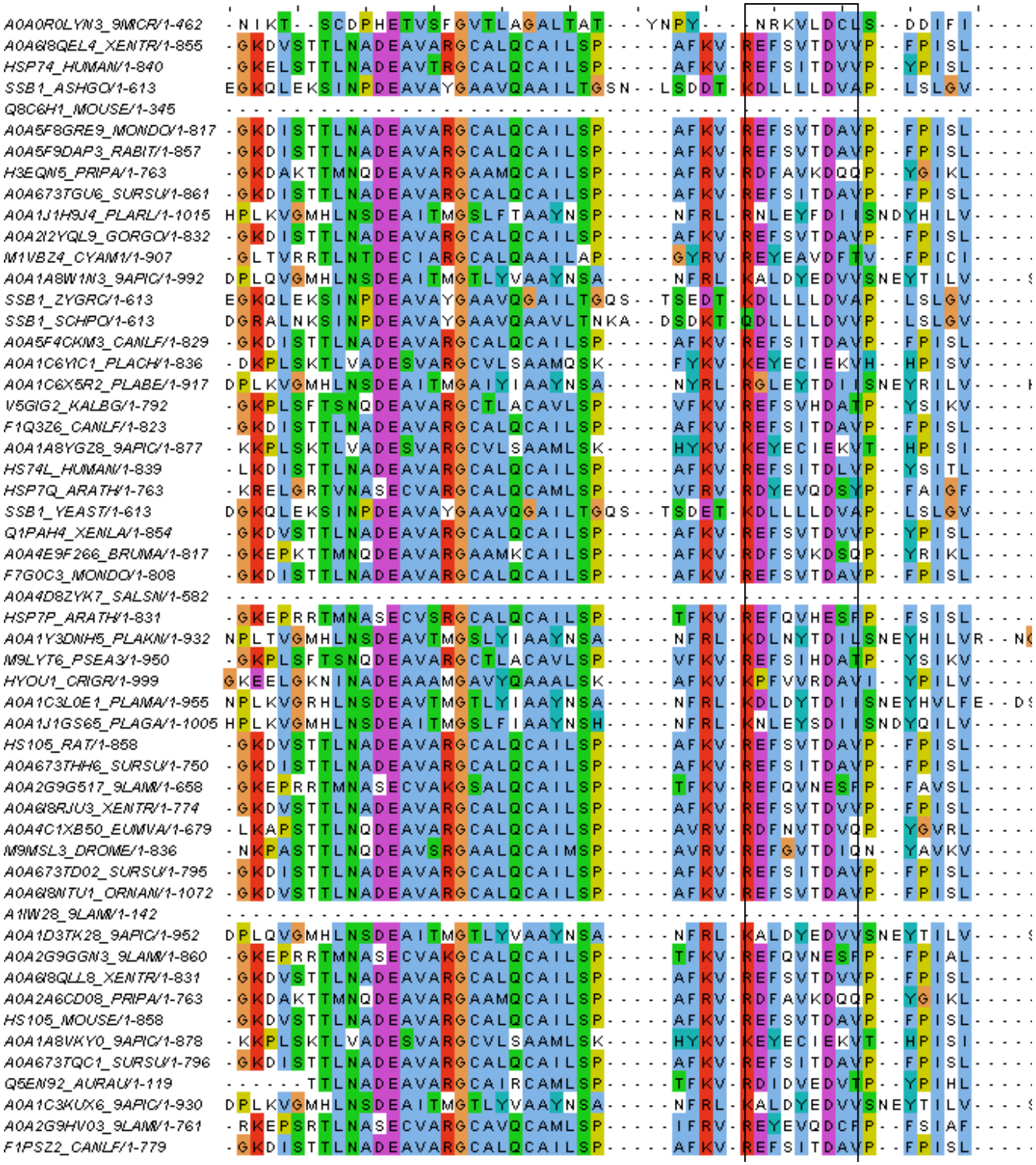

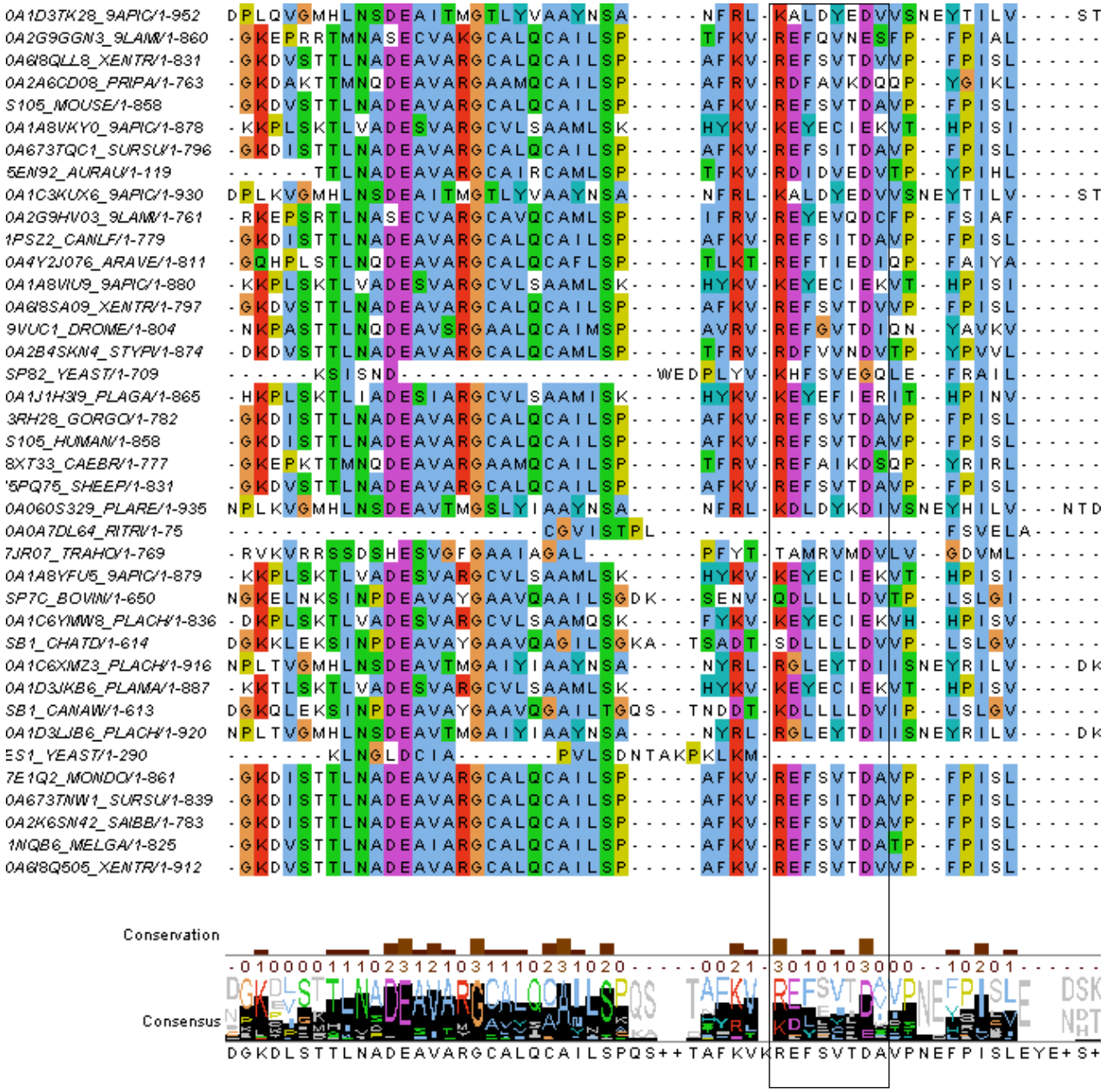

B6 Secondary structure prediction of PfHsp70-z$_{LS}$

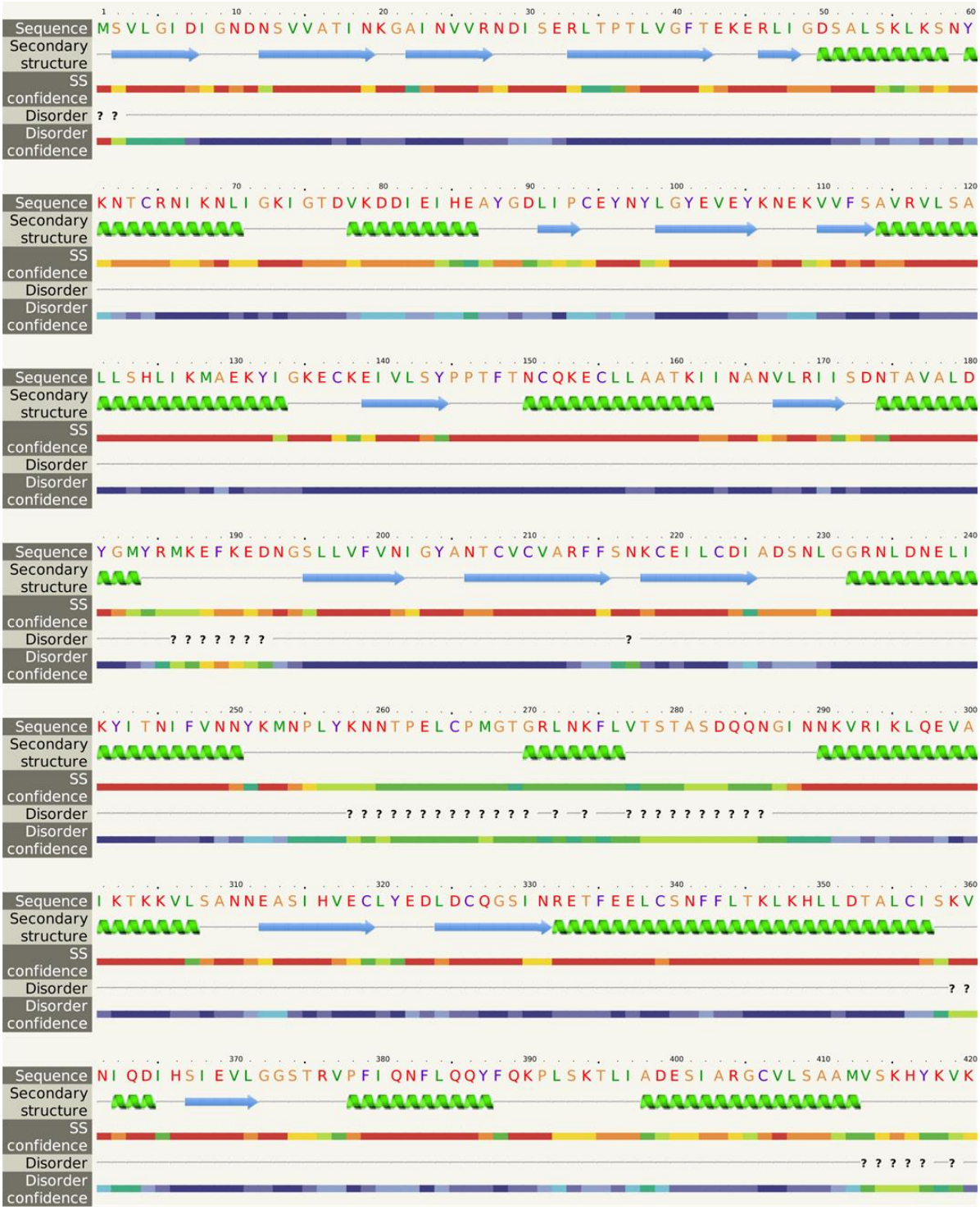

B7 Secondary structural prediction of PfHsp70-z

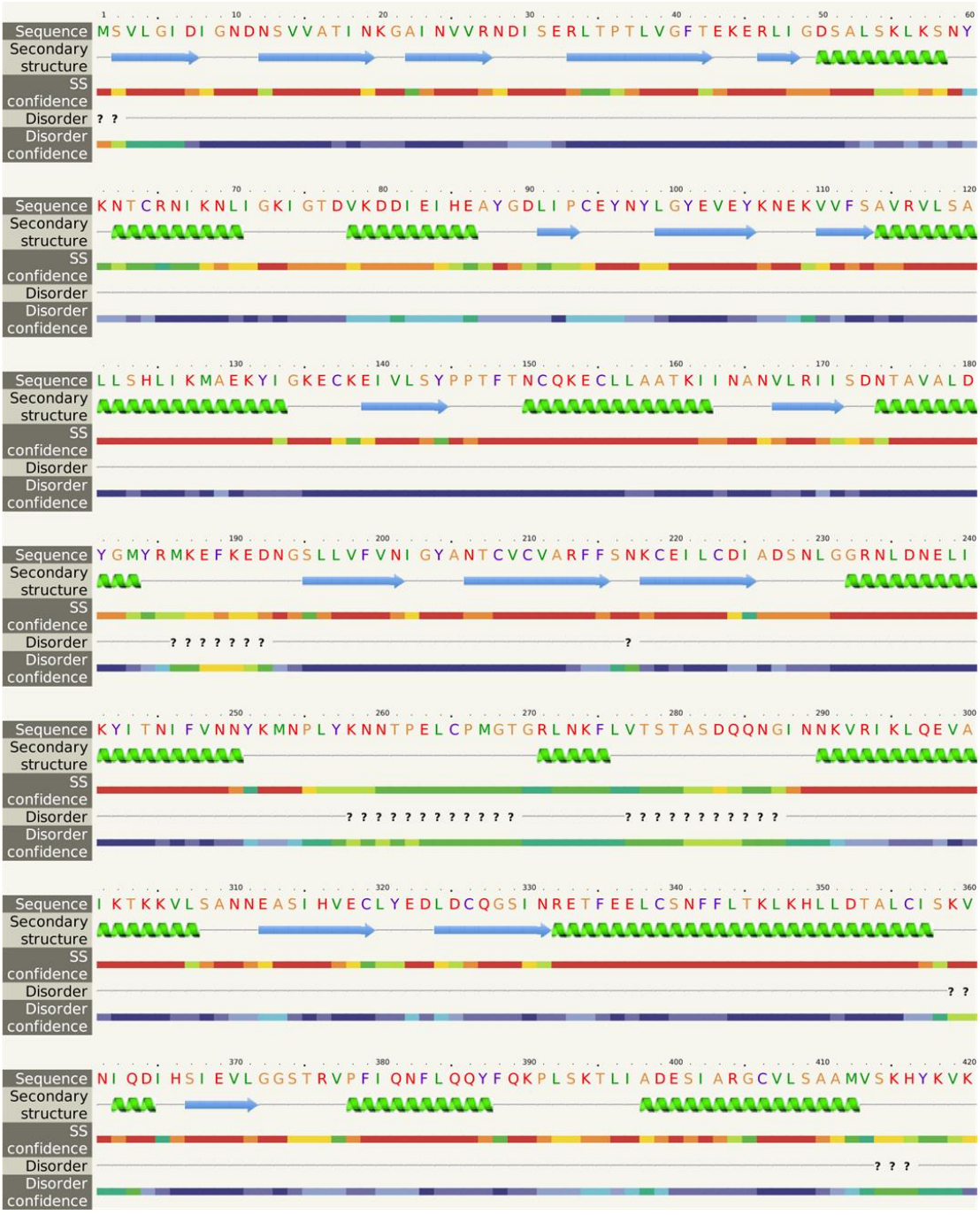

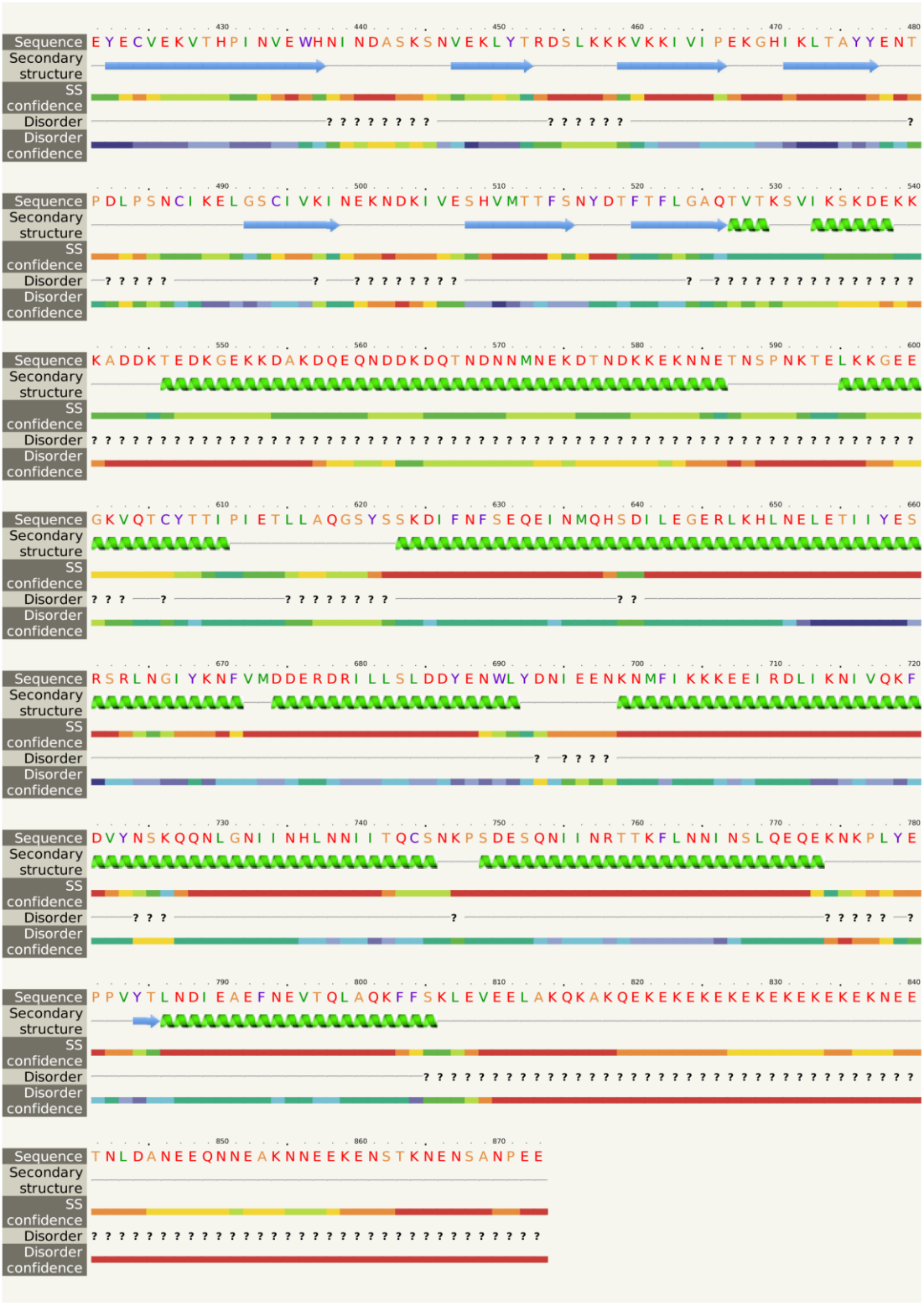

Confidence Key
High(9) Low (0)
? Disordered (28%)
Alpha helix (45%)
Beta strand (19%)

B8 PfHsp70-1 secondary structure

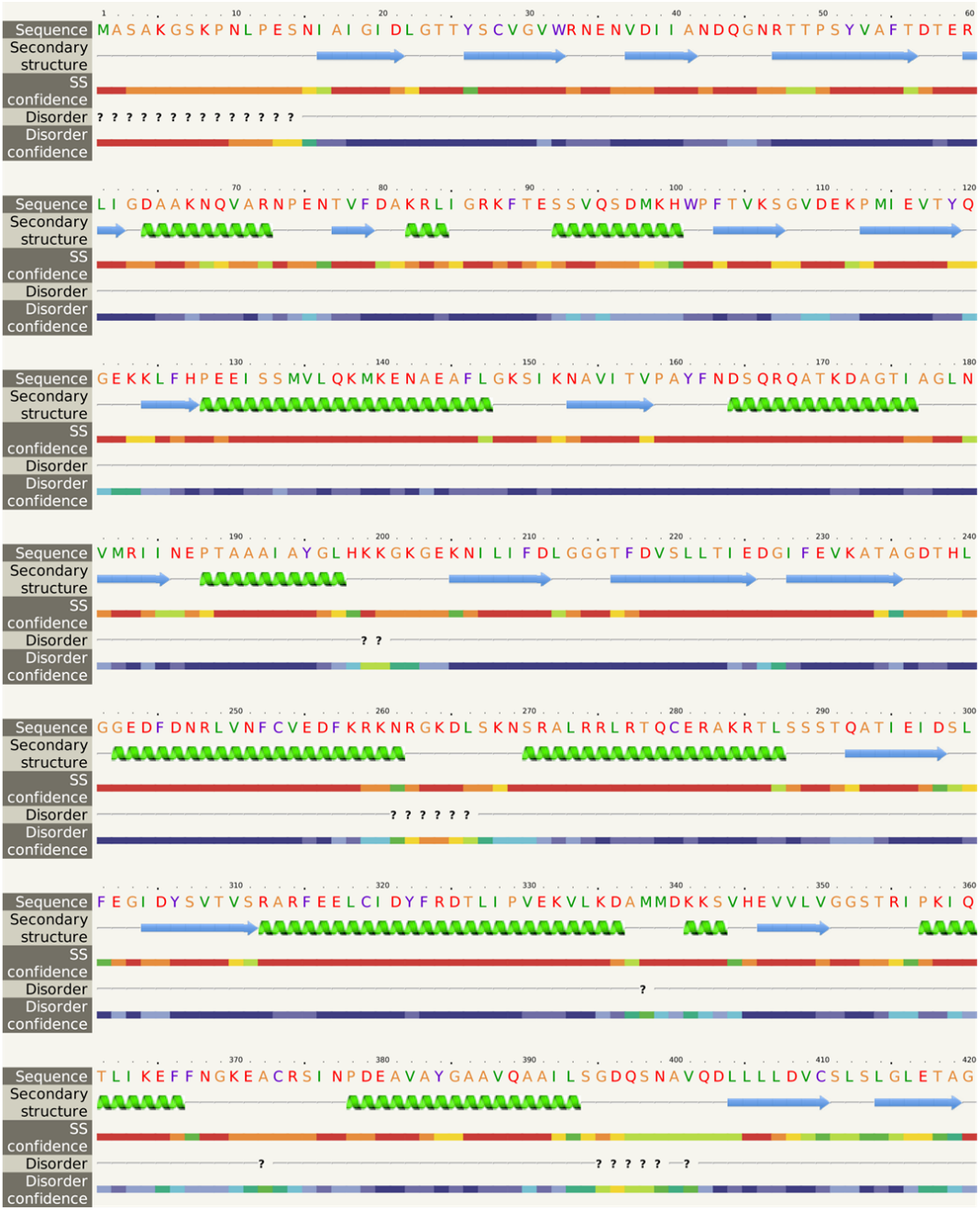

B9 Secondary structure prediction PfHsp70-1$_{LS}$

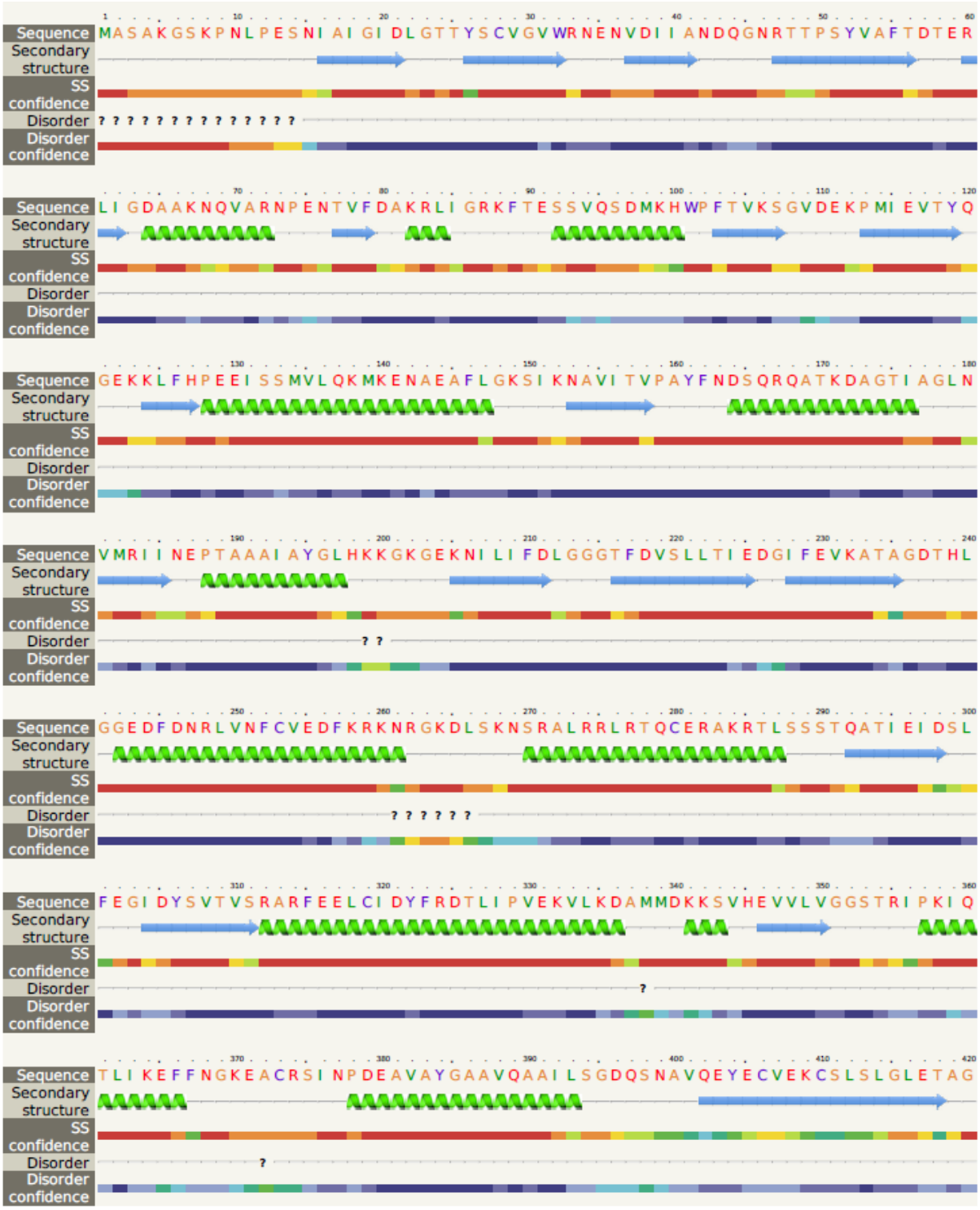

B10 Secondary structure prediction DnaK

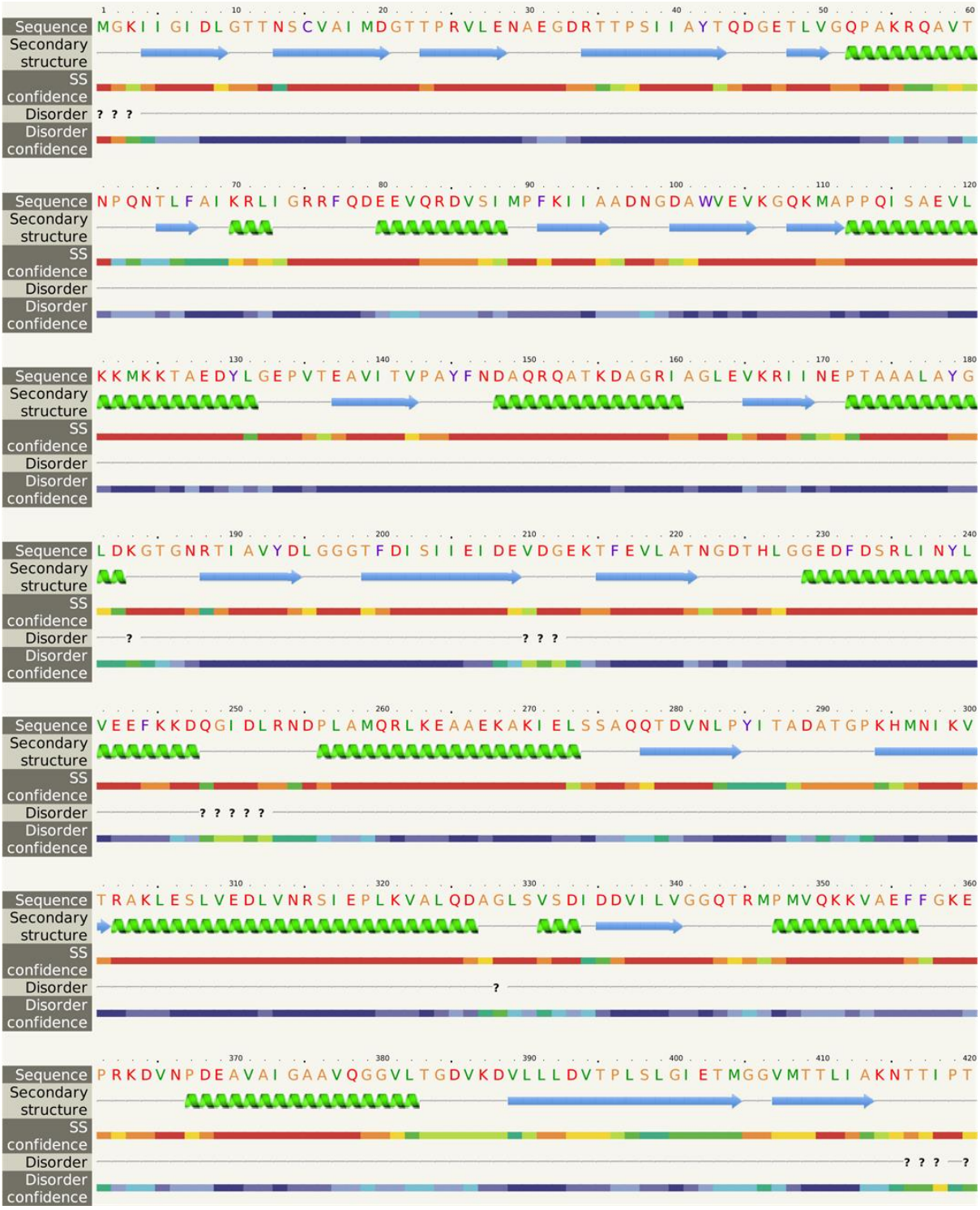

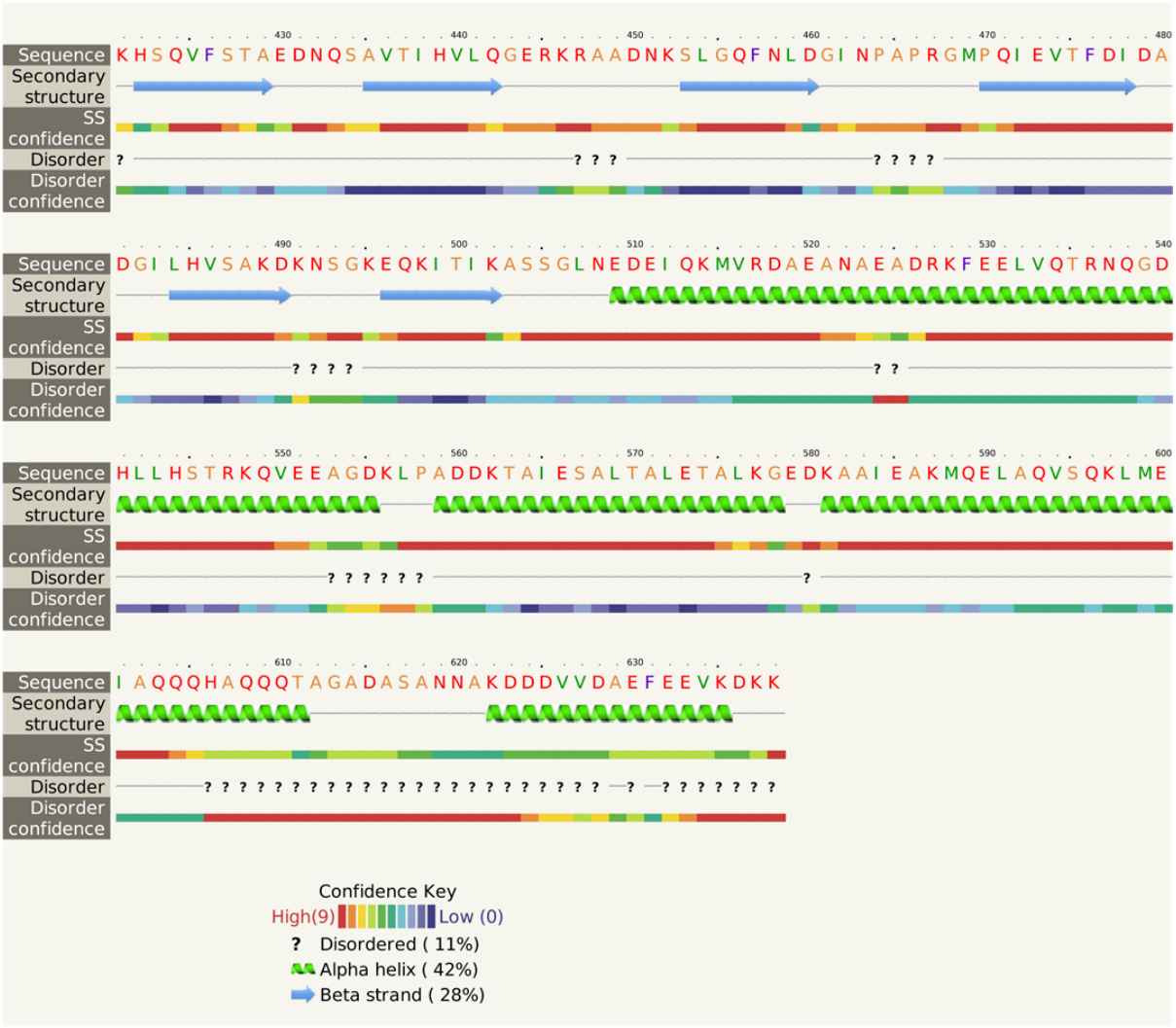

B11Secondary structure of DnaK$_{LS}$

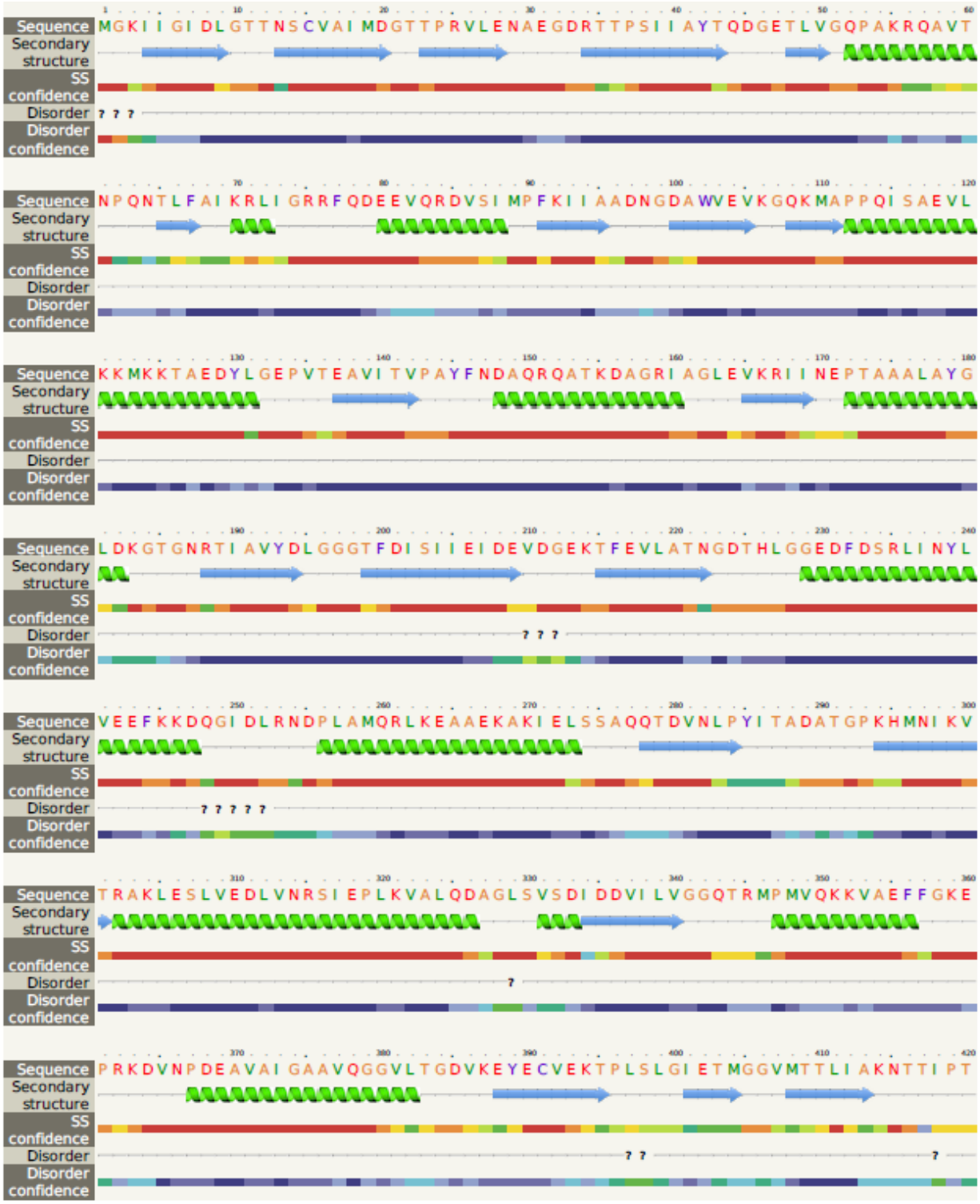

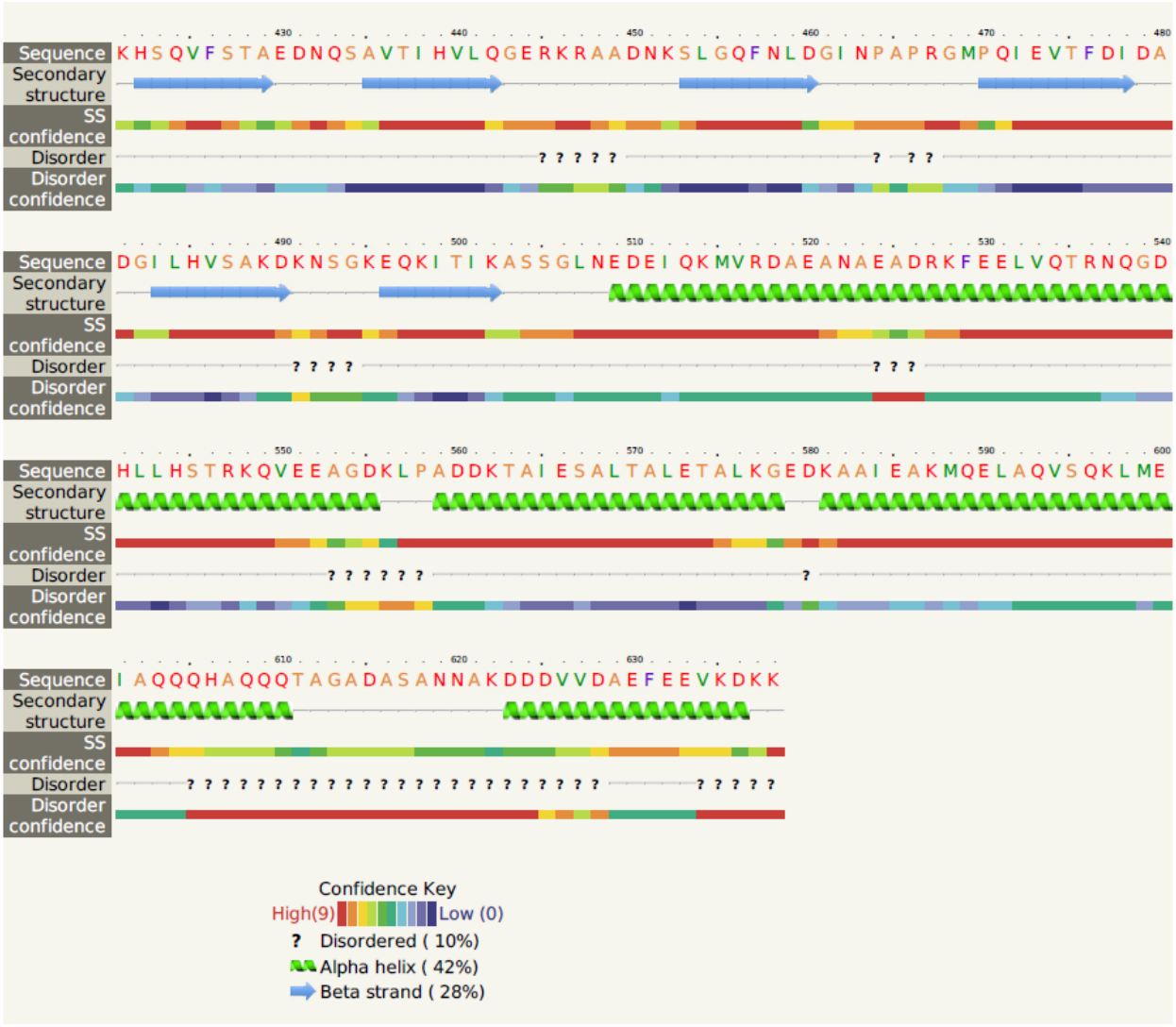

Table B.2 Interactome of PfHsp70-1

Protein	Description	Localization	Score
1. PF3D7_1357800	T complex protein 1 subunit delta	Cytosol	0.999
2. PF3D7_1308200	Carbamoyl phosphate synthetase	Cytoplasm	0.999
3. PF3D7_1333000	Co-chaperonin	Cytoplasm, Apicoplast	0.997
4. PF3D7_1357000	Elongation factor 1-alpha	Cytoplasm	0.996
5. PF3D7_1338300	Elongation factor gamma, putative	Cytoplasm	0.996
6. PF3D7_1309300	U4/U6 small nuclear ribonucleoprotein, putative	Nucleus	0.989
7. PF3D7_0213100	Heat shock protein 40kDa protein, putative (SIS1)	Cytosol	0.964
8. PF3D7_1317800	40S ribosomal protein S15/S19, putative	Cytosol	0.948
9. PF3D7_0213500	Conserved Plasmodium protein, tetratricopeptide repeat protein, putative	Cytoplasm	0.908
10. PF3D7_0707700	Ubiquitin-protein ligase E3, putative	Cytosol	0.906
11. PF3D7_0708800	Heat shock protein 110	Cytoplasm	0.904
12. PF3D7_0308200	T complex protein 1, subunit beta	Cytosol	0.893
13. PF3D7_0417200	Bifunctional dihydrofolate reductase-thymidylate synthase	Cytoplasm	0.891
14. PF3D7_0306800	T-complex protein beta subunit, putative	Cytosol	0.889
15. PF3D7_0920800	Inosine-5-monophosphate dehydrogenase	Cytoplasm	0.883
16. PF3D7_1202400	Cyclophilin, putative	Cytoplasm	0.875
17. PF3D7_1211400	Heat shock protein DnaJ homologue PfJ4	Cytoplasm, nucleus	0.867
18. PF3D7_1211800	Polyubiquitin	Cytoplasm	0.860
19. PF3D7_0922500	Phosphoglycerate kinase	Cytosol	0.878
20. PF3D7_0823800	DnaJ protein, putative	Nucleus, cytosol	0.850
21. PF3D7_1215300	Mitochondrial co-chaperonin	Cytoplasm, mitochondria	0.833
22. PF3D7_1216900	DNAJ-binding chaperone, putative	Nucleus	0.824
23. PF3D7_1224300	Polyadenylate binding protein	Cytoplasm	0.822
24. PF3D7_1229500	T-complex protein 1, gamma subunit, putative	Cytosol	0.811
25. PF3D7_0318200	DNA-directed RNA polymerase	Nucleus	0.807
26. PF3D7_1232100	Chaperonin, cpn60	Cytoplasm	0.806
27. PF3D7_0803000	SYF2 splicing factor, putative	Nucleus	0.806
28. PF3D7_1246200	Actin-1	Cytoplasm and cell surface	0.800
29. PF3D7_0320300	T-complex protein 1 epsilon subunit, putative	Cytosol	0.797
30. PF3D7_0322000	Peptidyl-propyl cis-trans isomerase	Cytosol, E.R	0.794
31. PF3D7_1359400	RNA binding protein, putative	Cytoplasm	0.797
32. PF3D7_1365900	60S ribosomal protein L40/UBI, putative	Cytosol	0.794
33. PF3D7_0209800	DEAD-box helicase 1	Cytoplasm, nucleus	0.783
34. PF3D7_1012600	GMP synthetase	Nucleus	0.780
35. PF3D7_1410600	Eukaryotic translation initiation factor 2 gamma subunit, gamma	Cytoplasm	0.777
36. PF3D7_1015600	Heat shock protein 60	Cytoplasm, mitochondria	0.776

37. PF3D7_1412500	Actin 2	Cytoplasm, cytoskeleton	0.764
38. PF3D7_1433500	DNA topoisomerase 2	Nucleus	0.764
39. PF3D7_1015900	Enolase	Cytoplasm	0.764
40. PF3D7_1030100	RNA helicase, putative	Cytoplasm	0.763
41. PF3D7_1434300	STI1-like protein	Cytosol, nucleus	0.761
42. PF3D7_1437900	Hssp40, subfamily A, putative	Cytosol	0.754
43. PF3D7_1115600	Peptidyl-propyl cis trans isomerase	Cytosol, E.R	0.749
44. PF3D7_1132200	T-complex protein 1 subunit alpha	Cytosol	0.748
45. PF3D7_1451100	Elongation factor 2	Cytosol	0.746
46. PF3D7_1304500	Small heat shock protein, putative	Cytosol	0.743
47. PF3D7_1318800	DnaJ/SEC63 protein, putative	Cytoplasm	0.730
48. PF3D7_1453700	P23 co-chaperone, putative	Cytosol	0.724
49. PF3D7_1462800	Glyceraldehyde-3-phosphate dehydrogenase	Cytosol, cell surface	0.713

Table B.3 Interactome of PfHsp70-z

Protein	Description	Localization	Score
1. PF3D7_1330300	Hsp40	Cytosol	0.985
2. PF3D7_0708400	Hsp86	Cytosol	0.976
3. PF3D7_1434300	Hsp70-Hsp90 organizing protein	Cytosol	0.972
4. PF3D7_1222300	Endoplasmin homologue	Cytosol	0.955
5. p23	SBA1	Cytoplasm	0.954
6. PF3D7_0410600	Conserved protein, unknown function	Nucleus	0.951
7. PF3D7_0308500	Activator of Hsp90 ATPase homologue	Cytosol	0.950
8. PF3D7_0308200	T complex protein 1 subunit eta	Cytosol	0.940
9. PF3D7_0818900	Hsp70	Cytoplasm	0.928
10. PF3D7_1232100	Chaperonin CPN60	Cytosol	0.926
11. PF3D7_1216900	DNA binding chaperone	Cytoplasm	0.922
12. PF3D7_1134000	Hsp70	Cytosol	0.906
13. PF3D7_1411300	DnaJ protein, putative	Cytoplasm	0.897
14. PF3D7_1015600	Chaperonin GroL/ Hsp60	Cytosol	0.897
15. PF3D7_1123400	Translation Elongation Factor 1	Cytoplasm	0.890
16. PF_110258	GrpE homologue	Cytosol	0.890
17. PF3D7_0409400	DnaJ	Cytoplasm	0.888
18. PF3D7_0608700	T complex protein 1 zeta	Cytoplasm,	0.887
19. PF3D7_1132200	T complex protein 1 alpha	Cytosol	0.874
20. PF3D7_0320300	T complex protein 1 epsilon	Nucleus, cytosol	0.874
21. PF3D7_1118200	Hsp90, putative	Cytosol	0.872
22. PF3D7_0214000	T complex protein 1 theta	Nucleus	0.864
23. PF3D7_0813300	Conserved protein, unknown function	Cytosol	0.856
24. PfCyP19	Peptidyl-propyl cis trans isomerase	Cytosol	0.856
25. PF3D7_1229500	T complex protein 1 gamma subunit	Nucleus	0.844
26. PFA_0660w	DnaJ domain	Cytosol	0.842
27. PF3D7_1338300	Elongation factor 1, gamma putative	Nucleus	0.838
28. PF3D7_1116800	Hsp101, ClpA/B family	Cytosol	0.833
29. PF3D7_0524000	Karyopherin beta	Cytosol	0.832
30. PF3D7_1473700	Nucleoporin NUP116/NSP116, putative	Cytosol, nucleus	0.826
31. PF3D7_0816600	Chaperone protein ClpB1	Cytoplasm	0.824
32. PF3D7_0826700	Receptor for activated c kinase	Cytosol	0.814
33. PF3D7_1232100	Chaperonin, Cpn60	Cytoplasm	0.814
34. PF3D7_0520000	40S ribosomal protein S9, putaive	Nucleus	0.804
35. PF3D7_1233600	Asparagine and aspartate rich protein	Cytoplasm	0.803
36. PF3D7_1124900	60S ribosomal protein L35, putative	Cytoplasm, mitochondria	0.803
37. PF3D7_1408100	Plasmepsin III	Cytosol	0.800
38. PF3D7_1451100	Elongation factor 2	Nucleus	0.799
39. PF3D7_1026800	40S ribosomal protein	Cytoplasm	0.796
40. PF3D7_1406600	ATP-dependent Clp protease	Cytoplasm	0.792
41. PF3D7_1355500	Serine/Threonine protein phosphatase	Cytosol, nucleus	0.792
42. PF3D7_1414300	60S ribosomal protein L10	Cytosol	0.784
43. PF3D7_0527500	Hsc70 interacting protein	Cytosol, E.R	0.791
44. PF3D7_1414300	60S ribosomal protein L10	Cytosol	0.784
45. PF3D7_1323400	60S ribosomal protein L23a	Cytosol	0.784
46. PF3D7_0816500	Small Hsp,Hsp20	Cytosol	0.782
47. PF3D7_1304500	Small Hsp, putative	Cytoplasm	0.780
48. PfCpn20	GroES family	Cytosol	0.780
49. PF10875w	Grp78 homologue	Cytosol	0.776
50. PF3D7_0312200	TPR domain containing protein	Cytosol	0.775

B12. Confirmation of plasmid constructs by restriction digestion

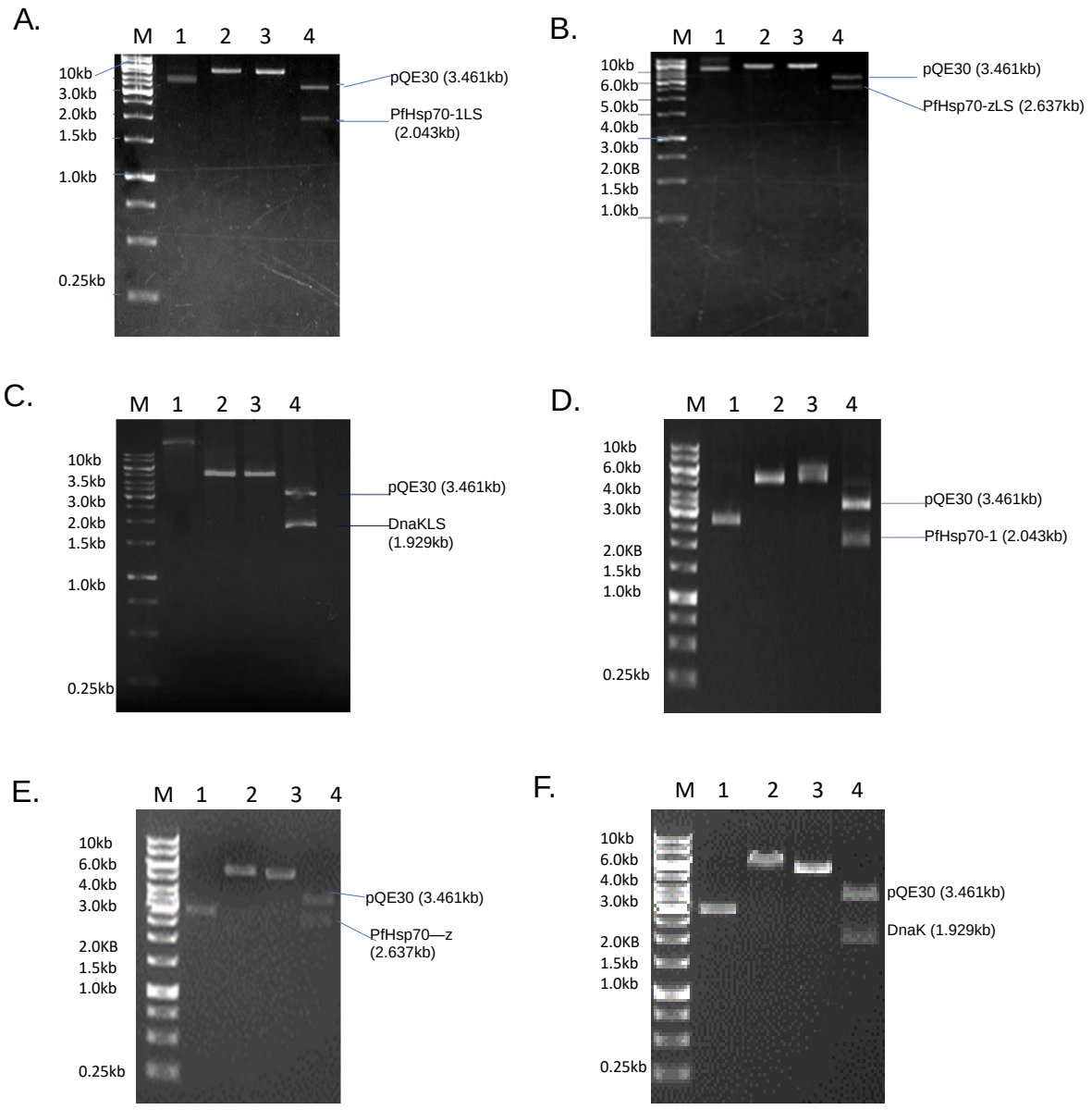

Figure B12 Restriction digestion of PfHsp70-1$_{LS}$, PfHsp70-z$_{LS}$ and DnaK$_{LS}$

Restriction digestion for pQE30/PfHsp70-1$_{LS}$ (A); pQE30/PfHsp70-1$_{LS}$ (B) and pQE30/DnaK$_{LS}$ DNA (C) plasmids using *Bam*HI and *Kpn*I. Llane 1, undigested plasmid DNA; lane 2 plasmid DNA digested with *Bam*HI; lane 3, plasmid DNA digested with *Kpn*I; lane 4, plasmid DNA digested with both *Bam*HI and *Kpn*I. Restriction digestion for pQE30/PfHsp70-1 (D); pQE30/PfHsp70-1$_{LS}$ (E) and pQE30/DnaK$_{LS}$ DNA (F) plasmids using *Bam*HI and *HindII*I. Llane 1, undigested plasmid DNA; lane 2 plasmid DNA digested with *Bam*HI; lane 3, plasmid DNA digested with *HindII*I; lane 4, plasmid DNA digested with both *Bam*HI and *HindIII*.

B13. PfHsp70-1$_{LS}$ expression and purification (full blots)

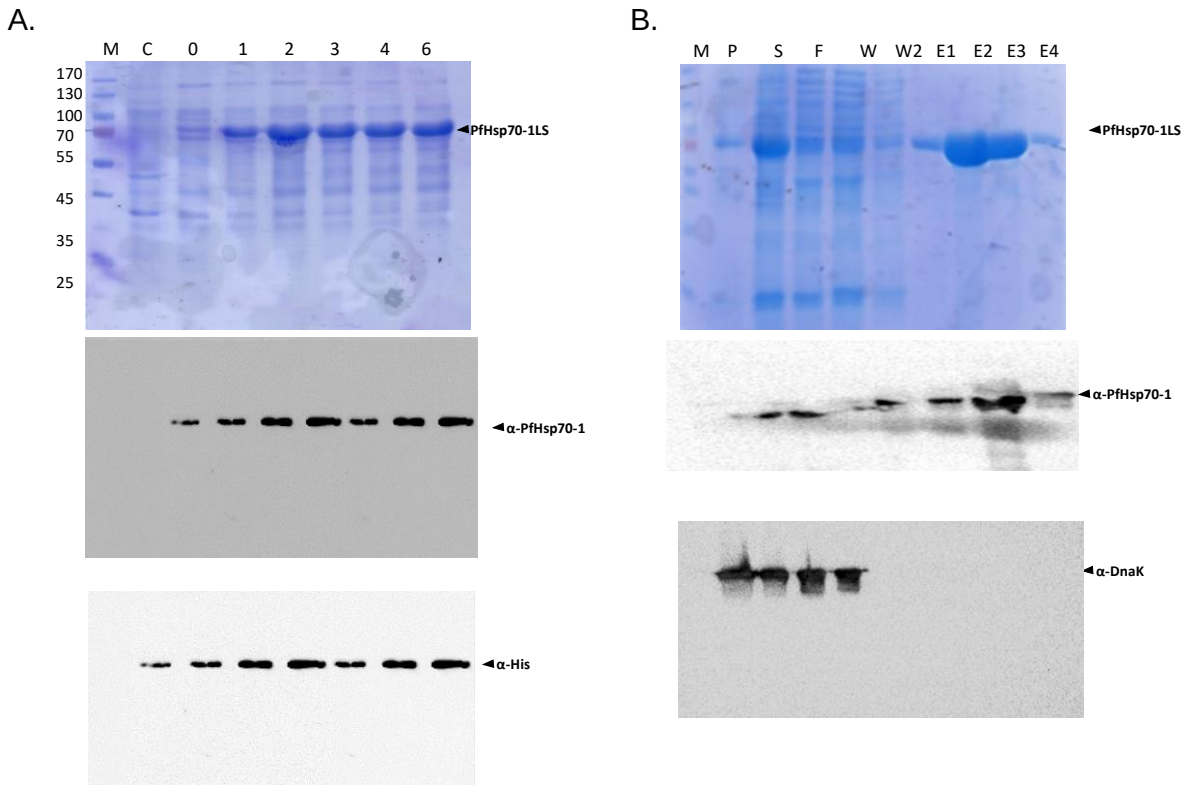

Figure B13 Expression and purification of PfHsp70-1$_{LS}$

(A) SDS-PAGE analysis for the expression of PfHsp70-1$_{LS}$. M represents the molecular weight marker (in kDa), C represents the pQE30 vector control with no insert. 0 represents the pre-induction samples. Samples 1-6 were hourly samples that were each collected at the respective hour after IPTG induction. Respective immunoblots for expression using α-PfHsp70-1 and α-His antibodies are labelled below expression. (B) Purification samples for PfHsp70-1$_{LS}$. P represents the pellet fraction, S: supernatant, F: flowthrough, W: washes, E: elutions.

B14. PfHsp70-1 expression and purification (full blots)

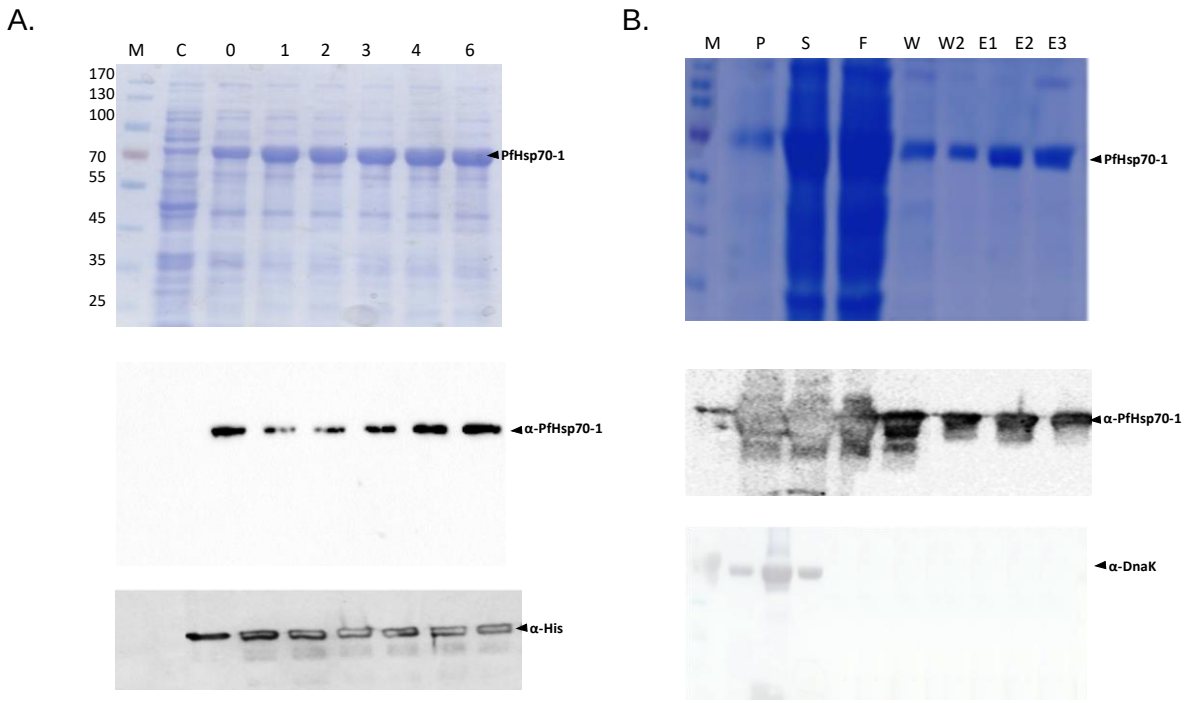

Figure B14 Expression and purification of PfHsp70-1

(A) SDS-PAGE analysis for the expression of PfHsp70-1. M represents the molecular weight marker (in kDa), C represents the pQE30 vector control with no insert. 0 represents the pre-induction samples. Samples 1-6 were hourly samples that were each collected at the respective hour after IPTG induction. Respective immunoblots for expression using α-PfHsp70-1 and α-His antibodies are labelled below expression. (B) Purification samples for PfHsp70-1. P represents the pellet fraction, S: supernatant, F: flowthrough, W: washes, E: elutions.

B15. PfHsp70-z$_{LS}$ expression and purification (full blots)

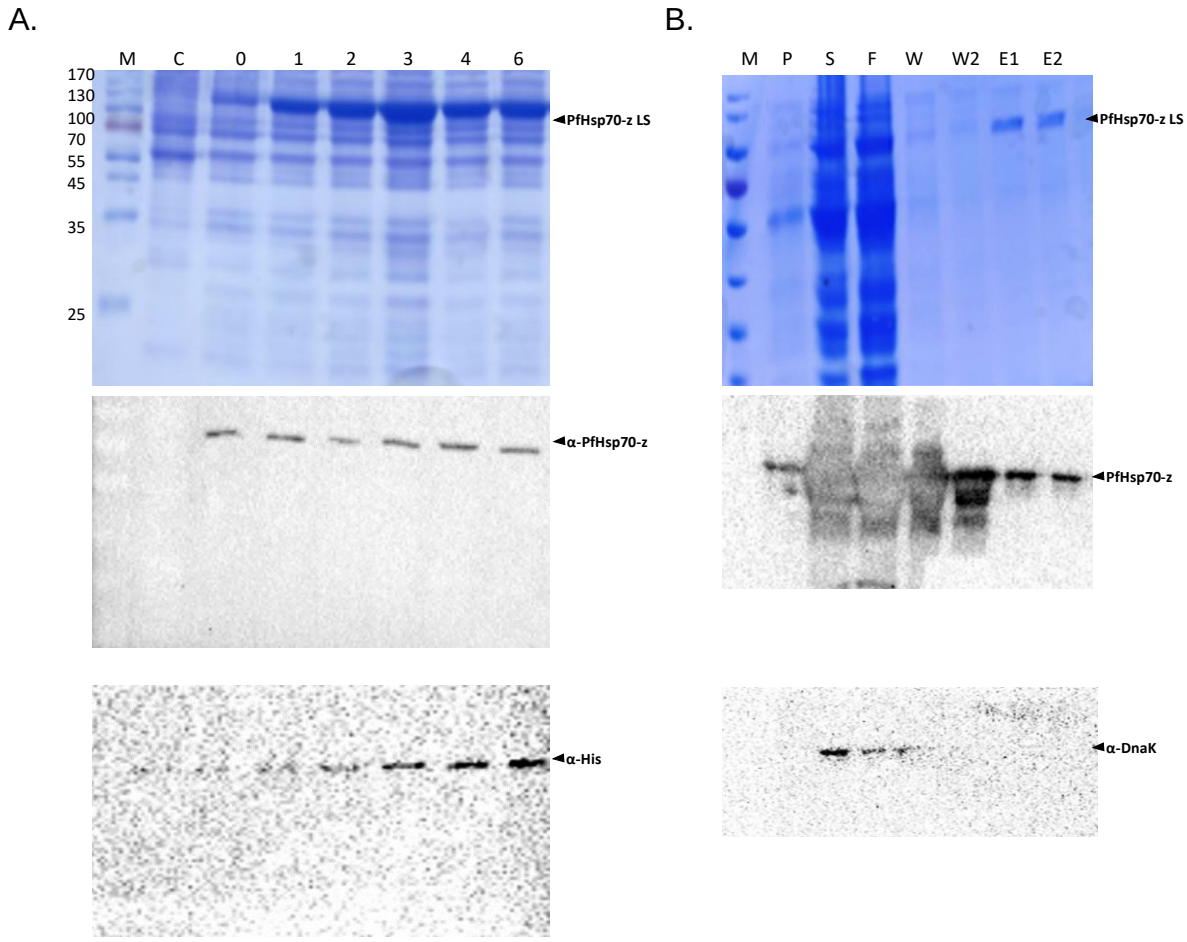

Figure B15 Expression and purification of PfHsp70-z$_{LS}$

(A) SDS-PAGE analysis for the expression of PfHsp70-z$_{LS}$. M represents the molecular weight marker (in kDa), C represents the pQE30 vector control with no insert. 0 represents the pre-induction samples. Samples 1-6 were hourly samples that were each collected at the respective hour after IPTG induction. Respective immunoblots for expression using α-PfHsp70-z and α-His antibodies are labelled below expression. (B) Purification samples for PfHsp70-z$_{LS}$. P represents the pellet fraction, S: supernatant, F: flowthrough, W: washes, E: elutions.

B16. Expression and purification of PfHsp70-z (full blots)

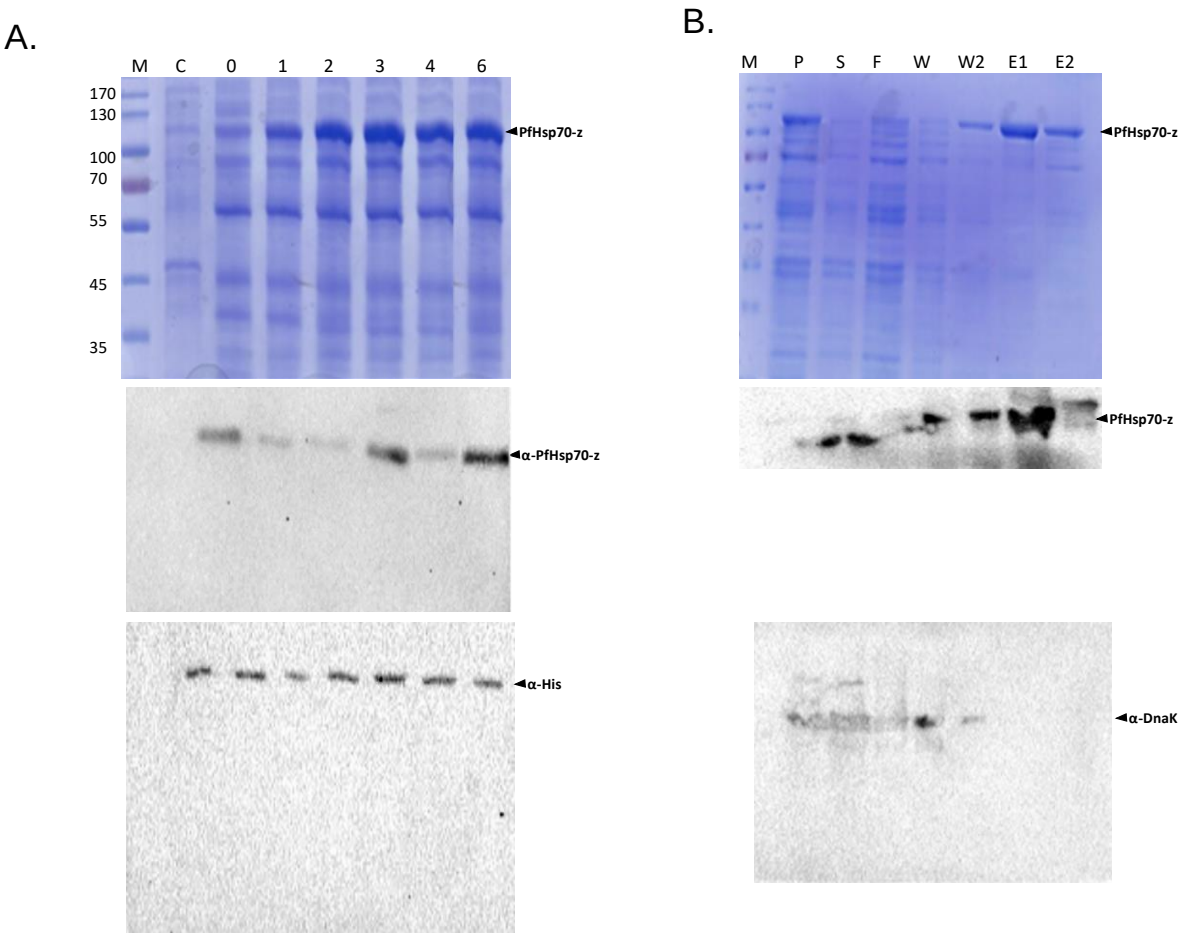

Figure B16 Expression and purification of PfHsp70-z

(A) SDS-PAGE analysis for the expression of PfHsp70-z. M represents the molecular weight marker (in kDa), C represents the pQE30 vector control with no insert. 0 represents the pre-induction samples. Samples 1-6 were hourly samples that were each collected at the respective hour after IPTG induction. Respective immunoblots for expression using α-PfHsp70-z and α-His antibodies are labelled below expression. (B) Purification samples for PfHsp70-z. P represents the pellet fraction, S: supernatant, F: flowthrough, W: washes, E: elutions.

B17. DnaK$_{LS}$ expression and purification

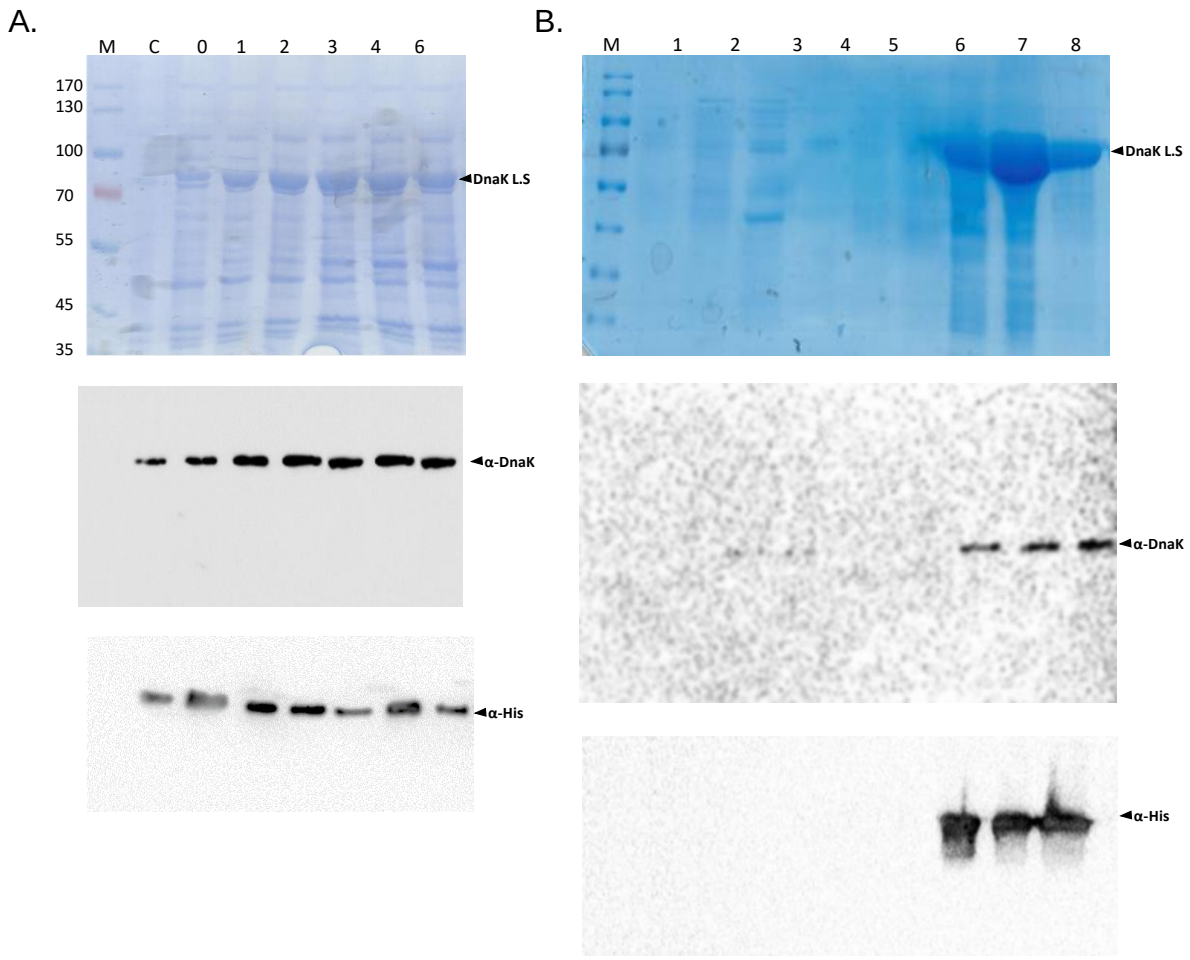

Figure B17 Expression and purification of DnaK$_{LS}$

(A) SDS-PAGE analysis for the expression of DnaK$_{LS}$. M represents the molecular weight marker (in kDa), C represents the pQE30 vector control with no insert. 0 represents the pre-induction samples. Samples 1-6 were hourly samples that were each collected at the respective hour after IPTG induction. Respective immunoblots for expression using α-DnaK and α-His antibodies are labelled below expression. (B) Purification samples for DnaK$_{LS}$. P represents the pellet fraction, S: supernatant, F: flowthrough, W: washes, E: elutions.

B18. DnaK expression and purification

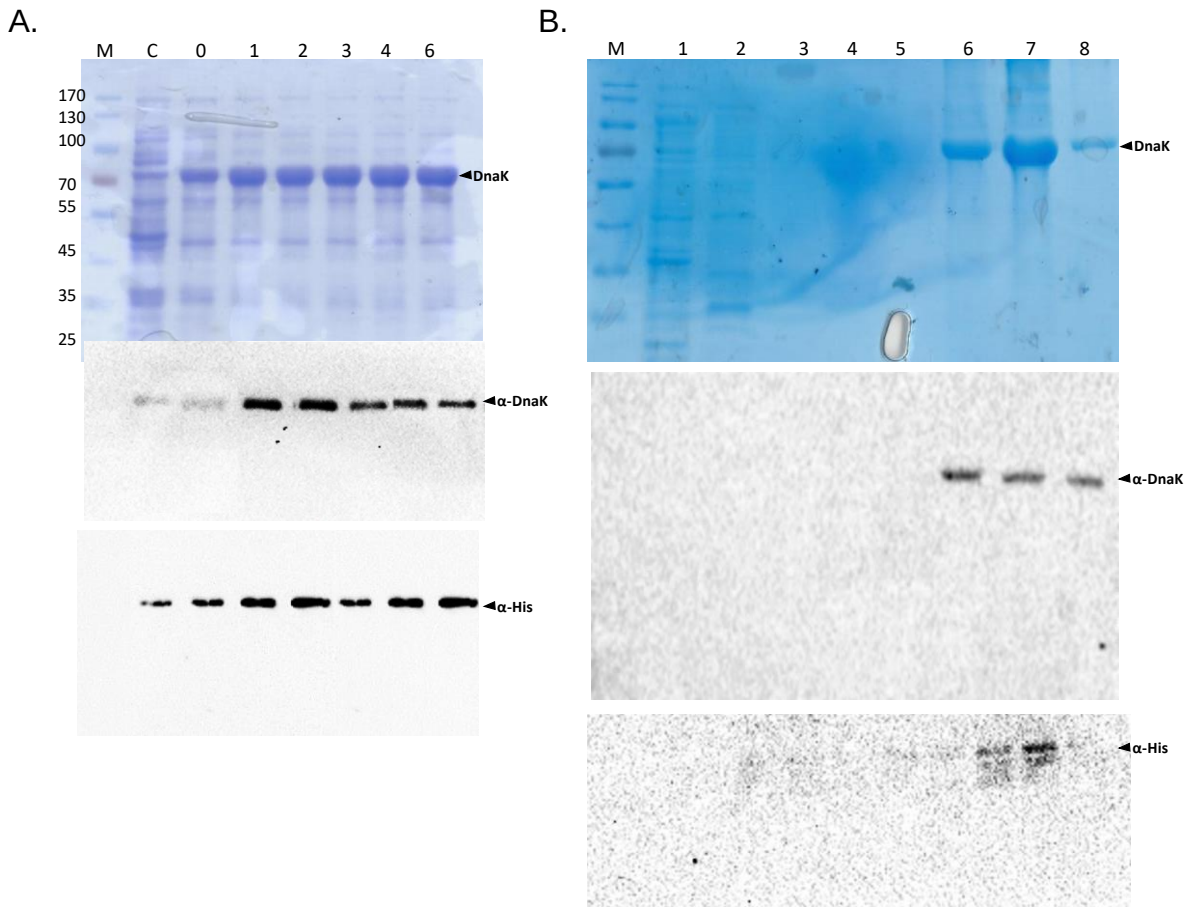

Figure B18 Expression and purification of DnaK

(A) SDS-PAGE analysis for the expression of DnaK. M represents the molecular weight marker (in kDa), C represents the pQE30 vector control with no insert. 0 represents the pre-induction samples. Samples 1-6 were hourly samples that were each collected at the respective hour after IPTG induction. Respective immunoblots for expression using α-DnaK and α-His antibodies are labelled below expression. (B) Purification samples for DnaK. P represents the pellet fraction, S: supernatant, F: flowthrough, W: washes, E: elutions.

B19. Urea denaturation CD Spectra

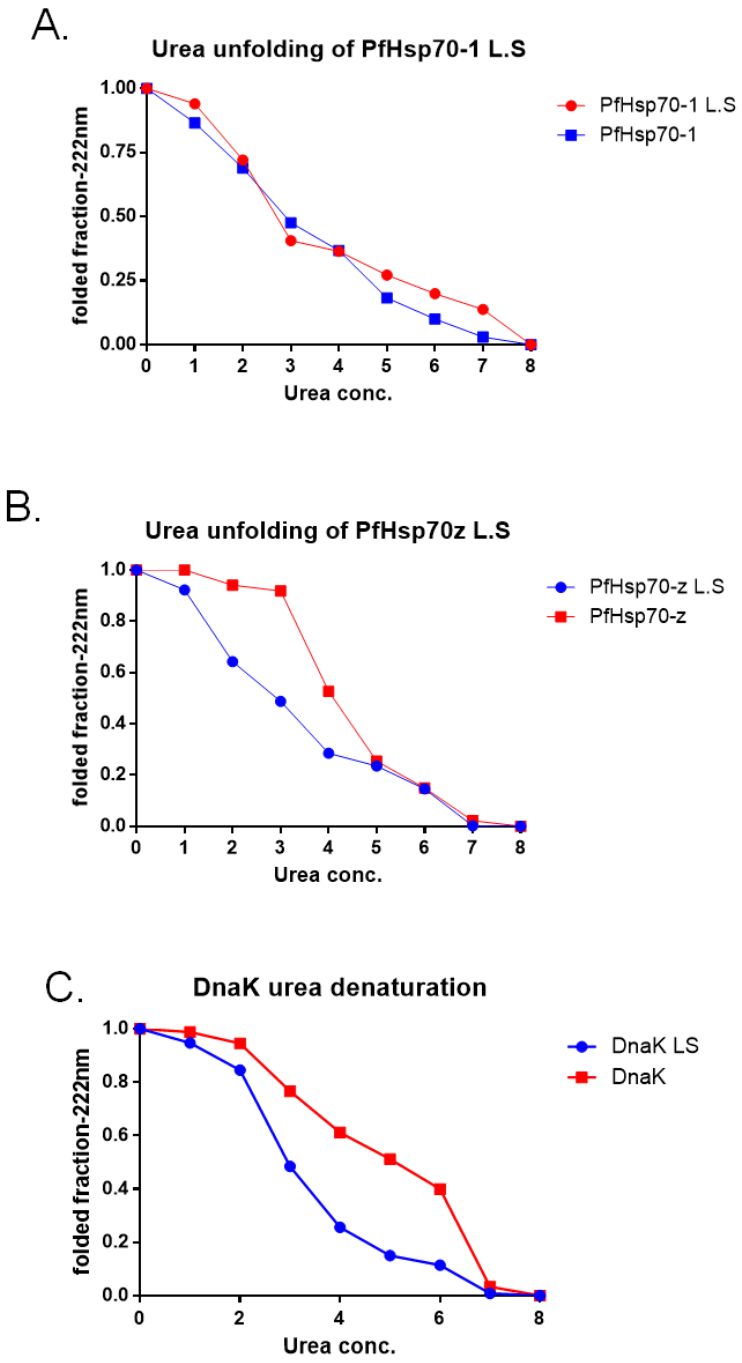

Figure B19 Urea induced changes in Hsp70 secondary structure

(A) PfHsp70-1 and PfHsp70-1$_{LS}$ had similar urea unfolding responses (B) PfHsp70-z is more stable compared to its L.S variant upon urea denaturation. (C) DnaK$_{LS}$ was shown to be less stable compared to its wild type form upon urea denaturation.

B20. Tertiary structures of recombinant Hsp70s

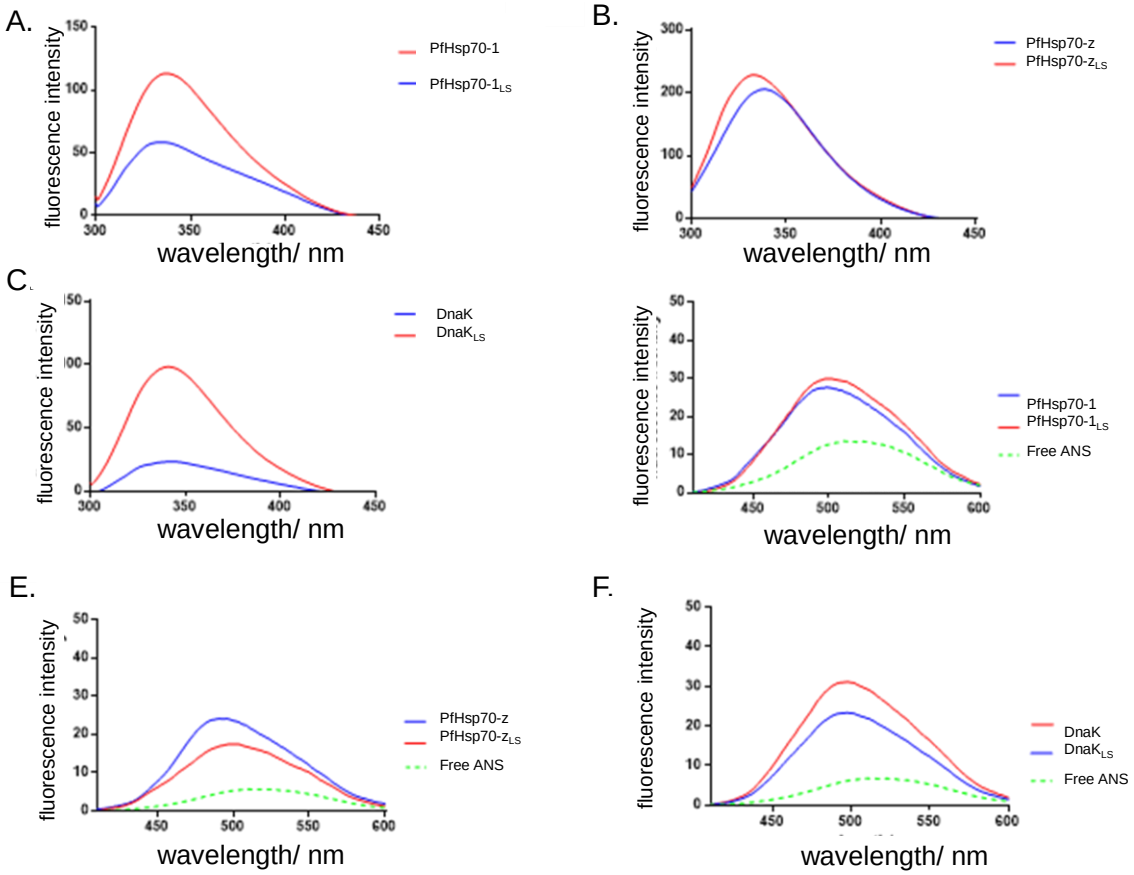

B20 Tertiary structural analysis of Hsp70s.

(A) Tryptophan fluorescence spectra curves for PfHsp70-1 and PfHsp70-1_{LS} show that PfHsp70-1_{LS} has a red shift from PfHsp70-1 structure. (B) PfHsp70-z_{LS} has a blue shift from PfHsp70-z structure. (C) $DnaK_{LS}$ exhibits a red shift from DnaK (wt). (D) ANS fluorescence spectroscopy analysis of PfHsp70-1 and PfHsp70-1_{LS}. (E) PfHsp70-z and PfHsp70-z_{LS} tertiary structures show variation in their response to ANS. (F) ANS fluorescence spectroscopy of DnaK (blue) and $DnaK_{LS}$ (red) showing a blue shift in the proteins in response to ANS.

B21. Effect of pH on tertiary structures

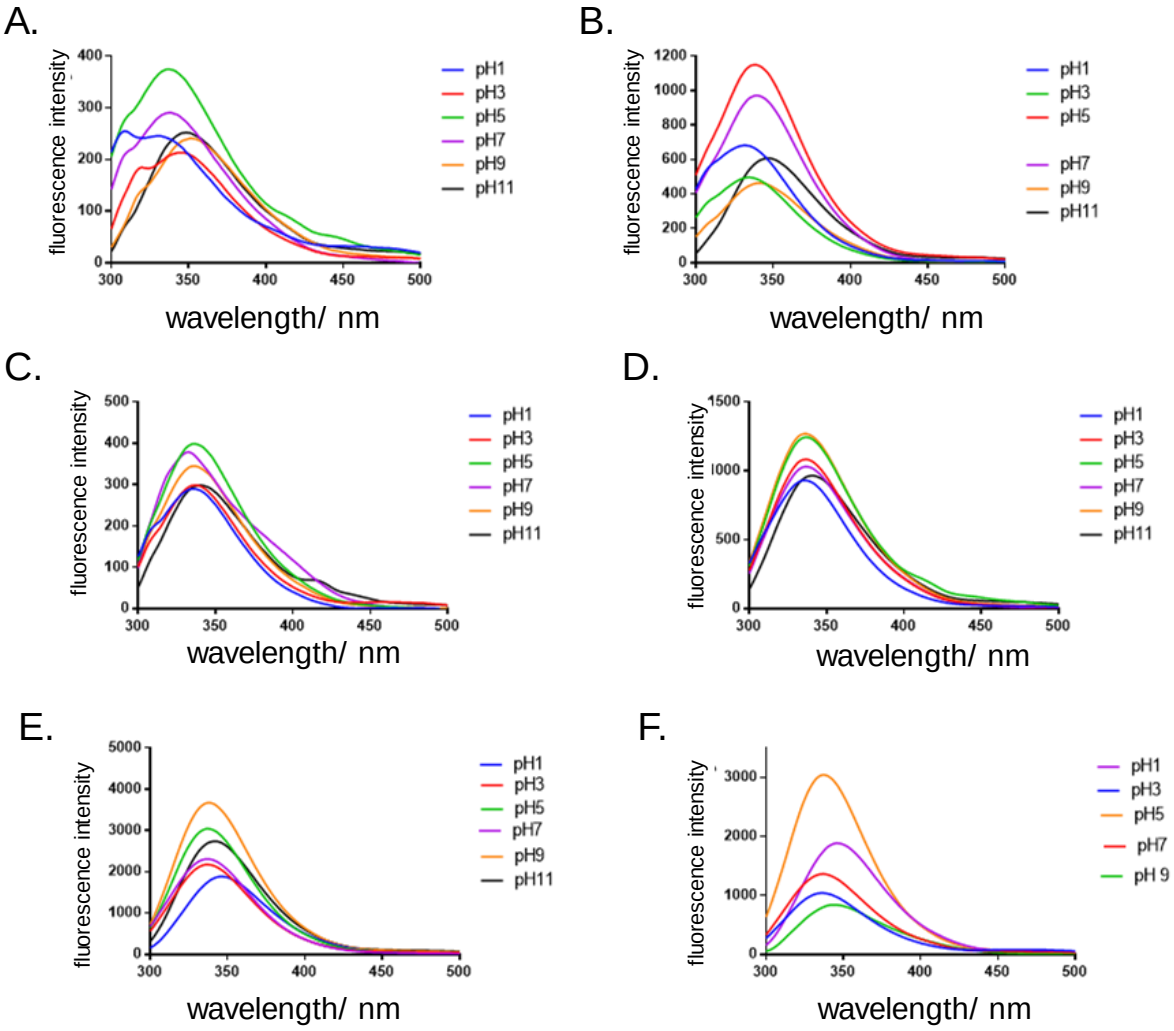

B21 Effect of pH on Hsp70 tertiary structure

(A) Effect of pH on tertiary structure conformation of DnaK. (B) Effect of pH on tertiary structure conformation of $DnaK_{LS.}$ (C) Effect of pH on tertiary structure conformation of PfHsp70-1 (D) Effect of pH on tertiary structure conformation of $PfHsp70\text{-}1_{LS.}$ (E) Effect of pH on tertiary structure conformation of PfHsp70-z were incubated in a pH range from 1-11 and the shifts in wavelengths were analysed. (F) Effect of pH on tertiary structure conformation of $PfHsp70\text{-}z_{LS}$.

B22 Nucleotide-induced tertiary structure conformations of Hsp70s

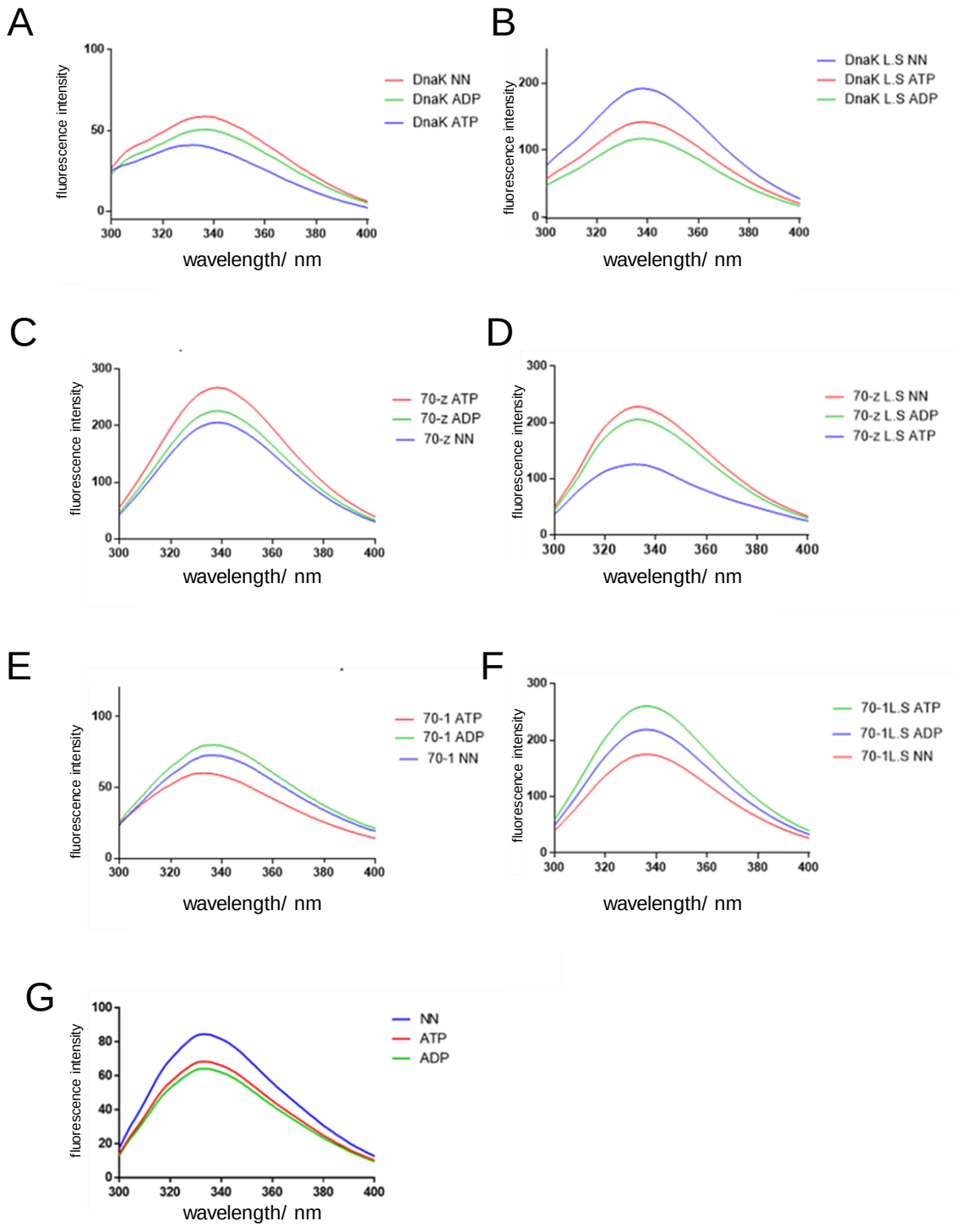

Figure B22 Effect of nucleotides on tertiary structure conformations of recombinant Hsp70s

Tertiary structure conformations of recombinant Hsp70s was investigated using tryptophan fluorescence in the absence of nucleotides (blue) and in the presence of ATP (red) or ADP (green). Tertiary structure conformations for the following proteins are represented in the curves (A) DnaK and (B) $DnaK_{LS}$; (C) PfHsp70-z and (D) $PfHsp70\text{-}z_{LS}$; (E) PfHsp70-1, (F) $PfHsp70\text{-}1_{LS}$ and (G) $PfHsp70\text{-}1_{NBD}$.

B23. Guanidine HCl Denaturation

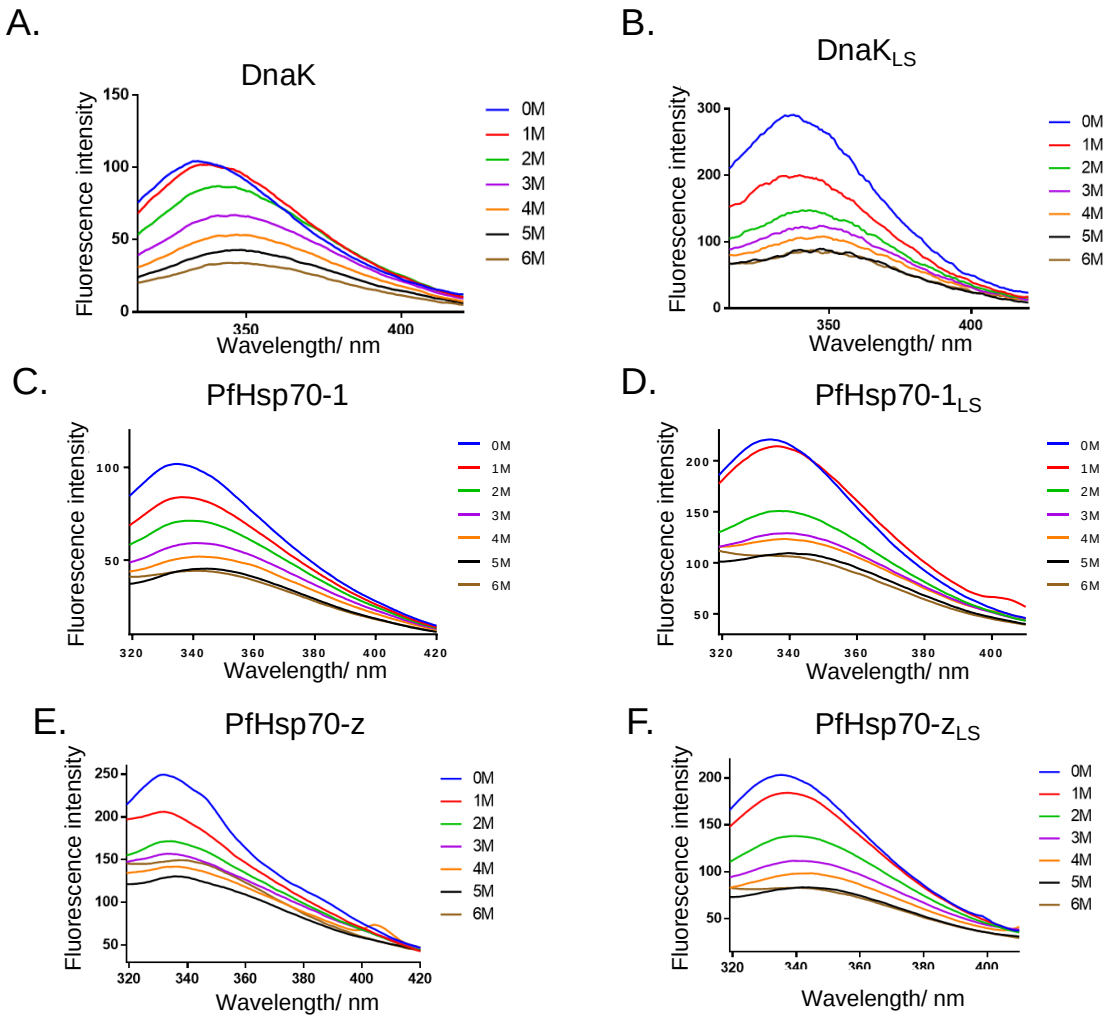

Figure B23 Guanidine HCl denaturation of recombinant Hsp70s

The recombinant Hsp70s were incubated in guanidine HCl concentrations ranging from 0-6 M and tryptophan fluorescence readings were taken at each concentration. Fluorescence spectra for (A) DnaK (B) DnaK$_{LS}$, (C) PfHsp70-1, (D) PfHsp70-1$_{LS}$, (E) PfHsp70-z and (F) PfHsp70-z$_{LS}$ are represented.

B.24 Urea denaturation

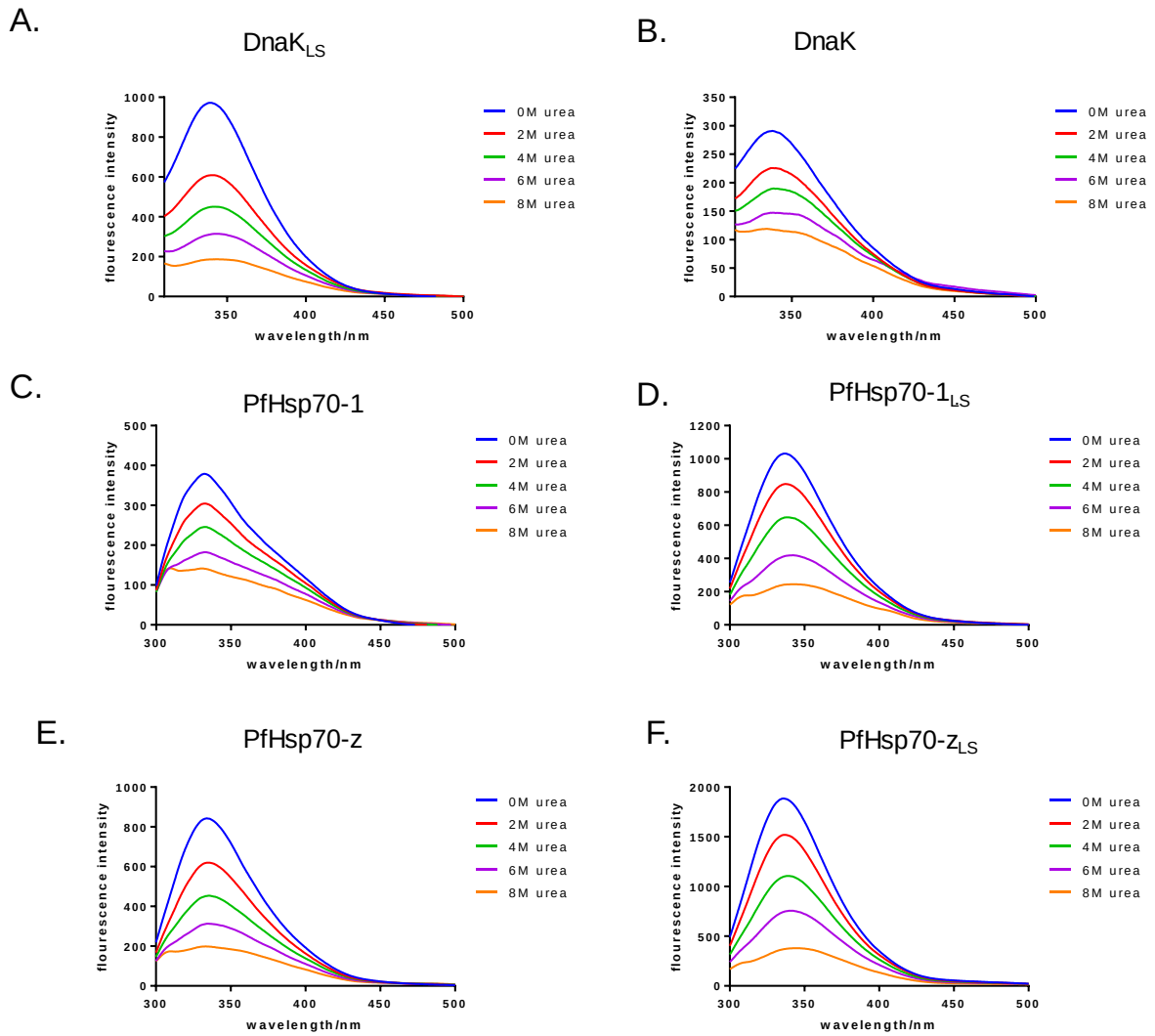

Figure B24 Urea denaturation of recombinant Hsp70s tertiary structure

The recombinant Hsp70s were incubated in urea concentrations ranging from 0-8 M and tryptophan fluorescence readings were taken at each concentration. Fluorescence spectra for (A) DnaK$_{LS}$ (B) DnaK, (C) PfHsp70-1, (D) PfHsp70-1$_{LS}$, (E) PfHsp70-z and (F) PfHsp70-z$_{LS}$ are represented.

B24. Effect of peptide binding on tertiary structure

A

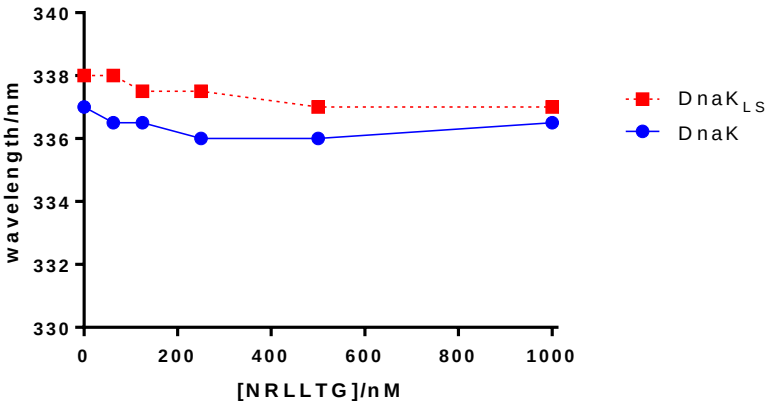

B

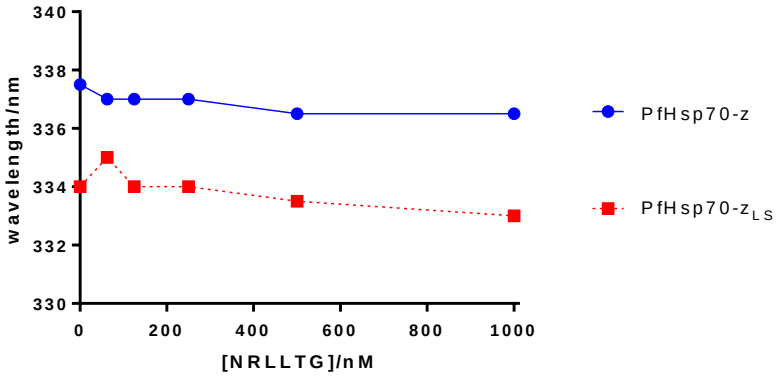

C

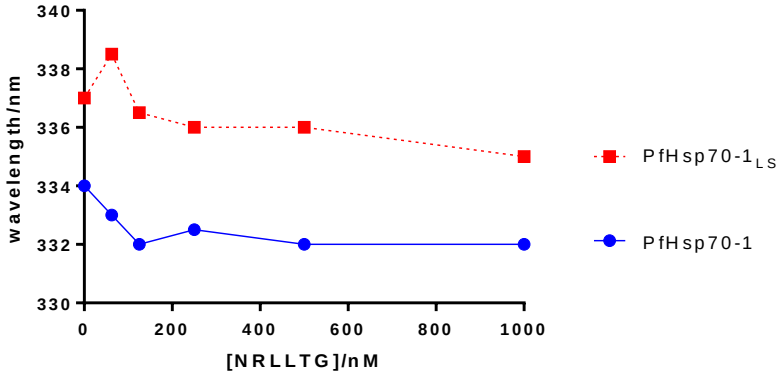

B27. Michaelis-Menten Curves

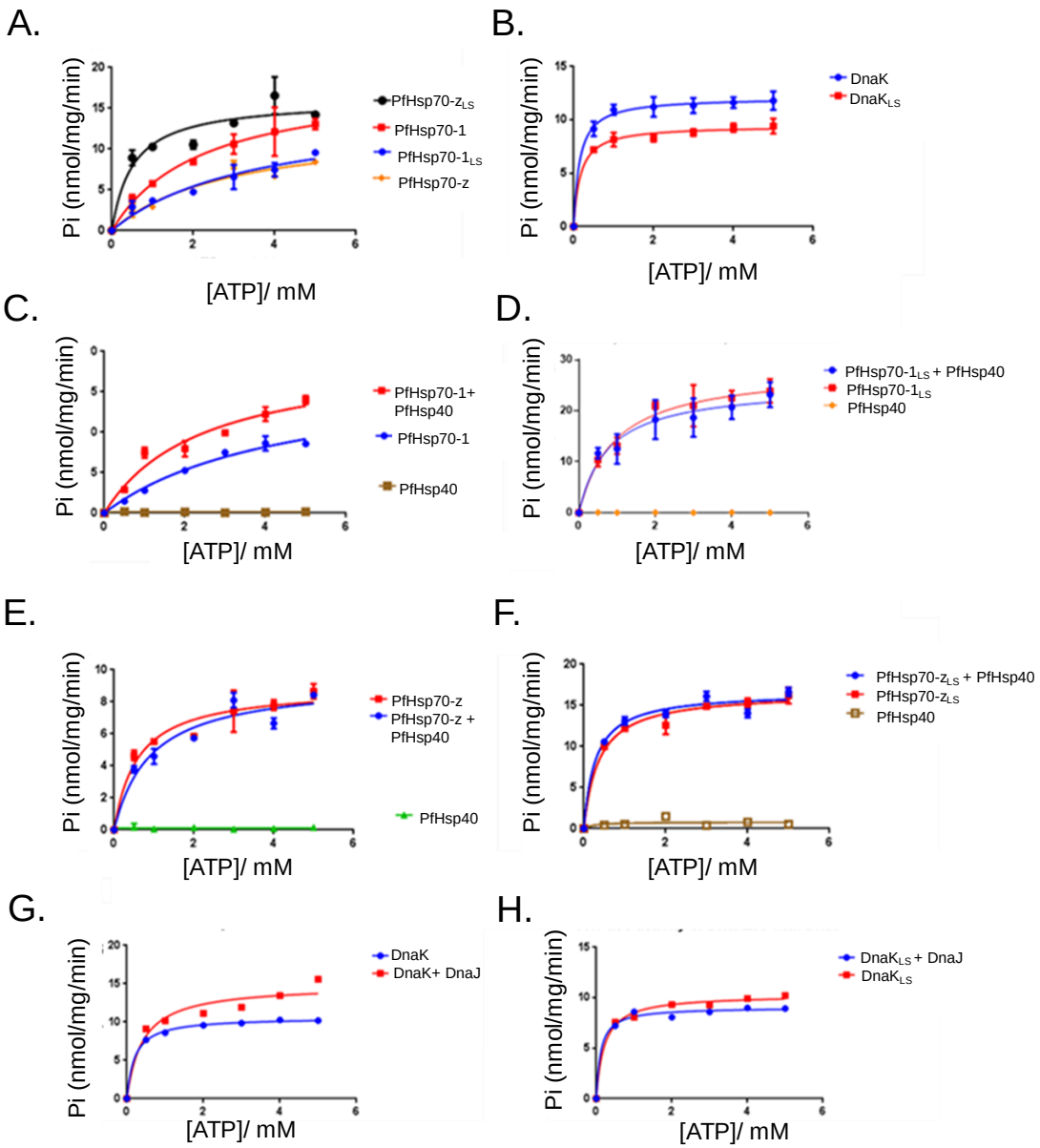

Figure B27 Comparative ATPase activity of wild type and LS Hsp70s

Michaelis-Menten plots of the ATPase activity were plotted based on the amount of P*i* released using a direct colorimetric assay. (A) Evaluation of the basal ATPase activities of PfHsp70-1$_{LS}$, PfHsp70-z$_{LS}$, and their wild type forms. (B) Basal ATPase activity of DnaK/K$_{LS}$. (C) ATPase activity of PfHsp70-1 in the presence of PfHsp40 and (D) represents the ATPase activity of PfHsp70-1$_{LS}$ in the presence of PfHsp40. (E) ATPase activity of PfHsp70-z in the presence of PfHsp40 and (F) represents the ATPase activity of PfHsp70-z$_{LS}$ in the presence of PfHsp40. (G) The Michaelis-Menten curve for the ATPase activity of DnaK in the presence of DnaJ and (H) is the curve for the ATPase activity of DnaK$_{LS}$ in the presence of DnaJ.

B28. Luciferase aggregation suppression assay data

A.

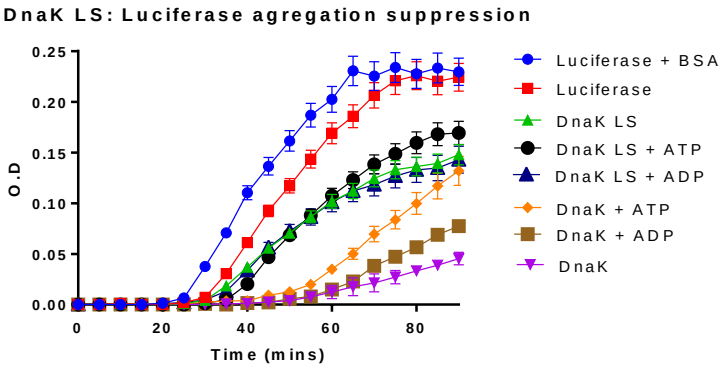

B.

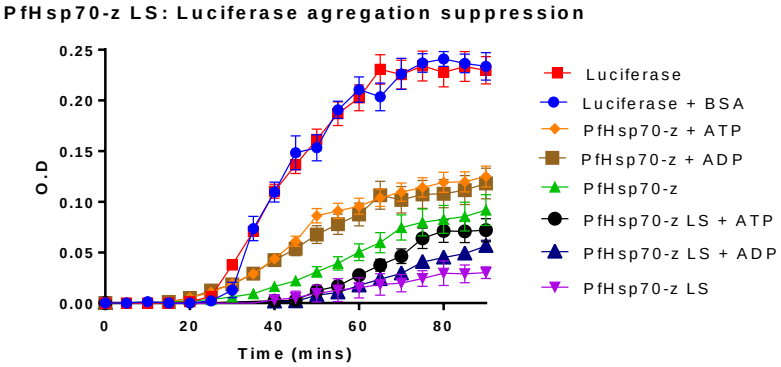

C.

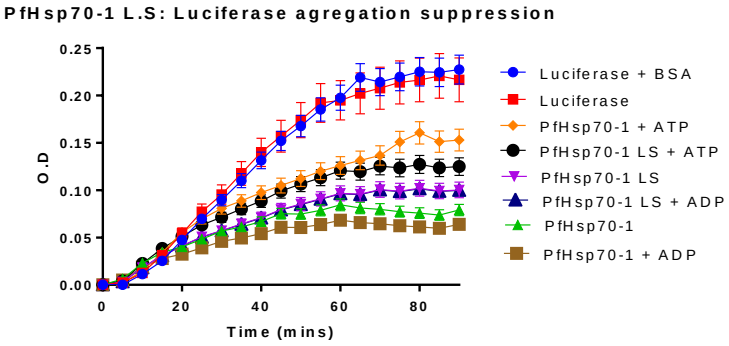

Figure B28 Aggregation suppression activity of wild Hsp70s and $_{LS}$ variants.

(A) represents aggregation suppression activity of DnaK and DnaK$_{LS}$ using the model protein substrate luciferase. (B) PfHsp70-z and PfHsp70-z$_{LS}$ aggregation suppression in the presence and absence of nucleotides. (C) PfHsp70-1 and PfHsp70-1$_{LS}$ aggregation suppression activity. The data represents results from three independent repeats of the assays.

B29 Thermal stability of proteins

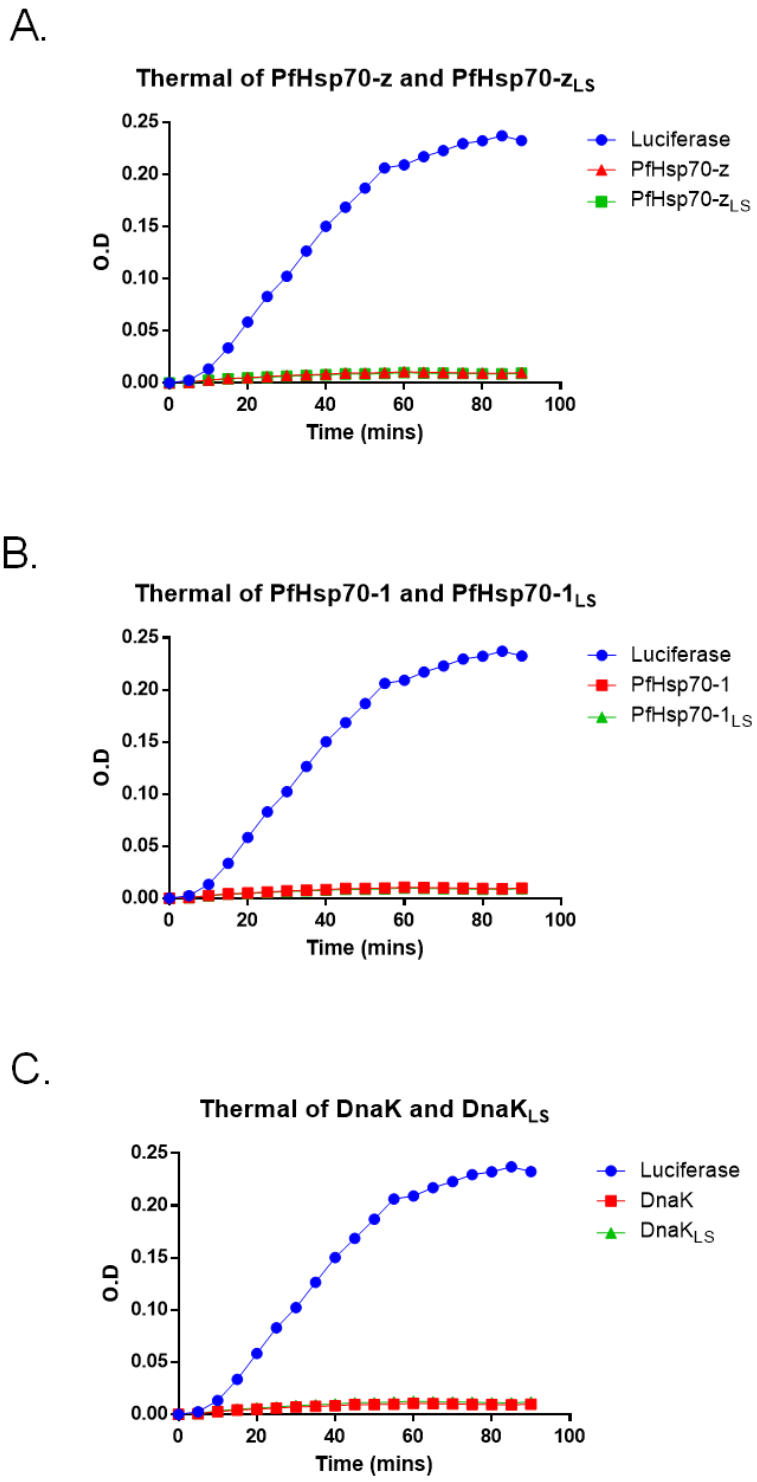

Figure B29 Thermal stability of wild Hsp70s and LS variants.

(A) represents the thermal stability of PfHsp70-1 and PfHsp70-1_{LS} which was demonstrated by the absence of aggregation over a 90 min period. (B) PfHsp70-z and PfHsp70-z_{LS} were also shown to be thermally stable at 51 °C over a 90min period. (C) DnaK and $DnaK_{LS}$ exhibited thermal stability.

Table B4. Peptide binding affinity of Hsp70s (ATP state)

Ligand	Peptides	Ka (1/Ms)	Kd (1/s)	KD (M)	χ^2
PfHsp70-1	1. ALLMYRR	4.21 (±0.01)e^{4}	5.90 (±0.90)e^{-2}	1.40 (±0.40)e^{-6}	0.08
	2. ANNMYRR	7.24 (±0.04)e^{4}	3.29 (±0.09)e^{-2}	4.57 (±0.07)e^{-7}	3.98
	3. NRLLTG	3.47 (±0.07)e^{4}	6.29 (±0.09)e^{-2}	1.81 (±0.01)e^{-6}	1.67
	4. NRNNTG	2.73 (±0.03)e^{4}	8.09 (±0.09)e^{-2}	2.96 (±0.06)e-^{6}	2.71
	5. GFRVLLMYRF	6.32 (±0.02)e^{4}	9.25 (±0.05)e^{-3}	1.46 (±0.06)e^{-7}	1.73
	6. GFRNNNMYRF	5.19 (±0.09)e^{4}	7.22 (±0.02)e^{-3}	1.39 (±0.09)e^{-7}	3.91
PfHsp70-1$_{LS}$	1. ALLMYRR	5.02 (±0.05)e^{5}	4.49 (±0.09)e^{-2}	8.94 (±0.04)e^{-8}	0.76
	2. ANNMYRR	5.28 (±0.08)e^{4}	4.11 (±0.01)e^{-2}	7.78 (±0.08)e^{-7}	3.29
	3. NRLLTG	4.76 (±0.06)e^{4}	3.25 (±0.05)e^{-2}	6.82 (±0.02)e^{-7}	1.82
	4. NRNNTG	5.11 (±0.01)e^{5}	6.76 (±0.06)e^{-2}	1.32 (±0.02)e^{-7}	3.91
	5. GFRVLLMYRF	3.25 (±0.05)e^{5}	5.27 (±0.07)e^{-2}	1.63 (±0.03)e^{-7}	1.69
	6. GFRNNNMYRF	1.62 (±0.02)e^{5}	4.89 (±0.09)e^{-2}	3.02 (±0.02)e^{-7}	1.96
PfHsp70-z	1. ALLMYRR	2.92 (±0.02)e^{5}	6.03 (±0.03)e^{-2}	2.07 (±0.07)e^{-7}	0.64
	2. ANNMYRR	6.70 (±0.70)e^{5}	3.99 (±0.09)e^{-2}	5.95 (±0.05)e^{-8}	4.94
	3. NRLLTG	1.13 (±0.03)e^{6}	4.12 (±0.02)e^{-2}	3.65 (±0.01)e^{-8}	4.41
	4. NRNNTG	2.87 (±0.07)e^{7}	5.79 (±0.09)e^{-2}	2.00 (±0.01)e^{-9}	1.31
	5. GFRVLLMYRF	5.20 (±0.20)e^{4}	6.27 (±0.07)e^{-3}	1.20 (±0.20)e^{-7}	0.21
	6. GFRNNNMYRF	4.83 (±0.03)e^{6}	5.40 (±0.40)e^{-2}	1.12 (±0.02)e^{-8}	0.34
PfHsp70-z$_{LS}$	1. ALLMYRR	6.72 (±0.02)e^{4}	3.53 (±0.03)e^{-2}	5.25 (±0.05)e^{-7}	0.07
	2. ANNMYRR	4.17 (±0.07)e^{5}	5.33 (±0.03)e^{-2}	1.28 (±0.08)e^{-7}	0.01
	3. NRLLTG	3.34 (±0.04)e^{5}	4.31 (±0.01)e^{-3}	1.29 (±0.09)e^{-8}	2.19
	4. NRNNTG	2.21 (±0.01)e^{5}	5.10 (±0.01)e^{-2}	2.31 (±0.01)e^{-7}	2.07
	5. GFRVLLMYRF	1.09 (±0.09)e^{5}	9.27 (±0.07)e^{-2}	8.50 (±0.50)e^{-7}	1.43
	6. GFRNNNMYRF	1.04 (±0.04)e^{5}	8.33 (±0.03)e^{-3}	8.01 (±0.01)e^{-8}	0.78
DnaK	1. ALLMYRR	9.25 (±0.05)e^{3}	4.12 (±0.02)e^{-2}	4.45 (±0.05)e^{-6}	5.76
	2. ANNMYRR	4.12 (±0.02)e^{3}	3.70 (±0.70)e^{-2}	8.96 (±0.06)e^{-6}	1.98
	3. NRLLTG	2.00 (±0.01)e^{4}	5.06 (±0.06)e^{-2}	2.53 (±0.03)e^{-6}	0.09
	4. NRNNTG	5.97 (±0.07)e^{3}	4.36 (±0.06)e^{-3}	7.31 (±0.01)e^{-6}	1.06
	5. GFRVLLMYRF	1.13 (±0.03)e^{4}	8.95 (±0.05)e^{-3}	7.92 (±0.02)e^{-7}	0.76
	6. GFRNNNMYRF	2.81 (±0.01)e^{3}	3.97 (±0.07)e^{-2}	1.41 (±0.01)e^{-5}	4.72
DnaK$_{LS}$	1. ALLMYRR	1.90 (±0.90)e^{4}	3.71 (±0.01)e^{-2}	1.95 (±0.05)e^{-6}	8.47
	2. ANNMYRR	2.81 (±0.01)e^{4}	4.97 (±0.07)e^{-2}	1.77 (±0.07)e^{-6}	6.74
	3. NRLLTG	4.21 (±0.01)e^{4}	3.75 (±0.02)e^{-2}	8.91 (±0.01)e^{-7}	5.42
	4. NRNNTG	4.08 (±0.08)e^{4}	2.92 (±0.02)e^{-2}	7.16 (±0.06)e^{-7}	4.72
	5. GFRVLLMYRF	2.19 (±0.09)e^{4}	4.21 (±0.01)e^{-2}	1.92 (±0.02)e^{-6}	2.74
	6. GFRNNNMYRF	4.97 (±0.07)e^{4}	5.07 (±0.07)e^{-2}	1.02 (±0.02)e^{-6}	1.59

Table B5. Peptide binding affinity of Hsp70s (NN state)

Ligand	Peptides	Ka (1/Ms)	Kd (1/s)	KD (M)	χ^2
PfHsp70-1	1. ALLMYRR	1.73 (±0.03)e^{4}	1.26 (±0.06)e^{-2}	7.31 (±0.01)e^{-7}	0.08
	2. ANNMYRR	3.02 (±0.02)e^{5}	1.20 (±0.20)e^{-2}	3.96 (±0.06)e^{-8}	3.98
	3. NRLLTG	1.68 (±0.08)e^{5}	2.23 (±0.03)e^{-2}	1.40 (±0.40)e^{-7}	1.67
	4. NRNNTG	3.92 (±0.02)e^{5}	3.34 (±0.04)e^{-2}	8.54 (±0.04)e^{-8}	2.71
	5. GFRVLLMYRF	3.89 (±0.09)e^{5}	9.78 (±0.08)e^{-2}	2.51 (±0.01)e^{-7}	1.73
	6. GFRNNNMYRF	1.41 (±0.01)e^{6}	4.98 (±0.08)e^{-2}	2.67 (±0.07)e^{-8}	3.91
PfHsp70-1_{LS}	1. ALLMYRR	7.93 (±0.03)e^{5}	8.33 (±0.03)e^{-2}	1.05 (±0.05)e^{-7}	0.76
	2. ANNMYRR	2.99 (±0.09)e^{6}	6.57 (±0.07)e^{-2}	2.98 (±0.08)e^{-8}	3.29
	3. NRLLTG	2.62 (±0.02)e^{5}	8.81 (±0.01)e^{-2}	3.37 (±0.07)e^{-7}	1.82
	4. NRNNTG	6.18 (±0.08)e^{5}	9.96 (±0.06)e^{-2}	1.61 (±0.01)e^{-7}	3.91
	5. GFRVLLMYRF	4.21 (±0.01)e^{5}	8.22 (±0.02)e^{-2}	1.95 (±0.05)e^{-7}	1.69
	6. GFRNNNMYRF	1.05 (±0.05)e^{5}	5.45 (±0.05)e^{-2}	5.20 (±0.20)e^{-7}	1.96
PfHsp70-z	1. ALLMYRR	6.57 (±0.07)e^{4}	2.83 (±0.03)e^{-2}	4.32 (±0.02)e^{-7}	0.64
	2. ANNMYRR	2.61 (±0.01)e^{6}	1.02 (±0.02)e^{-1}	3.89 (±0.09)e^{-8}	4.94
	3. NRLLTG	4.10 (±0.10)e^{6}	1.05 (±0.05)e^{-1}	2.56 (±0.06)e^{-8}	4.41
	4. NRNNTG	4.29 (±0.09)e^{6}	3.65 (±0.05)e^{-2}	8.50 (±0.50)e^{-9}	1.31
	5. GFRVLLMYRF	2.01 (±0.01)e^{6}	7.04 (±0.04)e^{-2}	3.49 (±0.09)e^{-8}	0.21
	6. GFRNNNMYRF	5.00 (±0.01)e^{6}	5.45 (±0.05)e^{-2}	1.09 (±0.09)e^{-8}	0.34
PfHsp70-z_{LS}	1. ALLMYRR	3.25 (±0.05)e^{4}	3.79 (±0.09)e^{-4}	1.16 (±0.06)e^{-8}	0.07
	2. ANNMYRR	1.35 (±0.05)e^{5}	4.19 (±0.09)e^{-2}	3.10 (±0.10)e^{-7}	0.01
	3. NRLLTG	7.27 (±0.07)e^{4}	2.13 (±0.03)e^{-4}	2.93 (±0.03)e^{-9}	2.19
	4. NRNNTG	5.53 (±0.03)e^{4}	4.47 (±0.07)e^{-2}	8.08 (±0.08)e^{-7}	2.07
	5. GFRVLLMYRF	1.98 (±0.08)e^{5}	7.34 (±0.04)e^{-2}	3.70 (±0.70)e^{-7}	1.43
	6. GFRNNNMYRF	1.05 (±0.05)e^{6}	8.96 (±0.06)e^{-2}	8.49 (±0.09)e^{-8}	0.78
DnaK	1. ALLMYRR	2.77 (±0.07)e^{5}	2.79 (±0.09)e^{-2}	1.01 (±0.01)e^{-7}	5.76
	2. ANNMYRR	1.05 (±0.05)e^{5}	8.68 (±0.08)e^{-2}	8.30 (±0.30)e^{-7}	1.98
	3. NRLLTG	6.62 (±0.02)e^{5}	5.67 (±0.07)e^{-3}	8.56 (±0.07)e^{-8}	0.09
	4. NRNNTG	1.00 (±0.01)e^{4}	6.45 (±0.05)e^{-3}	6.44 (±0.04)e^{-7}	1.06
	5. GFRVLLMYRF	5.82 (±0.02)e^{4}	2.48 (±0.08)e^{-4}	4.26 (±0.06)e^{-7}	0.76
	6. GFRNNNMYRF	3.78 (±0.08)e^{3}	3.65 (±0.05)e^{2}	9.65 (±0.05)e^{-6}	4.72
DnaK$_{LS}$	1. ALLMYRR	4.09 (±0.09)e^{4}	9.66 (±0.06)e^{-2}	2.36 (±0.06)e^{-6}	8.47
	2. ANNMYRR	1.65 (±0.05)e^{4}	2.36 (±0.06)e^{-2}	1.42 (±0.02)e^{-6}	6.74
	3. NRLLTG	1.00 (±0.01)e^{4}	1.65 (±0.05)e^{-2}	1.65 (±0.05)e^{-6}	5.42
	4. NRNNTG	1.14 (±0.04)e^{4}	1.31 (±0.01)e^{-2}	1.15 (±0.05)e^{-6}	4.72
	5. GFRVLLMYRF	3.43 (±0.01)e^{5}	7.49 (±0.09)e^{-2}	2.18 (±0.08)e^{-7}	2.74
	6. GFRNNNMYRF	1.34 (±0.04)e^{5}	5.43 (±0.03)e^{-2}	4.05 (±0.05)e^{-7}	1.59

Table B6. Peptide binding affinity of Hsp70s (ADP state)

Ligand	Peptides	Ka (1/Ms)	Kd (1/s)	KD (M)	χ^2
PfHsp70-1	1. ALLMYRR	5.29 (±0.09)e^{5}	3.27 (±0.07)e^{-2}	6.18 (±0.08)e^{-8}	0.08
	2. ANNMYRR	7.29 (±0.09)e^{5}	2.93 (±0.03)e^{-3}	4.02 (±0.02)e^{-9}	3.98
	3. NRLLTG	1.01 (±0.01)e^{5}	9.84 (±0.04)e^{-3}	9.74 (±0.04)e^{-8}	1.67
	4. NRNNTG	7.19 (±0.09)e^{5}	7.32 (±0.02)e^{-2}	1.02 (±0.02)e-^{8}	2.71
	5. GFRVLLMYRF	6.15 (±0.05)e^{4}	4.27 (±0.07)e^{-2}	6.94 (±0.04)e^{-8}	1.73
	6. GFRNNNMYRF	8.26 (±0.06)e^{4}	7.25 (±0.05)e^{-3}	8.77 (±0.07)e^{-8}	3.91
PfHsp70-1$_{LS}$	1. ALLMYRR	2.95 (±0.05)e^{5}	2.19 (±0.01)e^{-2}	9.93 (±0.03)e^{-8}	0.76
	2. ANNMYRR	5.23 (±0.03)e^{4}	5.11 (±0.01)e-^{2}	9.77 (±0.07)e^{-7}	3.29
	3. NRLLTG	4.16 (±0.06)e^{5}	7.25 (±0.05)e^{-2}	1.74 (±0.04)e^{-7}	1.82
	4. NRNNTG	1.13 (±0.03)e^{5}	5.27 (±0.07)e^{-2}	4.66 (±0.06)e^{-7}	3.91
	5. GFRVLLMYRF	1.61 (±0.01)e^{5}	3.29 (±0.09)e^{-2}	2.04 (±0.04)e^{-7}	1.69
	6. GFRNNNMYRF	2.72 (±0.02)e^{5}	4.29 (±0.09)e^{-2}	1.58 (±0.08)e^{-7}	1.96
PfHsp70-z	1. ALLMYRR	2.72 (±0.02)e^{5}	5.73 (±0.03)e^{-2}	2.11 (±0.01)e^{-7}	0.64
	2. ANNMYRR	2.03 (±0.03)e^{5}	5.20 (±0.20)e^{-2}	2.56 (±0.06)e^{-7}	4.94
	3. NRLLTG	9.98 (±0.08)e^{5}	4.15 (±0.05)e^{-2}	4.16 (±0.06)e^{-8}	4.41
	4. NRNNTG	1.45 (±0.05)e^{7}	4.76 (±0.06)e^{-2}	3.30 (±0.30)e^{-9}	1.31
	5. GFRVLLMYRF	5.59 (±0.09)e^{4}	5.62 (±0.02)e^{-3}	1.01 (±0.01)e^{-7}	0.21
	6. GFRNNNMYRF	3.57 (±0.07)e^{6}	5.35 (±0.05)e^{-2}	1.50 (±0.50)e^{-8}	0.34
PfHsp70-z$_{LS}$	1. ALLMYRR	1.06 (±0.06)e^{6}	4.79 (±0.09)e^{-2}	4.53 (±0.03)e^{-8}	0.07
	2. ANNMYRR	1.93 (±0.03)e^{5}	4.65 (±0.05)e^{-2}	2.41 (±0.01)e^{-7}	0.01
	3. NRLLTG	1.16 (±0.06)e^{7}	4.98 (±0.08)e^{-2}	4.31 (±0.01)e^{-9}	2.19
	4. NRNNTG	2.13 (±0.03)e^{5}	5.05 (±0.05)e^{-2}	2.37 (±0.07)e^{-7}	2.07
	5. GFRVLLMYRF	3.11 (±0.01)e^{5}	7.20 (±0.20)e^{-2}	2.32 (±0.02)e^{-7}	1.43
	6. GFRNNNMYRF	4.97 (±0.07)e^{5}	5.27 (±0.07)e^{-3}	1.06 (±0.06)e^{-8}	0.78
DnaK	1. ALLMYRR	2.77 (±0.07)e^{5}	2.79 (±0.09)e^{-2}	1.01 (±0.01)e^{-7}	5.76
	2. ANNMYRR	1.05 (±0.05)e^{5}	8.68 (±0.08)e^{-2}	8.30 (±0.30)e^{-7}	1.98
	3. NRLLTG	6.62 (±0.02)e^{5}	5.67 (±0.07)e^{-3}	8.56 (±0.06)e^{-8}	0.09
	4. NRNNTG	1.00 (±0.01)e^{4}	6.45 (±0.05)e^{-3}	6.44 (±0.04)e^{-7}	1.06
	5. GFRVLLMYRF	6.92 (±0.02)e^{4}	6.25 (±0.05)e^{-3}	9.03 (±0.03)e^{-8}	0.76
	6. GFRNNNMYRF	2.39 (±0.09)e^{3}	6.73 (±0.03)e^{-2}	2.82 (±0.02)e^{-6}	4.72
DnaK$_{LS}$	1. ALLMYRR	2.91 (±0.01)e^{4}	7.11 (±0.01)e^{-2}	2.44 (±0.04)e^{-6}	8.47
	2. ANNMYRR	2.97 (±0.07)e^{4}	5.03 (±0.03)e^{-2}	1.69 (±0.09)e^{-6}	6.74
	3. NRLLTG	3.15 (±0.05)e^{4}	3.03 (±0.03)e^{-2}	9.62 (±0.02)e^{-7}	5.42
	4. NRNNTG	5.02 (±0.02)e^{4}	4.29 (±0.09)e^{-2}	8.55 (±0.05)e^{-7}	4.72
	5. GFRVLLMYRF	1.99 (±0.09)e^{4}	5.11 (±0.01)e^{-2}	2.56 (±0.06)e^{-6}	2.74
	6. GFRNNNMYRF	4.03 (±0.03)e^{4}	2.72 (±0.02)e^{-2}	6.75 (±0.05)e^{-7}	1.59

B30. Peptide binding affinity of Hsp70s

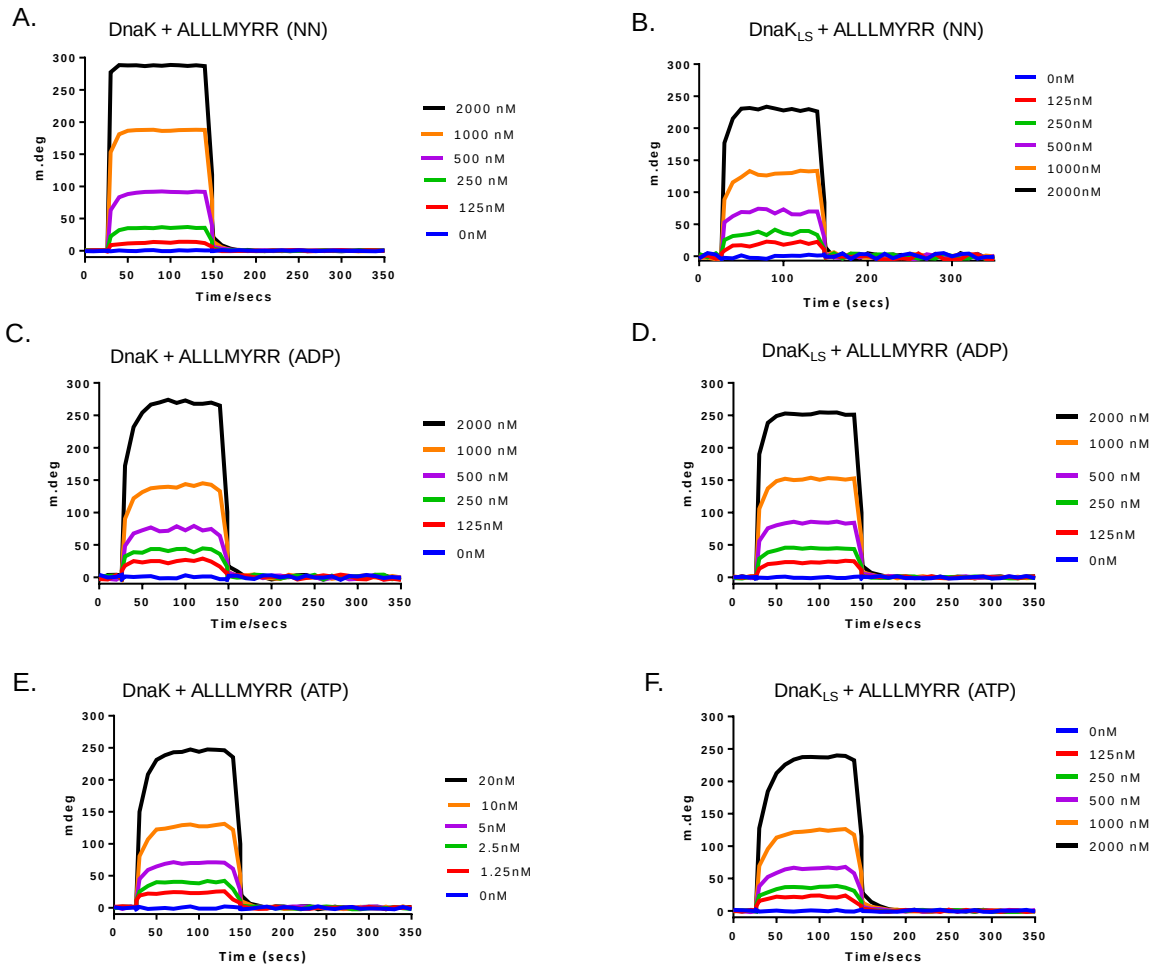

Figure B30 Comparative peptide binding affinity of Hsp70.

(A) Representative sensograms for the binding of DnaK for the peptide substrate ALLLMYRR in the NN state. (B) Sensograms for the binding affinity of DnaK$_{LS}$ to the peptide substrate ALLLMYRR (C) Sensogram for DnaK binding affinity for peptide substrate ALLLMYRR in the ADP state. (D) Sensogram for DnaK$_{LS}$ affinity for the peptide substrate ALLLMYRR in the ADP state. (E) Sensogram for DnaK affinity for the peptide substrate ALLLMYRR in the ATP state. (F) Sensogram for DnaK$_{LS}$ affinity for the peptide substrate ALLLMYRR in the ATP state.

Table B7. Luciferase refolding assay statistical analysis

Datasets	Significant (Y/N?)	Summary	p value
B vs. C	Yes	*	0.009
B vs. D	Yes	***	0.004
B vs. E	Yes	***	0.004
B vs. F	Yes	****	<0.001
B vs. G	Yes	****	<0.001
B vs. H	Yes	****	<0.001
B vs. I	Yes	****	<0.001
B vs. J	Yes	****	<0.001
C vs. D	No	ns	0.0822
C vs. E	No	ns	0.0801
C vs. F	Yes	***	0.004
C vs. G	Yes	**	0.006
C vs. H	Yes	***	0.005
C vs. I	Yes	***	0.002
C vs. J	Yes	***	0.002
D vs. E	No	ns	>0.999

*The following chaperone sets were used in the refolding assay

B- PfHsp70-1 + PfHsp40 + PfHsp70-z

C- PfHsp70-1_{LS} + PfHsp40 + PfHsp70-z

D- PfHsp70-1 + PfHsp40 + PfHsp70-z_{LS}

E- PfHsp70-1_{LS} + PfHsp40 + PfHsp70-z_{LS}

F- PfHsp40; G- PfHsp70-1; H- PfHsp70-1_{LS}

I- PfHsp70-z J- PfHsp70-z_{LS}

Table B8. Statistical analyses for Luciferase aggregation suppression assay (DnaK vs $DnaK_{LS}$)

Datasets	Significance	Summary	p value
DnaK NN vs. DnaK ATP	Yes	**	0.008
DnaK NN vs. DnaK ADP	No	ns	0.8938
DnaK NN vs. $DnaK_{LS}$ NN	Yes	*	0.009
DnaK NN vs. $DnaK_{LS}$ ATP	Yes	*	0.009
DnaK NN vs. $DnaK_{LS}$ ADP	No	ns	0.5531

Table B9. Statistical analyses for Luciferase aggregation suppression assay (PfHsp70-z vs PfHsp70-z_{LS})

Datasets	Significance (Y/N?)	Summary	p value
PfHsp70-z NN vs. PfHsp70-z ATP	No	Ns	0.987
PfHsp70-z NN vs. PfHsp70-z ADP	No	Ns	0.928
PfHsp70-z NN vs. PfHsp70-z_{LS} NN	Yes	**	0.004
PfHsp70-z NN vs. PfHsp70-z_{LS} ATP	No	Ns	0.105
PfHsp70-z NN vs. PfHsp70-z_{LS} ADP	Yes	**	0.003
PfHsp70-z ATP vs. PfHsp70-z ADP	No	Ns	0.672
PfHsp70-z ATP vs. PfHsp70-z_{LS} NN	Yes	**	0.003
PfHsp70-z ATP vs. PfHsp70-z_{LS} ATP	No	Ns	0.052
PfHsp70-z ATP vs. PfHsp70-z ADP	Yes	**	0.003
PfHsp70-z ADP vs. PfHsp70-z_{LS} NN	Yes	**	0.007
PfHsp70-z ADP vs. PfHsp70-z_{LS} ATP	No	Ns	0.290
PfHsp70-z ADP vs. PfHsp70-z_{LS} ADP	Yes	**	0.008
PfHsp70-z_{LS} NN vs. PfHsp70-z_{LS} ATP	No	Ns	0.088
PfHsp70-z_{LS} NN vs. PfHsp70-z_{LS} ADP	No	Ns	>0.99
PfHsp70-z_{LS} ATP vs. PfHsp70-z_{LS} ADP	No	Ns	0.097

Table B10. Statistical analyses for Luciferase aggregation suppression assay (PfHsp70-1 vs PfHsp70-1_{LS})

Datasets	Significance (Y/N?)	Summary	p value
PfHsp70-1 NN vs. PfHsp70-1 ATP	Yes	**	0.003
PfHsp70-1 NN vs. PfHsp70-1 ADP	No	Ns	0.928
PfHsp70-1 NN vs. PfHsp70-1_{LS} NN	No	Ns	0.004
PfHsp70-1 NN vs. PfHsp70-1_{LS} ATP	No	Ns	0.105
PfHsp70-1 NN vs. PfHsp70-1_{LS} ADP	No	Ns	0.030
PfHsp70-1 ATP vs. PfHsp70-1 ADP	Yes	***	0.004
PfHsp70-1 ATP vs. PfHsp70-1_{LS} NN	Yes	*	0.003
PfHsp70-1 ATP vs. PfHsp70-1_{LS} ATP	No	Ns	0.055
PfHsp70-1 ATP vs. PfHsp70-1 ADP	Yes	*	0.008
PfHsp70-1 ADP vs. PfHsp70-1_{LS} NN	Yes	*	0.009
PfHsp70-1 ADP vs. PfHsp70-1_{LS} ATP	No	**	0.003
PfHsp70-1 ADP vs. PfHsp70-1_{LS} ADP	Yes	*	0.008
PfHsp70-1_{LS} NN vs. PfHsp70-1_{LS} ATP	No	Ns	0.880
PfHsp70-1_{LS} NN vs. PfHsp70-1_{LS} ADP	No	Ns	>0.99
PfHsp70-1_{LS} ATP vs. PfHsp70-1_{LS} ADP	No	Ns	0.097

B31 PfHsp70-1 and PfHop ELISA curves

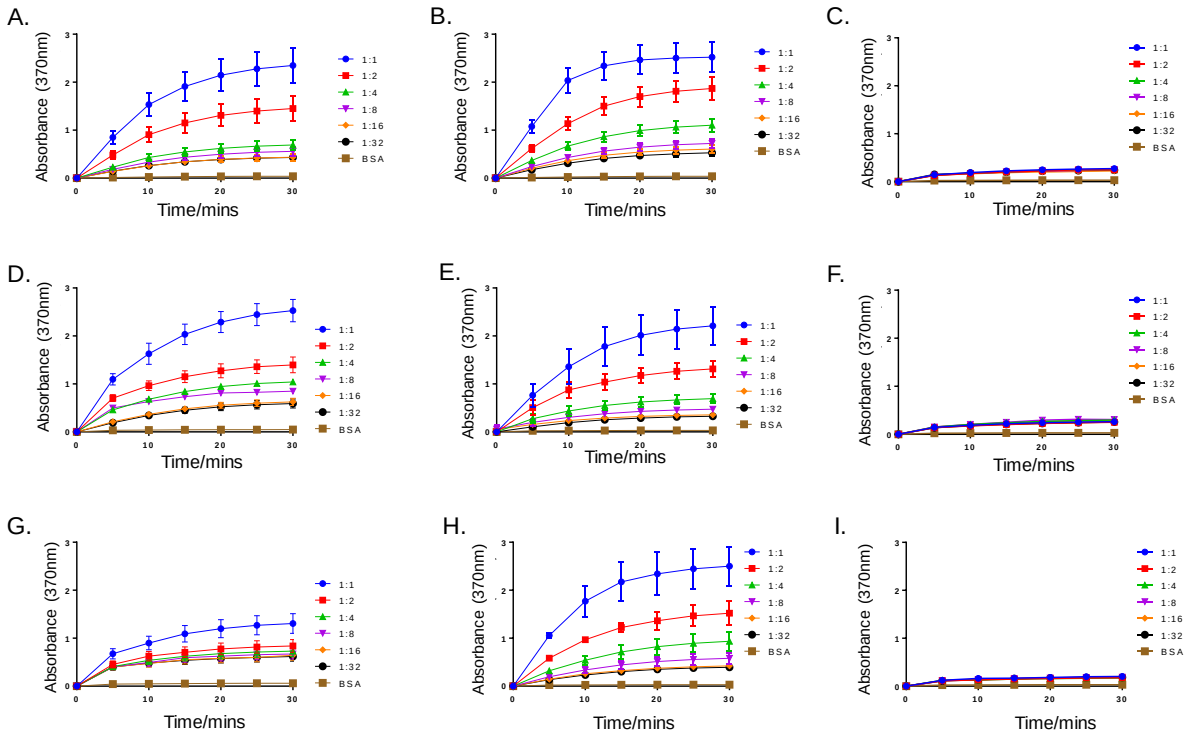

Figure B31. ELISA binding curves for PfHsp70-1/PfHsp70-1 $_{LS}$ and PfHop

(A) ELISA interaction curves for the association between PfHop with PfHsp70-1, (B) PfHsp70-1$_{LS}$ and (C) PfHsp70-1$_{NBD}$ in the absence of nucleotides. The assay was repeated in the presence of 5 mM ADP (D-F) and 5 mM ATP. The assays were observed to be dose dependent. The standard deviations obtained for at least 3 assays conducted independently are represented as error bars.

B32. PfHsp70-1 and PfHsp70-z ELISA curves

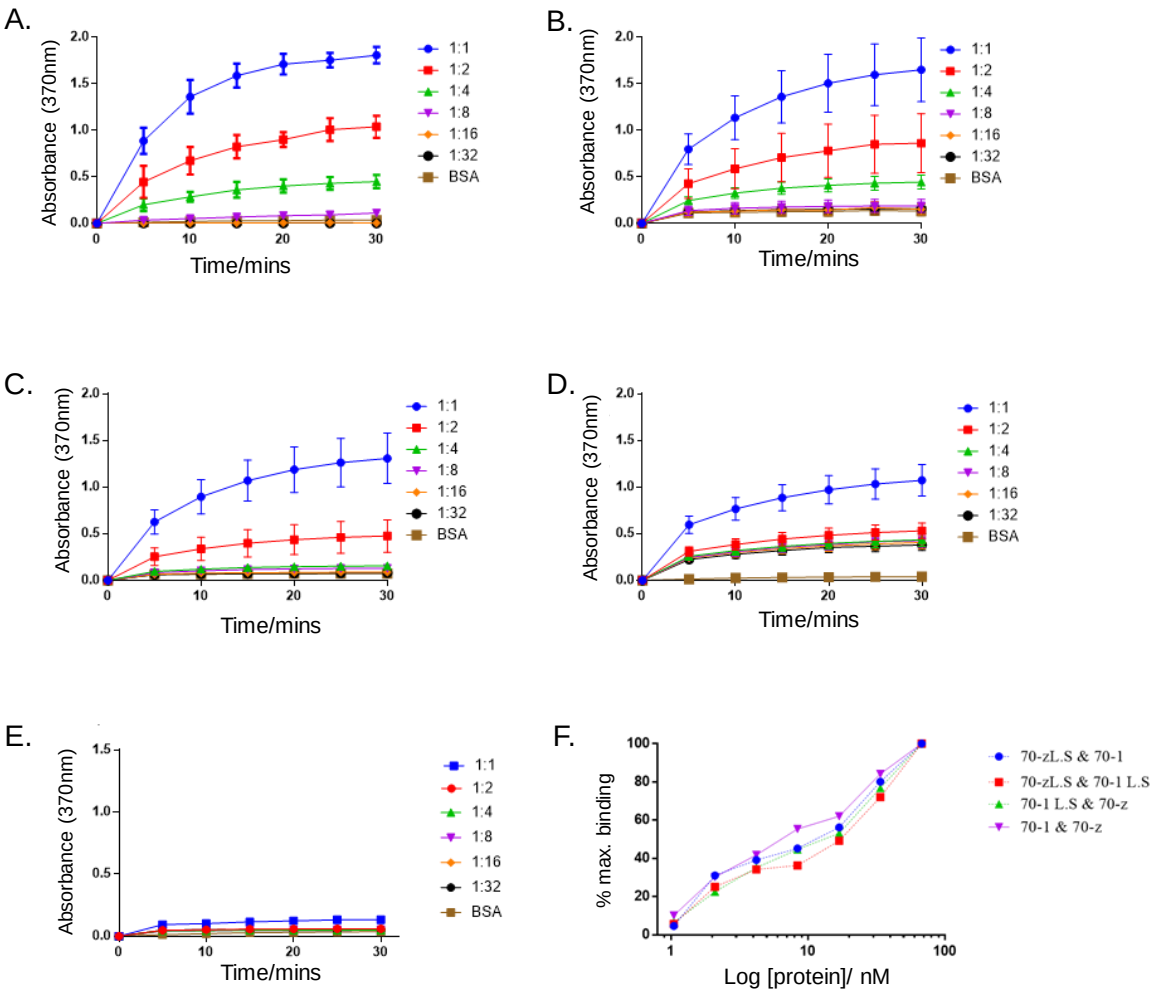

Figure B32. ELISA binding curves for PfHsp70-1/PfHsp70-1 $_{LS}$ and PfHsp70-z/PfHsp70-z $_{LS}$

(A) ELISA interaction curves for the association between PfHsp70-z with PfHsp70-1, (B) PfHsp70-1 $_{LS}$ and (C) PfHsp70-z$_{NBD}$ in the absence of nucleotides. The interaction of PfHsp70-z$_{NBD}$ with PfHsp70-1$_{LS}$ (D), PfHsp70-1$_{NBD}$ (E) was also investigated in the absence of nucleotides. (F) Protein binding curves to summarize PfHsp70-1/1$_{LS}$ and PfHsp70-z/z$_{LS}$ interaction.

Table B11. Self-association of Hsp70s

Ligand	Analyte	Ka (1/Ms)	Kd (1/s)	K_D (M)	χ^2
PfHsp70-1	PfHsp70-1 (NN)	2.36 (±0.06)e^{4}	8.83 (±0.03)e^{-2}	3.75 (±0.05)e^{-6}***	0.08
	PfHsp70-1 (ADP)	8.47 (±0.07)e^{3}	1.09 (±0.09)e^{-2}	1.29 (±0.09)e^{-6}	8.98
	PfHsp70-1 (ATP)	7.14 (±0.04)e^{4}	1.91 (±0.01)e^{-2}	2.68 (±0.08)e^{-7}	7.67
PfHsp70-1_{LS}	PfHsp70-1 (NN)	1.99 (±0.09)e^{4}	9.35 (±0.05)e^{-2}	4.70 (±0.70)e^{-6}	0.76
	PfHsp70-1 (ADP)	1.60 (±0.60)e^{4}	5.39 (±0.09)e^{-2}	3.37 (±0.07)e^{-6}	7.29
	PfHsp70-1 (ATP)	3.95 (±0.05)e^{4}	3.92 (±0.02)e^{-2}	9.98 (±0.08)e^{-7}	3.82
PfHsp70-1_{LS}	PfHsp70-1_{LS} (NN)	1.78 (±0.08)e^{3}	4.47 (±0.07)e^{-2}	4.24 (±0.04)e^{-5}***	0.64
	PfHsp70-1_{LS} (ADP)	3.67 (±0.07)e^{3}	6.33 (±0.03)e^{-2}	1.72 (±0.02)e^{-5}	4.94
	PfHsp70-1_{LS} (ATP)	1.13 (±0.03)e^{3}	6.66 (±0.06)e^{-2}	5.90 (±0.90)e^{-5}	3.93
DnaK	DnaK (NN)	2.72 (±0.02)e^{4}	6.21 (±0.01)e^{-2}	2.28 (±0.08)e^{-6}***	0.07
	DnaK (ADP)	4.38 (±0.08)e^{4}	8.19 (±0.09)e^{-2}	1.89 (±0.09)e^{-6}	0.01
	DnaK (ATP)	6.33 (±0.03)e^{4}	3.19 (±0.09)e^{-2}	5.04 (±0.04)e^{-7}	2.19
$DnaK_{LS}$	DnaK (NN)	4.57 (±0.07)e^{4}	9.21 (±0.01)e^{-2}	2.02 (±0.02)e^{-6}	5.76
	DnaK (ADP)	7.32 (±0.02)e^{4}	8.26 (±0.06)e^{-2}	1.13 (±0.03)e^{-6}	1.98
	DnaK (ATP)	6.32 (±0.02)e^{4}	5.71 (±0.01)e^{-3}	9.03 (±0.03)e^{-8}	0.09
$DnaK_{LS}$	$DnaK_{LS}$(NN)	2.39 (±0.09)e^{3}	7.14 (±0.04)e^{-2}	2.97 (±0.07)e^{-5}***	1.78
	$DnaK_{LS}$(ADP)	4.39 (±0.09)e^{3}	9.03 (±0.03)e^{-2}	2.05 (±0.05)e^{-6}	8.98
	$DnaK_{LS}$(ATP)	9.06 (±0.06)e^{3}	4.92 (±0.02)$^{-2}$	5.40 (±0.40)e^{-6}	2.76
PfHsp70-z	PfHsp70-z (NN)	3.79 (±0.09)e^{4}	5.27 (±0.07)e^{-5}	1.39 (±0.09)e^{-9}	8.47
	PfHsp70-z (ATP)	8.93 (±0.03)e^{3}	7.73 (±0.03)e^{-5}	9.08 (±0.08)e^{-9}	6.74
	PfHsp70-z (ADP)	1.15 (±0.05)e^{4}	3.37 (±0.07)e^{-5}	2.93 (±0.03)e^{-9}	5.42
PfHsp70-z_{LS}	PfHsp70-z (NN)	1.31 (±0.01)e^{4}	4.15 (±0.05)e^{-5}	3.17 (±0.07)e^{-9}	2.17
	PfHsp70-z (ATP)	2.37 (±0.07)e^{4}	4.36 (±0.06)e^{-5}	1.84 (±0.04)e^{-9}	0.19
	PfHsp70-z (ADP)	1.91 (±0.01)e^{4}	5.32 (±0.02)e^{-5}	2.79 (±0.09)e^{-9}	0.87
PfHsp70-z_{LS}	PfHsp70-z_{LS} (NN)	1.59 (±0.09)e^{4}	4.37 (±0.07)e^{-5}	2.75 (±0.05)e^{-9}	1.02
	PfHsp70-z_{LS} (ATP)	2.11 (±0.01)e^{4}	3.99 (±0.09)e^{-4}	1.89 (±0.09)e^{-8}	3.45
	PfHsp70-z_{LS} (ADP)	4.11 (±0.01)e^{4}	3.97 (±0.07)e^{-4}	9.66 (±0.06)e^{-9}	2.97

B34. PfHsp70-1 and PfHsp40 ELISA curves

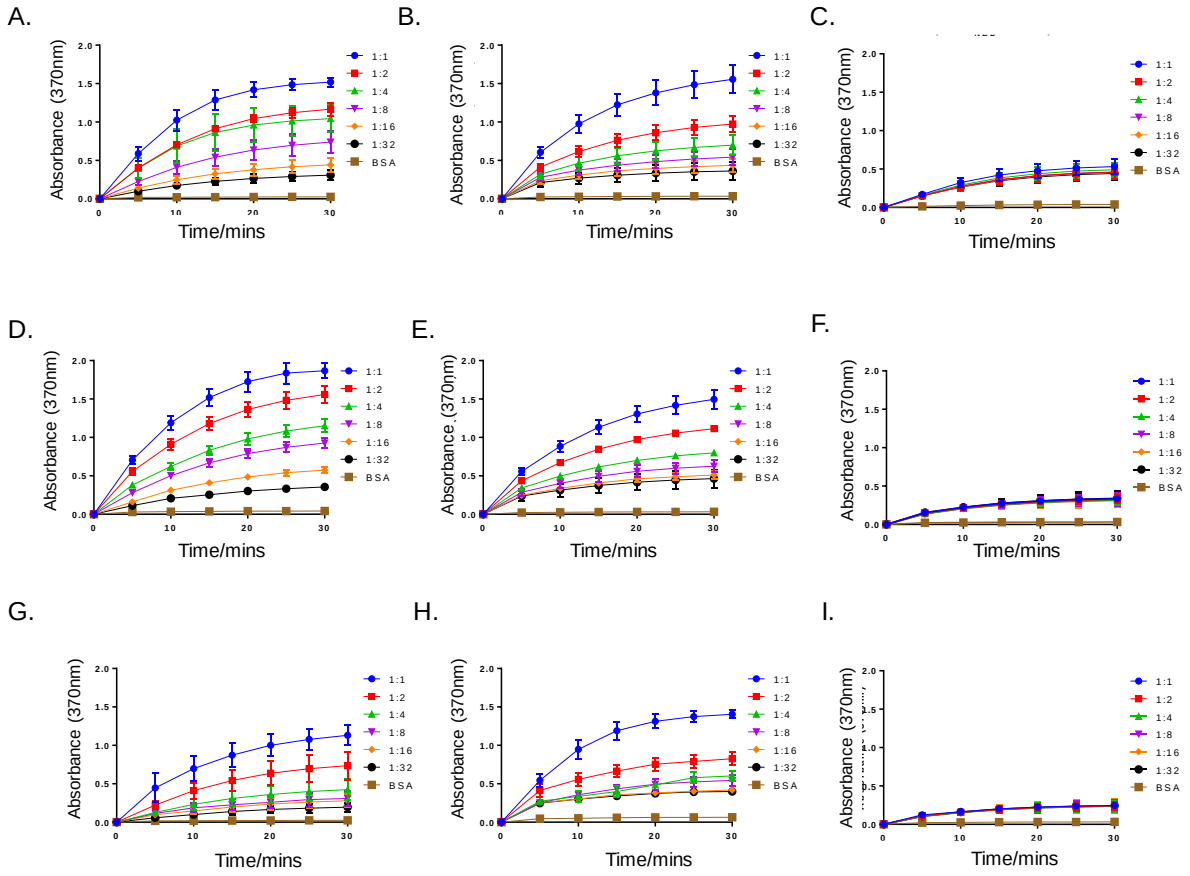

Figure B34 ELISA binding curves for PfHsp70-1 and PfHsp40

(A) ELISA interaction curves for the association between PfHsp40 with PfHsp70-1, (B) PfHsp70-1_{LS} and (C) PfHsp70-1_{NBD} in the absence of nucleotides. The assay was repeated in the presence of 5 mM ADP (D-F) and 5 mM ATP. The assays were observed to be dose dependent. The standard deviations obtained for at least 3 assays conducted independently are represented as error bars.

B36. Sensograms: DnaK and DnaJ interaction

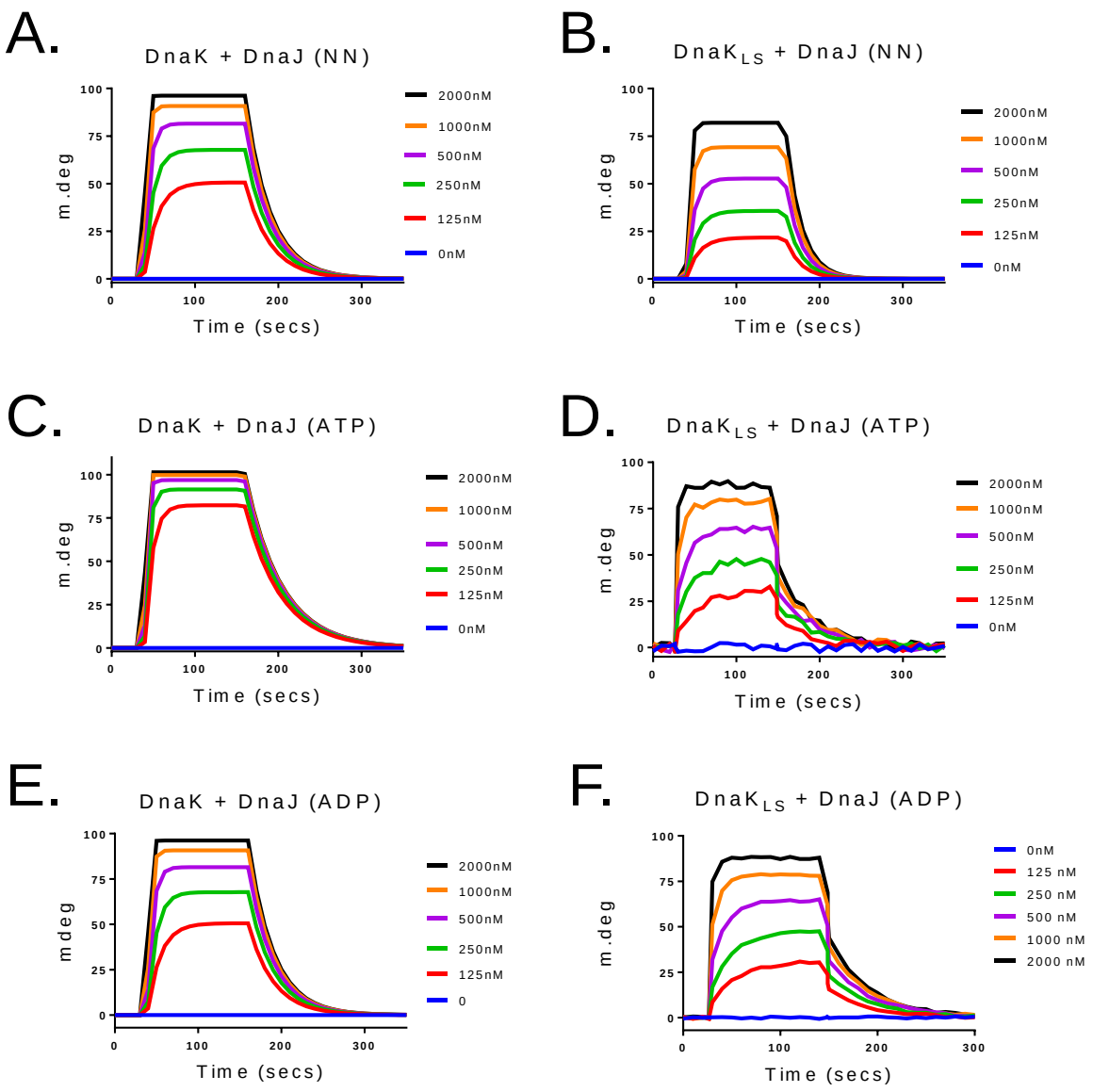

Figure B36 Sensograms for DnaK and DnaK$_{LS}$ association

SPR analyses was used to analyse association of DnaK/DnaK$_{LS}$ and DnaJ. The interaction showed concentration dependence, as response units (mdeg) increased with increasing analyte concentrations. The association was conducted in the absence of nucleotides (A, B) and in the presence of 5 mM ATP (C, D) as well as 5 mM ADP (E, F).

B37. Sensograms: PfHsp70-1 and PfHsp70-z self-interaction

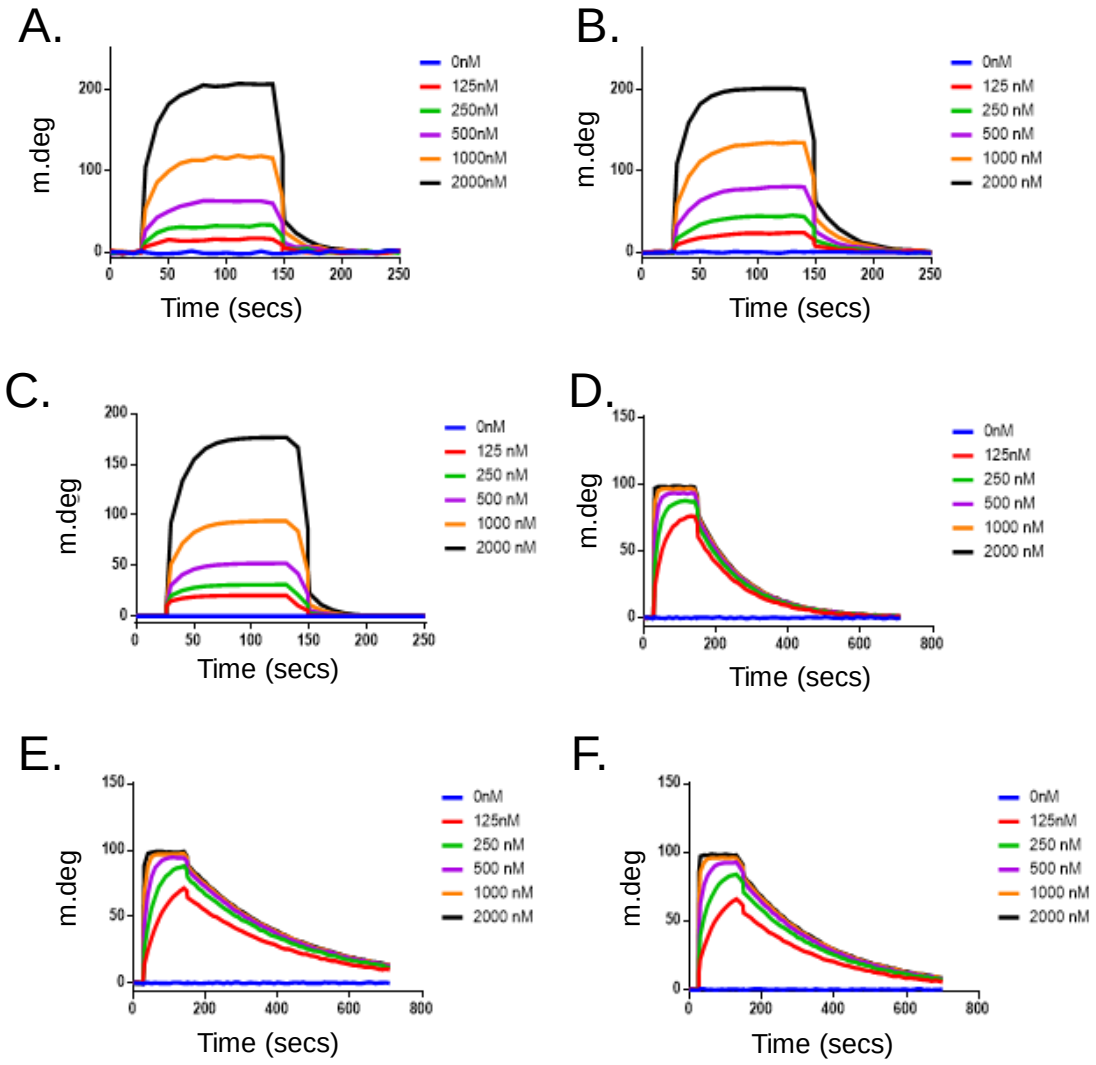

Figure B36 Sensograms for PfHsp70-1 and PfHsp70-z self-association.

(A) Sensograms for the self-association of PfHsp70-1 in the absence of nucleotides, (B) ATP state and (C) ADP state. (D) Sensograms for the self-association of PfHsp70-z in the ADP state, (E) ATP state and (F) absence of nucleotides.

B38. Sensograms: PfHsp70-z and PfHsp70-z $_{LS}$ interaction

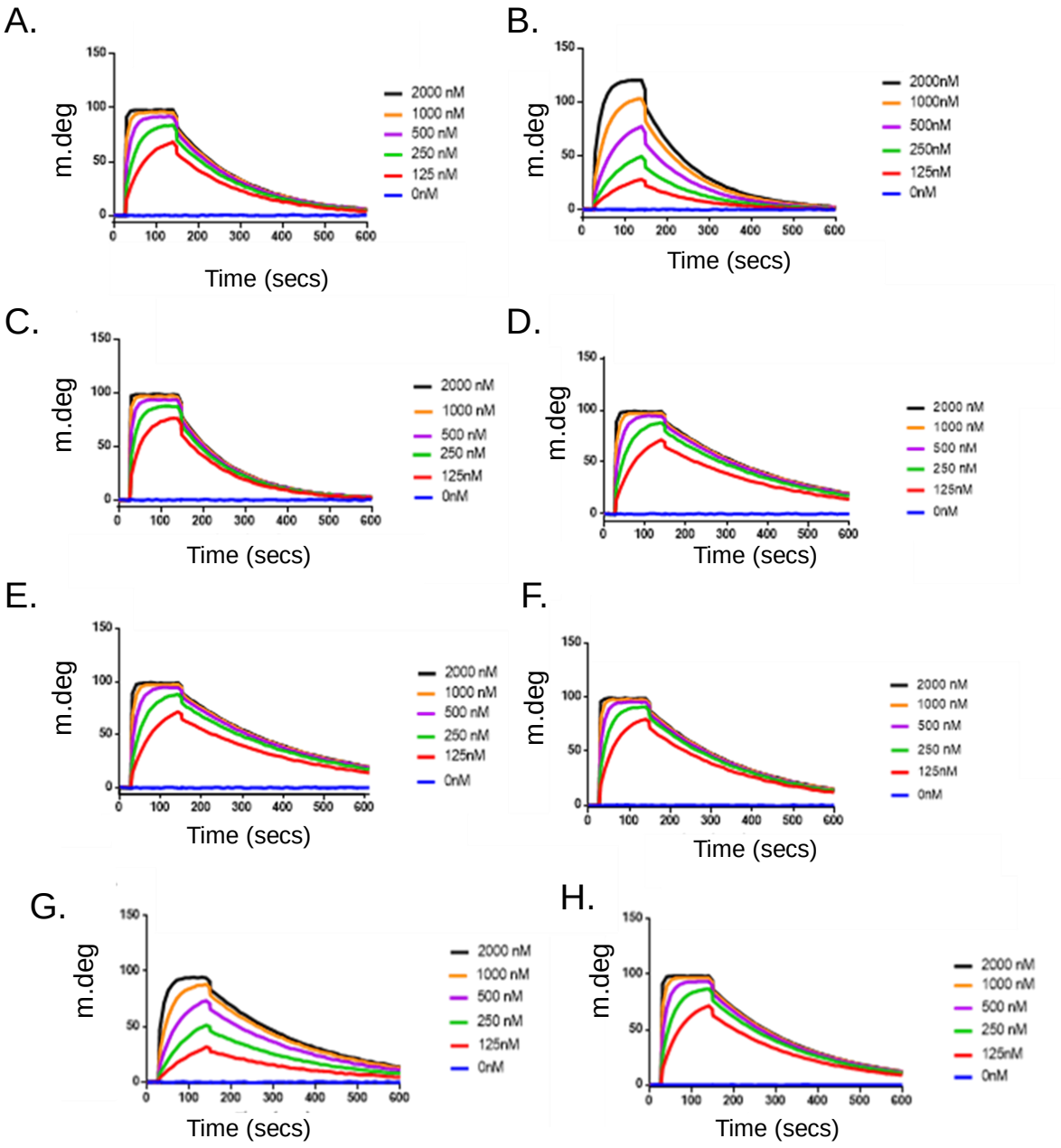

Figure B37 Sensograms for PfHsp70-z and PfHsp70-z $_{LS}$ self-association

SPR analyses was used to analyse self-association of wild type and linker mutant PfHsp70-z. The interaction showed concentration dependence, as response units (mdeg) increased with increasing analyte concentrations. The self-association of PfHsp70-z in the absence of nucleotides (A) and in the presence of 5 mM ATP (B) as well as 5 mM ADP (C). The experiment was repeated for the self-association of PfHsp70-z_{LS} (D, E, F). The association of PfHsp70-z with PfHsp70-z_{LS} was also investigated (G, H)

Appendix C: List of Reagents

REAGENT	SUPPLIER
Acetic acid	Merck, Germany
Adenosine triphosphate	Sigma, U.S.A
Agarose	Whitehead scientific, South Africa
Ammonium molybdate	Merck, Germany
Ammonium persulphate	Merck, Germany
Ampicillin	Sigma, U.S.A
Bovine serum albumin	Sigma, U.S.A
Bromophenol blue	Sigma, U.S.A
Calcium chloride	Merck, Germany
Chloramphenicol	Sigma, U.S.A
Coomasie brilliant blue R250	Merck, Germany
Diethiothreitol	Sigma, U.S.A
DreamTaq master mix	Thermo Scientific, U.S.A
Ethidium bromide	Sigma, U.S.A
Glacial acetic acid	Merck, Germany
Glycerol	Merck,
Glycine	Merck, Germany
Imidazole	Sigma, U.S.A
Isopropyl-1-thio-D-galacopyranoside	Sigma, U.S.A
Lysozyme	Merck, Germany
Magnesium chloride	Merck, Germany
Methanol	Merck, Germany
Monoclonal anti-His6-HRP antibodies	Sigma, U.S.A
Ni-NTA resin	Thermo Scientific, U.S.A
Nitrocellulose membrane	Pierce, U.S.A

Appendix C: List of Reagents

PagerRuler Prestained Protein Ladder	Thermo Scientific, U.S.A
Peptone	Merck, Germany
Phenylmethylsufonyl fluoride	Sigma, U.S.A
Polyacrylamide	Merck, Germany
Polyethylene glycol 2000	Sigma, U.S.A
Polyethylenimine	Sigma, U.S.A
Ponceau S	Sigma, U.S.A
Potassium chloride	Merck, Germany
Potassium dihydrogen phosphate	Merck, Germany
Proteinase-K	Sigma, U.S.A
Rapid ligation buffer	Promega, Germany
Restriction enzymes	Thermo Scientific, U.S.A
Sodium chloride	Merck, Germany
Sodium dodecyl sulphate	Merck, Germany
Sodium hydroxide	Merck, Germany
TEMED	Sigma, U.S.A
Tris	Merck, Germany
Tryptone	Merck, Germany
Tween 20	Merck, Germany
Urea	Melford, UK
Yeast extract powder	Merck, Germany
β-mercaptoethanol	Sigma, U.S.A